Urban scale phenomena and boundary layer processes in mountain valleys

Lorenzo Giovannini

UNIVERSITÀ DEGLI STUDI DI TRENTO

Dipartimento di Ingegneria Civile e Ambientale

2012

On the cover: looking to south-east from Molino Vittoria weather station, Trento

Acknowledgments

Contents

List of Figures

List of Tables

Chapter 1

Introduction

Scientific investigations towards a deeper understanding of weather and climate processes affecting urban areas have been increasingly stimulated in recent years by a number of motivations. An outstanding reason is that a majority of world population, estimated in around 3.3 billion people, lives nowadays in cities, and by 2030 is expected to raise to almost 5 billion (UNFPA 2007). Therefore it becomes more and more important to identify and investigate specific climatic conditions which an increasing number of citizens experiences every day. Moreover the growth of major urban areas is expected to induce appreciable modifications on weather and climate systems, affecting increasingly large regions, well beyond their close surroundings. The best known climatic phenomenon associated with urban areas is the Urban Heat Island (UHI), i.e. higher values of surface air temperature in the city center compared to surrounding rural areas. However the development of the UHI is only one of the modifications induced by the presence of a city. Indeed, as explained in the next Chapter, the artificial surfaces and high three-dimensional structures typical of urban built-up areas, alter the surface energy and hydrologic balances and produce an impact on surface temperatures, wind field and turbulence. Recent investigations have highlighted that local climatic modifications due to urban areas, often associated with higher temperatures, may have important consequences on human comfort and health, for example amplifying severe weather events such as heat waves (de'Donato et al. 2008; Tan et al. 2010). Citizens' health is also compromised by the high level of pollutants, which can be found inside urban areas due to high concentrations locally determined by the emissions from industrial activities, traffic and space heating. Pollutant dispersion is also affected by the specific microclimatic conditions of urban areas and by the interaction between cities and mesoscale atmospheric phenomena. Moreover, also the energy demand for space heating and cooling is affected by climatic conditions inside urban areas. For example in cities with a cold climate the presence of the UHI can have a positive effect, reducing the energy demand for space heating during cold months. On the other hand higher urban temperatures increase cooling needs in summer in cities displaying a hot climate.

1. Introduction

Most of the research on urban meteorology has so far concentrated on relatively big cities, which are mostly located over flat areas. The climate of large cities lying in widely open plains is relatively simple to characterize, as it mainly depends on synoptic scale factors and on boundary layer processes over flat terrain, which are very well known (Landsberg 1981; Oke 1987). The picture becomes more complicated for cities lying in areas displaying geographic inhomogeneities, such as coastal regions, as well as areas with strongly heterogeneous land use or located in complex terrain. In these cases the investigation of the urban climate must take into account the interactions between the built-up area and the non trivial phenomena typical of these contexts. In fact, while in flat areas weather conditions are mainly determined by synoptic scale situations, in complex terrain the influence of mesoscale to local-scale processes may be even more important, and affect phenomena at all scales down to the local-scale boundary-layer processes, which display features strongly marked by the local topography and ground properties (Rotach and Zardi 2007; de Franceschi et al. 2009). Several works have analyzed the climate of coastal cities and the interactions with sea breeze circulations (e.g. Gedzelman et al. 2003; Cenedese and Monti 2003; Thompson et al. 2007). On the other hand, the urban-climate properties of cities located in mountain valleys have received less attention, although various cases of midsized cities that have grown in mountain areas can be found all over the world, and only few works are available in the literature. Indeed mountain valleys are characterized by peculiar climatic conditions, which differ substantially from those found over flat areas. In particular daily-periodic, thermally-driven circulation systems are often present, such as slope winds, blowing along sidewall slopes, and along-valley winds (Whiteman 1990; Zardi and Whiteman 2011). Moreover in valleys diurnal temperature ranges are generally larger than over plains and in particular cooling rates are usually higher than over flat areas, due to cold air flowing down the slopes to the valley floor after sunset. As a result, thermal inversions are generally stronger in valleys than over the adjacent plains (de Wekker and Whiteman 2006). The investigation of the urban climate of cities located in valleys cannot neglect the possible interactions with these local atmospheric processes, which may play an important role for example in the transport and dispersion of air pollutants.

In the present thesis the city of Trento, located in the Alpine Adige Valley, is adopted as a typical case of urban weather and climate phenomena in a mid-sized city lying in a mountain valley. The urban climate of the city is investigated in detail, using different methods and focusing on different spatial scales, from the microclimatic conditions inside the urban canopy to the interactions between the urban area and the typical atmospheric phenomena of the valley environment. After a brief survey of the state of the art in urban meteorology presented in Chapter 2, the urban climate of Trento is first characterized analyzing the UHI of the city (Chapter 3). UHI intensity is evaluated by investigating the differences ΔT_{u-r} between air temperature taken at an urban automated weather station placed on the tower of a building, over mean rooftop level (T_u), and at five suburban/rural weather stations (T_r), located few kilometers

outside the city boundaries. This analysis concentrates especially on the evaluation of the temporal patterns of behavior of the UHI, both in the diurnal and in the yearly cycles, and on the influence of wind speed and cloud amount. The analysis focuses then on a smaller spatial scale, investigating the thermal field inside the urban canopy, by means of two experimental campaigns in a typical urban canyon in the city center, and using a simplified model, to simulate the energy balance of the different surfaces within the street. This analysis, along with comparisons with the measurements taken at the above mentioned weather station placed above roof level, is presented in Chapter 4. In the last part of the work the possible interactions between the urban area of Trento and the atmospheric processes in the Adige Valley, in particular local circulation systems, are investigated. To this purpose, first the main features of local circulation systems developing in the valleys around Trento are investigated by means of the analysis of a dataset from surface weather stations covering the period 2004-2011 (Chapter 5). After that, high-resolution numerical simulations with the mesoscale meteorological WRF model (Skamarock et al. 2008), coupled with an urban parameterization scheme, are utilized to study the urban climate of Trento in the Adige Valley context (Chapter 6). The numerical results, validated against measurements from surface weather stations, are analyzed to obtain more information about local circulation systems and the effects of the urban area of Trento on local climatic conditions. Finally in Chapter 7 some conclusions are drawn along with an outlook for future developments.

Chapter 2

Urban scale meteorology: an overview

Urban meteorology studies deal with a wide range of topics covering different spatial scales, ranging from the investigation of the microclimatic conditions inside the urban canopy including turbulence, to the study of the urban climate at a city-scale (UHI studies for example), to the evaluation of the impacts of urban areas on mesoscale processes. The present Chapter aims at giving an overview of the state of the art in urban meteorology, with no claim of being exhaustive, but focusing especially on the topics that will be explored in this work.

2.1 Energy balance

The particular characteristics of the urban climate are mainly caused by the alteration of the surface energy budget with respect to rural areas. The surface energy balance of an urban volume (Fig. 2.1) can be expressed in the following way (Oke 1988):

$$Q^\star + Q_F = Q_H + Q_E + \Delta Q_S + \Delta Q_A \qquad (2.1)$$

where Q^* is the net radiation, Q_F the anthropogenic heat flux, Q_H the sensible heat flux, Q_E the latent heat flux, ΔQ_S the storage heat flux and ΔQ_A the advection. The net radiation can be divided into four terms, expliciting the different components of the radiation balance at the surface:

$$Q^\star = K \downarrow + K \uparrow + L \downarrow + L \uparrow \qquad (2.2)$$

where $K \downarrow$ is the downward short-wave radiation, $K \uparrow$ the upward short-wave radiation, $L \downarrow$ the downward long-wave radiation and $L \uparrow$ the upward long-wave radiation.

The four radiation components are considerably altered inside cities with respect to rural
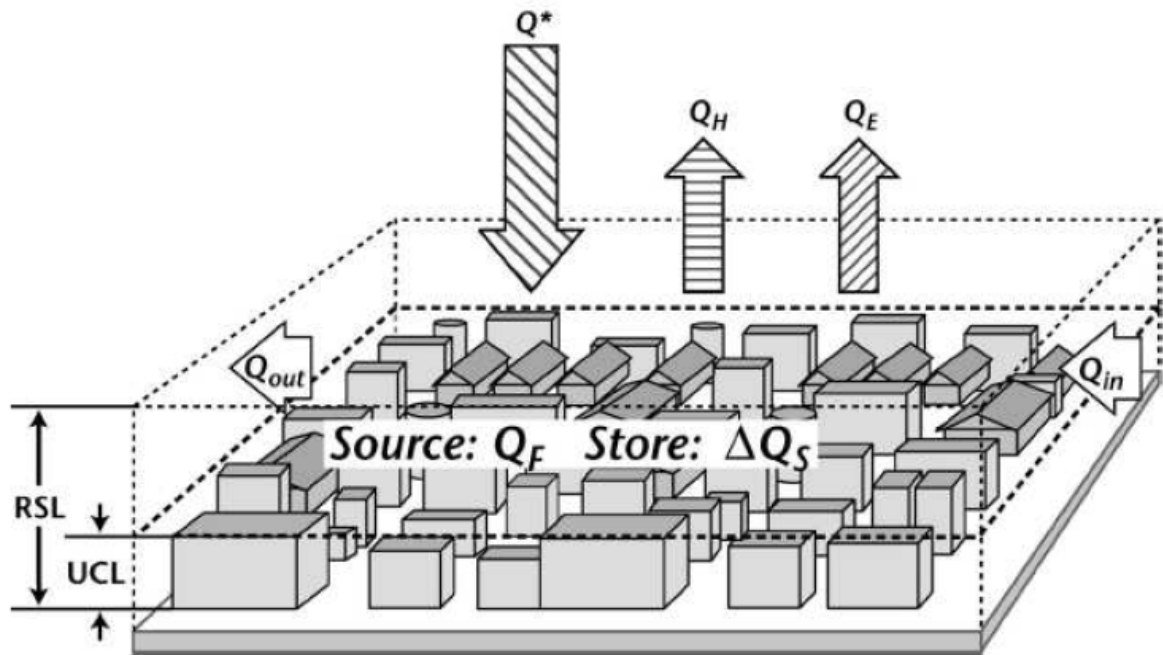
Figure 2.1: Representation of the various terms of the surface energy balance in an urban air-building volume (Oke 1988).

areas, due to the different surface conditions (high three-dimensionality, different surface materials) and the presence of a more polluted atmosphere (Oke 1987). The downward short-wave radiation $K \downarrow$ is generally attenuated by the more polluted urban atmosphere, which also causes an increase of the diffuse fraction, due to scattering and reflections. On the other hand the upward short-wave radiation $K \uparrow$ is generally lower in cities than in rural areas due to the lower albedo of urban surface materials and to the highly three-dimensional geometry of urban areas, which traps radiation between buildings within the streets. Oke (1987) states that there is roughly a balance between the two effects and for this reason the net short-wave radiation is similar in urban and rural areas. The temperature of urban surfaces is generally higher with respect to natural terrains, and as a consequence the upward long-wave radiation $L \uparrow$ is higher in cities, even though, similarly to $K \uparrow$, part of $L \uparrow$ is trapped within streets. Finally, the downward long-wave radiation $L \downarrow$ is greater in urban areas due to the more polluted atmosphere, roughly compensating the greater $L \uparrow$. Thus, also the net long-wave radiation is similar in urban and rural areas (Oke 1987).

The second term on the left-hand side of Eq. (2.1), the anthropogenic heat flux, represents an additional source of heat that is present only in urban areas. In some cases the anthropogenic heat flux can be a relevant term of the surface energy budget (even higher than $Q^\star$ in cold climates), and as a consequence it can play an important role in the development of the UHI

(e.g. Ohashi et al. 2007). The anthropogenic heat flux can be divided into three major sources (Sailor and Lu 2004):

$$Q_F = Q_V + Q_B + Q_M \qquad (2.3)$$

where Q_V is the anthropogenic heat from vehicles, Q_B the anthropogenic heat from buildings and industries and Q_M the anthropogenic heat from the human metabolism. This last term is usually very low compared to the others and for this reason neglected (Sailor and Lu 2004). The highest values of anthropogenic heat flux are generally found in cities with high population densities and well-developed industrial areas. Another factor influencing the magnitude of the anthropogenic heat flux is the climate, due to the contribution from space heating/cooling. The anthropogenic heat flux is generally not constant during the day, as can be seen in Fig. 2.2: the highest values are registered during daytime, with two peaks in the morning and in the late afternoon, corresponding to the rush hours. The seasonal variations depend mostly on climate conditions and the consequent energy need for space heating/cooling.
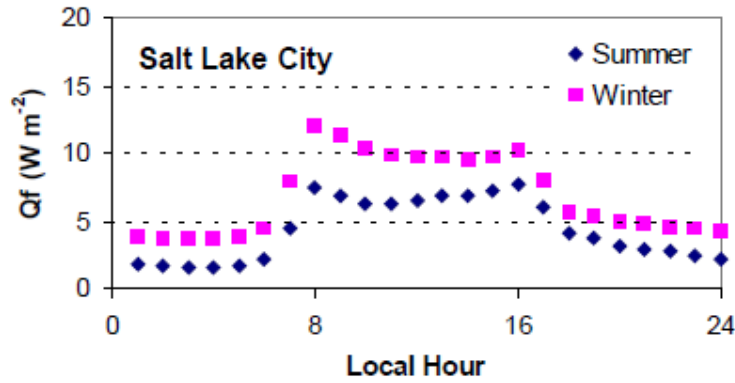
Figure 2.2: Anthropogenic heating profiles in summer and in winter for Salt Lake City (Sailor and Lu 2004).

Coming back to Eq. (2.1), the right-hand side terms present substantial differences between urban and rural areas, as can be seen in Fig. 2.3. The storage heat flux ΔQ_S is generally higher in urban areas than in the countryside due to the higher thermal admittance $\mu = (C \cdot \lambda)^{0.5}$ (C = thermal capacity, λ = thermal conductivity) of artificial materials and the three-dimensional structure of cities. Grimmond and Oke (1999) investigated the characteristics of the surface energy balance in ten cities of North and Central America, finding that the storage heat flux varies depending on the physical characteristics of the city: the highest values were measured in cities with high buildings and scarce presence of vegetation. In these cases ΔQ_S can be the highest term of the surface energy balance, as for example Oke et al. (1999) found in Mexico City. In cities the latent heat flux is generally very low, especially in the more densely urbanized areas, due to the impervious artificial materials which dry very fast after precipitations and the

efficiency of urban drainage systems. In fact Grimmond and Oke (1999) found a Bowen ratio $\beta = Q_H/Q_E$ higher than 1 in all the ten cities investigated, while in rural areas the sensible heat flux is generally lower than the latent heat flux. Similar values of sensible and latent heat fluxes were found only in residential areas, where vegetation is more present.
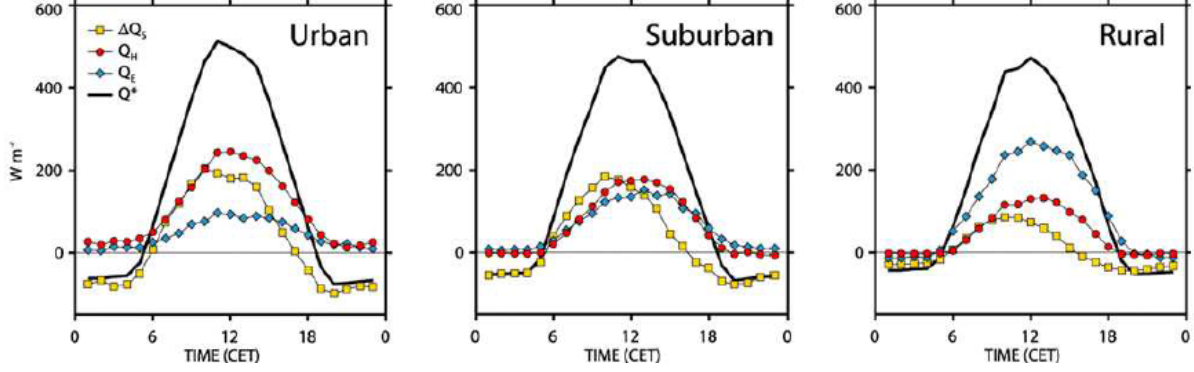
Figure 2.3: Surface energy balances in urban, suburban and rural areas as measured during BUBBLE (Basel UrBan Boundary Layer Experiment) project (Piringer et al. 2005).

2.2 The urban boundary layer

The presence of urban areas modifies not only the surface energy balance, but also the wind field, due to a drastic change in the aerodynamic surface conditions: tall buildings make cities among the roughest surfaces there are. The wind field has to adapt to these new aerodynamic boundary conditions, with the development of a zone influenced by the urban surface. Thus, starting from the city edge, there is the development of an internal boundary layer, called urban boundary layer. As shown in Fig. 2.4, the urban boundary layer can be divided into different sub-layers. The urban canopy layer extends from the ground to roof level and is a part of the roughness sublayer, which extends to a height where the influences of the single roughness elements are mixed together. This height is generally called blending height and varies in function of the height of the roughness elements, i.e. the buildings. According to Oke (2006), the blending height can be calculated as following:

$$\begin{cases} z_r = a \cdot z_H \\ a = 1.5 \div 4 \end{cases} \tag{2.4}$$

where z_H is the mean building height.

Rotach 1993a,b found that turbulent fluxes are not constant with height in the roughness layer and for this reason Monin-Obukhov Similarity Theory (MOST) cannot be applied. In the roughness sub-layer and in particular in the urban canopy layer the wind field is influenced

by microscale effects, i.e. the characteristics and the geometry of the nearest obstacles. As a consequence the wind field near the ground is generally rather complex with mechanical generation of turbulence and vortices. Wind speed and direction may vary considerably in short spatial scales, depending for example on the distance from the buildings or on the orientation of the streets. Wind speed is generally lower than at the same height in the open, due to the drag of the numerous obstacles. However, when the wind blows roughly parallel to the street axis, the flow may channel, with velocities even higher than in the open (Oke 1987). More details about the wind field in the canopy layer are given in Section 2.4.2.
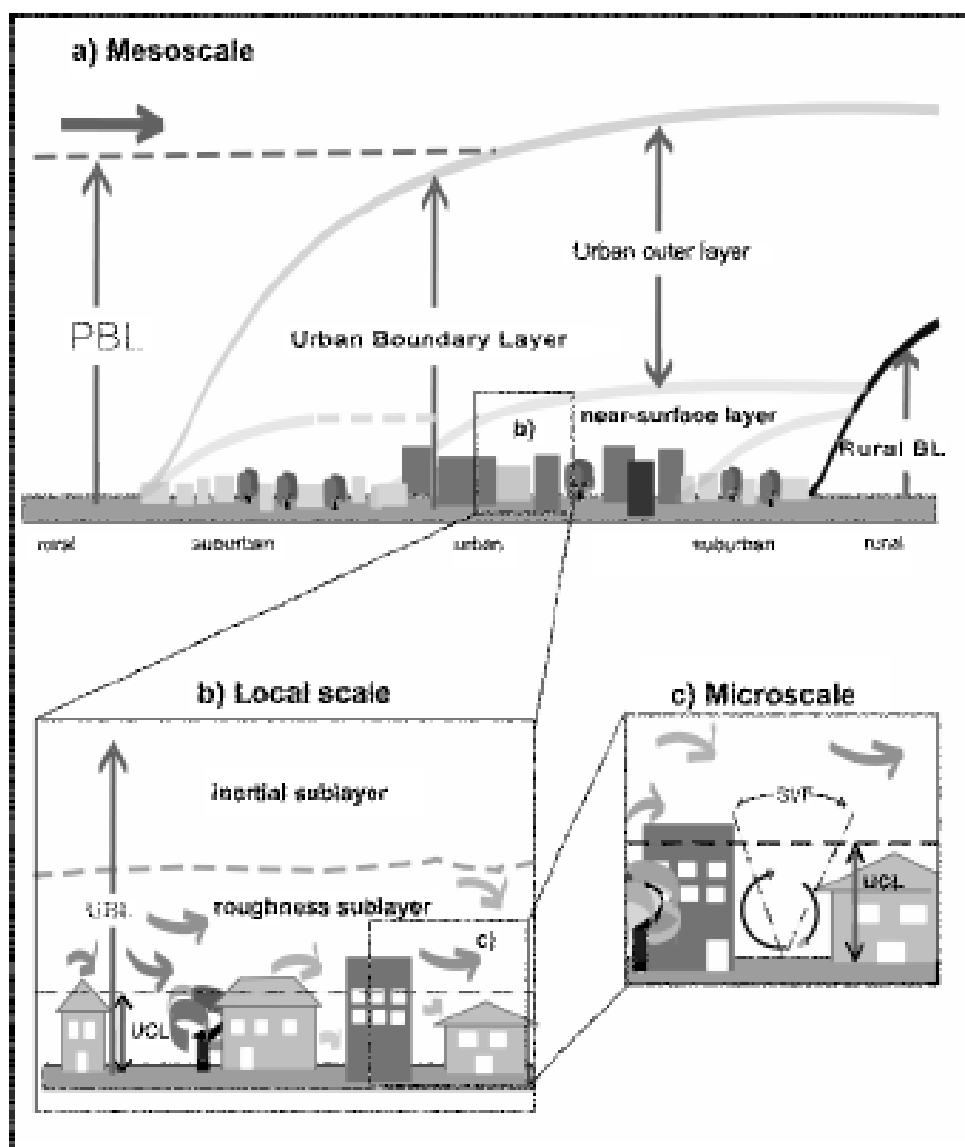
Figure 2.4: Urban boundary layer structure (Rotach et al. 2005).

Above the blending height there is the inertial sub-layer; here it may be expected that MOST holds (Rotach et al. 2005) and the wind speed profile follows the logarithmic law (Oke 2006):

$$U(z) = \frac{u_*}{k} \left[\ln \left(\frac{z-d}{z_0} \right) - \psi_m \left(\frac{z-d}{L} \right) \right]$$ (2.5)

where u^* is the friction velocity, k the Von Karman's constant, d the displacement height, z_0 the roughness length, ψ_m the integrated stability function for momentum, and L the Monin-Obukhov length:

$$L = \frac{-u_*^3}{k \left(\frac{g}{\theta_v} \right) Q_H}$$ (2.6)

where g is the gravitational acceleration, θ_v the virtual potential temperature, and Q_H the sensible heat flux.

The displacement height and the roughness length in urban areas can be estimated with morphometric or micrometeorological approaches (Grimmond and Oke 1999). The former utilizes expressions that relate these quantities to the geometry of the urban area, while the latter directly uses field measurements. The most important parameters used to describe the geometry of the urban area in the morphometric approach are (Grimmond and Oke 1999) :

- the building planar area fraction $\lambda_P = A_P/A_T$;

- the building frontal area index $\lambda_F = A_F/A_T$;

- the building surface area to plan area ratio $\lambda_B = (A_P + A_W)/A_T$;

where A_P is the plan area of buildings, A_T is the total area of the urban array, A_F is the plan area normal to the approaching wind direction, and A_W is the total area of the walls of buildings (Fig. 2.5).

Finally the highest part of the urban boundary layer is called urban outer layer, and is probably dominated by advection, but little is know about it (Rotach et al. 2005).

2.3   The urban heat island

The UHI is mainly amenable to the strong modifications produced in the surface energy budget by urban surfaces covered with artificial materials (buildings, paved roads, etc.), as described in Section 2.1. Another important factor is the highly three-dimensional character of the city structures (i.e buildings, streets, etc.), which determines a reduced ventilation of the gaps between buildings, a reduction of the sky view factor, and therefore the trapping of radiation within streets. Moreover, as said in Section 2.1, air temperature in urban areas may be affected by the presence of various sources of anthropogenic heat. The intensity of the UHI is usually
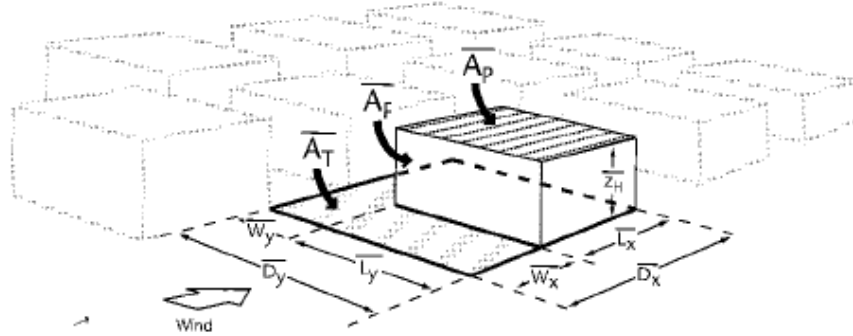
Figure 2.5: Schematic representation of the dimensions used in morphometric analysis (Grimmond and Oke 1999).

expressed by characterizing typical values of the difference $\Delta T_{u-r} = T_u - T_r$ between the air temperature T_u measured at a weather station inside the urban environment, and the temperature T_r taken at another station located in the countryside out of the city. In some cases the UHI has been studied by means of car transects across the urban area (e.g. Unger et al. 2001; Sofer and Potchter 2006). The UHI is usually characterized by a sharp air temperature jump at the outskirts of the city, where density of buildings is appreciably higher than in the adjacent countryside. Moving towards the inner urban area the temperature generally raises more slowly, reaching its maximum near the city center (Oke 1987) (Fig. 2.6). However the temperature field inside the city may be strongly nonuniform, due to the heterogeneity of the land use and of the urban morphology. In this regard, important factors affecting micrometeorological variations inside a city are building materials, canyon geometry and the degree of compactness of the urban texture (Pearlmutter et al. 1999a; Johansson 2006).

The presence of a city may also affect the vertical temperature profile: the atmosphere is generally neutral in urban areas during nighttime, in contrast with the stable stratifications present in the surrounding rural areas (Fig. 2.7).

UHI intensity is strongly variable depending on the time of the day: it is generally higher during nighttime than during daytime. A typical cycle of the UHI is shown in Fig. 2.8. The daytime values of the UHI are generally very low and in some cases the temperature in urban areas is even lower than in the countryside, with the development of the so-called urban cool island. In fact, especially in the morning, urban surface materials, displaying a higher thermal admittance, store a great amount of heat and therefore urban areas warm up slower than the nearby countryside (Oke 1987). Heat thus stored is then released after sunset, when the temperature in the city drops slower than in the countryside, thus resulting in higher nocturnal temperatures inside the urban area.

Also weather factors, especially wind speed and cloud cover, which basically modify tur-
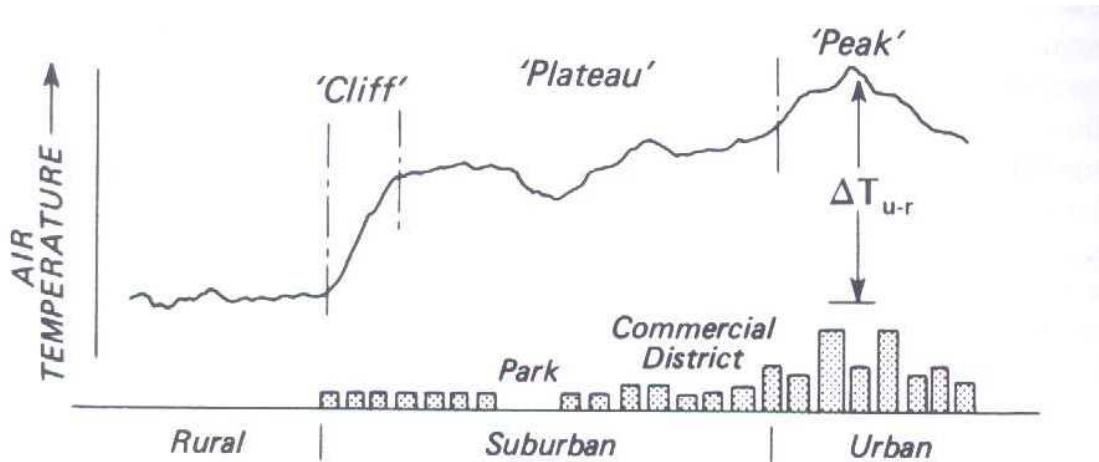
Figure 2.6: Typical spatial profile of the UHI (Oke 1987).
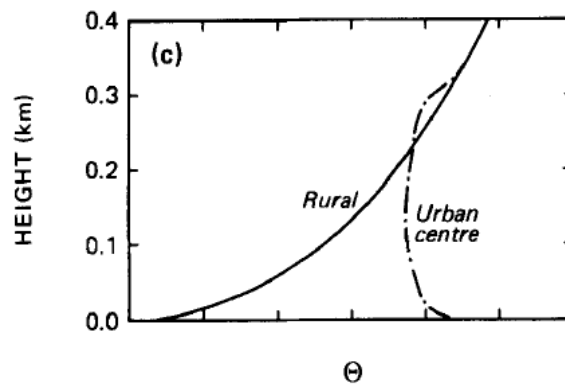
Figure 2.7: Comparison of urban/rural nocturnal potential temperature vertical profiles (Oke 1982).

bulent and radiative cooling at night (Morris et al. 2001; Kassomenos and Katsoulis 2006) influence the intensity of the UHI. Maximum UHI intensities are generally reached during clear nights under low wind speeds, when favorable conditions for a strong radiative cooling at night are present, and as a consequence cooling rate differences between urban and rural areas are stronger.

2.4 The urban canyon

As highlighted by Oke (1976), climatic conditions inside urban areas are generally very complex and highly variable on short space scales, reflecting the complexity of the urban environment, and are strongly influenced by site specific characteristics and microscale processes. In order to describe in a simple way the complex morphology of urban areas, the concept of urban
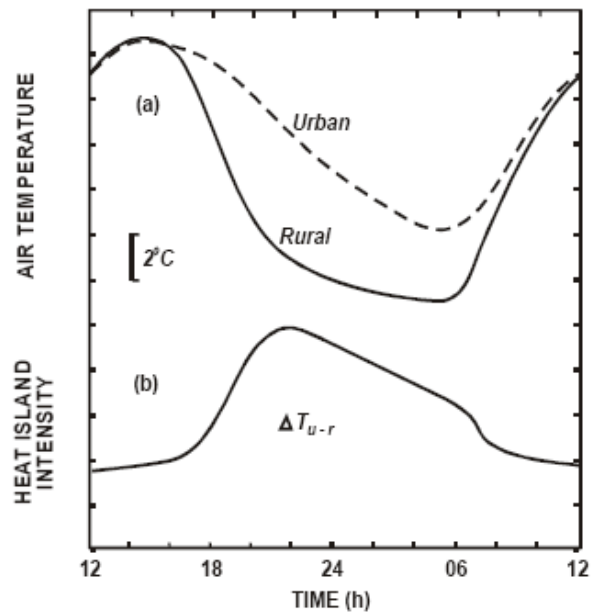
Figure 2.8: Typical temporal behavior of the UHI (Mills 2004).

canyon, that is a street flanked by two rows of buildings (Nunez and Oke 1977), is usually adopted (Fig. 2.9): the urban canyon is commonly considered as the fundamental unit of urban areas, which can be idealized as a repetition of these basic structures. The more important geometrical parameters used to describe an urban canyon are the aspect ratio, i.e. the ratio between the average height of the buildings flanking the canyon and the width of the street, and the orientation. These parameters, along with geographical and astronomical factors such as the latitude of the city and the time of the year, control the penetration of solar rays inside the canyon (and the radiative emission during the night) and thus the warming (cooling) of both the walls and the road (Offerle et al. 2007). The thermal properties of the materials employed for the adjacent buildings and the street paving are other important factors determining the urban canopy microclimate.

2.4.1 Temperature inside urban canyons

Climatic conditions at street level within urban canyons influence directly large communities of citizens living there and so the assessment of the typical thermal field inside the urban canopy is crucial in order to improve their thermal comfort and well-being. Moreover the thermal structure of the atmosphere in an urban canyon is a key factor controlling pollutant dispersion and heat exchange between buildings and the surrounding environment; accordingly these factors must be carefully evaluated in view of pursuing effective air quality management policies and an energy-efficient design of buildings adequate to the state of the art. To this
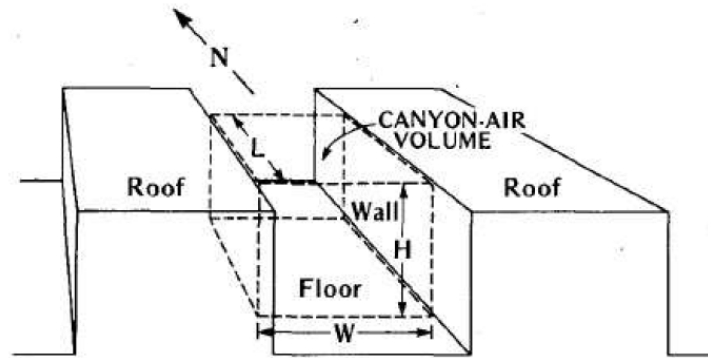
Figure 2.9: Schematic representation of an urban canyon (Oke 1987).

purpose several field measurements have been performed in the last few years to study the microclimatic conditions inside urban canyons (cf. Grimmond 2006 for a review). The results of these campaigns reflect partly site-specific characteristics, but some common features can also be highlighted. During daytime, if direct solar radiation can penetrate inside the urban canyon, thanks to a low or moderate aspect ratio and a low solar zenith angle, the air inside an urban canyon is generally warmer than above roof level (Kanda et al. 2005). This is the result of the warming of the walls and of the road and of the multiple reflections of both short- and long-wave radiations occurring inside the canyon. The above mentioned temperature difference is usually higher in summer, when the solar short-wave incoming radiation is stronger, as also described by Kanda et al. (2005) in their field measurements in the city of Tokyo. Furthermore they observed that the height, at which the maximum temperature inside the canyon occurred, varied depending on the season: it was at ground level during summer, at the middle of the canopy height in spring and in autumn, and at roof level in winter, confirming the dependence on the solar zenith angle and thus on the penetration of solar beams inside the urban canopy. Similar results were also found by Offerle et al. (2007) in their experimental campaign carried out in Gothenburg (Sweden), highlighting that temperature distribution inside the canyon was strongly influenced by short-wave solar radiation and thus by surface (walls and road) heating. On the other hand, when solar radiation cannot penetrate inside the urban canopy due to the high aspect ratio or the high solar zenith angle, air temperature inside the street can be lower than above roof level, as shown by the results of the field measurements carried out by Georgakis and Santamouris (2006) in a deep canyon (aspect ratio of 3.3) of Athens (Greece). These results are consistent with the measurements made by Bourbia and Awbi (2004) in the town of El Oued (Algeria), where they found that in the old part of the city, displaying a traditional structure with a dense network of narrow alleys, the average temperature was lower than at a reference station situated outside the city center. On the other hand in the modern part of the city, characterized by wide roads and large open spaces, the average temperature was higher than at

the reference site. An analogue conclusion was found by Johansson (2006) in his study on the thermal comfort in the city of Fez (Morocco).

During nighttime an opposite behavior with respect to the aspect ratio is generally found. In fact an elevated aspect ratio, and thus a low sky view factor, inhibits radiative cooling at night, resulting in higher temperatures than in wider streets (Svensson 2004). It is known in fact that the reduction of the sky view factors in cities is one of the main causes leading to the development of the nocturnal canopy-layer UHI (Oke 1981).

2.4.2 Wind field inside urban canyons

The determination of mean flow and turbulence characteristics inside urban canyons is of great importance for air pollutant dispersion studies. In this regard, in the last years several experimental campaigns with fast-response sensors and numerical studies with CFD models have been performed, but a comprehensive review of these works is well beyond the scope of this Chapter. In this Paragraph only a brief overview of the main features of the flow field inside urban canyons is given.

When the mean flow is roughly perpendicular to the street orientation, which is the configuration far more studied, one or more vortices are likely to develop within the canyon. Oke (1987), considering simple two-dimensional arrangements, proposed three main regimes (Fig. 2.10), depending on the canyon aspect ratio:
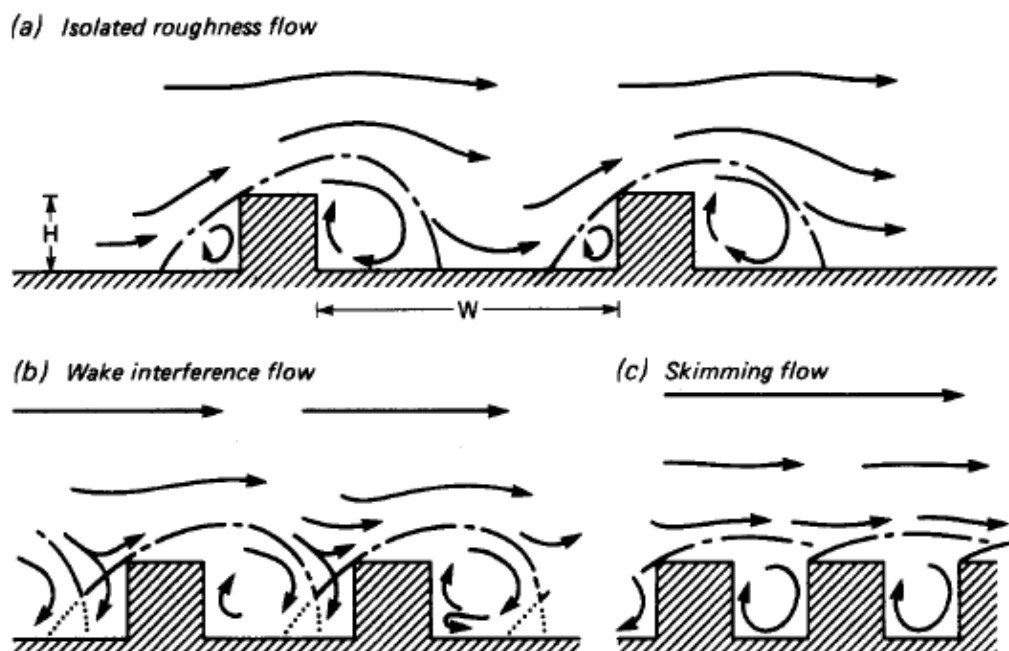
Figure 2.10: Flow regimes associated with different urban geometries (Oke 1987).

- the isolated roughness flow occurs for h/w < 0.3÷0.4; the flow pattern is similar as if there were isolated obstacles, with no interactions between the vortices upwind and downwind the buildings;

- the wake interference flow occurs for h/w up to 0.65÷0.7; the recirculating wake interacts with the vortex upstream the following building;

- the skimming flow occurs for h/w > 0.7; the main flow is not able to penetrate inside the canyon and a lee vortex develops inside the street.

Most numerical studies on wind flow characteristics within urban canyons have considered the skimming flow, which is more common in urban areas. In this regime complex urban geometries may lead to the development of a complex combination of vortices, as for example Zajic et al. (2011) highlighted analyzing the numerical experiments of Xiaomin et al. (2006) (Fig. 2.11).
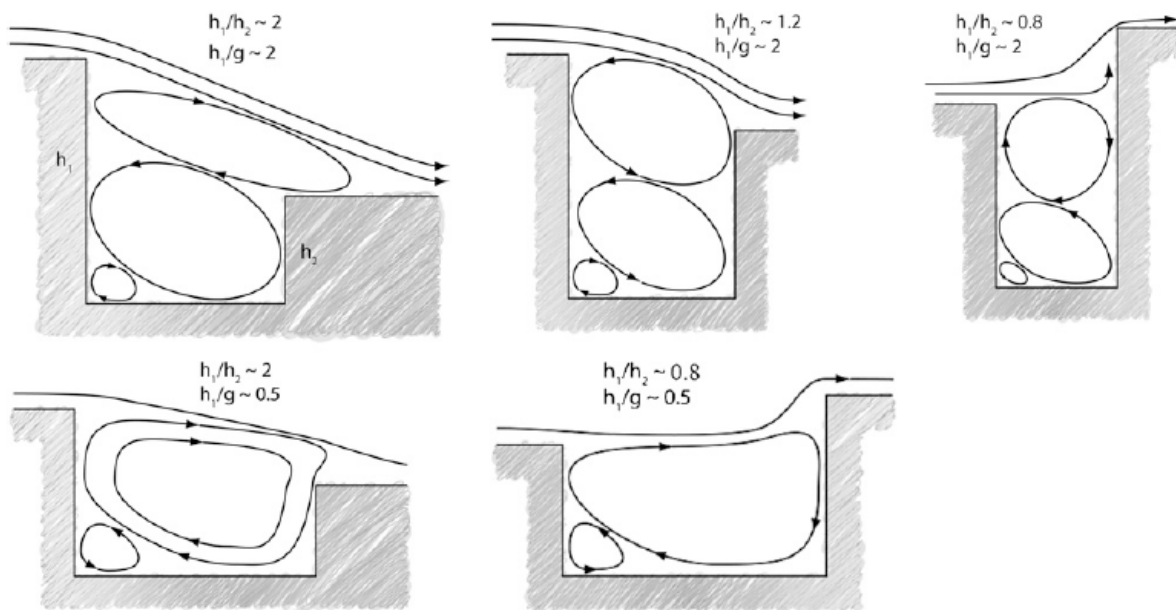
Figure 2.11: Vortices developing in canyons with unequal building heights following the numerical results of Xiaomin et al. (2006). g is the width of the road, h_1 and h_2 the height of the upwind and downwind buildings respectively (Zajic et al. 2011).

A more complete three-dimensional conceptual model was proposed by Coceal et al. (2007), based on the results of numerical simulations (Fig. 2.12). Hairpin-like vortices develop above roof level, associated with low momentum regions (blue areas). At roof-top level a strong shear layer is present, with ejection and sweep events. Within the canopy the flow is very complex

due to presence of eddies generating on the walls, vortices inside the canyon and due to the interactions with the structures in the shear layer at the canopy top.
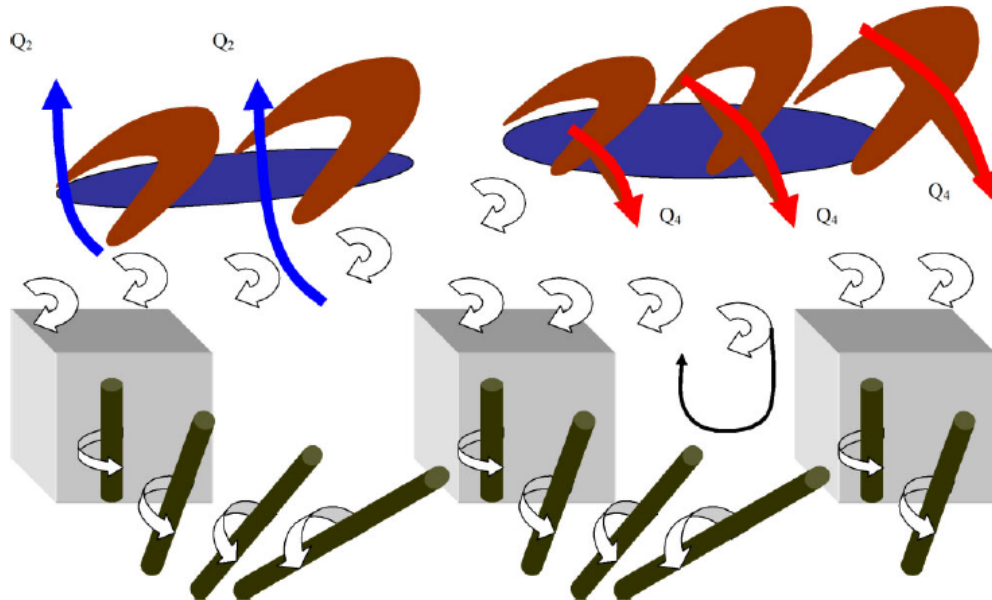
Figure 2.12: Conceptual scheme summarizing the complex flow patterns above and within the urban canopy (Coceal et al. 2007).

Numerical studies have suggested that also the heating of the surfaces within the canyon may influence the flow characteristics, due to buoyancy effects (e.g. Baik and Kim 1999), even though only little evidences about this fact have been found from observations (e.g. Idczak et al. 2007).

2.5 Urban areas in mesoscale models

Urban areas have an impact on local and mesoscale processes, affecting the climate conditions of large regions. In fact the higher surface and air temperatures and the enhanced roughness of built up areas interact with local wind systems (Wanner and Hertig 1984; Yoshikado 1992), influence the boundary layer structure and height (Lin et al. 2008) and may enhance convection (Chen et al. 2007). The use of building-resolving numerical models, such as CFD models, is not currently suitable for the study of the impact of urban areas on mesoscale processes, because of the too high computational cost. For this reason in the last years suitable parameterizations of urban effects have been developed to be included inside mesoscale models, which can be executed with grid spacings of order 0.5-1 km in urban climate studies (Chen et al. 2011). These urban parameterization schemes take into account the alterations caused by urban areas on the surface

energy balance and on the wind field. They supply the surface boundary conditions to the lowest atmospheric level of the mesoscale model. Masson (2006) classified these urban surface energy balance models in five categories: (1) empirical models, (2)-(3) vegetation models, with or without drag terms, adapted to urban areas, (4)-(5) single-layer and multi-layer urban canopy models. Empirical models try to reproduce the surface energy balance of urban areas from statistical relations obtained from measurements. These models are very simple, but being based on field measurements, the relations used are not applicable in all contexts. In the vegetation models adapted to include urban areas, the particular characteristics of the urban surface energy balance are generally simulated changing the physical parameters of the surface materials (thermal capacity and conductivity, albedo). The effects of urban areas on the mean flow are parameterized either with a larger roughness length or with a drag approach, adding a drag force in the equations of motions. Urban canopy models try to reproduce the surface energy balance of a real urban canyon, simulating separate surface energy budgets for roofs, walls and the road. Moreover in these models the shadowing and the multiple reflections of short-wave and long-wave radiations within the canyon are explicitly taken into account. In the mesoscale grid surface fluxes are calculated as they arise from an urban canyon having the average characteristics of the urban morphology. In the single-layer models the interaction between the surface scheme and the atmospheric model occurs only above the canyon (Fig. 2.13). On the other hand in the multi-layer models the interactions with the atmospheric model occur at several levels (Fig. 2.14); in these kind of schemes the drag approach is applied.

Several studies have highlighted that mesoscale models coupled with single- or multi-layer urban canopy schemes are able to simulate the modifications caused by cities on local climatic conditions and boundary layer processes. Miao et al. (2009) tried to simulate with the mesoscale WRF model coupled with a single-layer urban parameterization scheme the spatial and temporal characteristics of the UHI of Beijing, finding a reasonable agreement between measurements and numerical results. However the model was not able to capture the development of an urban cool island in the morning. The WRF model, coupled with a multi-layer urban parameterization scheme, was used also by Salamanca et al. (2011a) to analyze the UHI of Madrid. They found a good agreement with air temperature observations, but faced some problems in the correct simulation of the wind field. Moreover they highlighted that the presence of an urban area inhibits the development of strong ground-based thermal inversions. The intensity of the UHI and the boundary-layer development in the city of Taipei were simulated reasonably well by Lin et al. (2008), also in this case using the WRF model coupled with a single-layer scheme. Furthermore they found that the enhanced sensible heat flux over the urban area and the consequent stronger land-sea contrasts, may lead to a stronger sea breeze. On the other hand Thompson et al. (2007) and Dandou et al. (2009) highlighted, analyzing the case studies of New York and Athens respectively, that the sea breeze front is generally frictionally retarded in its penetration inland, due to the high roughness of the urban area. In both works the
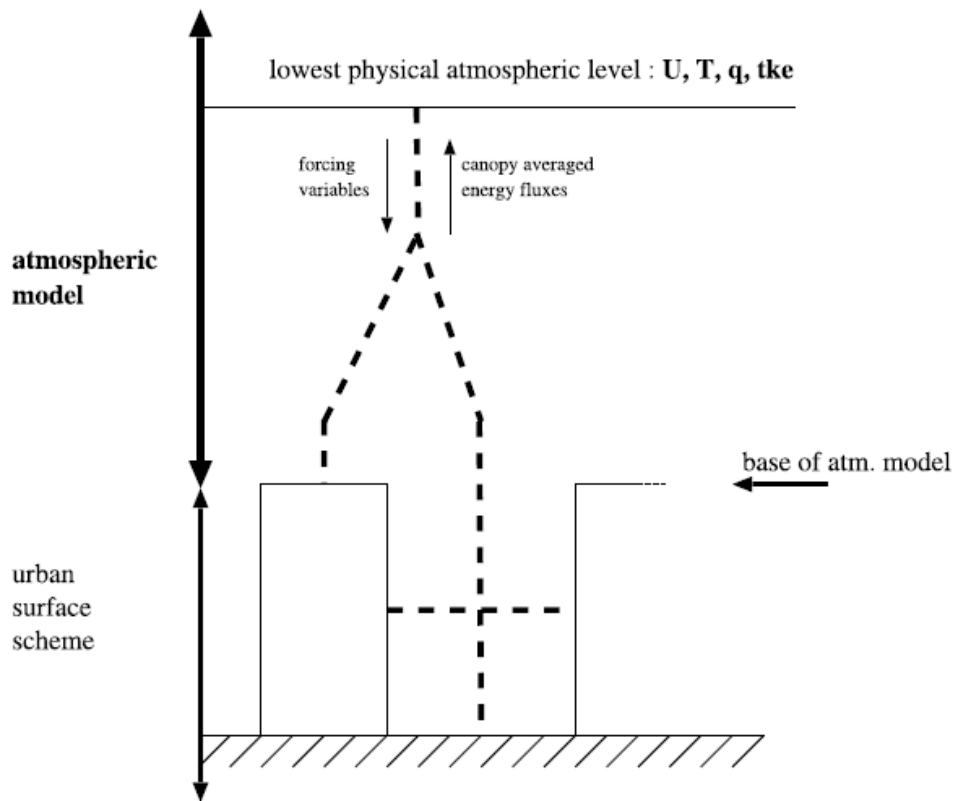
Figure 2.13: Scheme of a single-layer urban canopy model (Masson 2006).
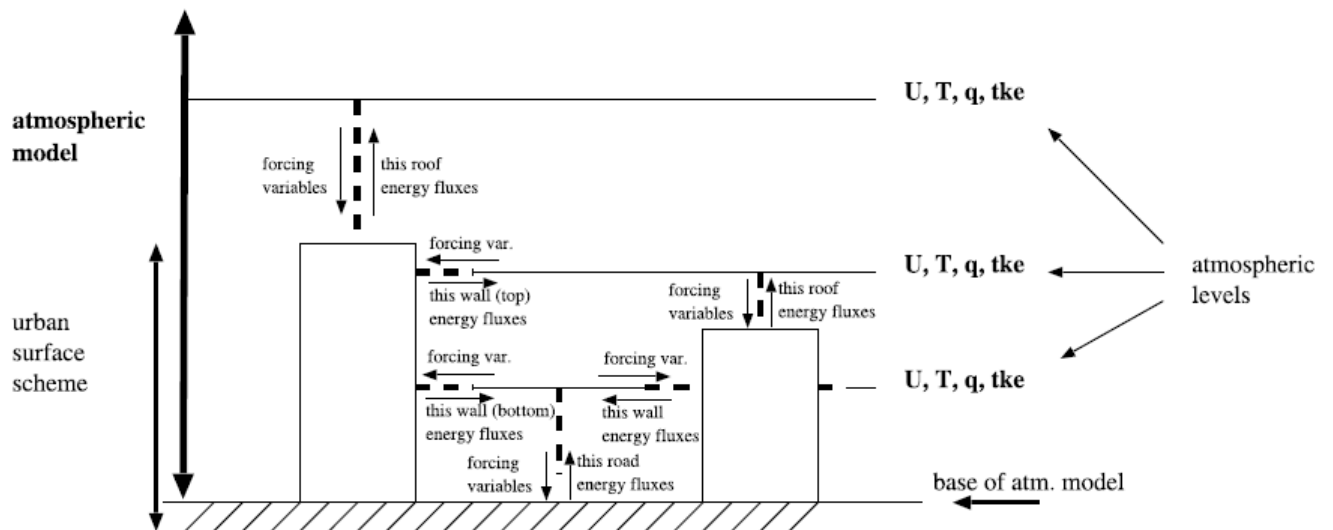
Figure 2.14: Scheme of a multi-layer urban canopy model (Masson 2006).

authors compared the results obtained performing an idealized run, replacing the urban area with natural surfaces, with those obtained simulating the real situation. They both found a delay of the sea breeze front of about 1 h, due to the presence of the urban area. Cities may have an impact also on precipitations, as highlighted by Miao et al. (2011), who analyzed an heavy rainfall event in Beijing with the WRF model coupled with a single-layer scheme. They found that the urban area influences the storm movement and as a consequence the amount and distribution of rainfall.

Chapter 3

Urban heat island effect in an Alpine valley: the case of Trento

As said in the Introduction, only few works regarding the climate of cities located in valleys are present in the literature. Wanner and Hertig (1984), working on both small and midsized Swiss cities, analyzed the possible interactions between the particular meteorological phenomena occurring in Alpine valleys and urban areas, emphasizing in particular the important influence of local winds. This aspect was also analyzed in detail by Kuttler et al. (1996), who highlighted how penetration of cold air drainage flow inside the urban canopy is a key factor affecting the development of the nocturnal UHI. In Stolberg - a small city in a narrow valley in western Germany - they found that the obstruction of the built up area, and the narrow valley cross-section, block the penetration of the drainage flow into the inner city in the first part of the night, leading to the development of a strong UHI in these hours. On the other hand, during the second part of the night, the drainage flow is partly able to penetrate in the most densely urbanized area, thus lowering UHI effects. However the authors concluded that the majority of the cold air flows around or over the town center, rather than penetrating into it. Kuttler et al. (1998) presented a similar analysis on the nighttime penetration of cold air in the inner city of Cologne (Germany), at the northern end of the Rhine Valley. In that case only the onset of the down-valley wind at 0100 LST (UTC+1) was effective in producing an appreciable cooling in the urban area.

The Austrian city of Graz, in the Mur Valley (eastern Alps), was analyzed by Pearlmutter et al. (1999b) and by Lazar and Podesser (1999). They pointed out that both the complex topography of the valley, and the presence of the urban area, contribute to develop remarkably heterogeneous temperature and wind fields, along with strong ground-based thermal inversions. The latter are an important aspect for the climate of a valley city, especially if the urban area spreads on the sidewalls, and thus topographic and urbanization effects may interplay (Goldreich 1984).

3.1 Study area
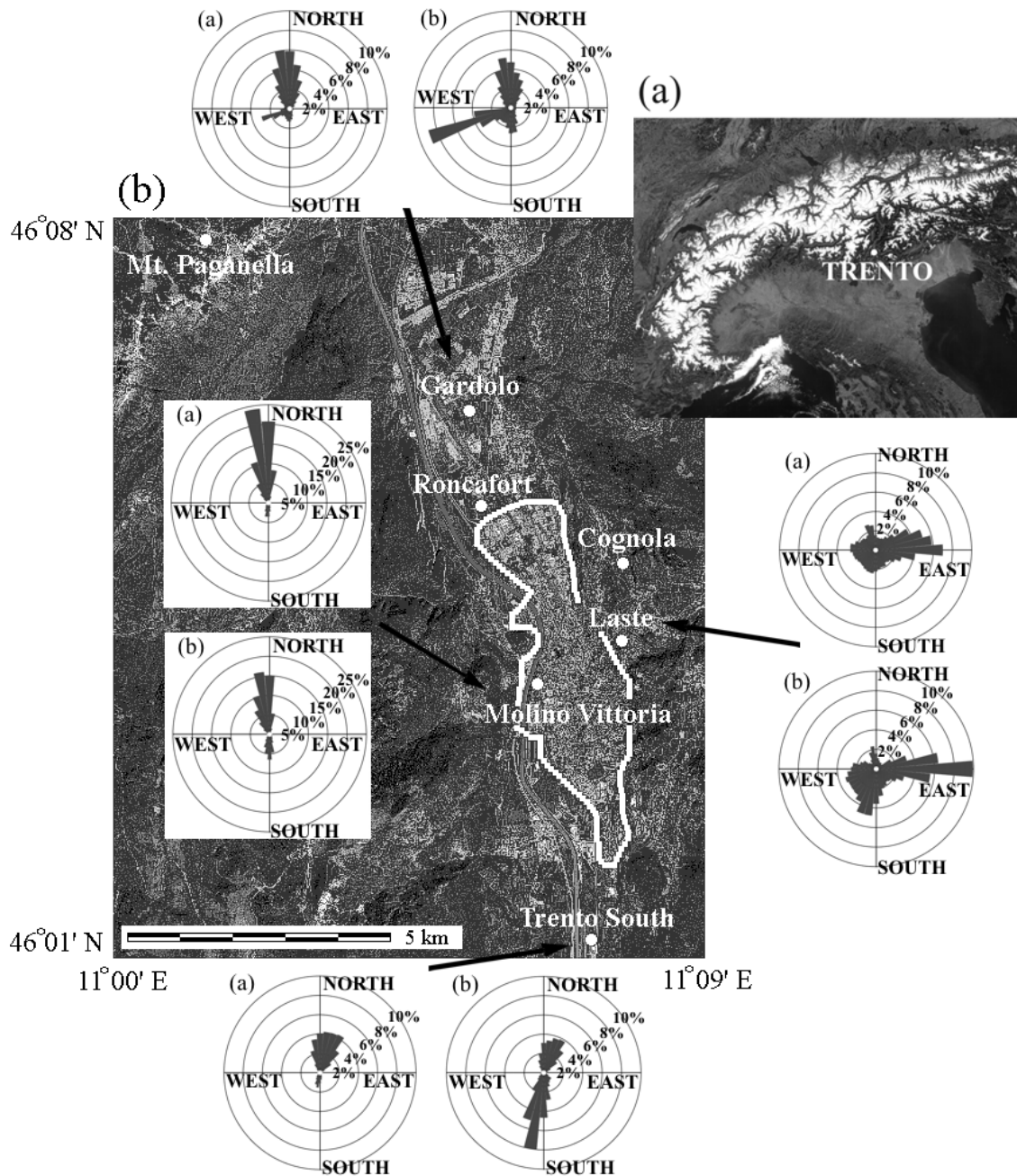
Figure 3.1: Location of the city of Trento (a) in northern Italy and (b) in the Adige Valley. White bullets indicate the weather stations analyzed in this study. The white boundary encloses the area of the city of Trento more uniformly urbanized, excluding the suburbs. The wind roses refer to the stations indicated by the arrows and cover respectively: (a) the cold semester (September-February), (b) the warm semester (March-August).

3. Urban heat island effect in an Alpine valley: the case of Trento

The city of Trento (46°4'N, 11°7'E) lies at 200 m MSL in the Adige Valley, which is the southern stretch of the main geographic corridor running approximately along a south-north direction in the Italian side of the Alps (Fig. 3.1), and connecting the Po Plain to the Brenner Pass. A population of about 56 000 citizens lives in the inner city of Trento, whereas a total of about 114 000 inhabitants is reached when all the surrounding suburbs are included. In fact in the last twenty years the city has grown, especially in the northern area, and incorporated some smaller urban conglomerations previously existing as suburbs. As a consequence nowadays the surroundings of the old city look like a single, continuously built-up area, spreading out by about 10 km along the valley and all across the valley width, which is about 2 km everywhere, except at the center of the urban area, where it gets reduced to about 1 km by the Doss Trento, a hill about 100 m high above the valley floor (Fig. 3.2). The latter is practically flat, with the only exception of the riverbeds of the River Adige and its tributaries, namely the Fersina creek, which flows inside the urban area, and the Avisio creek, flowing into the Adige 10 km north of the city center. The valley is flanked on the western side by Mount Bondone (2098 m MSL) and on the eastern side by Mount Marzola (1738 m MSL). Other two prominent massifs surrounding the city are Mount Paganella (2125 m MSL), north-west of the city, and Mount Vigolana (2150 m MSL), south-east of the urban area. The valley sidewall on the west is rather steep, whereas on the east it rises gently; for this reason the hills east of Trento are more intensely urbanized. Several narrow tributary valleys or gullies join the Adige Valley in the area surrounding Trento: Rio Vela Gully and Rio Gola Valley west of the city, and Fersina Gully east of Trento. A more important tributary valley (Lakes Valley) ends in the Adige Valley north-west of Trento through an elevated saddle about 400 m above the Adige Valley floor (Fig. 3.2).

The climate of Trento displays an annual temperature range of about 20°C, with cold winters and relatively hot summers. Average seasonal temperature values for the weather stations analyzed in this Chapter (see Section 3.2) are shown in Tab. 3.2. In wintertime, especially during clear nights, strong thermal inversions frequently occur over the Adige Valley floor, which can persist for the whole day or even more. This is a consequence of the weaker solar radiation input, determined not only by shorter day length and solar declination, but also by the reduced sky view factor (cf. Grigiante et al. 2011) and the low level cooling at the valley floor favored by nocturnal drainage winds. The average annual precipitation total is 940 mm (Sadler and Bellin 2004), and most of it occurs from April to November, while winters are usually quite dry. Summertime precipitations are mostly produced by short and strong convective rainstorms. The area surrounding Trento is known in the literature for its specific local circulations associated with the development of peculiar local valley winds, mainly occurring in spring and summer (Schaller 1936; Wagner 1938; de Franceschi et al. 2002). Local circulation systems in the valleys around Trento will be analyzed in Chapter 5. In the cold season winds are usually weak, excluding some cases of strong synoptic winds, usually blowing from the north and mainly related to Föhn episodes.
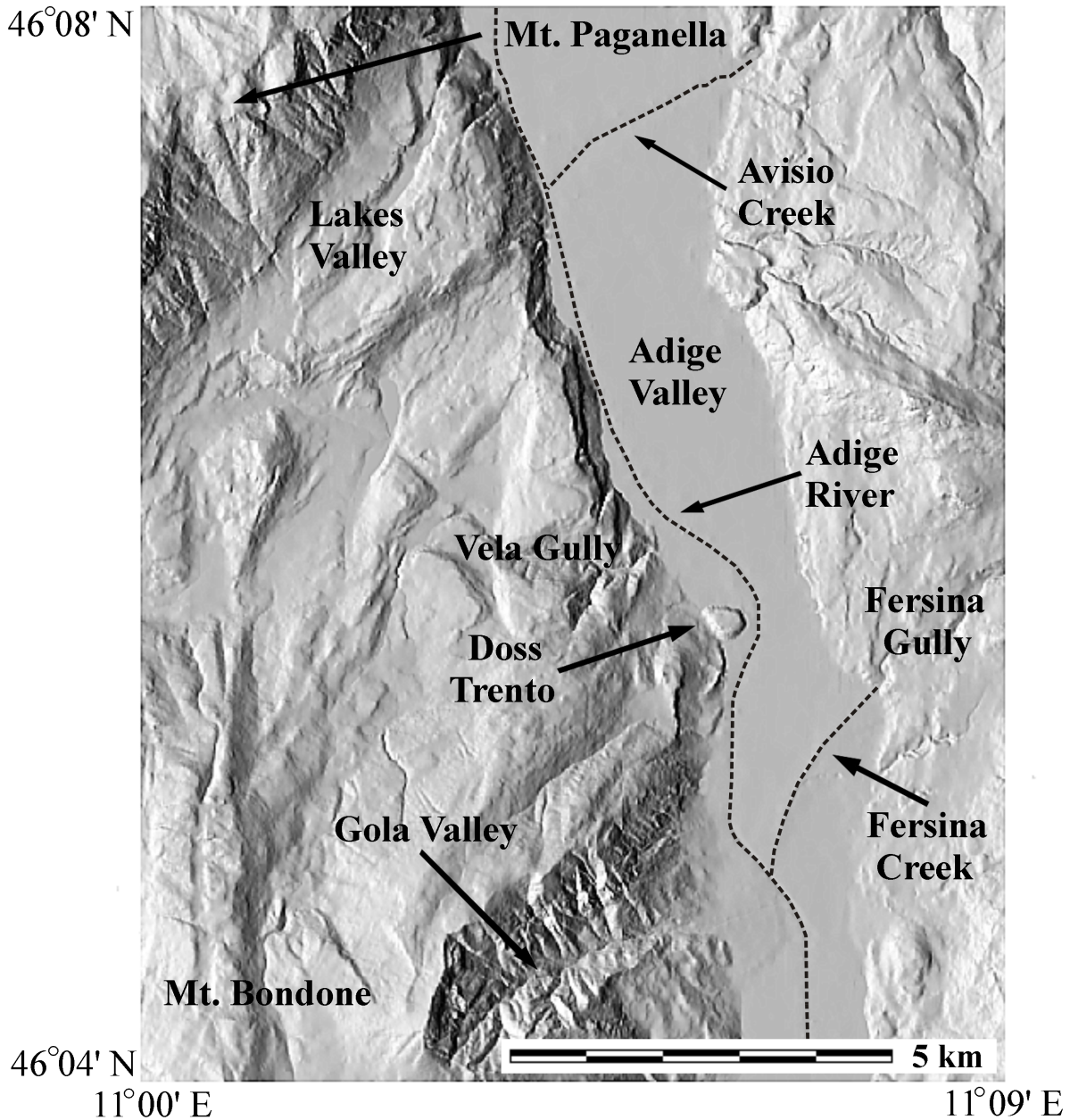
Figure 3.2: Digital Terrain Model (DTM) of the area shown in Fig. 3.1b, representing Trento and surroundings, including the Adige Valley and its sidewalls.

To better characterize the complex interaction of wind systems in the area surrounding Trento, wind roses were obtained from wind direction data, covering the time period 2003-08, taken at four meteorological stations. The latter are located respectively (Fig. 3.1) north of the city (Gardolo), inside the urban area (Molino Vittoria), south of Trento (Trento Sud) and on the sidewall east of the city (Laste) (see also Section 3.2 for more details). The emerging

dominant features are winds mainly blowing from north at all stations on the valley floor during the cold semester (i.e. autumn and winter), while in the warm semester (i.e. spring and summer) southerly winds (up-valley) become stronger. The wind rose at Gardolo clearly shows a prevailing direction from west-southwest in the warm semester, due to the interaction with the circulation blowing from the Lakes Valley (see Chapter 5 for more details). The presence of down-slope winds is evident in the wind rose at Laste, both in cold and in warm semesters, whereas the up-slope direction is less frequently met.

3.2 Measurement sites

In order to investigate the thermal structure and the UHI intensity of the city, a dataset of surface air temperature measurements was composed from data collected at six automated weather stations, routinely operated at different sites within or around the urban area (Fig. 3.1). The first station, hereinafter identified as "Molino Vittoria", is close to the city center and is assumed as representative of the inner urban area. It was installed in October 2002, on the roof of a tower in the building named Molino Vittoria (33 m AGL), and has continuously been operated thereafter by the Atmospheric Physics Group of the University of Trento (de Franceschi and Zardi 2007). The data recorded at this location, and used for the present analysis, are 10-min average values of air temperature, wind speed and global radiation. The station is close to the western boundary of the city center, whose core is built over the old-Roman-traced city, displaying a typical regular grid of narrow streets, crossing at right angles, either north-south or east-west oriented. The average building height in the city center is about 15-20 m and the aspect ratio of the main streets is about 1, while many narrower alleys display higher values. In this area the vegetation is very poor or totally absent, the building walls are covered with plaster, while the ground surface is covered with asphalt. This compact urban area surrounds the weather station in all the sectors from north-east to south-east, whereas in the direction west of the station the city is less compact: there is a parking lot covered by asphalt, and farther west, about 200 m from the station, the Adige River, close to the steep slope bounding the valley on the western side. Since the local circulation pattern displays a rather poor occurrence of westerly winds (Fig. 3.1), it can be inferred that the measurement station is mainly influenced by rather homogeneous surfaces, representative of the urban area. To substantiate this assumption with an objective and quantitative characterization of the urban morphology around the station, the building planar area fractions λ_p were calculated for the area. To this purpose the Digital Terrain Model and the Digital Elevation Model, calculated on the basis of airborne lidar scans, were obtained from the Municipality of Trento. The above models display an accuracy of 1 m in the horizontal and 0.15 m in the vertical. The city center, east of the weather station, displays rather high values of λ_p, ranging from 0.5 to 0.8. Lower values, of order 0.2, were found west of the tower over the parking lot and the Adige River. Furthermore, an estimate of the source

Table 3.1: Summary of the weather stations along with coordinates, altitude and measurements used for the analyses presented in this Chapter. T = temperature; R = global radiation; WV = wind velocity; WD = wind direction; CC = cloud cover.

STATION NAME	COORDINATES (lat,lon)	ALTITUDE (m MSL)	MEASUREMENTS				
			T	R	WV	WD	CC
MOLINO VITTORIA	46°03' N 11°06' E	224	X	X	X	X	
GARDOLO	46°06' N 11°06' E	197	X			X	
RONCAFORT	46°05' N 11°06' E	194	X			X	
TRENTO SUD	46°01' N 11°07' E	185	X			X	
COGNOLA	46°04' N 11°08' E	344	X				
LASTE	46°04' N 11°08' E	312	X		X	X	
PAGANELLA	46°09' N 11°02' E	2125					X

area of the urban weather station was also performed, based on the parameterization proposed by Kljun et al. (2004), by means of the online tool available at http://footprint.kljun.net/. The source area was found to fall inside the quite homogeneous urban area described above, for a reasonable range of the parameters used by the parameterization.

The remaining five weather stations are located in suburban or rural areas around the city, and temperature measurements are taken at 2 m AGL there. These stations will be identified from the name of their sites. Three extra-urban weather stations belong to an agrometeorological network, operated by the Institute for Agriculture of San Michele all'Adige, affiliated to the Edmund Mach Foundation. Two of them are located on the valley floor, respectively north and south of Trento. The station identified as Gardolo is located in the northern countryside, and is surrounded by croplands, while the other one - Trento Sud - is near the small city airport, in a green area few kilometers south of the city. The third station, identified as Cognola, is placed on the valley sidewall east of the city, and is surrounded by croplands and a deciduous broad-leaved forest. All of these stations provide hourly average values of air temperature. The other two extra-urban stations are operated by the Meteorological Office of the Autonomous Province of Trento, and are located respectively in an area dedicated to agriculture, north of the city (Roncafort), and in a suburban area on the valley slope east of Trento (Laste). This part of the sidewall is moderately urbanized, but open spaces and vegetation are also present, thus resulting in λ_p values of order 0.2-0.3 in the area surrounding this station. Both of these stations provide 15-min average values of air temperature.

To sum up, three of the five extra-urban weather stations (Gardolo, Trento Sud and Roncafort) are located, as is the urban site, on the valley floor, at about 200 m MSL, while the remaining two, Laste and Cognola, are placed on the eastern sidewall, respectively at 312 and 344 m MSL (Tab. 3.1). As a consequence, since UHI intensity is evaluated analyzing the temperature differences between the urban site and each of these stations, the results may reflect both effects due to topographic features and to urbanization. This question was already faced

by Lowry (1977), who pointed out that the climate of a particular location is given by the sum of three components: the "background" climate, the effects of the total landscape and of local urbanization. Therefore, when evaluating UHI intensity by analyzing temperature differences between "urban" and "rural" weather stations, it is implicitly assumed that the "background" climate and the landscape effects are identical at the two locations. This assumption is not easily met in complex terrain, where the overall landscape effects may vary significantly over space scales as short as few kilometers, for example due to the varying topography or to particular microclimatic features, closely related to complex terrain characteristics (e.g. slope winds). In the present case, it is reasonable to assume, at least as a first approximation, that the weather stations located on the valley floor are affected by similar landscape effects as the urban station. Therefore temperature differences between the urban weather station and these locations can be interpreted as urbanization effects. On the other hand Cognola and Laste, due to their different altitude in comparison with the urban site, are influenced by landscape effects which are slightly different from Molino Vittoria. For this reason it may be argued that the location of these two weather stations may not be an optimal one for the evaluation of UHI intensity. On the other hand their measurements specifically reflect phenomena really occurring on this urbanized sidewall, and a comparison between the urban site and the suburban weather station of Laste will provide information about the interaction between topography and urbanization (Goldreich 1984; Goldreich 2009). Moreover the comparison between Laste and Cognola temperature datasets can be useful to evaluate thermal differences between a suburban and a rural area being roughly at the same altitude.

In order to compensate for topographic effects, some authors used potential temperature (Oke and East 1971), or vertical profiles with constant lapse rates (Nkemdirim 1980; Junk et al. 2003). However such an approach does not take into account that the actual lapse rate is not constant and may change, not only on a seasonal basis, but also from day to day (Goldreich 1984). In the present case topographic effects affecting temperature differences between the valley floor and the weather stations on the sidewalls can be evaluated, at least as a first approximation, by comparing the average seasonal temperatures (Tab. 3.2) at the three weather stations on the valley floor and at Cognola. All of them are in the countryside, so they may be weakly affected by urbanization. Topographic differences turn out to be on average of order 0.6-0.7°C, being stronger in spring and summer, and lower in fall and winter. These results support the relevance of frequent ground-based thermal inversions during the cold season in reducing topographic effects. Following these considerations, in the present study UHI intensity has been evaluated using the actual air temperature, but the topographic effects estimated above have been taken into account in the interpretation of the results of the extra-urban weather stations placed on the valley sidewalls.

The dependence of UHI intensity on wind speed and cloud amount has also been analyzed. To this purpose wind speed data from routine measurements at Molino Vittoria (10 minute

Table 3.2: Average seasonal temperatures (°C) measured at the six weather stations taken into account for the evaluation of the UHI.

STATION NAME	WINTER	SPRING	SUMMER	FALL
Molino Vittoria	2.61	12.69	22.99	12.84
Gardolo	1.62	12.14	22.22	12.01
Roncafort	1.22	11.89	22.03	11.65
Trento Sud	1.67	12.19	22.63	12.22
Cognola	1.24	11.13	21.39	11.46
Laste	2.37	11.85	22.08	12.32

averages) were used, while hourly cloud cover observations (in oktas) were taken from Mount Paganella weather station. The latter is operated by the Meteorological Service of the Italian Air Force, ten kilometers north-west of Trento, at 2125 m MSL. Despite the high altitude, these cloud-cover observations are fairly well representative of the weather conditions over the city in most of the cases.

The station at Molino Vittoria is the most recently installed (October 2002), and this date sets the starting time for the whole dataset, which covers the period October 2002 - December 2008. Finally we note that, for the sake of consistency with the rest of the dataset, data from observations at Molino Vittoria, Roncafort and Laste were downsampled to hourly averages.

3.3 Data analysis

3.3.1 Average values of the UHI

As a first step, an average UHI intensity was evaluated by comparing all the hourly mean temperature values from Molino Vittoria (city center) with the corresponding values of the five extra-urban weather stations. Results from these comparisons are shown in Tab. 3.3. On the valley floor the average urban-rural temperature differences range between 0.6°C and 1.1°C. Such values are quite small, compared to typical UHI intensities found in larger cities. However these average temperature differences include every weather condition and every hour of the day, whereas, as shown below, UHI intensity is strongly dependent on these factors, as can be argued from the high values of the standard deviations (Tab. 3.3). As a consequence the above values should be considered only as a preliminary and partial representation of the UHI effect. The appreciable differences found between the average UHI intensities at the three rural weather stations on the valley floor are not easily explained. They can be caused by slightly different landscape effects, or by a partial influence of urbanization on the areas surrounding these weather stations. As to the two weather stations on the valley slopes, average temperature contrasts with the urban site are 0.7°C and 1.5°C at Laste and Cognola respectively. It is interesting to notice that the average temperature difference between the two stations on slopes,

Table 3.3: UHI average intensity (˚C; calculated as the difference between Molino Vittoria and the five extra-urban stations) during the full day and separated into daytime and nighttime. Here, N indicates the number of temperature data pairs, T_u and T_r, used to evaluate the mean difference, $\Delta T_{u-r} = T_u - T_r$, σ indicates the standard deviation.

Station name	All day			Daytime			Nighttime		
	N	ΔT_{u-r}	σ	N	ΔT_{u-r}	σ	N	ΔT_{u-r}	σ
Gardolo	53 359	0.76	1.61	29 415	0.03	1.30	23 944	1.67	1.49
Roncafort	42 704	1.07	1.50	23 391	0.49	1.24	19 313	1.79	1.47
Trento Sud	53 304	0.58	1.35	29 427	- 0.06	1.03	23 877	1.37	1.27
Cognola	52 849	1.48	1.56	29 153	0.74	1.47	23 696	2.39	1.13
Laste	50 288	0.65	1.07	27 827	0.54	1.20	22 461	0.79	0.88

one suburban and one rural, is comparable to those found between the urban and the rural weather stations located on the valley floor. Assuming that these two stations are affected by similar topographic effects, this fact suggests a considerable influence of urbanization at Laste. Indeed the average temperature difference between Molino Vittoria and Laste is of the same order of magnitude as the topographic effects estimated in the Section 3.2.

3.3.2 Diurnal-cycle variations of the UHI

The dataset was split into a daytime and a nighttime subset (simply identified on the basis of incoming solar radiation detected by the radiometer at Molino Vittoria), in order to evaluate separately the average intensity of the UHI during the two parts of the day. Based on the analysis of these subsets, three main aspects can be outlined (Tab. 3.3).

First, UHI intensity appears to be stronger during the night at the rural weather stations, following the well-established concept that urban-rural temperature differences are higher at nighttime (Oke 1987). As to the three weather stations on the valley floor, nocturnal urban-rural temperature contrasts seem to be slightly stronger in the countryside north of the city than south of it. However the temperature differences with the urban site are quite similar at these three weather stations, on the order of 1.5˚C. The highest temperature difference with the urban site, among the five extra-urban weather stations, is found at Cognola (2.4˚C). However part of this difference has to be attributed to topographic effects.

Second, it seems that during daytime on average urbanization effects do not significantly affect urban-rural temperature differences. Considering the three weather stations located on the valley floor, average temperature differences with the urban site during daytime are negligible at Gardolo and Trento Sud and low at Roncafort. On the other hand the value obtained at Cognola (0.7˚C) can be almost completely attributed to the altitude difference.

Third, concentrating on Laste, the temperature contrasts with Molino Vittoria are very similar during daytime and nighttime. Indeed the temperature diurnal cycle at this station
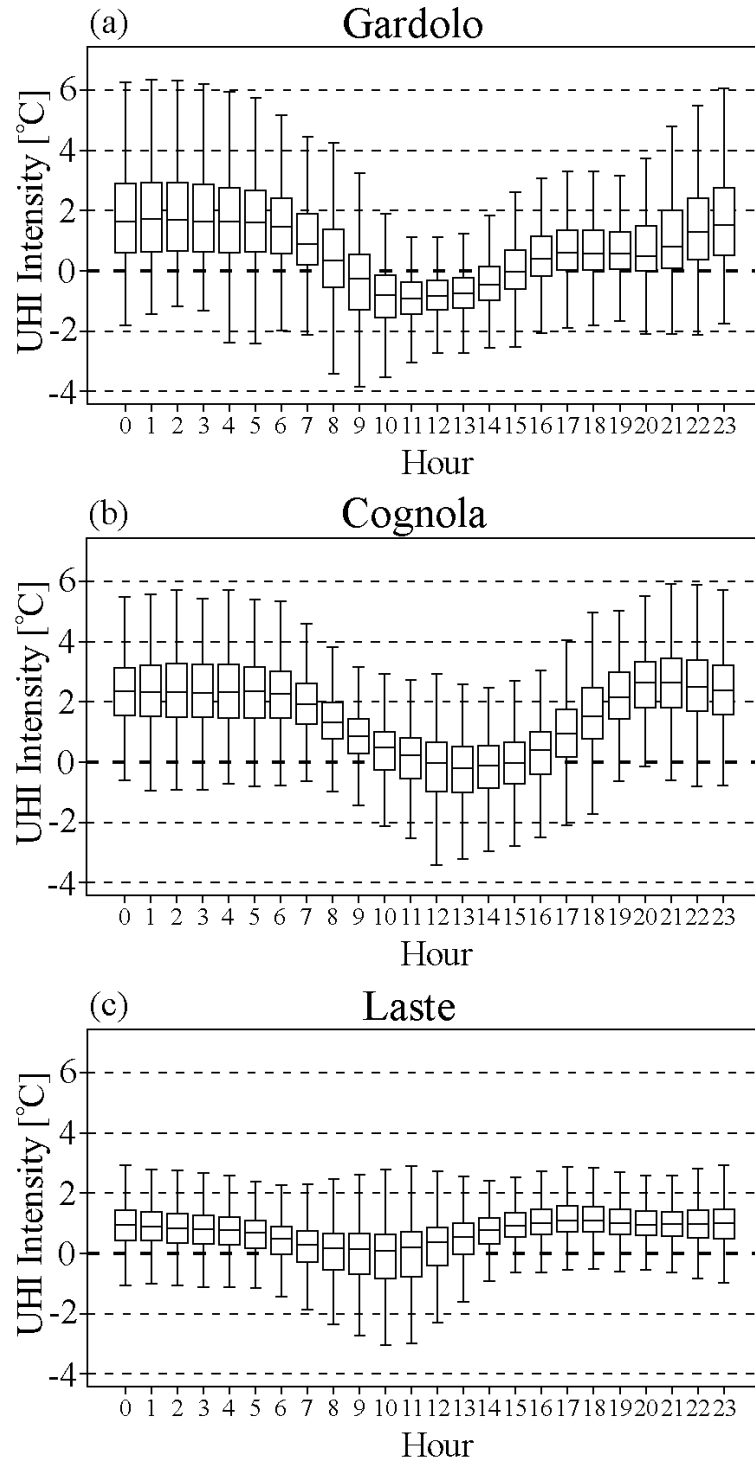
Figure 3.3: Box-plots of hourly temperature differences between Molino Vittoria and (a) Gardolo, (b) Cognola, (c) Laste. The bottom and the top of the boxes represent respectively the first and the third quartile (Q_1 and Q_3), while the line in the middle is the median (Q_2). The ends of the whiskers represent respectively the lowest datum still within $Q_1 - 1.5 \cdot (Q_3 - Q_1)$ and the highest datum still within $Q_3 + 1.5 \cdot (Q_3 - Q_1)$. This description applies to all the box-plots shown in this paper.

is similar to that registered at the urban site, confirming the strong influence of urbanization on the surrounding area. The same conclusion can be drawn by observing that during both daytime and nighttime the average temperature differences with Cognola are similar to urban-rural contrasts found on the valley floor.

The diurnal cycle of the UHI can be better understood analyzing its intensity on an hourly basis. In Fig. 3.3a a box-plot of the hourly intensity of the UHI is shown, with respect to the rural station of Gardolo, whose behavior was found to be similar to the other rural stations on the valley floor (not shown). It can be seen, as highlighted above, that UHI intensity is stronger at night, whereas urban-rural temperature differences progressively decrease in the morning. During the central hours of the day, when solar radiation is stronger, the temperature at the urban site becomes on average even lower than at the rural weather station, with the development of an urban cool island. The latter is a phenomenon observed in several cities of different sizes and with different climates. For instance Lee and Baik (2010) found an urban cool island in Seoul in 77% of the non-precipitating days in spring, while Unwin (1980) reported an average cool island of 0.49°C in Birmingham. Furthermore Steinecke (1999) found a strong urban cool island in Rejkjavíc in summer, due to the low solar altitude and the consequent overshadowing inside the urban area. In the present case the urban cool island develops mainly between 1000 LST and 1300 LST, when intensities higher than 1.5°C can be reached.

As found by Morris and Simmonds (2000), UHI intensity is roughly constant during the night, from 2300 LST to 0600 LST, and in the case of Trento the average value turns out to be, as seen above, of order 1.5°C. Nevertheless during these hours remarkable differences between urban and rural areas are reached: indeed the value of the third quartile is about 3°C, which means that in one night out of four the temperature in the city is almost 3°C higher than in the countryside. Thus, in contrast with the conclusions of Kuttler et al. (1996) for the valley city of Stolberg, in Trento the UHI intensity is rather constant during the night. This finding is supported by the fact that usually at Molino Vittoria a rather strong and persistent down-valley wind blows for the whole night (see Section 5.4.1), and therefore there is no evidence that the penetration of cold air drainage flow in the inner city is hindered in the early evening by the obstruction of the built-up area. However this finding may not be fully representative of processes occurring at ground level within the built up area, as far as the urban weather station is placed well above the urban canopy layer as discussed in Section 3.2.

At Cognola (Fig. 3.3b) the behavior of the diurnal cycle of the UHI is similar to that found on the valley floor, but in this case the maximum differences with the urban site are reached in the evening, probably because the drainage flow reaches the sidewalls earlier than the valley floor.

From the box-plot for Laste weather station (Fig. 3.3c) it can be seen that, as expected, the temperature differences with the urban site are less variable throughout the day in comparison with the rural stations. However the overall behavior is similar, with minimum differences in

the morning and maximum UHI intensity during the late afternoon and at night.

The height of the boxes and the distance of the whiskers in the box-plots in Fig. 3.3 provide an estimate of the scatter in the hourly data. At Gardolo the maximum spread around the median value is observed at night, while at Laste during daytime. At Cognola the dispersion in the hourly data is roughly constant throughout the day. Thus on the valley floor the temperature differences with the urban site are expected to be more affected at night than during daytime by factors such as weather conditions or the season. The opposite behavior is expected at Laste.

3.3.3 Diurnal maximum UHI intensity

The frequency distribution of the diurnal maxima of UHI intensity, computed on an hourly basis, is shown in Fig. 3.4. Considering the extra-urban weather stations lying on the valley floor, the maximum differences with the urban site range between 2°C and 4°C in more than 50% of the days. Higher values more often occur at Gardolo and Roncafort, in the northern countryside, than south of the city at Trento Sud. At Laste the maximum diurnal differences with the urban site fall most frequently between 1°C and 2°C. Values higher than 3°C are rarely reached. At Cognola the most frequent values of the diurnal maximum UHI intensity range between 3°C and 5°C.

Figure 3.5 shows a histogram of the frequency distribution of the local time of occurrence of the diurnal maxima of UHI intensity, confirming the results obtained from the analysis of the diurnal cycle of the UHI. At the rural locations on the valley floor the diurnal maximum UHI intensity is observed most often in the middle of the night. The same analysis for the sidewall weather stations shows that the maximum occurrence is reached in the afternoon (between 1400 LST and 1800 LST) at Laste, while some hours later (between 1800 LST and 2200 LST) at Cognola.

3.3.4 Seasonal variations of the UHI

In order to evaluate the seasonal variations of the UHI intensity, temperature differences between the urban site and the extra-urban weather stations were compared on a monthly basis. Following the different features characterizing the daytime and nighttime phases of the UHI, as outlined in Section 3.3.2, it seems convenient to analyze separately these two subsets.

Figure 3.6 shows the yearly cycles of the daytime UHI intensity at Gardolo (which is also representative of the other two extra-urban stations on the valley floor), and at Cognola (whose behavior is analogous to that found at the other sidewall station). At Gardolo, urban-rural temperature differences are quite constant throughout the year. On the other hand, taking into account Cognola, a completely different yearly cycle can be seen: maximum UHI intensities are reached during summer months, while the lowest differences are recorded in wintertime. This can be explained by observing, as discussed in Section 3.2, that in the Adige Valley the
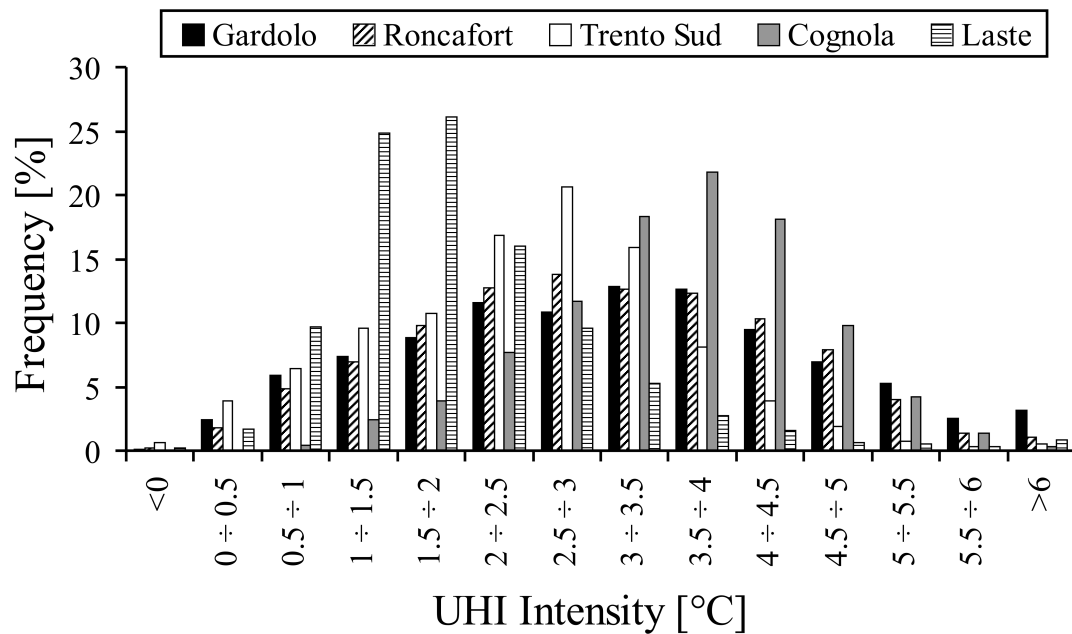
Figure 3.4: Frequency distribution of the diurnal maximum intensity of the UHI on an hourly basis, referred to the five extra-urban weather stations as indicated.
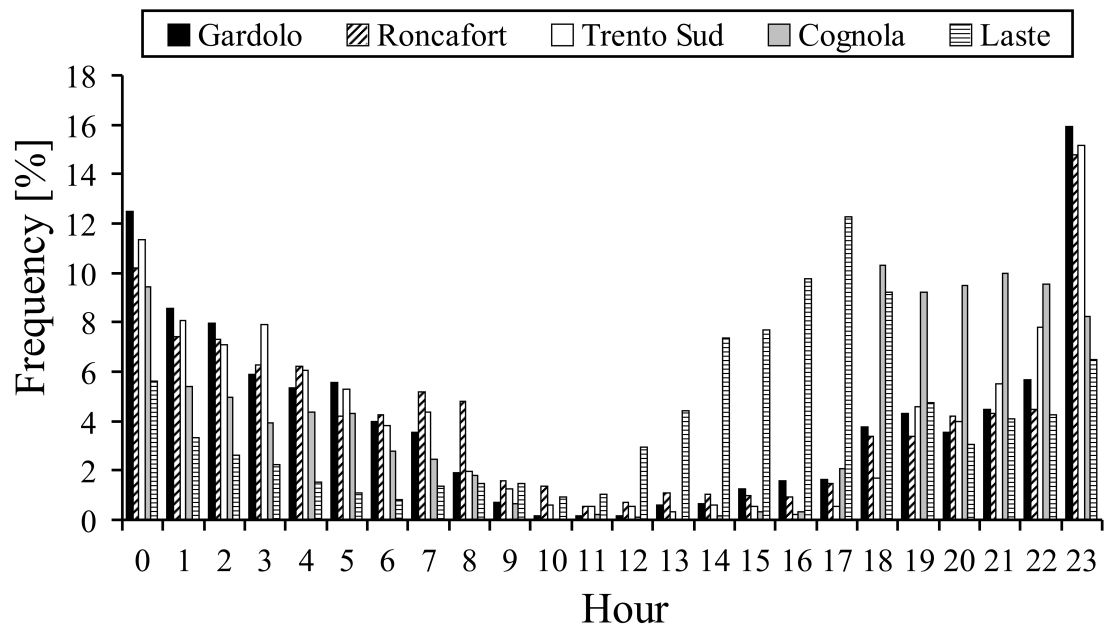
Figure 3.5: Frequency distribution of local time of occurrence of the diurnal maximum intensity of the UHI, referred to the five extra-urban weather stations as indicated.
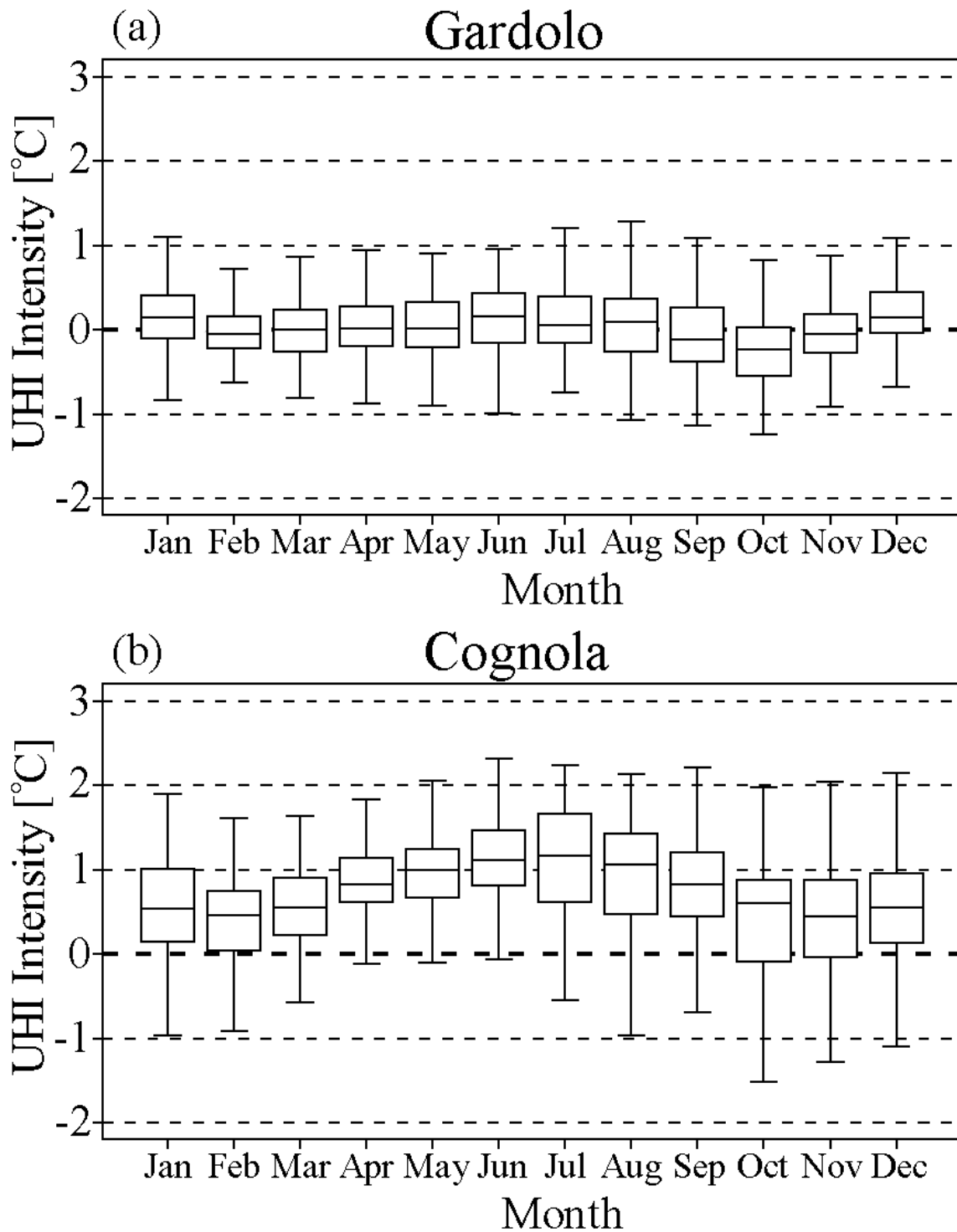
Figure 3.6: Box-plots of daytime monthly temperature differences between Molino Vittoria and (a) Gardolo, (b) Cognola.
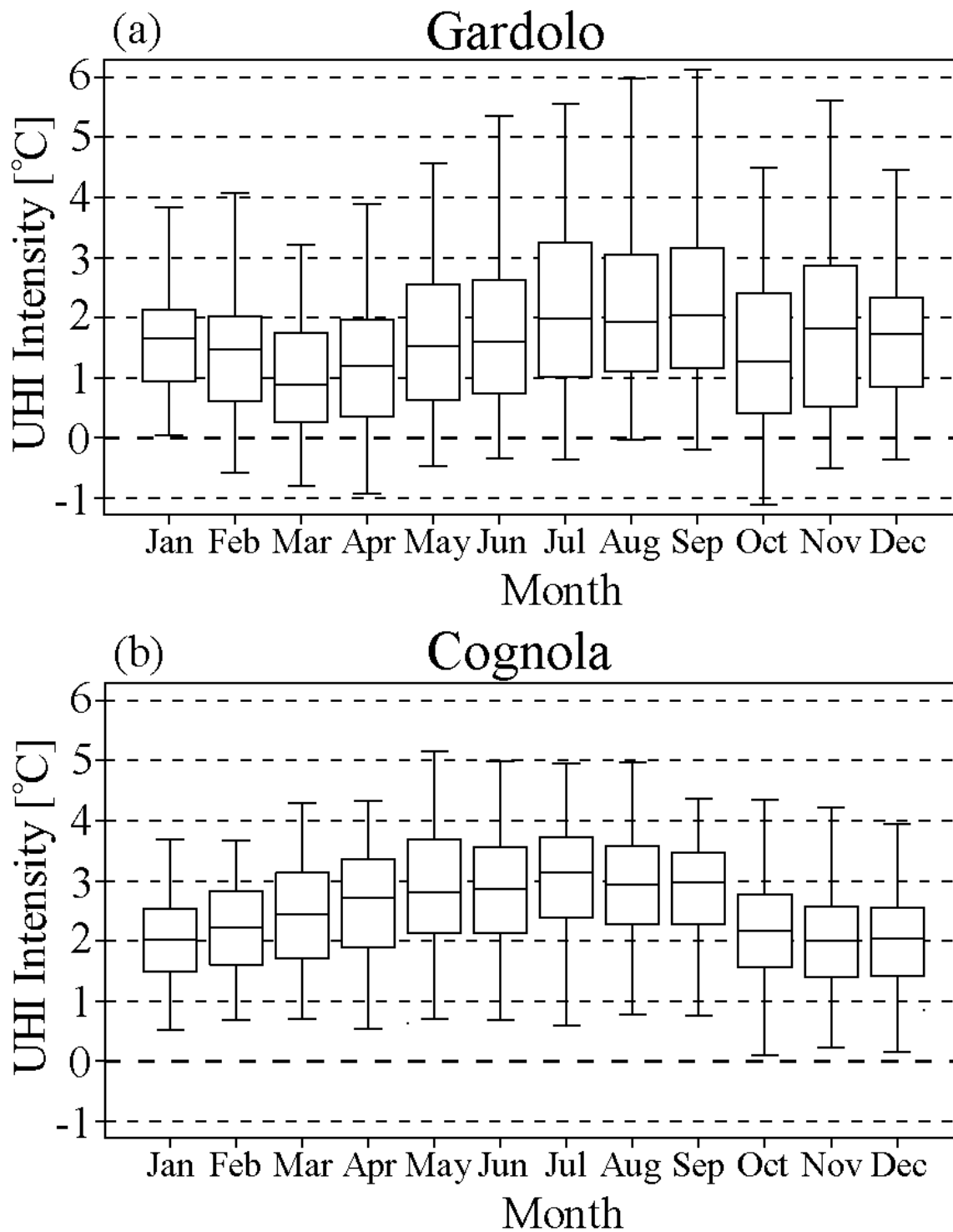
Figure 3.7: As in Fig. 3.6, but for nighttime.

mean lapse rate is lower during the cold season than in the summer months, partly due to the frequent thermal inversions in winter, hence the average temperature differences between the urban station, located on the valley floor, and those lying on the valley sidewalls are smaller.

The yearly cycle of the nocturnal UHI intensity (Fig. 3.7) shows that maximum intensities are reached at Gardolo during winter and summer months, while there are smaller differences in spring and in October. These results are consistent with the findings of Jauregui (1987) and Kim and Baik (2002): UHI intensity is stronger during dry periods, when conditions favorable to develop strongly different cooling rates between rural and urban areas are more likely to occur. In fact, as recalled above, spring and autumn are the rainiest seasons in Trento, while during wintertime frequent and persistent anticyclonic situations inhibit precipitations. The nighttime and daytime yearly cycles at Cognola are very similar, with maximum UHI intensities in summer, and minimum in winter.

3.3.5   Evaluation of cloud cover effects

As a further step in the evaluation of UHI effects in Trento, the possible dependence on cloud cover has been investigated, grouping the data into five classes, based on cloud cover observations at Mount Paganella weather station. This analysis was carried out on an hourly basis, so as to characterize the influence of cloud cover on the diurnal cycle of the UHI.

Figure 3.8 shows the box-plots for Gardolo, which are again representative also of the other rural stations on the valley floor. Urban-rural temperature differences decrease progressively as cloud cover increases, both during daytime and nighttime. Under clear sky conditions urban-rural temperature differences are positive and quite strong at night, whereas in the middle of the day the temperature at Molino Vittoria is lower than at Gardolo. On the other hand, when the sky is completely cloudy, temperatures at the urban site and at Gardolo are similar for the whole day. Also the scatter in the hourly data tends to decrease as cloud cover increases, especially at night. In cloudy conditions, at any hour, half of the data ranges within 0.5°C.

The behavior at Cognola is similar, with only minor differences (not shown). During night-time the UHI intensity seems less affected by cloud cover than at the rural weather stations on the valley floor, whereas during the central hours of the day the influence of cloud cover seems stronger. To explain these one should remember that temperature differences between Molino Vittoria and Cognola result from the combination of two factors, namely urbanization and topographic effects. It was found (not shown here) that temperature differences between the rural weather stations on the valley floor and Cognola become slightly stronger as cloud cover increases during both daytime and nighttime, as thermal inversions are more frequent in clear sky conditions. Thus it can be argued that temperature differences between Molino Vittoria and Cognola due to topographic effects also become stronger as cloud cover increases. On the other hand the analysis carried out at the rural weather stations on the valley floor shows that
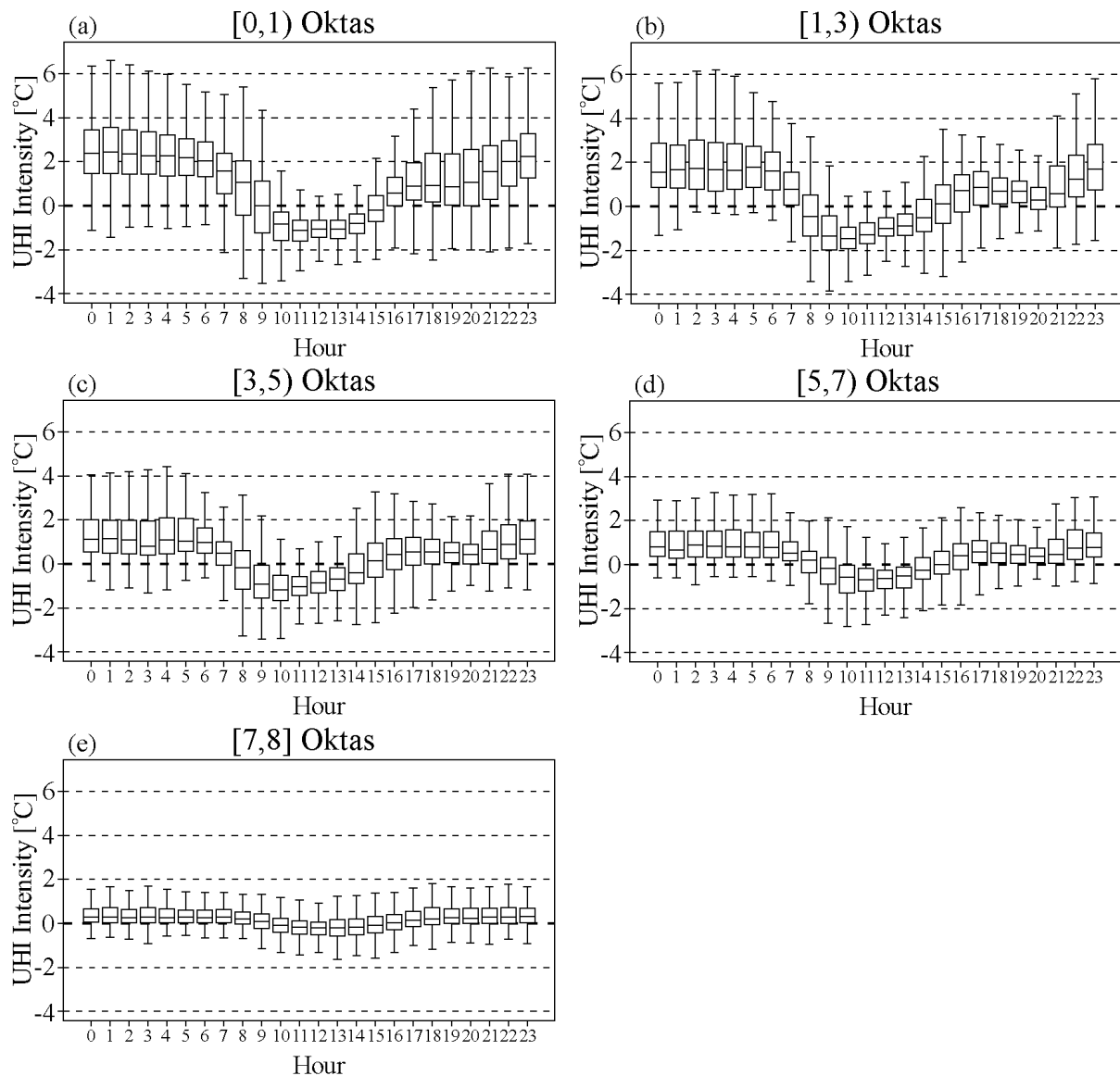
Figure 3.8: Box-plots of hourly temperature differences between Molino Vittoria and Gardolo classified by cloud cover classes in oktas observed at Mount Paganella weather station.

the temperature differences between urban and rural areas due to urbanization effects decrease as cloud cover increases. Therefore during nighttime the two contrasting effects result in a lower influence of cloud clover on UHI intensity at Cognola than on the valley floor. On the other hand during the central hours of the day the temperature differences due to both topographic and urbanization effects have the same behavior as cloud cover increases, and therefore the net result is an enhanced influence of cloud cover on the temperature contrasts between the urban site and Cognola.
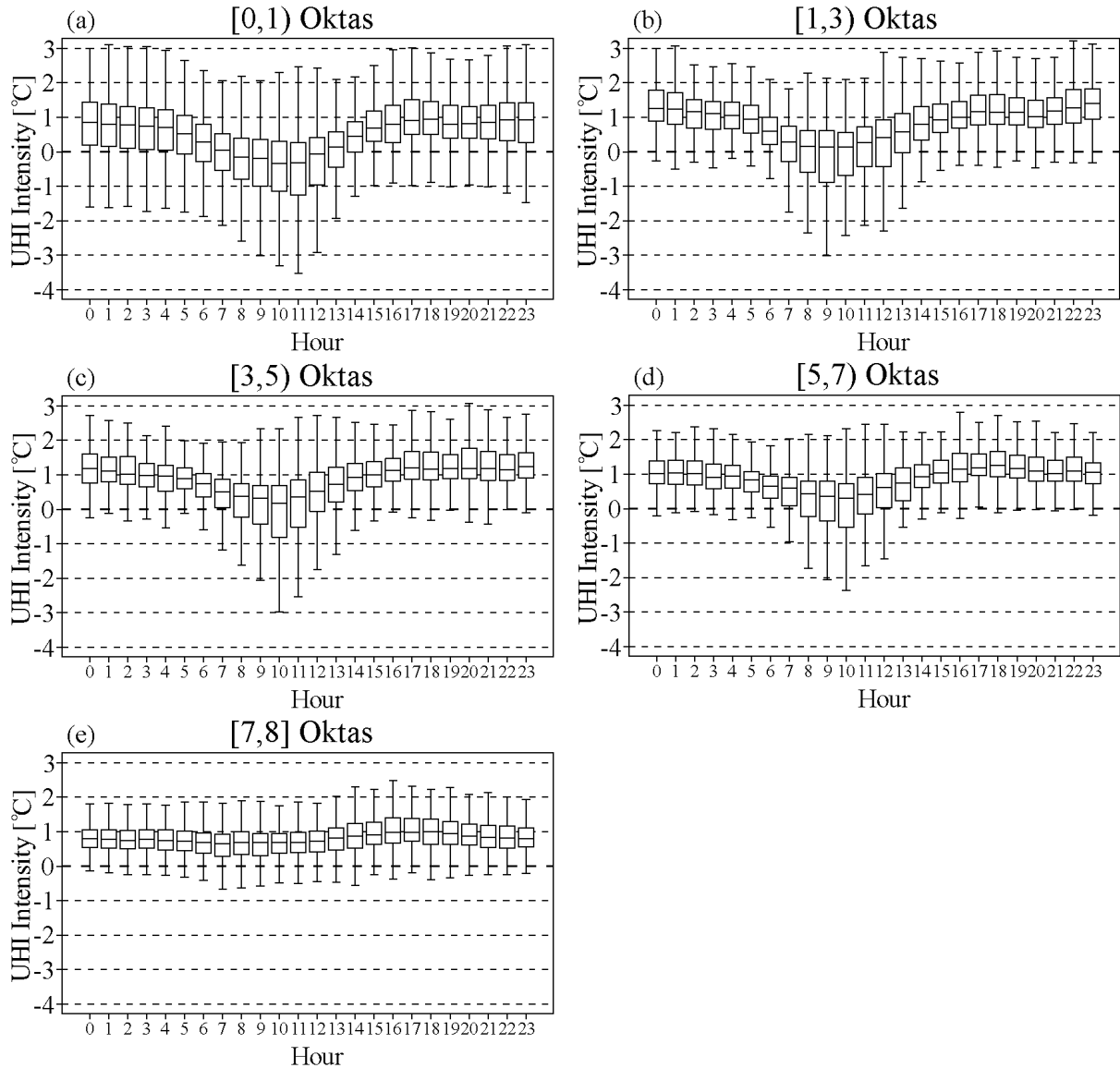
Figure 3.9: As in Fig. 3.8, but for between Molino Vittoria and Laste.

Also at Laste (Fig. 3.9) the temperature contrasts with Molino Vittoria tend to become constant throughout the day as cloud cover increases, but in this case only the temperature differences in the middle of the day seem to be affected by cloud cover, since during nighttime UHI intensity remains roughly similar in all cloud cover conditions. Thus the behavior found at Laste at night is different from that found at Cognola. It can be supposed that at Cognola, in a rural area, cloud cover affects more the local nocturnal radiative cooling than the lapse rate, whereas at Laste, in a suburban location, where nocturnal cooling is lower, the two contrasting effects are balanced, and therefore cloud cover does not significantly affect temperature
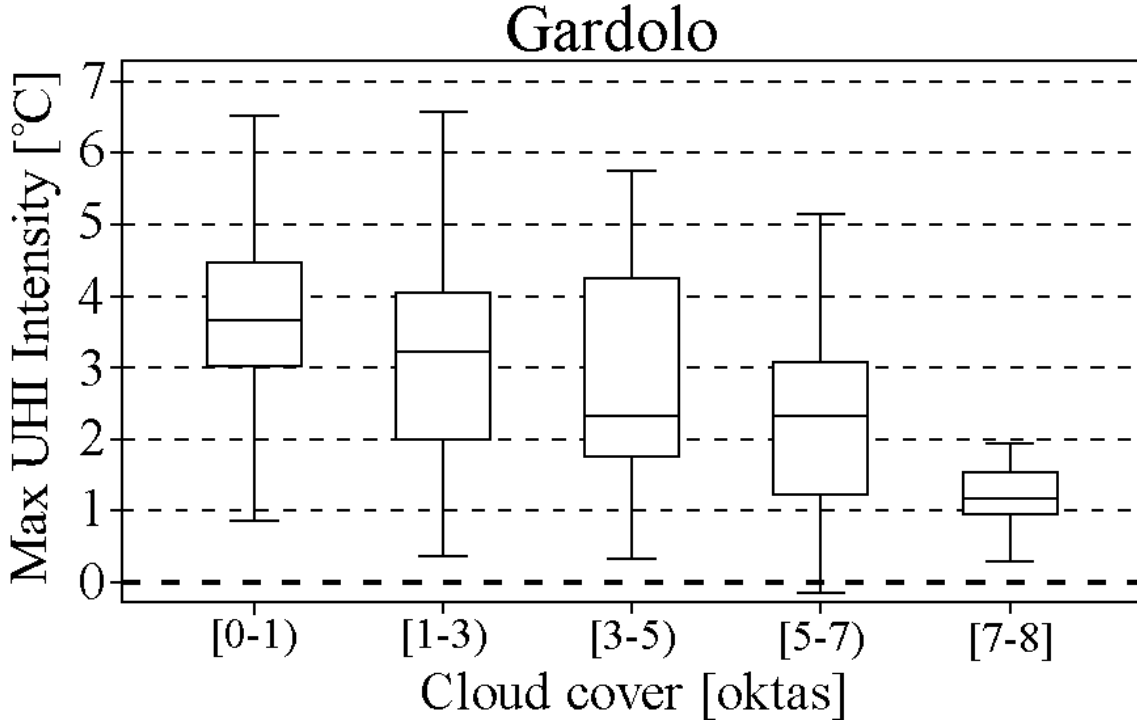
Figure 3.10: Box-plot of the maximum diurnal temperature differences between Molino Vittoria and Gardolo classified by cloud cover classes in oktas observed at Mount Paganella weather station.

differences with the urban site at night. On the other hand during the central hours of the day the temperature differences between Molino Vittoria and Laste, negative in clear sky conditions, become positive as cloud cover increases, due to the combination of urbanization and topographic effects.

Figure 3.10 shows the dependence of the diurnal maximum intensity of the UHI on cloud cover for Gardolo weather station, analyzing situations with wind speed less than 1 m s^{-1}, so as to isolate the effects of cloud cover only. The maximum UHI intensity decreases roughly linearly as cloud cover increases, and from the relative scatter-plot (not shown here) the statistics are: slope = -0.26°C oktas^{-1}, intercept = 3.72°C (with $R^2 = 0.17$, a rather small value due to the large scatter of the data). The value of the intercept indicates the average maximum UHI in "ideal" conditions, with low wind speeds and cloudless skies. This value is lower than predicted by Oke's (1973) formula for European cities,

$$\Delta T_{u-r} = 2.01 \log(P) - 4.06 \tag{3.1}$$

where P is the city population. In the case of Trento, use of the population in the inner city provides $\Delta T_{u-r} = 5.5$°C. From Fig. 3.10 it can be seen that this value is also 1°C higher than the third quartile in low wind speed and cloudless conditions. However, due to the high variability

in the data, values even higher than 5.5°C are possible, as can be noted by the high whiskers. Thus the maximum intensity of the UHI in Trento substantially agrees with the value given by Eq. (3.1), as well as with the intensities reported for European cities (Oke 1973) of similar size as Trento (maximum UHI intensities ranging from 4.4°C to 7°C). Notice that Kuttler et al. (1996) found a similar maximum UHI intensity (6°C) in Stolberg (60 000 inhabitants), located, as is Trento, in a narrow valley and thus influenced by similar local conditions. The same analysis was also carried out for the weather stations on the valley sidewall (not shown). As expected from the previous results, at Cognola the dependence of the maximum UHI intensity on cloud cover is less than on the valley floor, but still significant, whereas at Laste the influence of cloud cover is negligible.

3.3.6 Evaluation of wind effects

A further analysis has been carried out to assess the impact of wind speed; accordingly temperature differences with the urban site were grouped into six wind speed classes, based on wind intensity recorded at Molino Vittoria, so as to include in every class a representative number of values.

Figure 3.11 shows the box-plots for Gardolo, on the valley floor: during nighttime the UHI intensity tends to decrease as wind speed increases, whereas during daytime urban-rural temperature differences seem not significantly affected by wind speed. During nighttime wind speed affects UHI intensity to a smaller extent than cloud cover.

On the valley slopes the diurnal cycle of the UHI seems to be little affected by the wind speed recorded at Molino Vittoria, during both daytime and nighttime: at Cognola and Laste the diurnal cycles of the UHI remain similar to those shown in Fig.3.3 in every wind condition (not shown). This finding may be attributed to the fact that wind speed measured at Molino Vittoria is not fully representative of the conditions at the sidewalls, where local down-slope winds typically occur (Fig. 3.1): a correlation analysis (not shown here) highlighted that wind speeds at Molino Vittoria and at Laste are well correlated during daytime, whereas there is a poor correlation at night, when, as found above, wind speed affects temperature differences with the urban site. For this reason generally valid conclusions for the stations on the sidewalls cannot yet be drawn.

In order to assess the influence of wind speed on the maximum diurnal UHI intensity, an analysis similar to that carried out for cloud cover was performed. In this case only the situations with cloud cover less than 2 oktas were analyzed. Results for Gardolo, on the valley floor, are shown in Fig. 3.12. The maximum UHI intensity displays only a weak dependence on wind speed. In particular, it is constant for wind speeds less than $2 \, \text{m s}^{-1}$, while beyond this value it slightly decreases as wind speed increases. This result is remarkably different from the relation proposed by Oke (1973), who found a strong dependence of UHI intensity on wind speed, with a variation as $u^{-0.56}$. A similar dependence on wind speed was found also by Runnals and
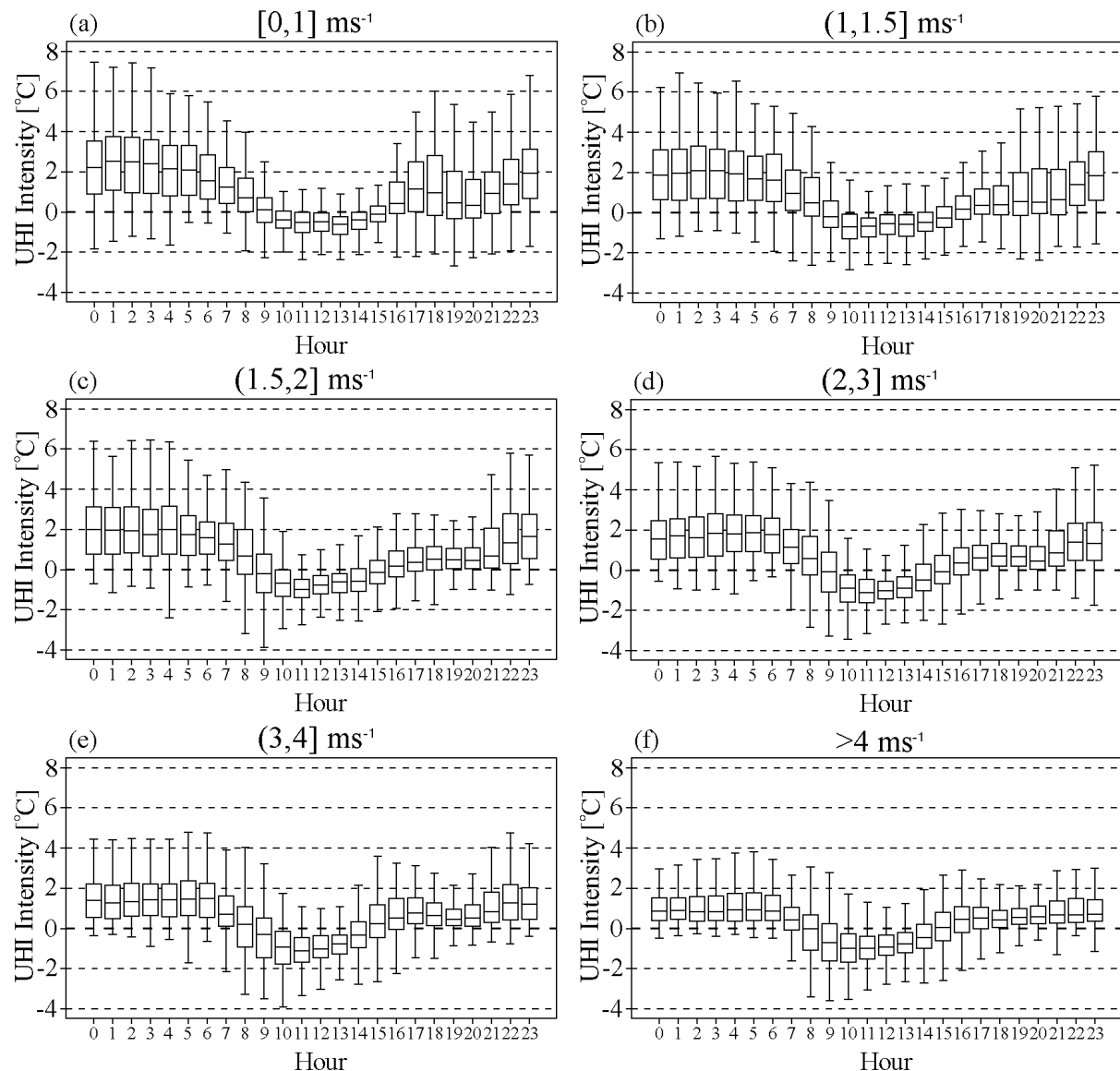
Figure 3.11: Box-plots of hourly temperature differences between Molino Vittoria and Gardolo classified by wind speed classes measured at Molino Vittoria.

Oke (2000), while Morris et al. (2001) reported a slightly lower dependence. Furthermore it is interesting to notice from Fig. 3.12 that, even with strong winds, high UHI intensities are possible (under cloudless conditions).

3.3.7 Combination of cloud cover and wind effects: the weather factor

The weather factor ϕ_w (Runnals and Oke 2000) was used to evaluate the combined effects of cloud cover and wind speed on the maximum diurnal UHI intensity. The original formulation
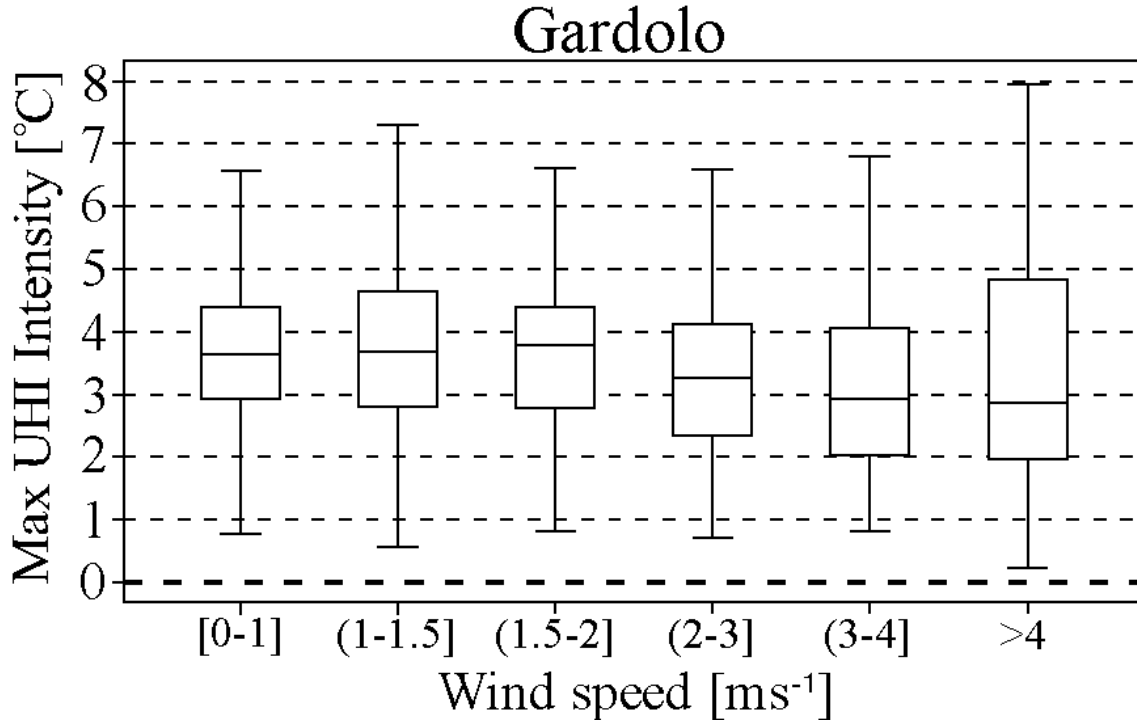
Figure 3.12: Box-plot of the maximum diurnal temperature differences between Molino Vittoria and Gardolo classified by wind speed classes measured at Molino Vittoria.

of Runnals and Oke (2000) is the following:

$$\phi_w = u^{-0.5} \cdot (1 - kn^2) \tag{3.2}$$

where u is the wind speed, n the cloud cover fraction (from 0 to 1), and k an empirical parameter taking into account the fact that cloud base temperature decreases with height. Since measurements of cloud base height were not available for this study, k was taken constant and equal to 0.7, which is the average of the values proposed by Oke (1987) for different cloud types. The weather factor can range from 0 to 1, setting the cut-off for low speeds at 1 m s^{-1}, with higher values indicating lower wind velocity and cloud cover.

In Fig. 3.13 the resulting box-plot for Gardolo, on the valley floor, is shown. The maximum diurnal intensity of the UHI increases roughly linearly with the weather factor, with a slope of 2.53°C m$^{0.5}$ s$^{-0.5}$ and an intercept of 1.32°C. However, as can also be seen from the box-plot, the data are quite scattered and the value of R^2 is only 0.20. Notice that, for any value of the weather factor, the maximum diurnal UHI intensity may be negligible at some days, as highlighted by the low whiskers, whereas the high whiskers indicate strong UHI intensities occurring even with a weather factor as low as 0.4.
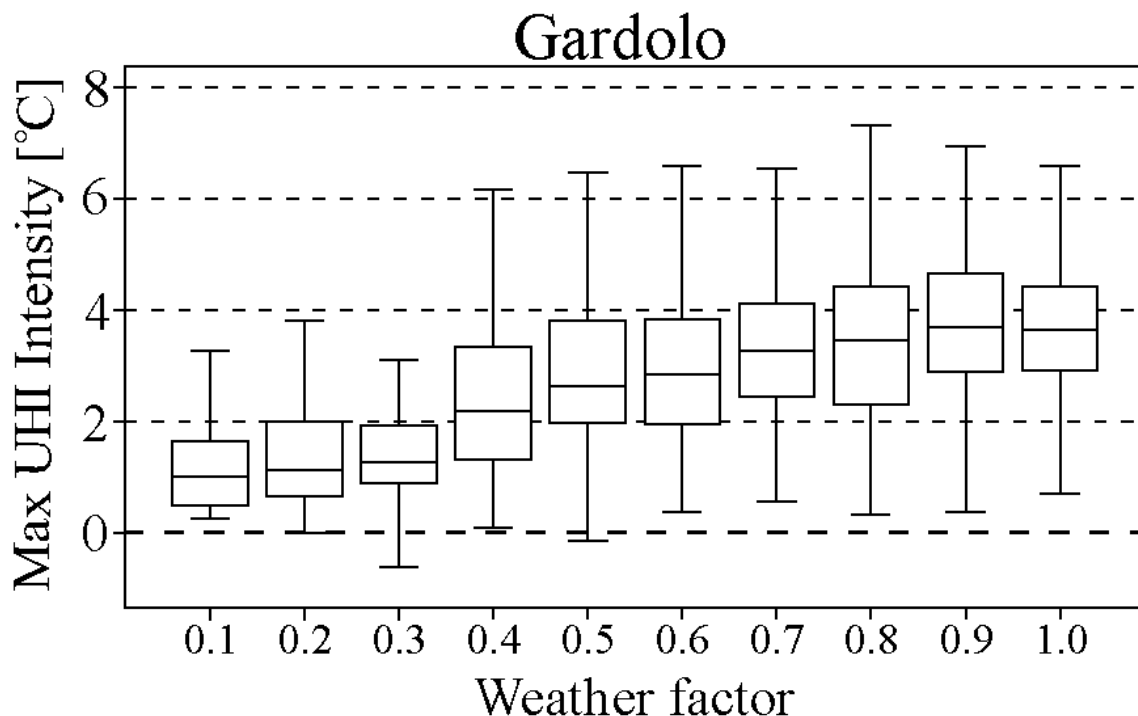
Figure 3.13: Box-plot of the maximum diurnal temperature differences between Molino Vittoria and Gardolo as a function of the weather factor.

3.4 Conclusions

The analyses presented in this Chapter provide a first insight into the UHI of the city of Trento, by analyzing the differences between air temperature time series registered at an urban station and at five surrounding extra-urban weather stations over the period October 2002 - December 2008. Temperature contrasts strongly depend on the position of the extra-urban weather stations. These are affected by different landscape and urbanization effects, reflecting the situation of a city located in a complex topography. In particular three of the extra-urban weather stations are located, as is the urban site, on the valley floor, while the other two are on the eastern slopes of the valley, one in the countryside and one in a suburban area. For these reasons the average temperature differences with the urban site vary considerably (between 0.6°C and 1.5°C), if different extra-urban weather stations are taken into account. These results emphasize the importance of carefully considering the position and local surroundings of the weather stations adopted to evaluate UHI intensity, in order to distinguish urbanization effects from site-dependent, local meteorological features, and to correctly interpret the results (Stewart 2010). On the other hand some general conclusions can be drawn from the diurnal cycles of the UHI intensity, which display similar properties at all the extra-urban weather stations. The UHI is stronger during nighttime, when urban-rural temperature differences are quite constant

for the whole night. In the same hours maximum diurnal UHI intensities are generally reached, with average values ranging between 2°C and 4°C at the extra-urban stations on the valley floor. During the middle of the day the temperature at the urban site is usually lower than at the extra-urban locations, with the development of an urban cool island. As a consequence, the diurnal temperature range at the urban site is considerably lower than at the extra-urban weather stations, where both warming and cooling rates are stronger.

The analysis of the maximum diurnal intensity of the UHI highlighted that, under "ideal" conditions, values higher than 6°C can be reached. This result seems in agreement with maximum UHI intensities found in other European cities of similar size to Trento, and in particular Stolberg (Kuttler et al. 1996), one of the few studied cities located in a valley. As to the urban cool island effect, its typical maximum intensity was found to be of order 1.5°C on the valley floor.

Considering the extra-urban weather stations located on the valley floor, the seasonal variations of UHI intensity are negligible over daytime. On the other hand during nighttime UHI intensity is slightly stronger during dry months, when weather conditions favor stronger radiative cooling. As to the extra-urban stations located on the slopes, the seasonal variations of UHI intensity seem mainly affected by the seasonal change in the mean lapse rate rather than by urbanization effects. In fact during both daytime and nighttime UHI intensity is lower during winter months, when the mean lapse rate is lowered by frequent thermal inversions.

The analyses of the impact of cloud cover and wind speed on the diurnal UHI cycle highlighted that in the case of Trento the former is the meteorological factor which most influences UHI intensity: being connected with solar radiation during daytime and with radiative cooling at night, it affects directly both heating and cooling rates, and hence their differences between urban and rural areas. For this reason temperature contrasts due to urbanization effects are appreciable under clear sky conditions, becoming negligible for a completely cloudy sky.

As to the wind speed influence, it was found that this meteorological factor affects the diurnal cycle of the UHI at the extra-urban weather stations on the valley floor only at night, when urban-rural temperature differences slightly decrease as wind speed increases. No significant results were found for the two extra-urban weather stations on the sidewalls, probably because wind speed at Molino Vittoria is not fully representative of the situation on the slopes of the valley.

The analyses presented in this Chapter have some inherent limits, as they are based on single surface data only, which cannot give a complete spatial representation of the phenomena. For this reason some aspects, such as the assessment of the three-dimensional temperature and wind fields in the surroundings of the city, will be further investigated in Chapter 6 by means of numerical simulations with a mesoscale meteorological model. Among the few evidences of local wind effects on UHI intensity, it was noted (not shown here) that on the valley floor in spring and summer, as opposed to the winter period, UHI intensity is very low or negligible in the late

evening. This behavior may be caused both by the later sunset, and (mostly) by the strong up-valley wind, which inhibits radiative cooling in the rural areas and tends to homogenize the surface temperature in the whole region. Moreover the interaction between cold air drainage flow and the built up area is not completely clear. The drainage flow contributes to an earlier onset of strong UHI intensities on the sidewalls, but the situation on the valley floor needs further investigations. Wind measurements at the urban reference station, located at about twice the height of the surrounding buildings, suggest that down-valley wind is generally rather strong and persistent at night over the urban area. However, in the absence of measurements inside the urban canopy layer, it is not clear if the flow penetrates below roof level. One possibility is that the down-valley wind bypasses the urban area flowing along preferential lanes, such as the lower level corridor offered by the Adige riverbed.

Chapter 4

Evaluation of the thermal structure in an urban street canyon: field measurements and validation of a numerical model

In this Chapter the microclimatic conditions inside an urban canyon located in the city center of Trento are evaluated using both an experimental and a modeling approach. In particular first the results of two measurement campaigns carried out in the summer 2007 and in the winter 2008-2009 in a north-south oriented urban street canyon are presented. The results of these urban canyon field campaigns are then used, along with wall surface temperature observations collected during the ATREUS PICADA experiment (Idczak et al. 2007), to evaluate the performance of a simple canyon model, similar to the single-layer model by Kusaka et al. (2001), which is able to simulate the average temperature inside an urban canyon, calculating the energy budgets of the different surfaces inside the street.

4.1 Field measurements

4.1.1 Site description and instrumental set-up

Two fields measurements were carried out respectively from 26 July to 20 August 2007 and from 23 December 2008 to 22 January 2009 in a street canyon of the city of Trento. The purpose of these measurements was to investigate the thermal field inside the urban canopy under various situations, and in particular to better highlight the effects of the different penetration of solar radiation inside the street. The urban canyon selected for the two field measurements, namely Via Rosmini, lies close to the historic city center of Trento, approximately in the middle of the

whole urban area (Fig. 4.1). As highlighted in Section 3.2, the core of the city center is built over the old Roman city and displays the typical regular grid of streets crossing at right angles. The selected street offers a suitable test case, being characterized by a very simple geometry, with buildings of equal heights flanking the street, and by a poor vegetation (low trees on the sidewalks). The building walls facing the street are constructed with brick and concrete and covered with plaster, while the street ground is covered with asphalt. Via Rosmini is roughly north-south oriented (354°N) and is 20 m wide, while the buildings at both sides display a rather uniform height of about 17 m, which implies an average aspect ratio of 0.85. It is one of the main streets of the city, running straight for about 350 m in both directions from the measurement points (Fig. 4.1).

Figure 4.1: Aerial photo showing the street canyon adopted as test case, Via Rosmini, and Molino Vittoria weather station. The dashed line in Via Rosmini indicates the cross section where instruments were placed during the field campaigns (photo courtesy of Municipality of Trento).

Five devices Onset Inc. Mod. HOBO H8 Pro were used for the measurements. These instruments are composed of a temperature and humidity sensor covered by a solar-radiation

screen, with eight superimposed plates. These low-cost instruments display good characteristics of accuracy (0.2°C declared by the manufacturer) and have been widely used, under various setups, for meteorological research, also in the urban environment (Whiteman et al. 2000; Doran et al. 2003; Fast et al. 2005). After a preliminary campaign, performed in 2005 (Lora et al. 2006), the HOBOs were considered suitable for the scope of this work. Before the field measurements the sensors were inter-compared in a controlled ambient room, and the resulting data were all within the accuracy interval provided by the manufacturer (not shown here). The sensors were setup in order to take measurements every 5 minutes in the so-called high resolution mode (12-bit).

In both campaigns four sensors were placed on the two opposite walls of Via Rosmini, two per wall at a height of about 7 and 11 m AGL respectively. In the winter campaign an additional HOBO was installed on a traffic light in the center of the street at 7 m AGL, in order to evaluate also a temperature inside the street not directly influenced by any surface (Fig. 4.2). For convenience the sensors on the walls are referred to with a label indicating what direction they were facing (E = East, W = West) and at what level they were placed (1 = higher, 2 = lower): e.g. E1 means the east-facing higher sensor at 11 m AGL. The sensor on the traffic light is referred to as TL.

Figure 4.2: Positions of the five HOBOs used during the field measurements.

4. Evaluation of the thermal structure in an urban street canyon: field measurements and validation of a numerical model

Since temperature measurements were performed near canyon walls, it is important to evaluate the influence of the thermal boundary layer developed on the wall directly lit by solar radiation. The experimental campaign performed by Idczak et al. (2007) in a 1:5 scale street canyon showed that the thermal boundary layer of the heated wall was about 50 mm thick, this thickness being rather independent from temperature. Farther from the wall the air temperature remained higher than in the center of the canyon, but the temperature gradient became nearly negligible. Following these results, the HOBO sensors in the two measurement campaigns in Trento were installed at about 0.3 m from the walls, in order to evaluate the effects of the surface heating on the air temperature near the walls, yet outside the thermal boundary layer. A similar setup, with sensors installed near building walls to evaluate the temperature field inside an urban canyon, was adopted by Santamouris et al. (1999) in Athens and by Erell and Williamson (2007) in Adelaide (Australia).

Via Rosmini is approximately 250 m far away from the automated meteorological station of Molino Vittoria (Fig. 4.1). As said in Section 3.2, the station is based on top of a tower at 33 m AGL, i.e. roughly twice the height of the surrounding buildings. For the purpose of the present analysis it is worth remarking that, given the site characteristics, these measurements are taken at the lower boundary of the inertial sub-layer, where the single microclimatic anomalies are mixed (see Section 2.2). So the station sensors record a blended, spatially averaged signal, representative of the local scale (Oke 2006). For this reason, measurements taken at this station can be assumed as representative of weather conditions above the average roof-top level and for comparison with data taken inside the canyon. The temperature measurements taken at Molino Vittoria are recorded as 10-min averages.

4.1.2 Direct solar radiation

The penetration of direct solar radiation inside the street is a key factor for temperature distribution in the canopy layer, as it controls the heating of the walls and of the street and as a consequence it strongly influences the temperature field inside the urban canyon and its contrast with the air temperature above roof level (Offerle et al. 2007). Figure 4.3 shows the sky lines viewed at ground level from the two walls flanking Via Rosmini, along with the path of the sun in the sky during the periods of the two field campaigns: the upper arch corresponds to the period of the summer field measurements (the upper curve is 26 July, while the lower curve is 20 August), whereas the lower arch to the period of the winter field measurements (the upper curve is 22 January, while the lower curve is 23 December). The two walls are lit by direct solar radiation over periods that vary considerably between the two campaigns. In the summer period the east-facing wall (Fig. 4.3a) is lit by direct solar radiation at ground level approximately from 0800 to 1200 LST, whereas the wall facing to the west (Fig. 4.3b) from 1200 to 1630 LST. In winter these periods are considerably shorter: at ground level the east-facing wall is lit from

1030 to 1200 LST, while the west-facing from 1200 to 1430 LST. Obviously, the higher portions of the walls are lit by direct solar radiation for longer than the lower ones: indeed sunrise time at the top of the east-facing wall is as early as 0600 LST during the summertime and at 0930 LST in winter, while sunset time at the top of the west-facing wall is delayed at 1815 LST in summertime and at 1500 LST during the wintertime.
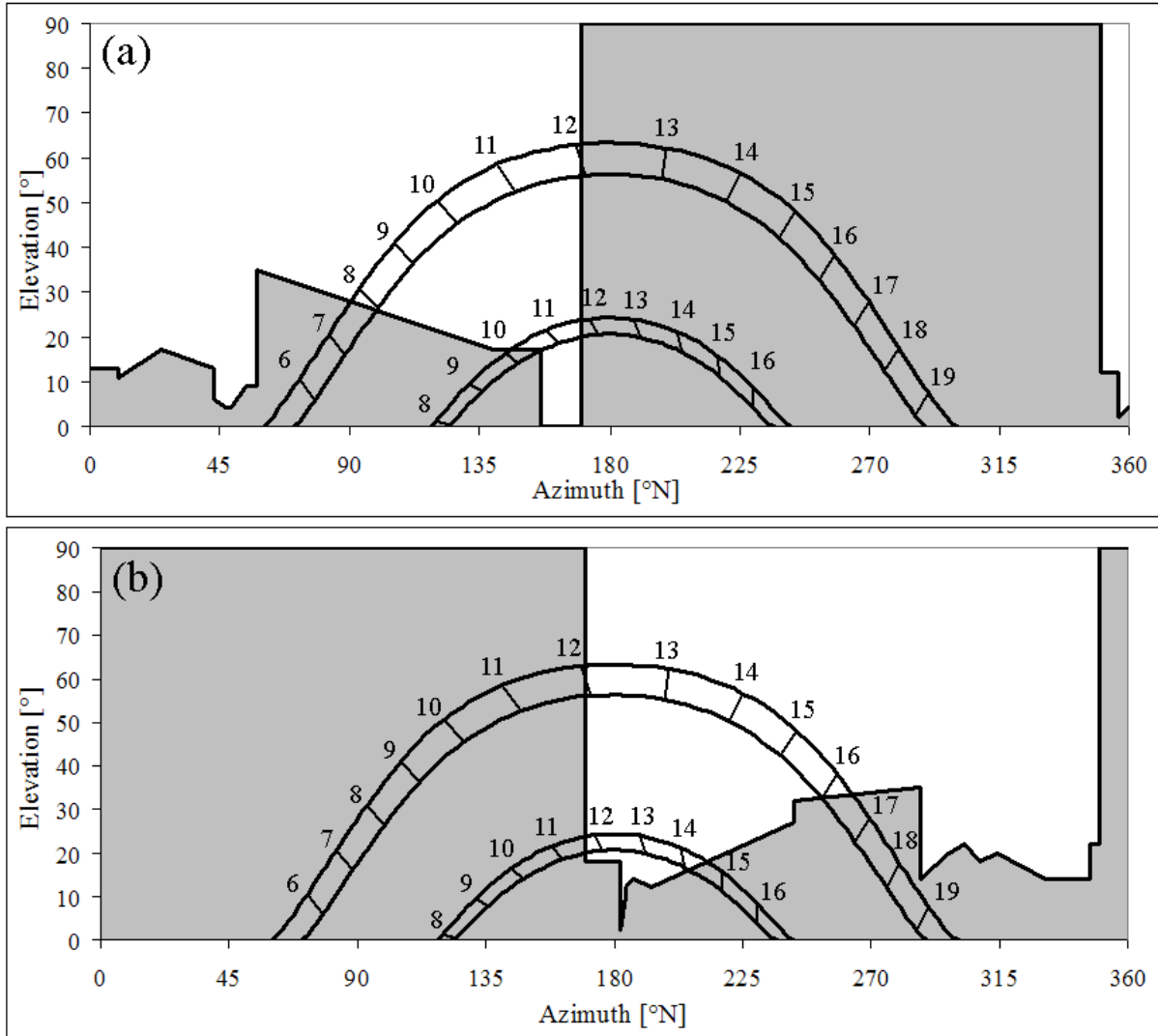
Figure 4.3: Sky lines as viewed at ground level from (a) the east-facing and (b) the west facing walls of Via Rosmini. In both Figures the diurnal path of the sun in the sky and the relative hourly position are shown. The upper arch corresponds to the period of the summer field campaign (lower curve 20 August and upper curve 26 July), whereas the lower arch to the period of the winter field campaign (lower curve 23 December and upper curve 22 January).

4.1.3 Weather conditions

Weather conditions occurred during the field measurements are well documented also in this case by cloud cover observations taken at the weather station, operated by the Italian Air Force Weather Service, at 2125 m MSL on top of Mount Paganella flanking on the west the Adige Valley, 10 km north-west of Trento. The record consists of hourly observations of cloud cover measured in oktas. Accordingly days were grouped into three weather categories, based on the average daily cloud cover: sunny days (0-2 oktas), partly cloudy days (2-6 oktas) and cloudy or rainy days (6-8 oktas). In the summer campaign 11 sunny days, 12 partly cloudy days and 3 cloudy or rainy days were registered. Air temperature measured at Molino Vittoria ranged from 14.0°C to 33.6°C. In the winter campaign there were 17 sunny days, 9 partly cloudy days and 4 cloudy or rainy/snowy days and air temperature at Molino Vittoria ranged from -6.2°C to 11.6°C.

4.1.4 Data analysis

Summer field measurements

During the summer field measurements the four HOBOs worked correctly for all the period and all the data registered could be used in the data analysis. Therefore the dataset is composed of 7488 temperature measurements for each HOBO and 3744 data registered at Molino Vittoria. The measurements taken inside the canyon and at Molino Vittoria in a clear day (5 August), which was adopted as a reference, are shown in Fig. 4.4. For the sake of clarity data have been downsampled to 30-min averages. During the morning the east-facing sensors warm up faster than the other ones, while in the afternoon the west-facing instruments are the warmest. In the morning the temperature measured by the sensors placed near the wall lit by direct solar radiation is on average about 2°C higher than that registered by the sensors in the shade, while in the afternoon the temperature difference is slightly lower, 1.5°C on average. During daytime, and especially when both sensors on the same wall are hit by direct solar radiation, the lower instrument systematically records a temperature slightly higher (about 0.5°C). This difference suggests that inside the canyon the highest temperatures are reached at low levels, probably due to the influence of the warming of the asphalt of the road, which can reach temperatures as high as 50-60°C during hot summer days (cf. Niachou et al. 2008). At night the temperature values are generally similar for all the four instruments, with differences mostly below 0.5°C. Temperature differences between the four HOBOs during partly cloudy days follow the same behavior as during sunny days, but with smaller differences, due to the lower solar forcing. On the other hand in cloudy or rainy situations, when solar radiation is very low, temperature differences between the four HOBOs are negligible.

The air temperature measured by the four sensors inside the canyon is systematically higher than above roof level at Molino Vittoria, under every weather condition. In clear sky situations

during nighttime the temperature inside the canyon is about 1°C higher than above roof level for all the four HOBOs, while during daytime the temperature differences between the sensors inside the canyon and Molino Vittoria vary in connection with the presence of direct solar radiation. The sensors lit by direct solar radiation are on average 2-2.5°C warmer than at Molino Vittoria, and in some days, especially when the sky is completely clear and thus the direct solar radiation is stronger, irrespectively from wind intensity, differences of 3-3.5°C are recorded. In the morning the temperature of the sensors in the shade is about the same as that measured at Molino Vittoria. On the other hand during the afternoon also the sensors in shade register temperatures higher than Molino Vittoria, with differences changing day by day, but displaying an overall average difference of order 1°C. Finally the temperature measured by the four instruments in the canyon is constantly higher than that recorded at Molino Vittoria also during cloudy or rainy days, with average differences of order 1°C.
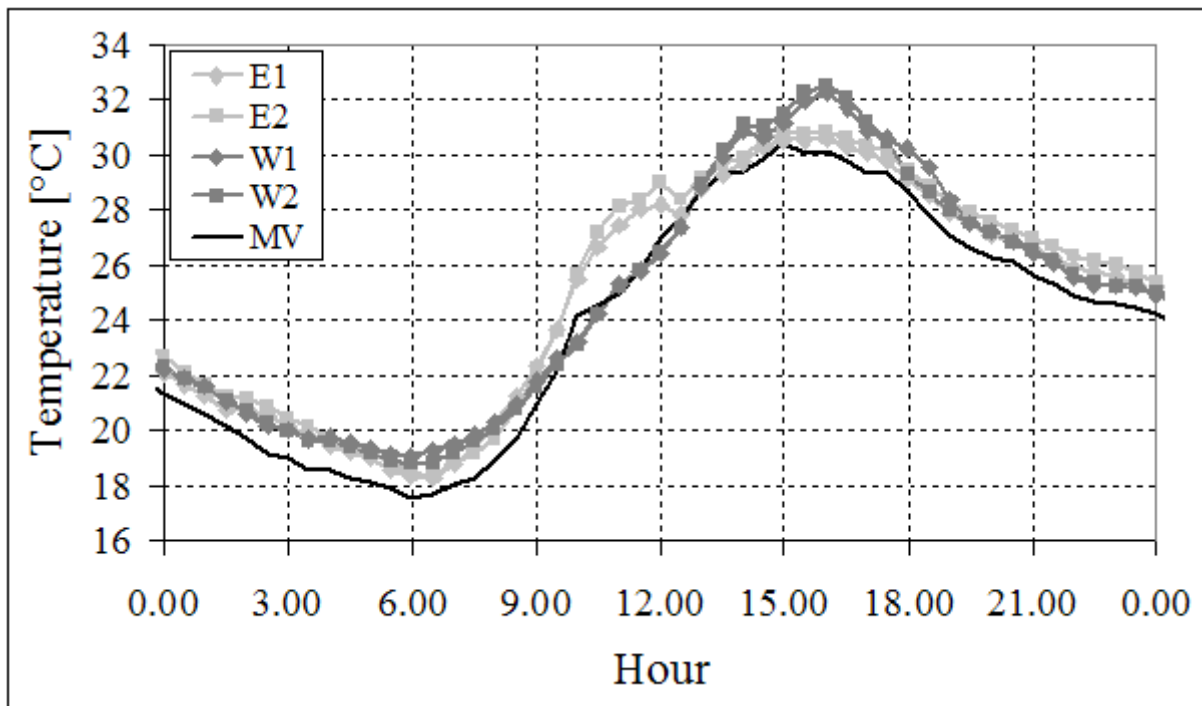
Figure 4.4: Comparison of air temperature measurements taken inside the urban canyon and at Molino Vittoria. The values presented here are 30-min averaged temperatures for 5 August 2007, a sunny day. Each curve refers to one sensor, identified with a label as explained in Section 4.1.1: E, W indicate sensors facing respectively east and west; 1 and 2 indicate higher and lower heights respectively. MV indicates measurements taken over roof level at Molino Vittoria.

4. Evaluation of the thermal structure in an urban street canyon: field measurements and validation of a numerical model

Winter field measurements

During the winter field measurements some technical problems occurred with the west-facing sensors and for this reason after a quality check some data recorded by these HOBOs were discarded. In particular 7 and 19 days of data registered respectively by W1 and W2 could be used for the present analysis (i.e 2016 and 5472 temperature measurements respectively). The other sensors performed correctly for all the 31 days of the field measurements and therefore contributed to the dataset with 8928 data each. The dataset from Molino Vittoria weather station is composed of 4464 data.

Figure 4.5 shows the daily cycle for all the available sensors 30-min averaged for a completely sunny day (11 January). The temperature of the sensors near canyon sidewalls are influenced by direct solar radiation as in the summer field measurements, but with some remarkable differences. In particular the overheating of the east-facing sensors in the morning is almost negligible, as solar radiation is very weak during these hours and hits this wall for a shorter time (Fig. 4.3a). On the other hand during the afternoon the overheating of the west-facing sensors is considerable (2°C on average). The temperature measured by TL, which is not influenced by any surface, is always close to that registered by the sensors in shade during the whole diurnal cycle. For this reason it can be inferred that the thermal field inside the canyon is quite horizontally homogeneous, with appreciable gradients only close to the sunlit surfaces. At night and in cloudy or rainy/snowy days the five HOBOs display, as in the summer period, similar temperatures, with differences below the sensors accuracy, as can be seen in Fig. 4.6, where the diurnal cycle for a rainy/snowy day (6 January) is shown.

Also during the winter period the temperature inside the urban canyon is generally higher than that measured above roof level at Molino Vittoria, although differences are lower than those registered during the summer field measurements. At night and during rainy days the temperature inside the canyon is slightly higher (on average about 0.5°C) than above roof level. During daytime on sunny days (Fig. 4.5) the morning temperature above roof level is similar to that measured by all sensors, due to the low overheating of E1 and E2. However in the afternoon the HOBOs facing west are on average 2°C warmer than Molino Vittoria, while the east facing sensors and TL measure a temperature similar to Molino Vittoria. In some cases in the afternoon the temperature at Molino Vittoria is even higher than that registered inside the canyon by the sensors in the shade (not shown).

4.2 Model description

The simple two-dimensional model tested here and validated against field measurements is a modified version of the single-layer model by Kusaka et al. (2001). This model can simulate the average air temperature in an urban canyon by calculating separate surface energy budgets for
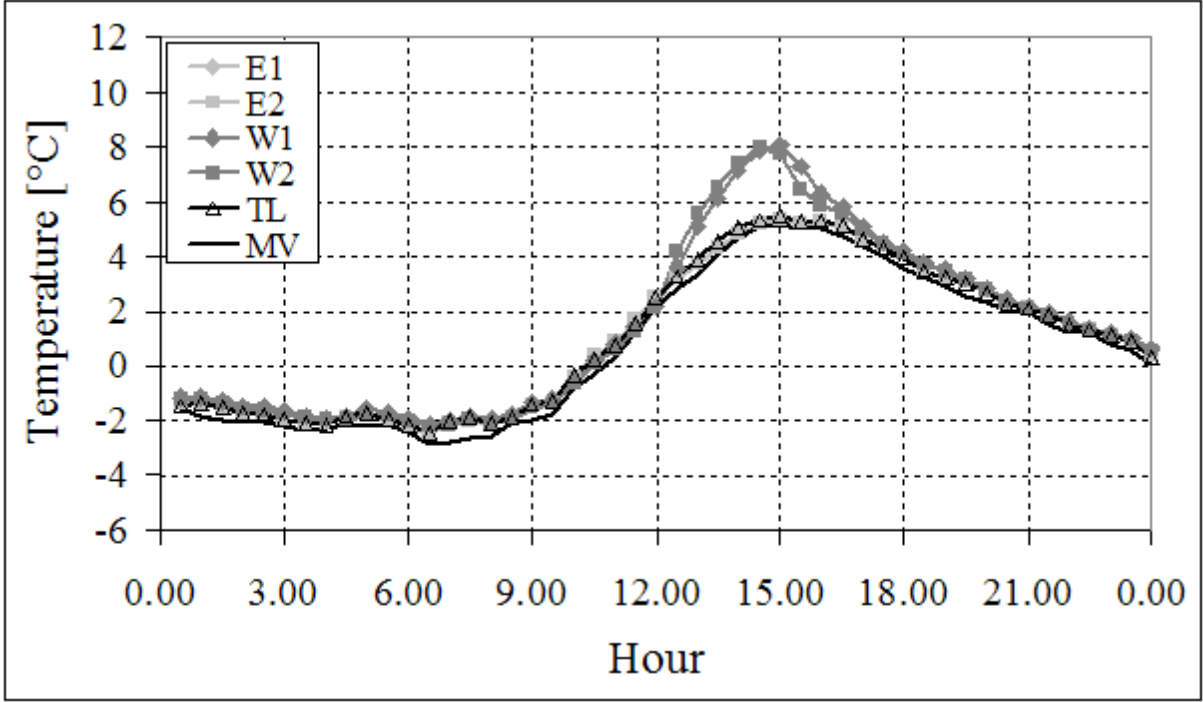
Figure 4.5: As in Fig. 4.4, but for 11 January 2009, a sunny day. TL indicates data taken on a traffic light in Via Rosmini.

each surface (road, wall, roof) and balancing the heat fluxes inside a suitable control volume, so that the heat exchanged through the top of the canyon (which is the interface between the canyon and the over-the-canopy atmosphere) equals the heat released/absorbed by the "physical" surfaces, i.e. walls and road, and the anthropogenic heat flux released from vehicular traffic:

$$wH_{top} = hH_{w,1} + hH_{w,2} + wH_r + wQ_v \qquad (4.1)$$

where $H_{w,1}$, $H_{w,2}$ and H_r represent the heat fluxes from the two walls and the road respectively, while Q_v the anthropogenic heat flux from vehicular traffic.

The model takes into account the shadowing inside the street and the multiple reflections of both short- and long-wave radiations between the road and the walls. The heat through the surfaces is calculated with the heat conduction equation dividing each surface in several layers of variable thickness, depending on the real composition of the surfaces modeled. Furthermore the walls and the road are divided into sub-areas, so that different temperature values can be found in different portions of the same surface. The model implemented here calculates a simplified surface energy budget, since latent heat flux is not accounted for. However it can be safely assumed that in an urban environment characterized by very scarce vegetation, such as the present cases, the latent heat flux displays very low or negligible values (Oke et al.
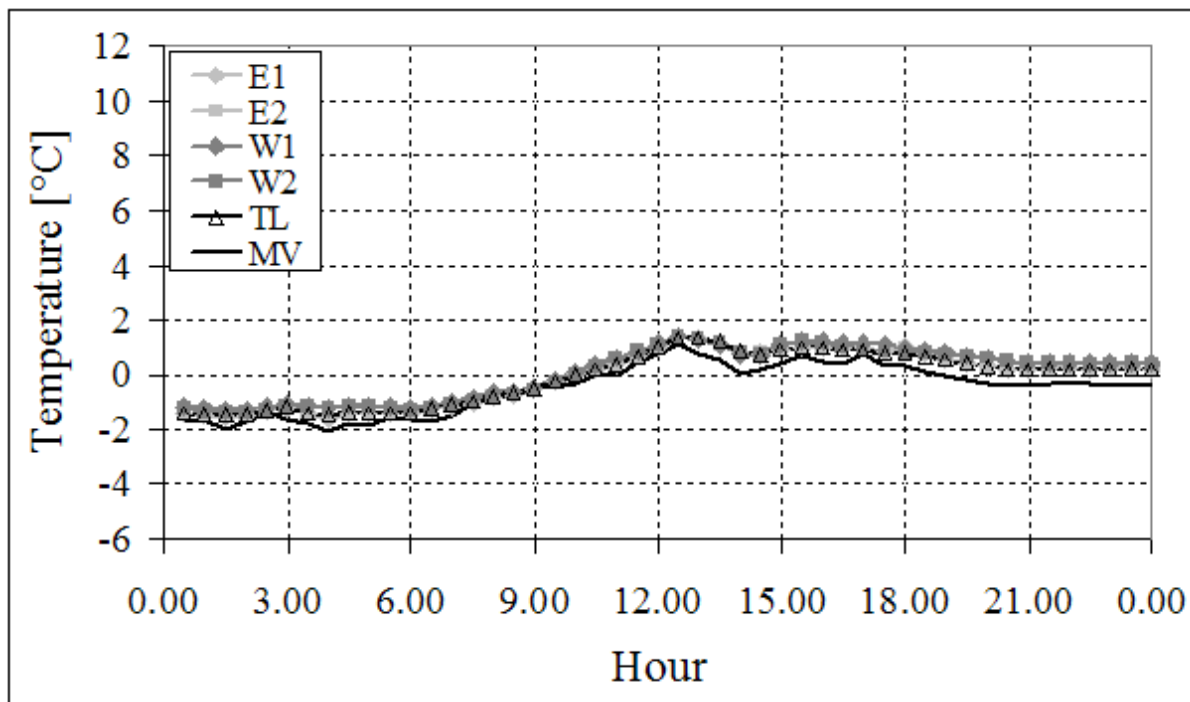
Figure 4.6: As in Fig. 4.4, but for 6 January 2009, a rainy/snowy day. TL indicates data taken on a traffic light in Via Rosmini.

1999). The model takes directly into account the anthropogenic heat flux from vehicular traffic, with a daily cycle that can be added to the heat balance of the canyon, while heat fluxes due to domestic heating or cooling are implicitly considered setting a constant temperature inside the buildings. On the other hand, at the present stage, heat directly released from other anthropogenic activities such as air conditioners [which may be relevant at an urban-canyon scale (Ohashi et al. 2007)] has been neglected.

The upper boundary conditions needed by the model are the basic meteorological parameters normally measured by standard weather stations: air temperature, relative humidity, incoming short-wave radiation, and wind speed measured above roof level. The other basic inputs needed by the model are the cloud cover, the geometrical parameters of the canyon and the properties of the surface materials.

4.2.1 Wind speed

Although recent investigations highlighted the complexity of the wind field across urban areas (e.g. Mochida and Luna 2008), in view of the rather simplified approach of the model presented here, it has been assumed a logarithmic wind profile above roof level, including atmospheric

stability effects, as in Kusaka et al. (2001). Thus wind speed at roof level V_{top} is obtained as:

$$V_{top} = V_{ref} \frac{[ln(\frac{h-d}{z_0}) - \psi_m(\frac{h-d}{L})]}{[ln(\frac{z_{ref}-d}{z_0}) - \psi_m(\frac{z_{ref}-d}{L})]} \tag{4.2}$$

where d is the displacement height, z_0 is the aerodynamic roughness length, ψ_m is the universal function of relative stability, L is the Monin-Obukhov length (Stull 1988), h is the height of the buildings and z_{ref} is the height of the reference weather station.

The wind speed inside the canyon V_{can} has been evaluated as having an exponential profile (Kusaka et al. 2001):

$$V_{can} = V_{top} \exp(-0.386\frac{h}{w}) \tag{4.3}$$

where w is the width of the road.

4.2.2 Surface temperatures

Surface temperatures are calculated from the surface energy budget, following the approach proposed by Masson (2000). For the generic i-th surface:

$$C_{i,1} \frac{\partial T_{i,1}}{\partial t} = \frac{1}{d_{l_{i,1}}} (S_i^* + L_i^* - Q_{H_i} - \Delta Q_{S_{i,1-2}}) \tag{4.4}$$

where C is the heat capacity, d_l the thickness of the layer, S^* and L^* are short-wave and long-wave net radiations, Q_H the sensible heat flux and ΔQ_S the storage heat flux between layers 1 and 2. Equation (4.4) is applied at the first layer of every surface, i.e. that directly in contact with external air: this layer is assumed to be very thin (1 cm) in order to utilize its temperature for the evaluation of surface turbulent fluxes.

The temperatures of the internal layers are obtained by means of a monodimensional heat conduction equation. For the k-th layer (Masson 2000):

$$C_{i,k} \frac{\partial T_{i,k}}{\partial t} = \frac{1}{d_{i,k}} (\Delta Q_{S_{i,(k-1)-k}} - \Delta Q_{S_{i,k-(k+1)}}) \tag{4.5}$$

The internal boundary condition has been set as a constant temperature: the temperature of the air inside the buildings for the walls and the roof, and the temperature of the ground (at a depth greater than 1 m where it can be safely supposed that the ground temperature is not affected by the air temperature diurnal cycle) for the street.

4.2.3 Solar and long-wave radiations

The only radiation measurement needed by the model is the incoming solar radiation. The partitioning of global solar radiation into direct and diffuse components is calculated according

to Carroll (1985):

$$\alpha_{diff} = 0.88 - 1.024 K_t \qquad (4.6)$$

with:

$$K_t = \frac{S_{glob}}{(K_{sun} cos(\theta_z))} \qquad (4.7)$$

where S_{glob} is the global short-wave radiation measured at the reference level, K_{sun} is the solar constant (1353 W m^{-2}) and θ_z is the solar zenith angle.

The incoming long-wave radiation is calculated by the model according to Brutsaert (1975) and Unsworth and Monteith (1975), to take into account the effects of cloud cover. The atmospheric emissivity with clouds ϵ_a(c) is calculated with the following expression:

$$\epsilon_a(c) = (1 - 0.84c)\epsilon_a(0) + 0.84c \qquad (4.8)$$

where c is the fraction of sky covered by clouds and $\epsilon_a(0)$ is the atmospheric emissivity with completely clear sky:

$$\epsilon_a(0) = 1.24 (\frac{e_{ref}}{T_{ref}})^{\frac{1}{7}} \qquad (4.9)$$

where e_{ref} and T_{ref} are the vapor pressure and the temperature at the reference level respectively.

Finally the incoming long-wave radiation L is simply calculated from the Stefan-Boltzmann relationship:

$$L = \epsilon_a(c)\sigma T_{ref}^4 \qquad (4.10)$$

where σ is the Stefan-Boltzmann constant.

The penetration of solar radiation inside an urban canyon is hindered by the buildings that border the street and directly depends on the height of the buildings, the orientation of the main axis of the canyon and the position of the sun in the sky. The following expression has been adopted to evaluate the extension of the part of the street which lies in shade (Kusaka et al. 2001):

$$l_{shadow} = \min[h \tan(\theta_z) \sin(\theta_n), w] \qquad (4.11)$$

where θ_n is the difference between solar azimuthal angle and the orientation of the canyon axis. The fraction of wall lit by direct solar radiation has been calculated in a similar way (Kusaka et al. 2001).

The view factors for the walls have been calculated as in Sakakibara (1996), thus for a generic point on the wall the sky view factor ψ_{w-s} is given by:

$$\psi_{w-s} = \frac{1}{2} \left[1 - \frac{z}{(z^2 + w^2)^{0.5}} \right] \qquad (4.12)$$

where z is the distance of the point from the top of the canyon. The wall-road view factor ψ_{w-r}

is then calculated as the following:

$$\psi_{w-r} = \frac{1}{2}\left[1 - \frac{h-z}{((h-z)^2 + w^2)^{0.5}}\right] \tag{4.13}$$

The wall-wall view factor ψ_{w-w} can be calculated as the remaining part of the view after subtracting wall-sky and wall-road view factors:

$$\psi_{w-w} = 1 - \psi_{w-s} - \psi_{w-r} \tag{4.14}$$

The sky view factor for the entire wall is calculated with the expression proposed by Noilhan (1981):

$$\overline{\psi}_{w-s} = \frac{1}{2}\frac{\left[\frac{h}{w} + 1 + \left[\left(\frac{h}{w}\right)^2 + 1\right]^{0.5}\right]}{\frac{h}{w}} \tag{4.15}$$

Considering the geometry of the canyon, the road view factor for the entire wall is equal to $\overline{\psi}_{w-s}$, while the wall-wall view factor for the entire wall $\overline{\psi}_{w-w}$ is simply the remaining part of the view:

$$\overline{\psi}_{w-w} = 1 - 2\overline{\psi}_{w-s} \tag{4.16}$$

The sky view factor for the entire road $\overline{\psi}_{r-s}$ is calculated with the expression proposed by Noilhan (1981):

$$\overline{\psi}_{r-s} = \left[\left(\frac{h}{w}\right)^2 + 1\right]^{0.5} - \frac{h}{w} \tag{4.17}$$

while the road-wall view factor $\overline{\psi}_{r-w}$ is given by:

$$\overline{\psi}_{r-w} = \frac{1 - \psi_{r-s}}{2} \tag{4.18}$$

It has also been supposed that the roof is not hindered by obstacles, thus the sky view factor of the roof $\overline{\psi}_{rf-s}$ is 1.

For both solar and long-wave radiations, the multiple reflections between the walls and the road have been taken into account, similarly to Kusaka et al. (2001). For sake of simplicity here are reported only the expressions for the entire surfaces. The expressions for the sub-areas are very similar, taking into account the geometry of the canyon. The net short-wave radiation received by the sunlit part of the walls S_w is calculated as following:

$$\begin{aligned}S_w = &S_{dir,w}(1 - \alpha_w) + S_{dif}\overline{\psi}_{w-s}(1 - \alpha_w) + S_{dir}\frac{(w - l_{shadow})}{w}\overline{\psi}_{w-r}\alpha_r(1 - \alpha_w) + \\ &S_{dif}\psi_{r-s}\overline{\psi}_{w-r}\alpha_r(1 - \alpha_w) + S_{dif}\overline{\psi}_{w-s}\overline{\psi}_{w-w}\alpha_w(1 - \alpha_w)\end{aligned} \tag{4.19}$$

where S_{dif} is the diffuse solar radiation, α_w and α_r are the albedo of the walls and of the road

4. Evaluation of the thermal structure in an urban street canyon: field measurements and validation of a numerical model

respectively and $S_{dir,w}$ is the direct solar radiation received by the wall:

$$S_{dir,w} = \begin{cases} S_{dir}\frac{w}{h} & \theta_z > \theta_{lim} \\ S_{dir}\tan(\theta_z)\sin(\theta_n) & \theta_z \leq \theta_{lim} \end{cases} \quad (4.20)$$

where S_{dir} is the direct solar radiation on a horizontal surface and θ_{lim} is the solar zenith angle for which the road begins to be lit by direct solar radiation. The net short-wave radiation for the shaded part of the walls is:

$$\begin{aligned} S_w =& S_{dif}\overline{\psi}_{w-s}(1-\alpha_w) + S_{dir}\frac{(w-l_{shadow})}{w}\overline{\psi}_{w-r}\alpha_r(1-\alpha_w)+ \\ & S_{dif}\overline{\psi}_{w-r}\overline{\psi}_{r-s}\alpha_r(1-\alpha_w) + S_{dir,w}\overline{\psi}_{w-w}\alpha_w(1-\alpha_w) + S_{dif}\overline{\psi}_{w-s}\overline{\psi}_{w-w}\alpha_w(1-\alpha_w) \end{aligned} \quad (4.21)$$

Similarly, the net short-wave radiation for the entire road is:

$$\begin{aligned} S_r =& S_{dir}\frac{(w-l_{shadow})}{w}(1-\alpha_r) + S_{dif}\overline{\psi}_{r-s}(1-\alpha_r)+ \\ & S_{dir,w}\overline{\psi}_{r-w}\alpha_w(1-\alpha_r) + 2S_{dif}\overline{\psi}_{w-s}\overline{\psi}_{r-w}\alpha_w(1-\alpha_r) \end{aligned} \quad (4.22)$$

Assuming that there are no reflections and shadows above the canyon, the expression for the roofs is very simple:

$$S_{rf} = S_{dir}(1-\alpha_{rf}) + S_{dir}(1-\alpha_{rf}) \quad (4.23)$$

The net long-wave radiation for each surface is calculated in a similar way, also in this case as in Kusaka et al. (2001), taking into account the multiple reflections inside the canyon. The net long-wave radiation absorbed by each wall L_w is calculated as following:

$$\begin{aligned} L_w =& \epsilon_w\overline{\psi}_{w-s}L - \epsilon_w\sigma T_w^4 + \epsilon_w\overline{\psi}_{w-r}\sigma\epsilon_r T_r^4 + \epsilon_w^2\overline{\psi}_{w-w}\sigma T_w^4 + \epsilon_w(1-\epsilon_r)\psi_w\psi_r L+ \\ & \epsilon_w(1-\epsilon_r)\overline{\psi}_{w-r}\overline{\psi}_{r-s}L + \epsilon_w(1-\epsilon_w)\overline{\psi}_{w-s}\overline{\psi}_{w-w}L + \epsilon_w^2(1-\epsilon_w)\overline{\psi}_{w-w}^2\sigma T_w^4+ \\ & \epsilon_w^2(1-\epsilon_r)\overline{\psi}_{w-r}\overline{\psi}_{r-w}\sigma T_w^4 + \epsilon_w(1-\epsilon_w)\overline{\psi}_{w-r}\overline{\psi}_{w-w}\sigma\epsilon_r T_r^4 \end{aligned} \quad (4.24)$$

where ϵ_w and ϵ_r are the emissivity coefficients for the walls and the road respectively, $T_{w,1}$, $T_{w,2}$ and T_r are the surface temperatures of the two walls and of the road.
The net long-wave radiation for the entire road L_r is:

$$\begin{aligned} L_r =& \epsilon_r\overline{\psi}_{r-s}L - \epsilon_r\sigma T_r^4 + \epsilon_r\epsilon_w\overline{\psi}_{r-w}\sigma T_{w1}^4 + \epsilon_r\epsilon_w\overline{\psi}_{r-w}\sigma T_{w2}^4+ \\ & 2\epsilon_r(1-\epsilon_w)\overline{\psi}_{r-w}\overline{\psi}_{w-s}L + \epsilon_r\epsilon_w(1-\epsilon_w)\overline{\psi}_{r-w}\overline{\psi}_{w-w}\sigma T_{w1}^4+ \\ & \epsilon_r\epsilon_w(1-\epsilon_w)\overline{\psi}_{r-w}\overline{\psi}_{w-w}\sigma T_{w2}^4 + 2\epsilon_r(1-\epsilon_w)\overline{\psi}_{r-w}\overline{\psi}_{w-r}\sigma\epsilon_r T_r^4 \end{aligned} \quad (4.25)$$

The long-wave balance for the roof is calculated without any reflection:

$$L_{rf} = \epsilon_{rf}L - \epsilon_{rf}\sigma T_{rf}^4 \quad (4.26)$$

Table 4.1: Physical properties of the materials composing the canyon surfaces of the physical model of the ATREUS-PICADA experiment. Here d_l is the thickness of each layer (m), α the albedo, ϵ the emissivity, λ the thermal conductivity (W m^{-1} K^{-1}), and C the heat capacity (J m^{-3} K^{-1}).

		d_l	α	ϵ	λ	C
	Cement	0.013	0.60	0.95	0.90	1600000
WALLS	Air layer	0.030	-	-	0.026	1206
	Steel	0.003	-	-	45.3	3915000
GROUND	Gravel	0.35	0.20	0.95	1.6	2288000
	Soil	2.0	-	-	1.0	2160000
ROOFS	Steel	0.003	0.20	0.95	45.3	3915000

where ϵ_{rf} is the emissivity of the roof and T_{rf} is its surface temperature.

4.2.4 Sensible heat flux

The sensible heat flux Q_H at the generic j-th surface is calculated as:

$$Q_{H_j} = K_j(T_s - T_a) \tag{4.27}$$

where T_s and T_a are surface and air temperatures respectively and the coefficient K is a function of wind velocity (Kusaka et al. 2001):

$$K_j = \begin{cases} 7.51V^{0.78} & V < 5 \text{ m s}^{-1} \\ 6.15 + 4.18V & V \geq 5 \text{ m s}^{-1} \end{cases} \tag{4.28}$$

The sensible heat flux at the top of the canyon $Q_{H_{top}}$, i.e. that exchanged between the air within the canyon and the atmosphere above roof level is (Kusaka et al. 2001):

$$Q_{H_{top}} = \rho c_p \frac{k u_*}{\Psi_h}(T_{can} - T_{ref}) \tag{4.29}$$

where ρ is the air density, c_p is the heat capacity of dry air, k is the Von Karman constant, u_* the friction velocity, Ψ_h the integrated universal function, and T_{can} the canyon air temperature.

4.3 Model set-up

4.3.1 Atreus-Picada simulation

The ATREUS-PICADA experimental campaign (Idczak et al. 2007) was carried out from 7 July 2004 to 20 October 2004 to study the microclimatic conditions inside urban canyons using a physical model at 1:5 scale. The physical model was composed by four rows of buildings (18.3 m in length, 5.2 m in height and 2.4 m in width), formed by steel containers simulating

4. Evaluation of the thermal structure in an urban street canyon: field measurements and validation of a numerical model

Table 4.2: As in Tab. 4.1, but for Via Rosmini.

		d_l	α	ϵ	λ	C
WALLS	Concrete	0.01	0.30	0.90	1.51	1540000
	Concrete	0.09	-	-	1.51	1540000
	Insulation	0.01	-	-	0.03	250000
	Concrete	0.30	-	-	1.51	1540000
GROUND	Asphalt	0.01	0.10	0.95	0.82	1740000
	Asphalt	0.04	-	-	0.82	1740000
	Gravel	0.20	-	-	2.1	2000000
	Soil	1.0	-	-	0.4	1400000
ROOFS	Tile	0.01	0.20	0.90	1.4	1510000
	Tile	0.04	-	-	1.4	1510000
	Insulation	0.01	-	-	0.03	250000
	Concrete	0.20	-	-	1.51	1540000

three urban canyons. The orientation of the street was 54°N, while the street width was 2.1 m, resulting in an aspect ratio of 2.5. The walls of the canyon were lined with white cement panels. Intensive measurements of the most important atmospheric parameters, as well as of surface temperatures, were conducted inside and outside the canyons. In the present work data from their measurements of wall surface temperature at different heights in a sunny day (Fig. 10 of Idczak et al. 2007) are used to test the performance of the model. To this purpose the numerical scheme has been slightly modified to account for the fact that the physical model is not infinitely long and, as a consequence, solar radiation can reach the walls and the ground also through the canyon ends. The forcing meteorological parameters needed to run the model are provided in Idczak et al. (2007), along with the geometric characteristics of the canyon. The composition of the surfaces of the canyon are taken from Idczak et al. (2010), where the authors compared the observations of the experimental campaign with the results of numerical simulations with a 3D finite elements model. Values adopted for the simulations are reported in Tab. 4.1. The estimation of the aerodynamic roughness length z_0 and of the displacement height d is difficult due to the particular configuration of the physical model and the non-uniform conditions around the site. On the other hand, some preliminary tests have highlighted that the wall temperatures simulated by the model are not so sensitive to these parameters. Accordingly, for the purpose of the present work, the values proposed by Grimmond and Oke (1999) in their Fig. 1a for isolated roughness elements were adopted, namely $d/h = 0.1$ and $z_0/h = 0.04$. In this simulation the integration time step is 1 s, results are then averaged and compared with the 30 min-averaged measurements.

4.3.2 Simulations in the real canyon

The ability of the model to simulate the air temperature inside an urban canyon was tested with the measurements performed during the above mentioned field campaigns in Via Rosmini. The model calculates the average air temperature inside the canyon, so the results of the model have been compared with the measurements from the field campaigns which reasonably represent an average canyon air temperature. It can be safely assumed that the latter is provided by the HOBO placed in the center of the street on the traffic light during the winter field campaign. As to the summer campaign (when no measurements were taken at the street center), it can be supposed that the temperature field is rather homogeneous during the night inside the street. So the numerical results are compared with the average of the four sensors. Instead during daytime the sensors directly hit by solar radiation are influenced by the wall surface heating, so the HOBOs in the shade only can be taken as representative of the average conditions inside the street. In fact, as seen above, during the winter campaign it was found that the temperature measured by the sensors in the shade is always similar to that measured in the center of the street. For this reason during daytime the model results are compared with the average of the observations of the two sensors in the shade.

In these simulations the meteorological upper boundary conditions are supplied by Molino Vittoria weather station, that, as mentioned before, is taken as representative of the situation above roof level, while the canyon geometry input parameters are set using Via Rosmini characteristics. The displacement height d and the aerodynamic roughness length z_0 are assumed to be constant for all possible wind directions around the test site. In fact the urban morphology in the area surrounding the canyon is quite homogeneous, as resulted from an analysis of the building planar area fractions λ_p and of the heights of the buildings calculated on the basis of the high-resolution (1 m) lidar data of the Municipality of Trento. The values of λ_p obtained in the area surrounding the canyon range between 0.5 and 0.7, while the height of the buildings between 13 and 18 m. The values of the displacement height and of the aerodynamic roughness length used in the model have been adopted again from those suggested by Grimmond and Oke (1999) in their Fig. 1a. Planar area ratios in the area surrounding the canyon correspond to d/h = 0.8 and z_0/h = 0.08. In this case the height h has been taken equal to 17 m, i.e. the mean height of the buildings flanking the canyon, which is also representative of the surroundings of the test site. Furthermore, for these values of λ_p, the width of the buildings has been set equal to 30 m. For what concerns the real composition of the canyon physical surfaces, materials and widths of the different layers have been assigned considering the usual engineering practice in the region (Tab. 4.2). It was assumed that walls are made of concrete with a thin layer of insulating material, while roofs are made of tiles covering a thin layer of insulating material and an internal layer of concrete. The temperature inside buildings has been set constant at 26°C during summertime and 21°C during wintertime, assumed as average working conditions.

Finally it was supposed that the road is made of asphalt over a layer of gravel, and natural soil at deeper levels. Moreover at 1.25 m underground a constant temperature of 20°C in summer and 10°C in winter has been assigned. The anthropogenic heat flux from vehicular traffic was calculated, following Grimmond (1992), from the vehicular fluxes data contained in the Urban Mobility Plan of the Municipality of Trento. The daily cycle presents two peaks, one in the morning and one in the evening, with maximum values of order 7-8 W m^{-2}. In these simulations the integration time step is 60 s, results are then averaged and compared with the 30 min-averaged data from the field measurements, for consistency with the results presented before.

4.4 Model validation

4.4.1 Comparison with measurements in a physical model (ATREUS-PICADA experiment)
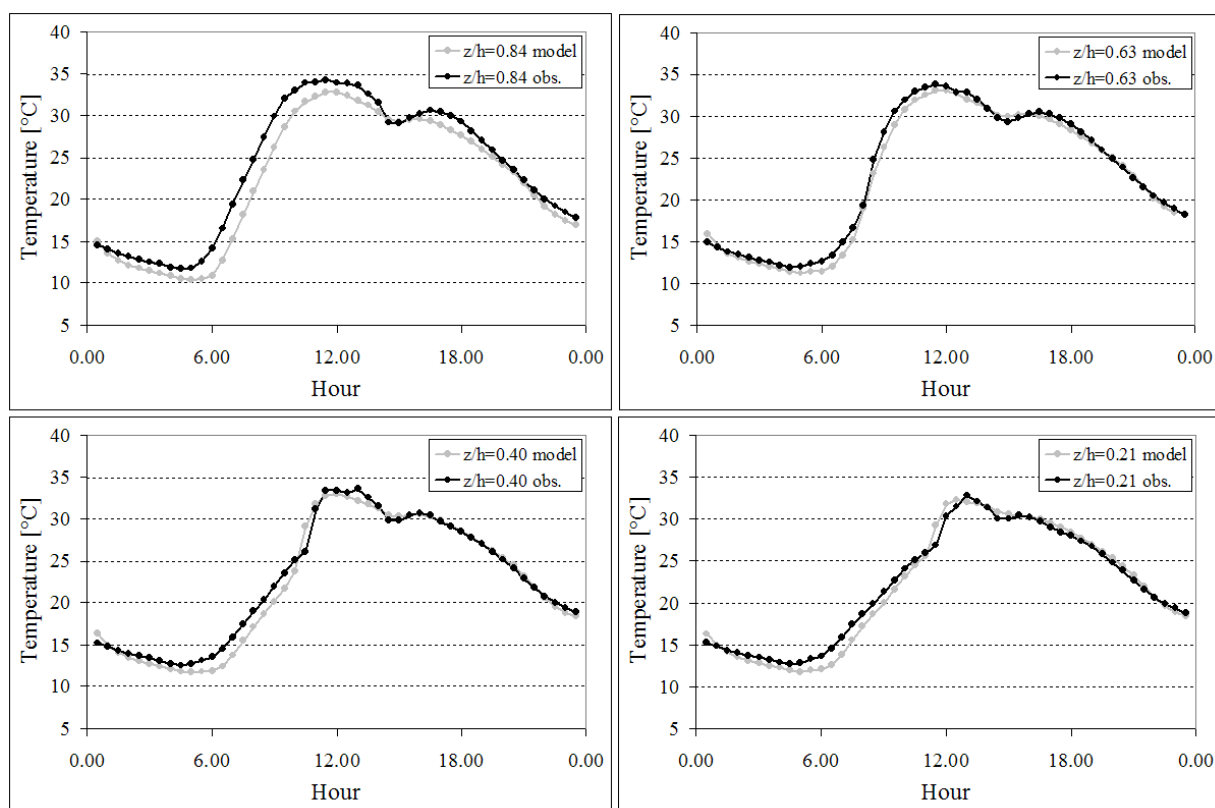
Figure 4.7: Comparison between the south wall temperatures measured at different heights during a sunny day of the ATREUS-PICADA experiment (black) and those simulated by the model (gray).
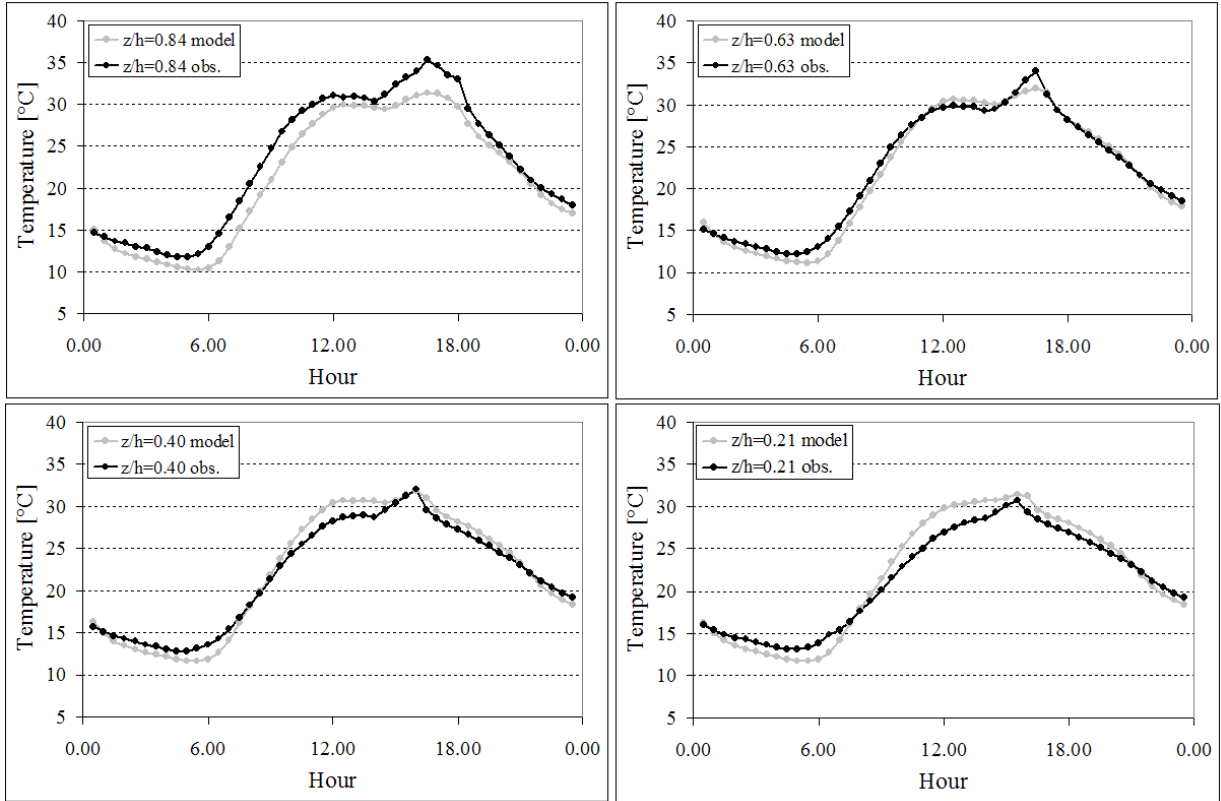
Figure 4.8: As in Fig. 4.7, but for the north wall.

The comparison between the wall temperatures simulated by the model and those measured during a sunny day of the ATREUS-PICADA experiment is shown in Fig. 4.7 and in Fig. 4.8 for the south and north walls respectively. It can be seen that the model reproduces reasonably well the principal features of the daily cycles, including the primary peak caused by direct solar radiation and the secondary peak due to reflections and emissions from the opposite wall. The mean absolute error ($MAE = \frac{1}{n} \sum_{i=1}^{n} |f_i - y_i|$ where f_i is the model result and y_i the observation) of the model is 0.9°C for the south wall and 1.2°C for the north wall. The highest errors are registered at the uppermost measurement points for both walls (the mean absolute errors are 1.6°C and 1.9°C for the south and north walls respectively), where the model constantly underestimates the temperature. During nighttime these errors might be caused by an underestimate of the downward long-wave radiation (minima are underestimated at all the measurement points), while during daytime the heating of the steel roof of the container, factor not taken into account by the model, might play a role.

When a wall is not lit by direct solar radiation, the model provides a wall temperature slightly increasing from the roof down to ground level. This behavior is caused by the fact that the lower parts of the walls receive the highest amount of reflections and emissions from

the opposite wall and from the ground, due to the highest view factors. The experimental results confirm this behavior on the south wall, where, apart from underestimating the highest measurement point, the agreement between simulations and observations looks very good. On the other hand on the north wall observations show an opposite behavior, with the highest temperatures near the roof. As a consequence, the model overestimates the temperature at the two lowest measurement points in the morning and in the first part of the afternoon.

4.4.2 Comparison with measurements in the real urban canyon
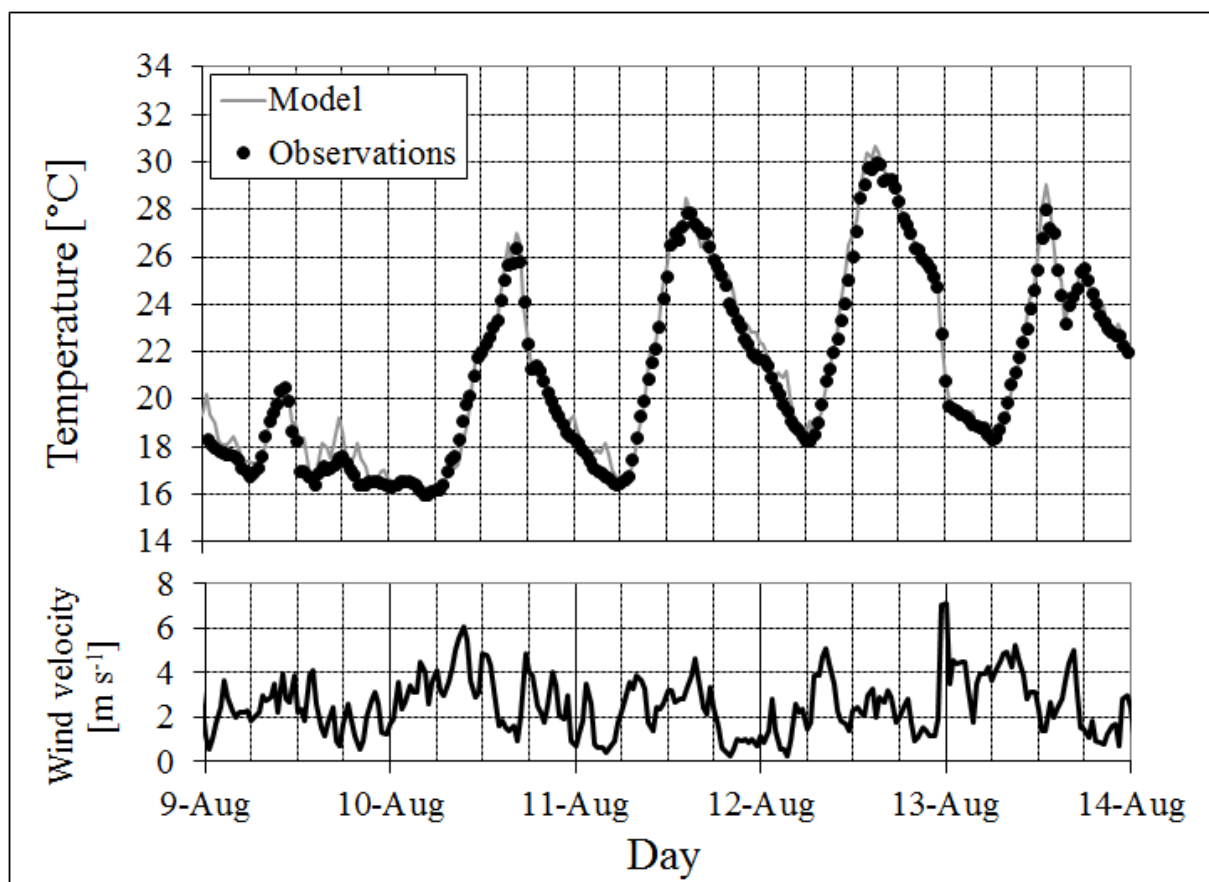
Figure 4.9: Comparison between the temperatures measured inside the canyon (black dots) and those simulated by the model (gray line) during five consecutive days of the summer field campaign, along with wind velocity measured at Molino Vittoria (lower panel).

The comparison between the model results and the observations during five consecutive days of the summer field campaign is shown in Fig. 4.9, along with wind speed measured at Molino Vittoria. 9 August was a rainy day, 10, 11 and 13 August were partly cloudy days, while 12 was sunny. At a first glance it can be seen that the model generally simulates very well the
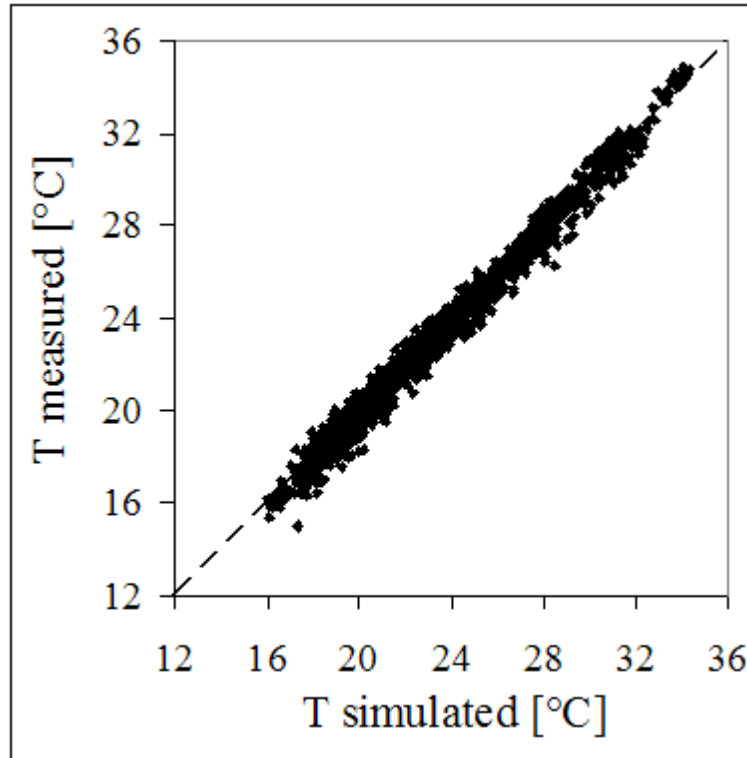
Figure 4.10: Scatterplot of the air temperature inside the urban canyon measured and simulated by the model for all the summer field campaign.

air temperature inside the urban canyon over the whole period of changing weather conditions. There are only some overestimates in low wind speed conditions, when the heat exchange between the canyon and the atmosphere above, as simulated by the model, is too low (the heat exchanged is proportional to the wind velocity, see Eq. (4.29)), with a consequent overheating of the canyon air. Nevertheless it is noticeable that, taking into account all the summer field measurements, the mean absolute error of the model is only 0.4°C. The model simulates better minima than maxima, with mean absolute errors of 0.4°C and 0.5°C respectively. In Fig. 4.10 the scatterplot of the measured and simulated temperatures during the whole summer measurements is presented. The agreement between measured and simulated temperatures appears very satisfactory for all the data available from the field experiment: most of the data are within 0.5°C and the maximum errors are few overestimates of order 2°C.

Figure 4.11 shows the comparison between the model results and the measurements during five consecutive days of the winter field campaign. Again days with different weather conditions have been chosen: 6, 7 and 8 January were cloudy days, while 9 and 10 January were sunny. It can be seen that the model is able to simulate with a good accuracy, even better than during the summer period, the average temperature inside the urban canyon. In fact the mean absolute
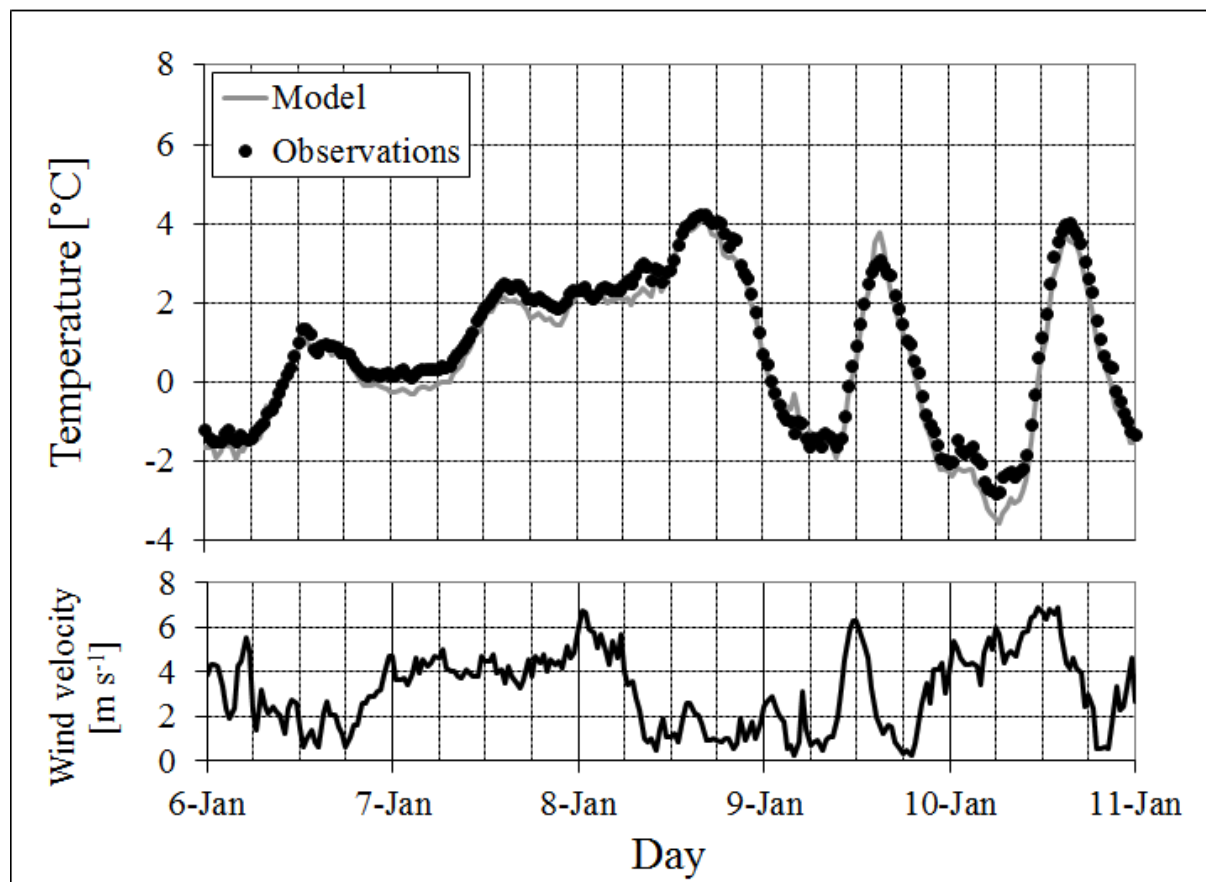
Figure 4.11: As in Fig. 4.9, but for five consecutive days of the winter field campaign.

error of the model during the whole winter field campaign is 0.3°C. Also in this case minima are simulated better than maxima, with mean absolute errors of 0.3°C and 0.4°C respectively. The good performance of the model during the whole winter field campaign is confirmed also in this case by the scatterplot in Fig. 4.12, where all the measurements and the simulated temperatures are compared. It can be seen that the model tends to slightly underestimate low temperatures, as can be partly observed also in Fig. 4.11. The greatest errors are few overestimates of order 1.5°C, again registered in low wind speed conditions.

4.4.3 Surface energy balance

Apart from direct comparison of measured and simulated air and wall temperatures, it is interesting to inspect how the model simulates the daily cycles of the heat fluxes. Although no data for these variables were available from the experimental datasets used in this work, yet some comparisons can be made with similar cases reported in the literature. The results presented in this Section refer to the real canyon test case and the surface fluxes are calculated as they
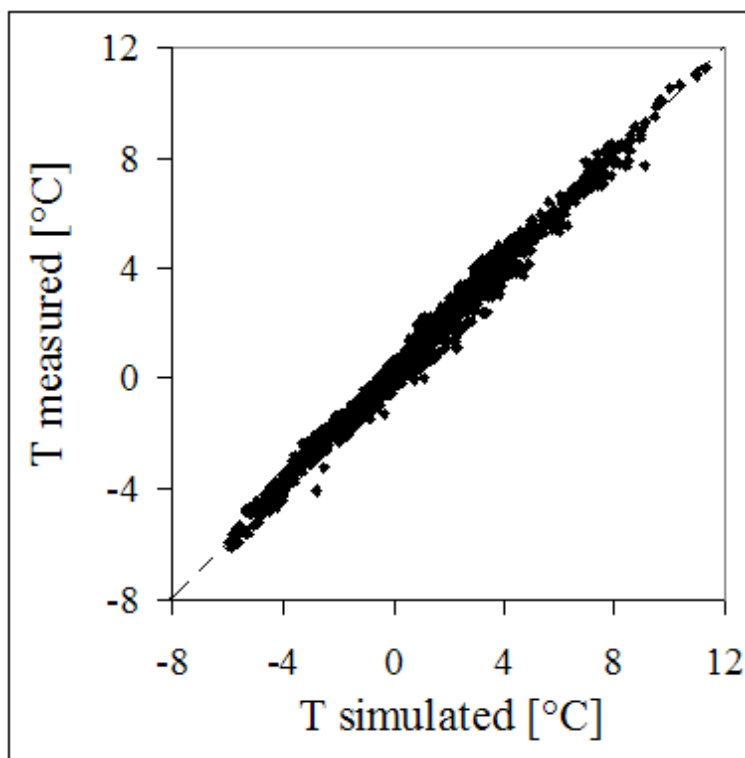
Figure 4.12: As in Fig. 4.10 , but for the winter field campaign.

arise from an area having the geometrical characteristics of Via Rosmini. Figure 4.13a shows the average daily cycle of the surface energy budget during the sunny days of the summer field measurements. It can be seen that the storage heat flux is the dominant component of the surface energy budget, as was also found in different field measurements in dense urban areas (e.g. Oke et al. 1999 in Mexico City). Another typical feature of the surface energy budget in urban areas (e.g. Coutts et al. 2007), well captured by the model, is the asymmetry of the peaks in the storage and sensible heat fluxes terms: the former peaks around noon, while the latter in the early afternoon. Furthermore the sensible heat flux remains positive even during nighttime, supported by the heat released by the surfaces. The results for the sunny days of the winter field measurements are presented in Fig. 4.13b. In this case in the central part of the day the sensible and the storage heat fluxes display comparable values, and the asymmetry in their peaks is not present. Furthermore, similarly to what observed and simulated with the TEB single-layer model (Masson 2000) during the winter period by Pigeon et al. (2008) in Marseille, during nighttime the sensible heat flux presents higher values than in the summer period, probably due to releases from space heating.
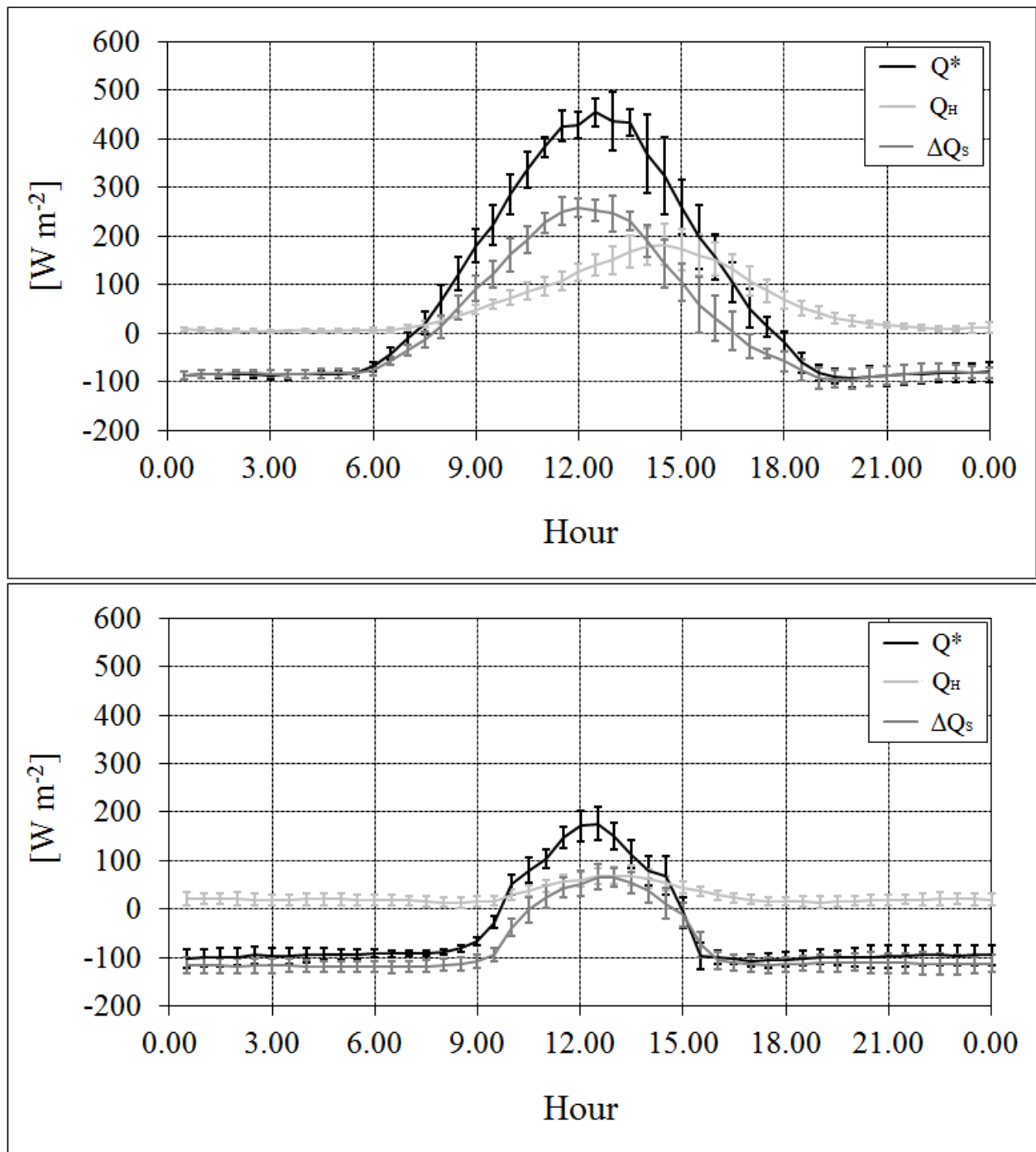
Figure 4.13: Average daily cycles of the surface fluxes calculated by the model during the sunny days of the (a) summer and (b) winter field measurements. The vertical bars represent the standard deviation.

4.5   Conclusions

The results of two experimental field campaigns, carried out inside an urban street canyon in the center of the city of Trento (Italy) in the summer 2007 and in the winter 2008-2009,

have been analyzed to characterize the temperature field in the urban canopy and to validate a simple urban canyon model, similar to the single-layer model proposed by Kusaka et al. (2001). Moreover the performances of the model have been further tested with wall temperature measurements collected in a physical model during the ATREUS-PICADA experiment.

The results of the field measurements confirmed that the microclimatic conditions inside an urban canyon are strongly influenced by the penetration of direct solar radiation inside the canopy and the consequent surface heating. In fact during sunny days the highest temperatures are measured by the east-facing sensors in the morning, whereas in the afternoon by the west-facing ones. Only in the winter period the overheating of the east-facing sensors in the morning is very low, as the wall is hit by the sun for a short time and the morning solar radiation in this period is very weak. Also the heating of the road seems to play a role in the air temperature distribution inside the canyon. In fact during daytime, especially when both sensors on the same wall are hit by direct solar radiation, in the summer period the HOBO at a lower height records higher temperatures (about 0.5°C) than the other instrument on the same wall. For this reason it can be supposed that maxima inside the canyon are reached near ground level in summer, as pointed out by Kanda et al. (2005). When solar radiation is absent, i.e. during the night or in cloudy or rainy days, the temperatures registered by the instruments in the canyon are similar, in most of the cases within the instrumental accuracy. The temperature in the center of the street, not influenced by any surface, is always similar to that registered by the sensors in shade. This fact suggests that the temperature field inside the urban canyon is quite homogeneous horizontally, with stronger gradients only near the sunlit surfaces.

The air temperature measurements taken at an automatic weather station above roof level, close to the instrumented street, have also been analyzed in order to evaluate the temperature differences with the canopy layer. The temperature inside the street is generally higher than above roof level, both in summer and in winter. Higher differences are found during the summer period, also in this case probably due to the stronger overheating of the walls and of the road, similarly to the results found by Offerle et al. (2007) in an urban canyon in Gothenburg, Sweden. The average temperature differences between the air above roof level and inside the street are 1°C in summer and 0.5°C in winter. In Chapter 3 it was shown that the UHI intensity, calculated as the temperature difference between the weather station above roof level and measurements collected at rural locations, may reach values up to 5-6°C during clear nights with low wind speeds. The results of the urban canyon field campaigns suggest that the UHI inside the canopy layer can be even stronger, with a consequent serious discomfort for the citizens, especially during summer evenings and nights.

As to the validation of the single-layer urban canyon model, the results suggest that the simple numerical scheme is able to simulate with good accuracy both wall and air temperatures inside the canopy layer, especially when considering the low level of complexity of the numerical code and the simplifications made. This conclusion is in agreement with the findings of Grim-

mond et al. (2011) from an intercomparison of different urban surface energy balance models: in particular they pointed out that also simple schemes display good performances, stating also that an increased model complexity does not necessarily lead to an increase in the performance of the model. As to the air canyon temperature, the agreement between the measurements performed during the two field campaigns and the numerical results is good both during the summer and the winter periods and in different weather conditions. However the model shows some weaknesses in low wind speed conditions, when the numerical scheme tends to overestimate the air temperature. This behavior is probably to be attributed to the parameterization of the heat exchange between the canyon air and the atmosphere above roof level, which is proportional to the wind velocity.

The comparison with the wall temperatures measured in the 1:5-scaled street canyon of the ATREUS-PICADA project, demonstrates that the model is able to reproduce reasonably well also the daily cycles of wall temperatures. The model performs better for the south wall, where there is only an underestimate of the temperature at the highest measurement point. However some minor problems affect the simulation of the north wall temperatures. According to the observations, the temperature of the wall increases from ground level up to the top, while the model results show an opposite behavior. This is due to the fact that in the model the lower parts of the wall receive a greater amount of the radiation emitted and reflected from the opposite wall and from the ground, due to the high view factors. Further tests on different datasets might highlight if the problem found is due to local effects not taken into account by the model (for example the heating of the steel roof might play a role in the underestimate in the highest part of the walls) or if it is caused by an imperfect characterization of the reflections inside the canyon or by an overestimate of the ground temperature. However it is noticeable that the accuracy of the results obtained with the simple urban canyon model is comparable to that obtained with the more complicated 3D finite elements model utilized in Idczak et al. (2010). In particular, also in Idczak et al. (2010) the temperature was underestimated at the top of both walls and overestimated at the lowest measurement points of the north wall.

Chapter 5

Characterization of daily-periodic circulations in Alpine valleys

Mountain valleys are often characterized, especially during fair weather days, by daily-periodic local circulation systems, developing in both the along-valley and cross-valley directions. The first scientific studies on this topic date back to 1920's and 30's, and were carried out mainly by Austrian and German meteorologists. Observational, theoretical and modeling studies (cf. Whiteman 1990; Zardi and Whiteman 2011 for a review) have then grown in the last decades, especially in view of the important practical applications in several different fields, ranging from detailed weather forecasts for tourism or agriculture, to climatological analyses in mountain areas, to the transport and diffusion of air pollutants, just to cite a few (cf. Zardi and Whiteman 2011). The latter application is particularly important in densely urbanized valleys, as is the case of the Adige Valley, with several urban areas and major roads that run in the quite narrow valley floor, connecting the Po Plain to Central Europe.

In the present Chapter the development of local circulation systems in the Alpine valleys around the city of Trento is investigated on the basis of a dataset from surface weather stations from the Provinces of Verona, Trento and Bolzano, covering the period 2004-2011 (Fig. 5.4). Particular attention is given to the evaluation of the main features of the along-valley wind in the Adige, Sarca and Lakes valleys, highlighting the substantial differences between the "combined" valley/lake wind system blowing in the Sarca and Lakes valleys and the regular valley wind system in the Adige Valley.

5.1 Diurnal valley wind systems: basic concepts

Daily-periodic thermally-driven local circulation systems in valleys can basically be divided into two categories: slope winds, blowing along sidewall slopes, i.e perpendicular to the valley axis, and along-valley winds, parallel to the valley longitudinal direction. Slope winds are generated

by the buoyancy forces arising from the heating/cooling of the air close to the valley slopes; they are generally up-slope (anabatic) during daytime and down-slope (katabatic) during nighttime. They react almost instantly to changes in the insolation: up-slope winds start few minutes after sunrise, while down-slope winds few minutes after sunset. The depth of the down-slope flow layer ranges generally between 3 and 100 m, with maximum velocities of order 1-4 m s^{-1}, while the upslope flow layer has a depth of 20-200 m and a maximum wind speed of 1-5 m s^{-1} (Zardi and Whiteman 2011). The along-valley winds, which typically blow up-valley during the day and down-valley at night, are generated by the horizontal pressure gradients due to the temperature differences between different cross sections of the valley or between the valley and the adjacent plain. In fact the diurnal temperature range is generally larger in valleys than over plains (Whiteman 1990).

The typical daily cycle of valley and slope winds is well represented by the classical Defant's (1949) scheme (Fig. 5.1):

(A) dawn: onset of up-slope winds, the down-valley wind continues from the night;

(B) morning: up-slope winds, transition from down-valley to up-valley;

(C) noon: weakening of up-slope winds, up-valley wind fully developed;

(D) late afternoon: up-slope winds cease, the up-valley wind continues;

(E) evening: onset of down-slope winds, weakening of the up-valley wind;

(F) first part of the night: well developed down-slope winds, transition from up-valley to down-valley;

(G) central part of the night: down-slope winds continue, well developed down-valley wind;

(H) last part of the night: down-slope winds cease, down-valley wind continues.

It can be noticed that the valley wind reversal lags that of the slope flows both after sunrise and after sunset. This lag is due to the fact that the whole valley air volume must be heated or cooled before the pressure gradient can reverse.

The larger temperature range in valleys, which causes the alternating down- and up-valley winds, is generally explained with geometric factors. In fact during daytime in a valley a given amount of energy is used to heat a smaller volume than over a plain, due to the presence of the valley slopes, with a consequent overheating of the valley air (Whiteman 1990). Similarly at night the same loss of energy cools a smaller volume, resulting in lower temperatures in the valley. This concept was first proposed by Wagner (1932) and can be quantified with the Topographic Amplification Factor (TAF) τ:
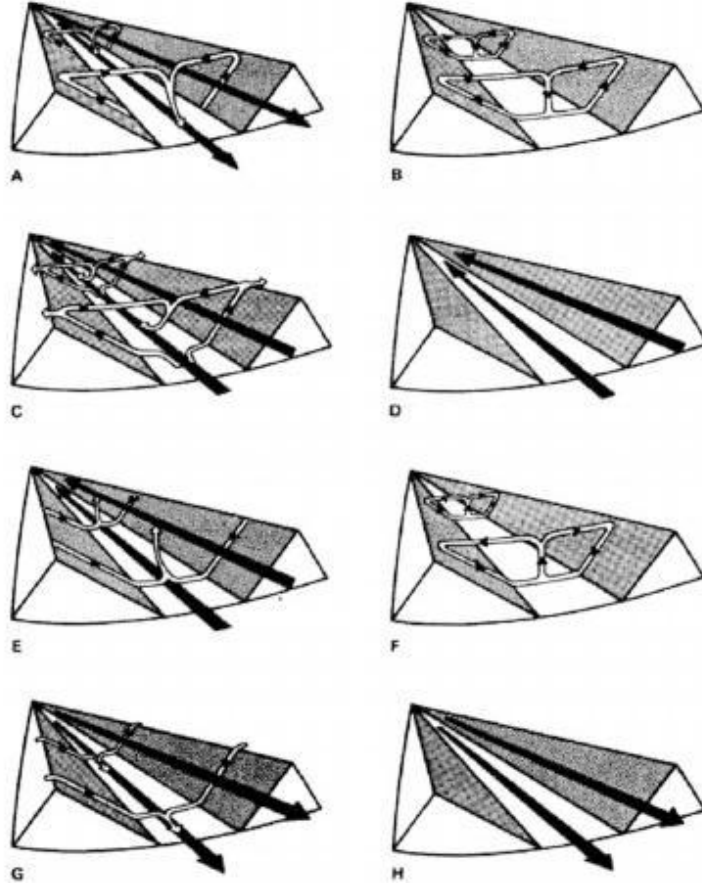
Figure 5.1: Schematic diagram showing the diurnal cycle of slope and valley winds (Defant 1949).

$$\tau = \frac{\left[\frac{A_{xy}(h)}{V_{valley}}\right]}{\left[\frac{A_{xy}(h)}{V_{plain}}\right]} \qquad (5.1)$$

where A_{xy} is the horizontal area through which energy enters at height h, V_{valley} is the valley air volume and V_{plain} is the plain air volume. The assumption made is that no heat is exchanged with the atmosphere above the valley (Schmidli and Rotunno 2010). However recent investigations (e.g. Rampanelli et al. 2004, Weigel et al. 2006) showed that this assumption is generally not true. In particular Rampanelli et al. (2004) highlighted the important role of subsidence in warming the valley core. The subsidence in the center of the valley during daytime is caused by the return flow induced by up-slope winds, which in turn export heat above the valley top, reducing the heating of the valley.

Following Schmidli and Rotunno (2010), the Reynolds-averaged momentum equation for the along-valley wind can be written as follows (neglecting the Coriolis force and assuming an

horizontal valley floor):

$$\frac{\partial v}{\partial t} = -\frac{1}{\rho}\frac{\partial p_l}{\partial y} - \frac{1}{\rho}\frac{\partial p_h}{\partial y} - \mathbf{v}\cdot\nabla v - \frac{1}{\rho}\nabla\cdot\mathbf{T}_v \qquad (5.2)$$

where p_h is the contribution to surface pressure from upper levels, p_l the contribution from lower levels and $\mathbf{T}_v$ is the turbulent flux of along-valley momentum. It can be seen that the rate of change of the along-valley velocity is associated with upper and lower levels pressure gradients or with advective and turbulent transport of along-valley momentum. If the advective term can be neglected, then the rate of change of the along-valley velocity depends only on the balance between pressure gradients (active force) and turbulent fluxes (resistances).

5.2 Diurnal valley wind systems in the valleys around Trento: characterization from early works

Various works investigated some of the main features of daily-periodic local circulation systems in the valleys surrounding Trento (de Franceschi et al. 2002; Santin 2007; Bee 2010), but a comprehensive study has not yet been performed. The Adige Valley, where the city of Trento lies (Fig. 5.4), is roughly north-south oriented and connects the Po Plain to the city of Merano. The valley is 160 km long with an average slope of about 1.25‰. The altitude of the valley floor ranges from 100 m MSL at the end in the Po Plain to 300 m MSL at Merano. During sunny days a well developed valley wind system occurs throughout the Adige Valley, and consists in a light down-valley wind during nighttime till early morning, and a stronger up-valley wind in the afternoon and in the evening.

Also the Sarca Valley is roughly north-south oriented and starts from the north shores of Lake Garda, which is the largest lake in Italy. The Lakes Valley is geographically connected to the Sarca Valley one one side, while on the other joins the Adige Valley through an elevated saddle at about 400 m above the Adige Valley floor (Fig. 5.4). Sarca and Lakes valleys are about 50 km long with an altitude ranging from 70 m AGL on the shores of Lake Garda to 500 m AGL above the saddle where the Lakes Valley joins the Adige Valley. The local circulation in the Sarca and Lakes valleys is strongly affected by Lake Garda. In the early morning a typical lake breeze front develops from Lake Garda and propagates north through the valley. This wind, named "Ora del Garda", goes up in the Sarca and Lakes valleys during the day, and in the early afternoon reaches the Adige Valley through the above mentioned elevated saddle, north-west of Trento, interacting with the local up-valley wind (Fig. 5.2). For this reason, following the Ora del Garda outbreak into the Adige Valley, in the early afternoon the wind direction in the middle of the valley north of Trento rapidly turns from the previous 180°N (normal up-valley wind) to 270°N, becoming stronger and persistent till a couple of hours after sunset.

As can be seen from the scheme proposed by de Franceschi et al. (2002) in Fig. 5.2, after

Figure 5.2: Schematic representation of the interaction between the up-valley wind in the Adige Valley and the Ora del Garda north of Trento (de Franceschi et al. 2002).
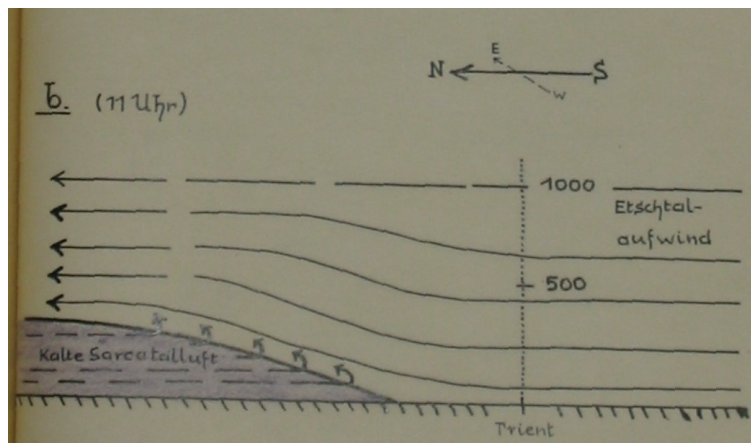
Figure 5.3: Picture representing the along-valley section of the Adige Valley in the area north of Trento, with the interaction between the Ora del Garda blowing from the Lakes Valley and the up-valley wind in the Adige Valley, as proposed by Schaller (1936).

arriving into the Adige Valley the Ora del Garda partly channels northward, joining the local up-valley wind, but partly flows southward, i.e. in the opposite direction with respect to the local up-valley wind. Therefore it can be argued that the northern part of the city is influenced by the interaction between these two opposing circulations. Indeed there are quantitative observations supporting this idea, but a comprehensive study on this phenomenon has not yet been performed. Schaller (1936) investigated the interaction between the Ora del Garda and

the up-valley wind in the Adige Valley with measurements with balloons, proposing the scheme shown in Fig. 5.3. According to Schaller (1936), the up-valley wind in the Adige Valley flows over the cooler air flowing down the saddle and originating from Lake Garda, which reaches a depth of about 300 m in the area north of Trento.

5.3 Weather stations analyzed
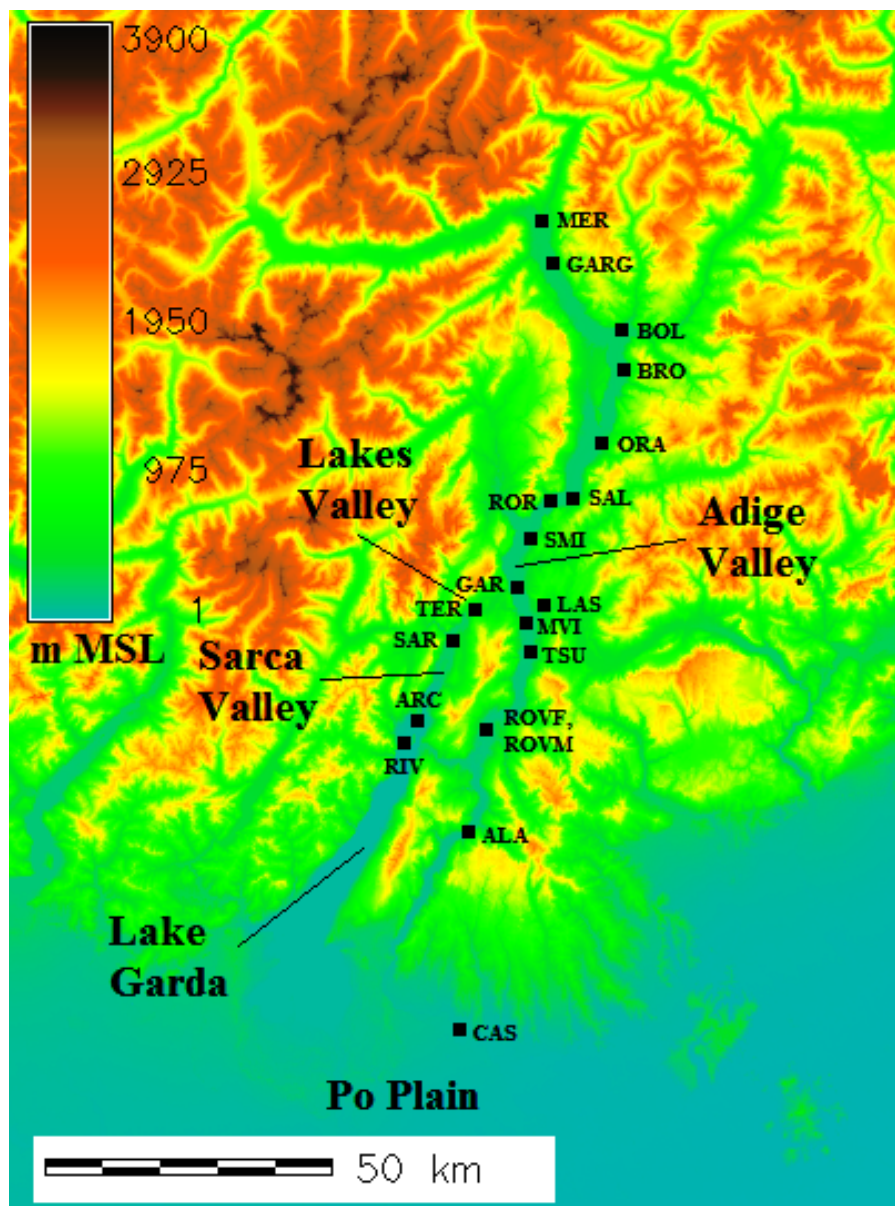
Figure 5.4: Weather stations utilized for the analyses presented in this Chapter.

Table 5.1: Weather stations along with their coordinates, altitude, data time period, and measurements used for the analyses presented. WV = wind velocity; WD = wind direction; P = pressure. * indicates wind measurements at 3 m AGL instead of the standard 10 m AGL of all the other stations.

ORGANIZ.	STATION NAME	COORD. (lat,lon)	ALTITUDE (m MSL)	PERIOD	SENSORS			LABEL
					WV	WD	P	
FEM	ALA	45°47' N 11°01' E	172	2004-2011	X	X	X	ALA
	ARCO	45°55' N 10°53' E	84	2004-2011	X	X		ARC
	GARDOLO	46°07' N 11°06' E	197	2004-2011	X*	X*		GAR
	RIVA DEL GARDA	45°53' N 10°51' E	66	2004-2010	X	X		RIV
	ROVERE' DELLA LUNA	46°15' N 11°11' E	220	2004-2009	X	X		ROR
	ROVERETO	45°53' N 11°01' E	170	2004-2011	X	X		ROVF
	S. MICHELE ALL'ADIGE	46°11' N 11°07' E	204	2004-2011	X	X		SMI
	SARCHE	46°02' N 10°57' E	248	2010-2011	X*	X*		SAR
	TERLAGO	46°05' N 11°03' E	428	2011	X*	X*		TER
	TRENTO SUD	46°01' N 11°08' E	185	2004-2011	X	X	X	TSU
METEO TRENTINO	ROVERETO	45°54' N 11°03' E	203	2005-2006 2011	X	X	X	ROVM
	TRENTO LASTE	46°04' N 11°08' E	312	2004-2011	X	X		LAS
IDR BZ	BOLZANO	46°30' N 11°19' E	254	2006-2011	X	X	X	BOL
	BRONZOLO	46°24' N 11°19' E	226	2008-2011	X	X	X	BRO
	GARGAZZONE	46°35' N 11°12' E	290	2004-2011	X	X	X	GARG
	MERANO	46°40' N 11°09' E	324	2004-2011	X	X	X	MER
	ORA	46°21' N 11°18' E	250	2004-2010	X	X	X	ORA
	SALORNO	46°14' N 11°11' E	212	2009-2011	X	X	X	SAL

5. Characterization of daily-periodic circulations in Alpine valleys

ORGANIZ.	STATION NAME	COORD. (lat,lon)	ALTITUDE (m MSL)	PERIOD	SENSORS			LABEL
					WV	WD	P	
ARPAV	CASON	45°28' N 10°55' E	91	2004-2011	X	X	X	CAS
UNITN	MOLINO VITTORIA	46°03' N 11°06' E	224	2004-2011	X	X	X	MVI

The dataset used to analyze the main features of local circulation systems in the valleys around Trento has been composed collecting data from several surface weather stations located in the Provinces of Verona, Trento and Bolzano and operated by various agencies, as shown in Tab. 5.1. The stations located in the Province of Verona are operated by ARPAV (the environmental agency of the Veneto Region), those in the Province of Trento by MeteoTrentino, i.e. the Meteorological Office of the Autonomous Province of Trento, the Edmund Mach Foundation (FEM) and the University of Trento (UNITN). Finally the stations in the Province of Bolzano are operated by the Meteorological Office of the Autonomous Province of Bolzano (IDR BZ). The dataset used covers rather completely the time period 2004-2011.

The stations operated by ARPAV and the Edmund Mach Foundation provide hourly-averaged data, those operated by MeteoTrentino 15-min averaged data, while Molino Vittoria, operated by the University of Trento, and the stations operated by the Meteorological Office of the Autonomous Province of Bolzano provide 10-min averaged data. As can be seen from Tab. 5.1, most of the wind measurements are taken at the standard height of 10 m AGL, but some stations provide values of wind velocity and directions registered at 3 m AGL. In these cases the following expression has been used to evaluate wind speed at 10 m:

$$v_h = v_{10}[0.233 + 0.656 \log(h + 4.75)] \tag{5.3}$$

where v_h is the wind speed at a height h [m] and v_{10} is the wind speed at 10 m.

The analysis has focused only on fair weather days, with no appreciable synoptic winds, when valley winds can develop without the influence of any external forcing. Accordingly suitable days have been selected from the days in the months of May, June, July and August with an average cloud cover ≤ 2 oktas. Cloud cover data have been taken from observations at Mount Paganella weather station (Fig. 3.1). From these days 148 "valley wind days" (Vergeiner and Dreiseitl 1987) have been chosen from a direct inspection of wind velocity and direction daily cycles.

5.4 Analysis of local circulations in the Adige Valley

5.4.1 Wind odographs

In order to characterize the general features of local circulation systems in the Adige Valley, wind hodographs were plotted for some of the weather stations analyzed (Figs 5.5-5.15). It can be seen that on the valley floor the wind blows mainly in the along-valley direction, down-valley during the night and in the first part of the morning and up-valley from around mid-morning to the late evening. In fact the wind vectors follow the axis of the valley, which is roughly north-south oriented in all the stations, but Roverè della Luna, where the valley turns and the axis is locally roughly west-east oriented. The only exception is Gardolo, located north of Trento, where a strong cross-valley flow occurs during the afternoon, following the outbreak of the Ora del Garda into the Adige Valley, as described in Section 5.2. The up-valley wind reaches maximum average intensities of order 4-6 m s^{-1} in the late afternoon. Lower velocities, of order 2 m s^{-1}, are recorded at the northernmost stations Bolzano and Merano, and at Molino Vittoria. The behavior at this last weather station is influenced by the interaction between the Ora del Garda and the up-valley wind of the Adige Valley, as it will be investigated in Section 5.6. The down-valley wind is generally quite weak at all the stations, with maximum average velocities of 1-2 m s^{-1}. Stronger intensities are registered only at Molino Vittoria in the early morning (Fig. 5.8). However it is worth remembering that this weather station is located on a tower at 33 m AGL in the urban area. On the other hand at Bronzolo a light up-valley wind seems to blow also during the night. The weather stations placed close to the valley sidewall or near a junction with a secondary valley register light cross-valley circulations, as is the case of Ala, influenced in the evening by katabatic winds flowing from a secondary valley, and S. Michele all'Adige, reached by down-slope winds flowing from the nearby hills.

Figure 5.15 shows the wind hodograph for Laste weather station, located on the eastern sidewall of the Adige Valley, to give an example of slope winds. It can be seen that a significant down-slope wind occurs at night, while in the morning, between 0800 and 1000 LST a light up-slope wind develops. In the afternoon also this part of the slope (about 100 m above the valley floor level) is influenced by a light up-valley wind.

Figure 5.16 shows, as a summary, all the wind odographs in the Adige Valley, along with the position of the weather stations to which they refer.

5.4.2 Along-valley wind daily cycles

Along-valley wind daily cycles for the weather stations located in the Adige Valley have been analyzed to better characterize the main features of up and down-valley winds. The along-valley directions have been derived from the orientation of the valley in the sections where the weather stations lie. Some weather stations located in the Province of Bolzano were installed recently
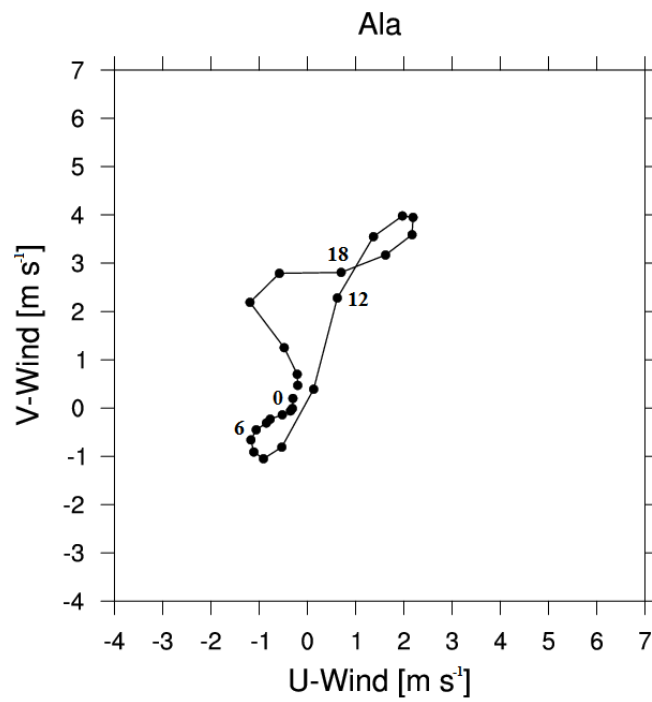
Figure 5.5: Wind hodograph at Ala weather station.
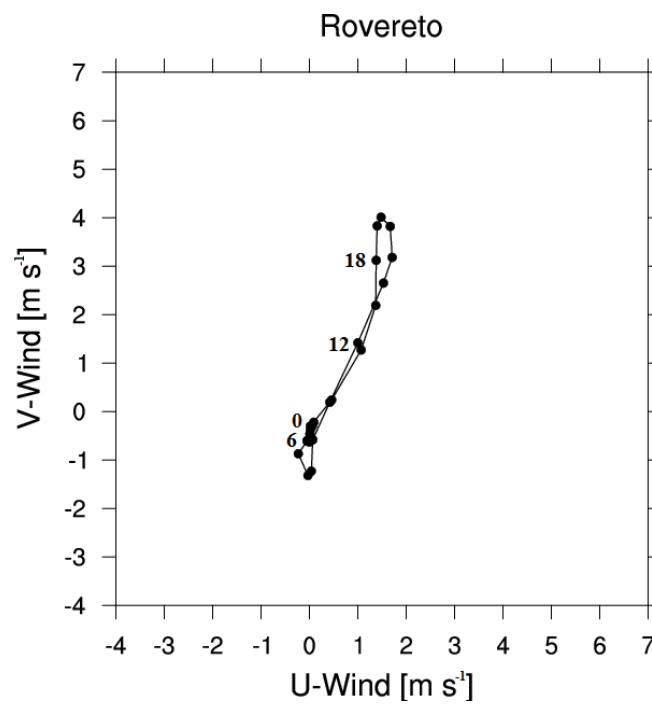
Figure 5.6: As in Fig. 5.5, but at Rovereto IASMA weather station.
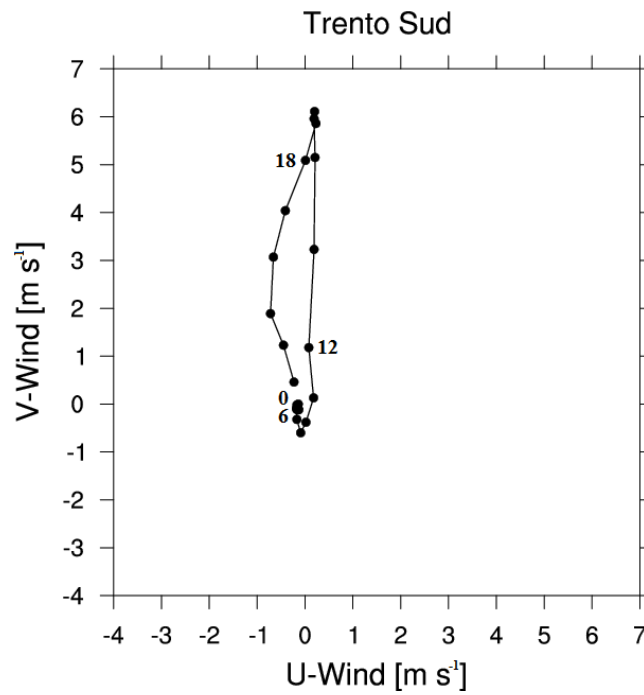
Figure 5.7: As in Fig. 5.5, but at Trento Sud weather station.
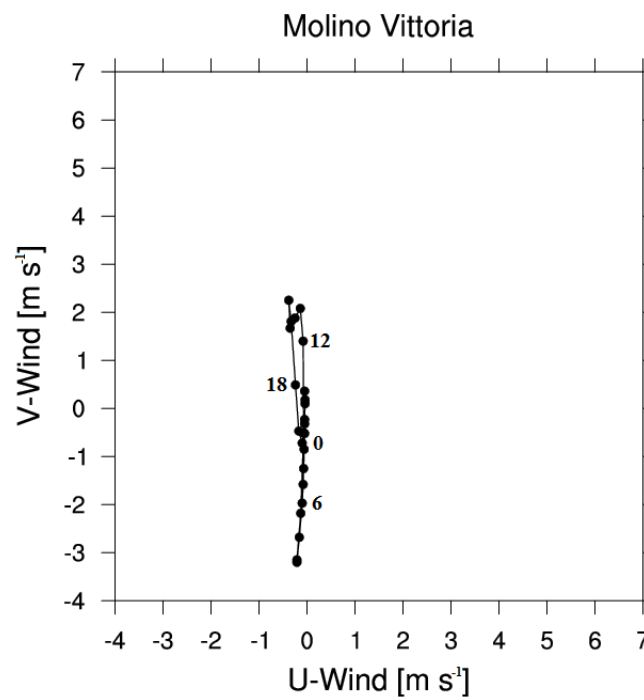
Figure 5.8: As in Fig. 5.5, but at Molino Vittoria weather station.
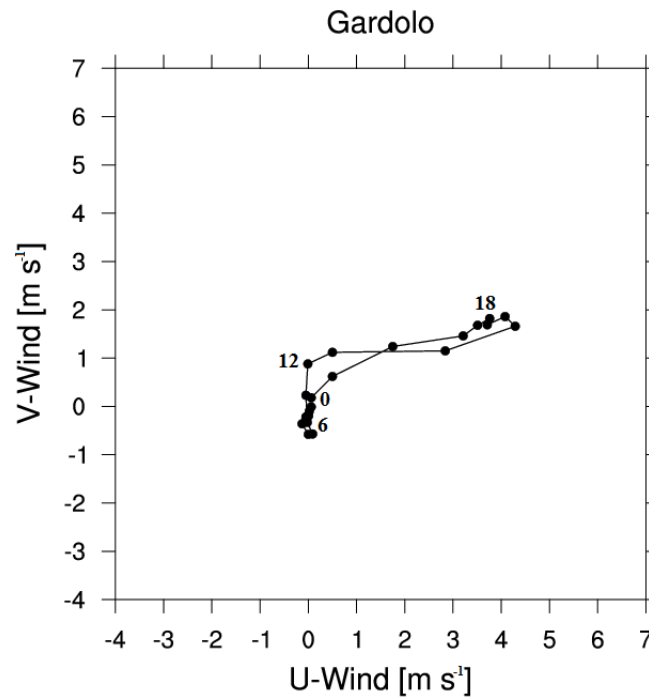
Figure 5.9: As in Fig. 5.5, but at Gardolo weather station.
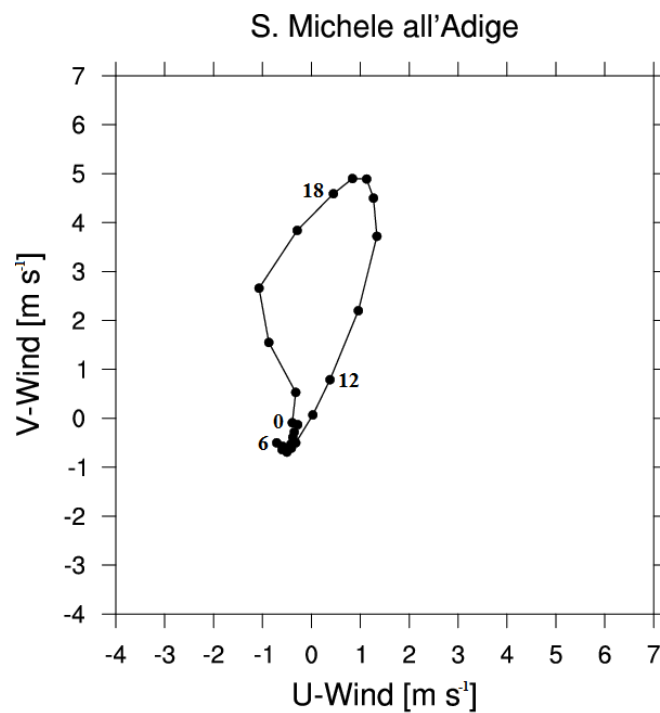
Figure 5.10: As in Fig. 5.5, but at S. Michele all'Adige weather station.
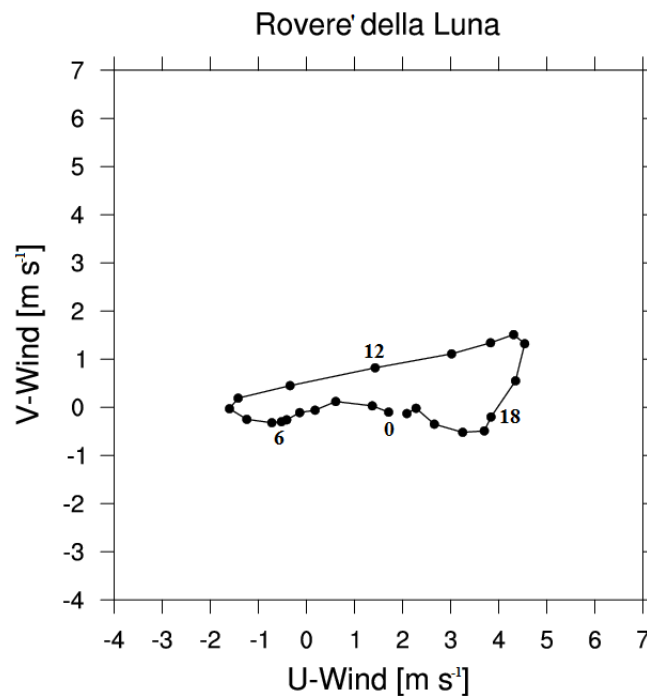
Figure 5.11: As in Fig. 5.5, but at Roverè della Luna weather station.
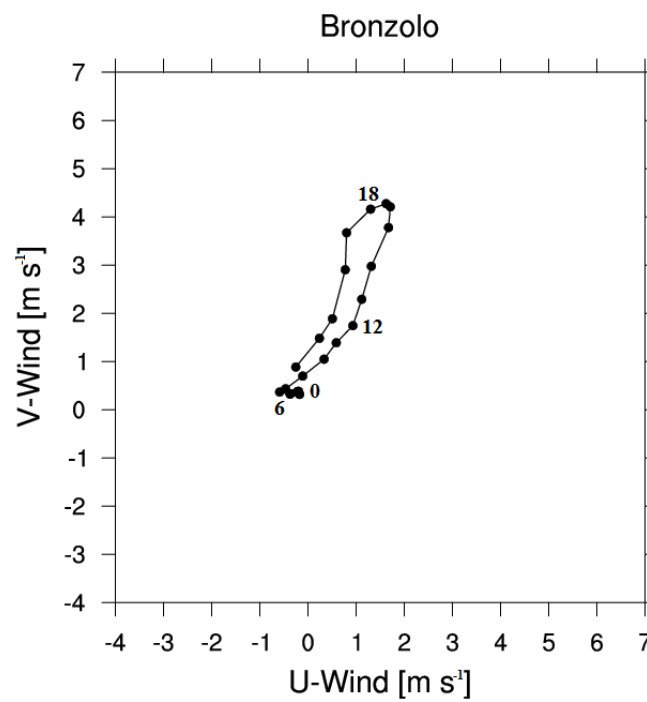
Figure 5.12: As in Fig. 5.5, but at Bronzolo weather station.
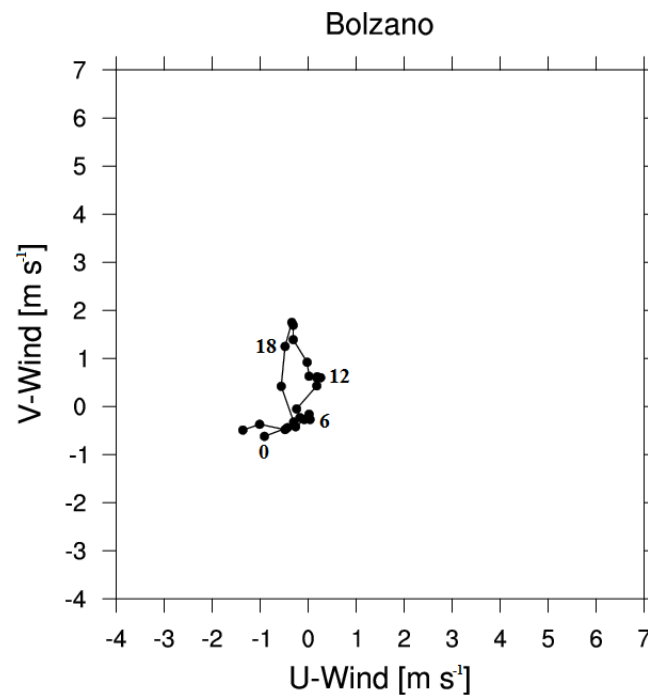
Figure 5.13: As in Fig. 5.5, but at Bolzano weather station.
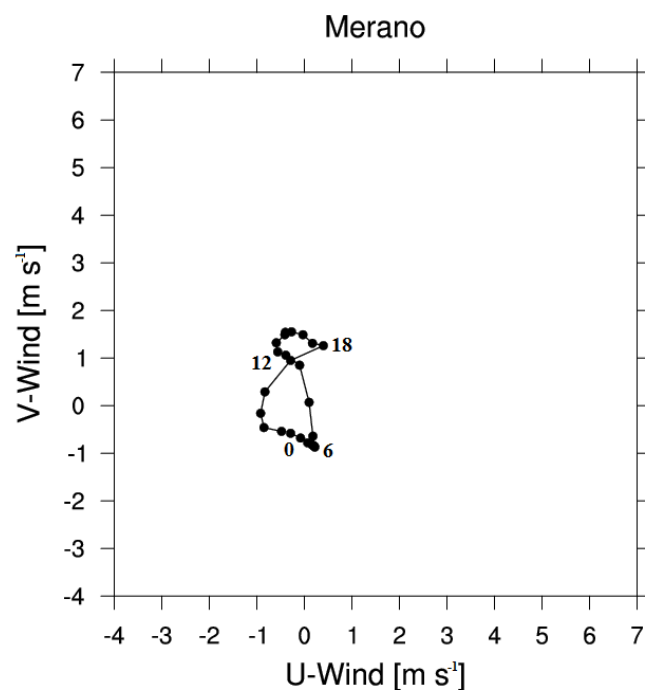
Figure 5.14: As in Fig. 5.5, but at Merano weather station.
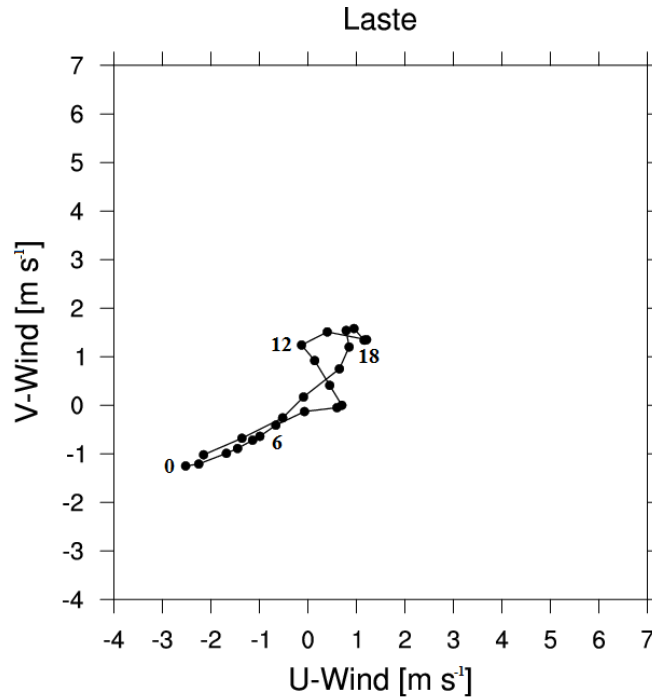
Figure 5.15: As in Fig. 5.5, but at Laste weather station.

(see Tab. 5.1) and for this reason only few "valley wind days" are available from these stations. Therefore in the calculation of the average along-valley wind daily cycles it was decided to separate the weather stations of the Provinces of Trento and Bolzano, so as to utilize a greater number of days for the former stations. Moreover in this way the graphics and the comparisons are clearer. The average along-valley wind daily cycles for the Province of Trento are calculated starting from 111 "valley winds days", while those for the Province of Bolzano using only 12 days. All data presented are hourly-averaged values.

The average daily cycles are very similar for all the stations located in the Province of Trento (Fig. 5.17), with only minor differences. Focusing on the onset of the up-valley wind in the late morning, it seems that it occurs roughly at the same time at all the stations. Only at Ala, the southernmost station, the onset seems to occur slightly earlier than at the other locations, while at S. Michele all'Adige slightly later. Also the maximum wind velocities of both down and up-valley winds are similar, apart from a stronger up-valley wind at Trento Sud. At Roveré della Luna the up-valley wind lasts until 0300 LST.

At the weather stations in the Province of Bolzano (Fig. 5.18) the along-valley wind daily cycles display more variability: three different behaviors can be recognized. At Salorno, the southernmost weather station, the daily cycle is very similar to those found in the Province of Trento. At Bronzolo there is an earlier onset of the up-valley wind in the morning and lower intensities during the afternoon. Moreover at this station, as seen from the wind hodograph, a
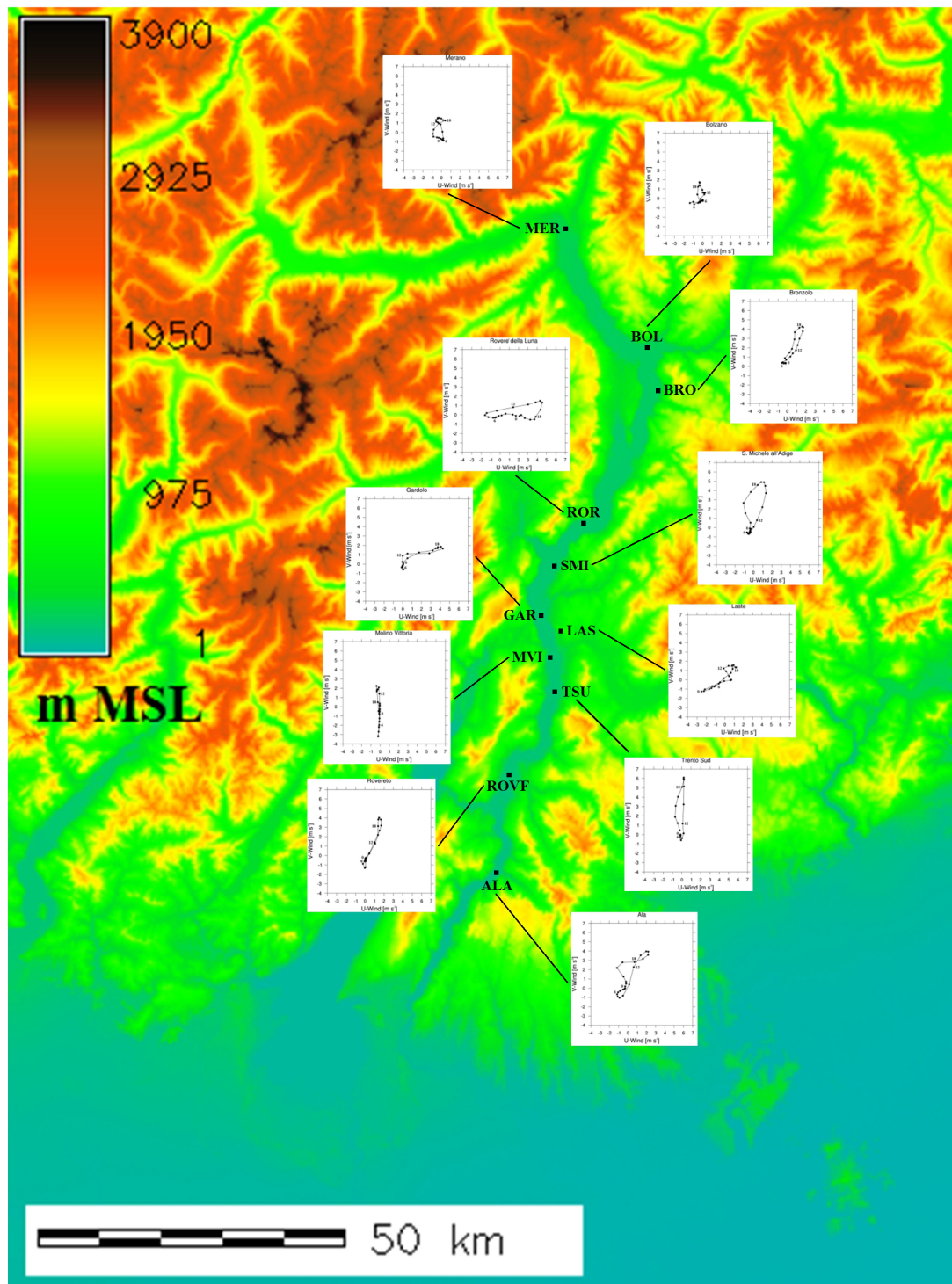
Figure 5.16: Summary of the wind odographs in the Adige Valley, along with the position of the weather stations to which they refer.
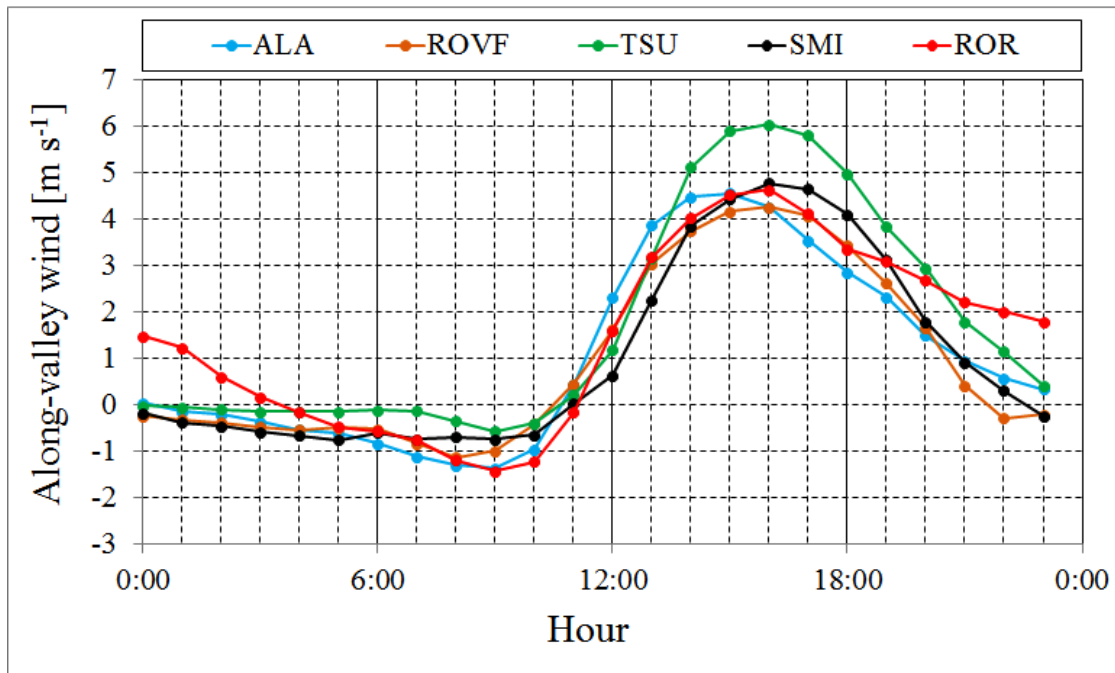
Figure 5.17: Average daily cycles of the along-valley wind during "valley wind days" for several weather stations in the Adige Valley in the Province of Trento.
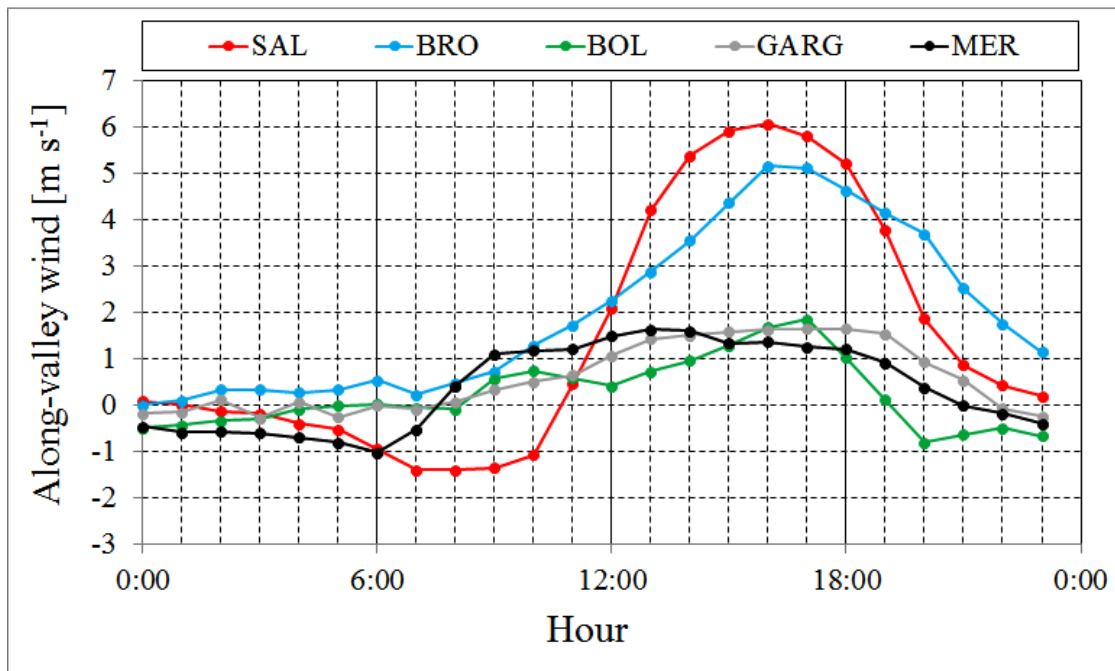
Figure 5.18: As in Fig. 5.17, but in the Province of Bolzano.

light up-valley wind is present also at night. Bronzolo is located north of a bifurcation, where a secondary valley roughly parallel to the Adige Valley originates (Fig. 5.4). This secondary valley is about 15 km long and joins again the Adige Valley in the basin of Bolzano. Starting from the bifurcation, the geometry of the Adige Valley changes substantially. In fact the Adige Valley and the secondary valley are separated only by a low hill, reaching an average height of 400 m above the Adige Valley floor level. South of the fork the distance between the mountains flanking the Adige Valley is about 2.5-3 km, while it becomes larger further north, reaching about 7 km in the basin of Bolzano. Therefore, neglecting the small hill in the middle, the valley becomes considerably larger, with a consequent different behavior of the heating and cooling rates of the valley atmosphere. Moreover it can be supposed that part of the up-valley wind blowing from south channels in the secondary valley, thus contributing to the different along-valley wind daily cycle at Bronzolo with respect to Salorno. The along-valley wind daily cycles in the basin of Bolzano and north of it seem completely decoupled from the situation in the Adige Valley south of the basin. At these weather stations the onset of the up-valley wind occurs earlier than at Salorno, and it remains weak also during the afternoon, as seen from the wind hodographs. The down-valley wind is very weak at Bolzano and Gargazzone, while it is slightly stronger at Merano. As it will be shown in the next Section, where pressure daily cycles are analyzed, it is likely that the basin behaves like a "small plain", thus decoupling the wind behavior north and south of it. Moreover north of the basin of Bolzano the Adige Valley changes from its previous north-south orientation and continues towards north-west, with an average valley floor width of about 2.5 km. After Merano the valley axis changes again orientation and becomes roughly west-east; the penetration of solar radiation inside the valley is therefore different, with a consequent difference in the timing of the heating of the valley atmosphere. These are other geometric factors which may contribute to the different behavior of the along-valley wind daily cycles.

In order to obtain more information about the characteristics of the along-valley wind, the single daily cycles during the "valley wind days" have also been analyzed. Here some examples are shown, along with comments about the recurrent features found. The variability of the single daily cycles is not very marked, and for this reason the average values can be considered representative of the phenomenon, even though some minor differences between the single days can be appreciated. Focusing on the onset of the up-valley wind in the Province of Trento, in some days the up-valley phase starts at the same hour at all the weather stations (see Fig. 5.19 for example), while in other cases, as partly highlighted also by the average cycles, the wind reversal occurs 1-2 hours earlier at Ala, the southernmost weather station (see Fig. 5.21 for example). Moreover also at Roveré della Luna in some days the wind reversal happens earlier than at Rovereto, Trento Sud and S. Michele all'Adige (see Fig. 5.21 for example). The earlier onset of the up-valley wind at Roveré della Luna may be caused by the east-west orientation of the valley at this weather station, with a consequent different timing of the morning heating
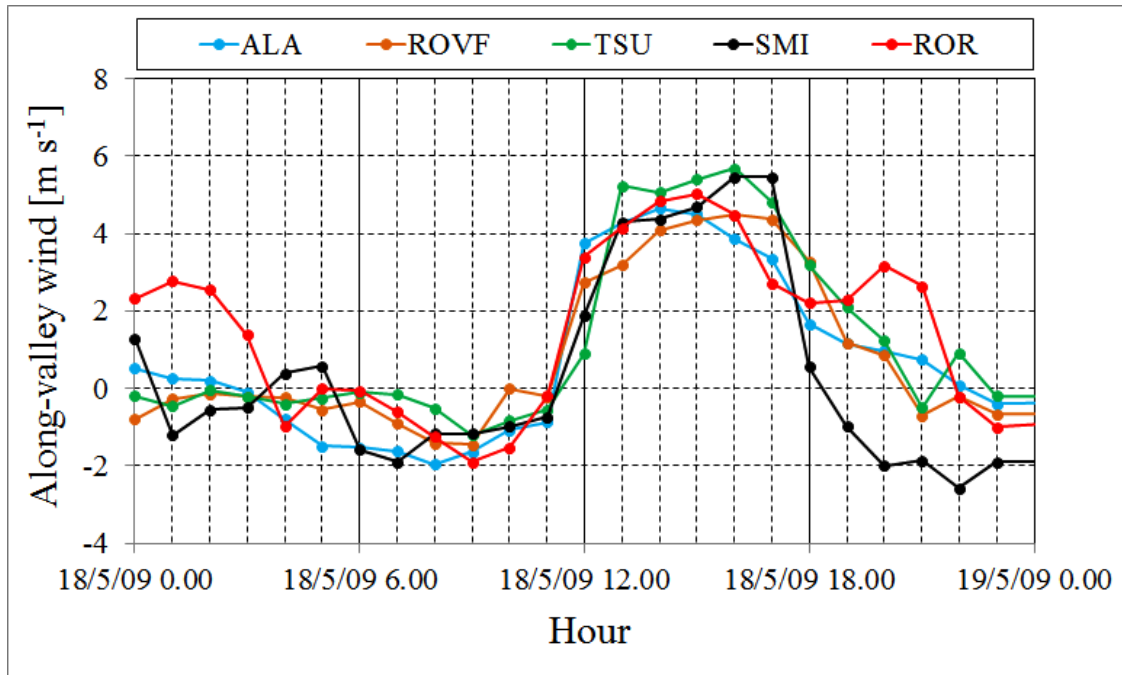
Figure 5.19: Daily cycles of the along-valley wind for 18 May 2009 for several weather stations in the Adige Valley in the Province of Trento.
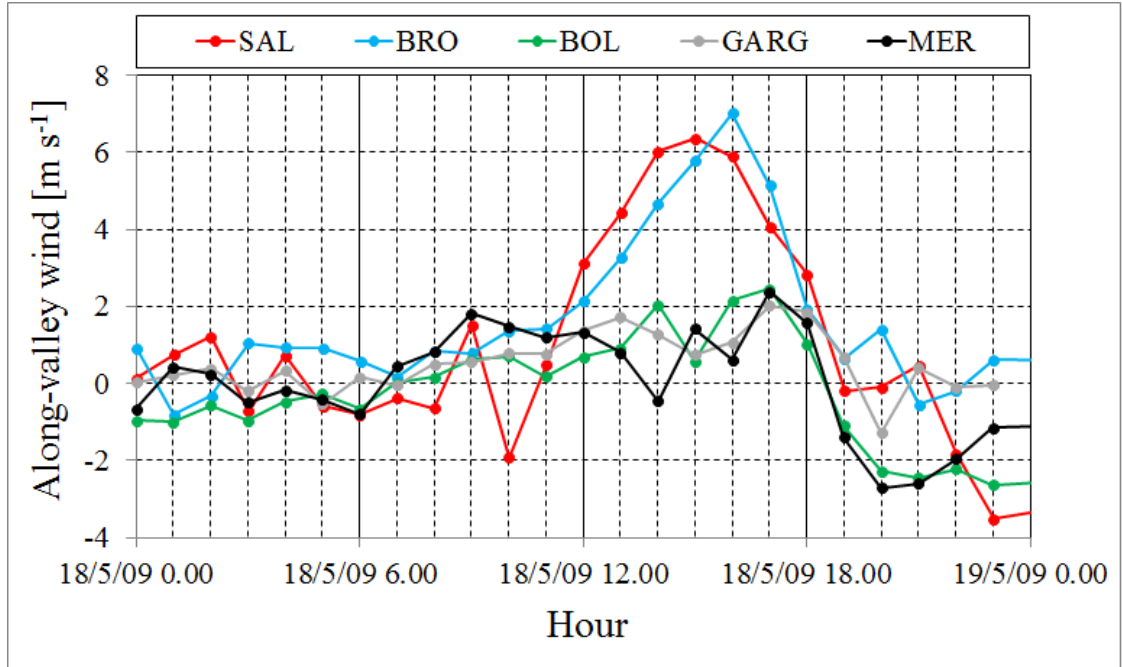
Figure 5.20: As in Fig. 5.19, but for the weather stations in the Province of Bolzano.
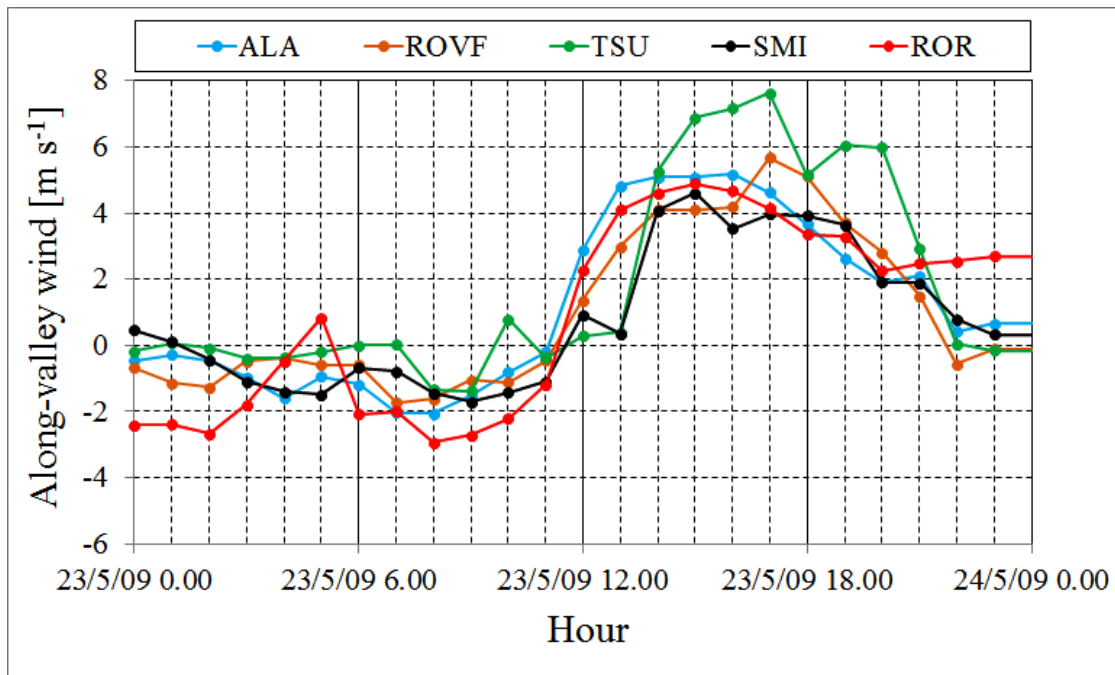
Figure 5.21: Daily cycles of the along-valley wind for 23 May 2009 for several weather stations in the Adige Valley in the Province of Trento.
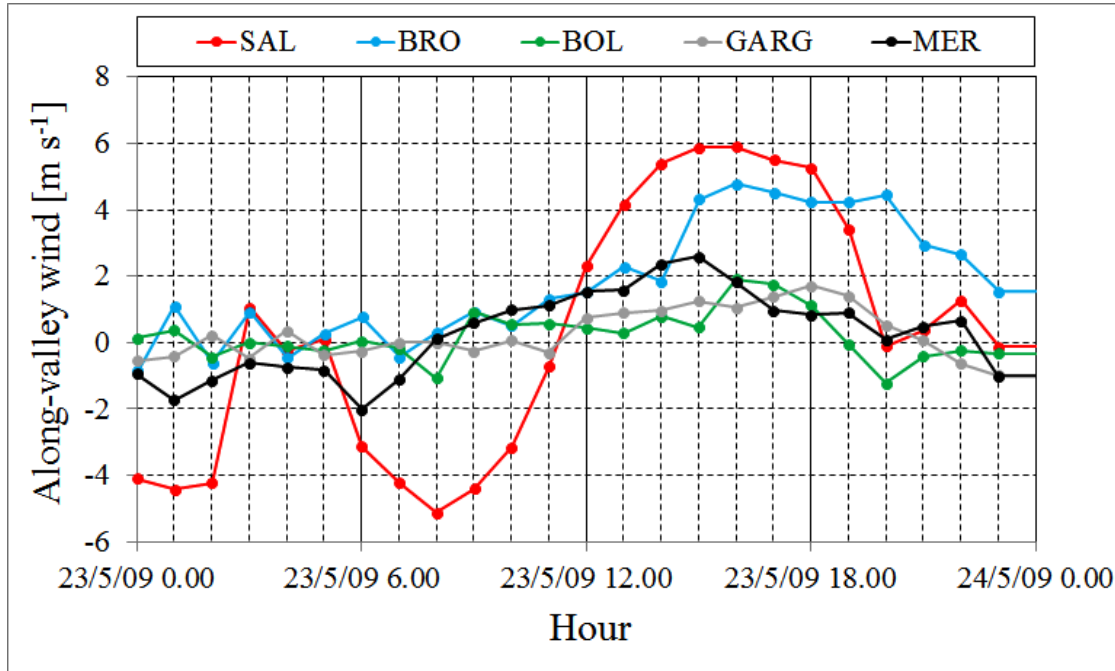
Figure 5.22: As in Fig. 5.21, but for the weather stations in the Province of Bolzano.

with respect to the other sections of the valley. From these considerations it seems that the development of a breeze front moving from south towards north is not present, especially in the central parts of the valley; it seems that the onset of the up-valley wind is to some extent connected to local factors, as for example the local topography, which influences the heating of the different sections of the valley.

At Roveré della Luna, as highlighted by the average cycles, the up-valley wind lasts until 0300 LST in most days; in these days a light up-valley wind is present also at Salorno weather station some kilometers north of Roveré della Luna, in the Province of Bolzano. On the other hand in some days a quite strong down-valley wind is observed in the first hours of the morning at these two weather stations, especially at Salorno (Fig. 5.22). Also this strong down-valley wind is probably caused by the east-west orientation of the valley at these two weather stations and the consequent thermal contrasts with the other sections of the valley. In fact it generally begins around 0600-0700 LST, when the sun begins to heat the valley atmosphere. Finally the analysis of the single daily cycles confirms that a weak up-valley wind is present in most days at Bronzolo for the whole night and that the up-valley wind is very weak at Bolzano, Gargazzone and Merano.

5.4.3   Pressure daily cycles

Along-valley winds are caused by the pressure differences between the valley and the adjacent plain, or between two different sections of the valley. For this reason an analysis of the pressure gradients in the Adige Valley highlights the mechanisms leading to the development of the along-valley wind. In no one of the selected valley wind days data covering all the weather stations were available, due to the different periods during which the weather stations were operative. For this reason also in this case it has been decided to separate the weather stations in the Province of Trento (plus Cason) and those in the Province of Bolzano. In this way data from 55 days could be used to obtain the average cycles in the Province of Trento, while 18 days were utilized for the stations in the Province of Bolzano. Pressure has been normalized subtracting from the values measured at each weather station the difference between the average pressure at that weather station and the average pressure at a weather station taken as a reference. In this way the average pressure is the same at every weather station and only the fluctuations from the average are highlighted. The weather station located at the highest altitude, S. Michele all'Adige in the Province of Trento and Merano in the Province of Bolzano, has been taken as the reference. Also in this case data presented are hourly averages.

Figure 5.23 shows the daily cycles of the mean pressure fluctuations from the average for the weather stations in the Province of Trento plus Cason, in the Po Plain. As expected, the daily pressure range tends to become larger and larger going from the Po Plain to the inner parts of the Adige Valley. This behavior is in agreement with the twice a day reversal of the
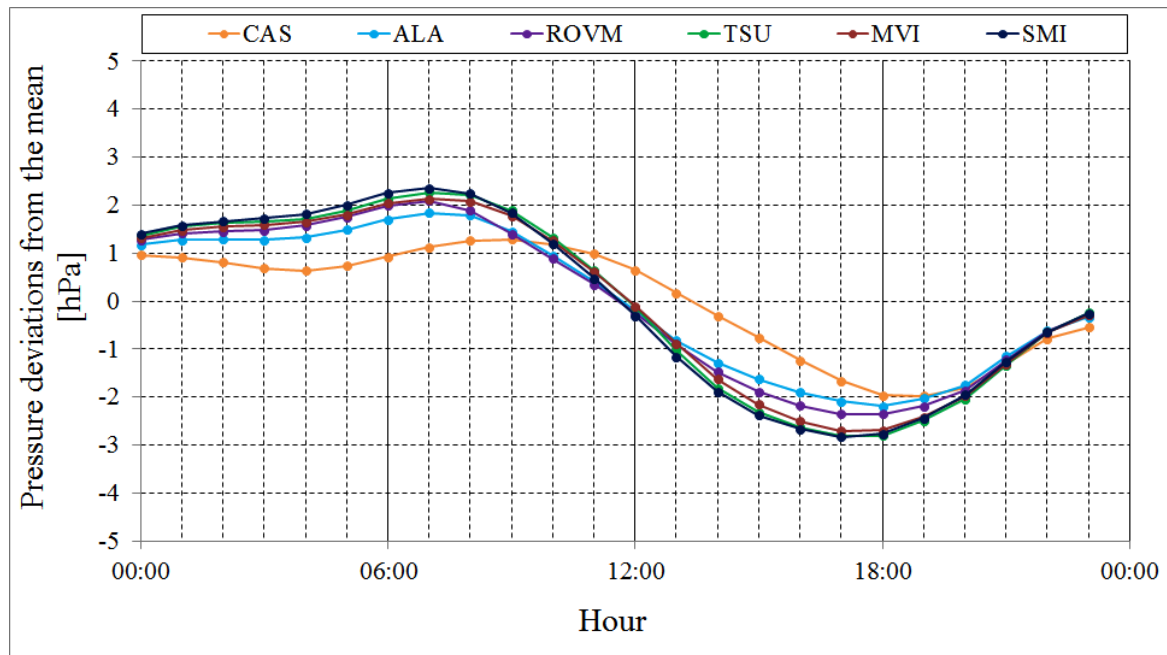
Figure 5.23: Daily cycles of the average pressure fluctuations at several weather stations in the Adige Valley in the Province of Trento and in the Po Plain.
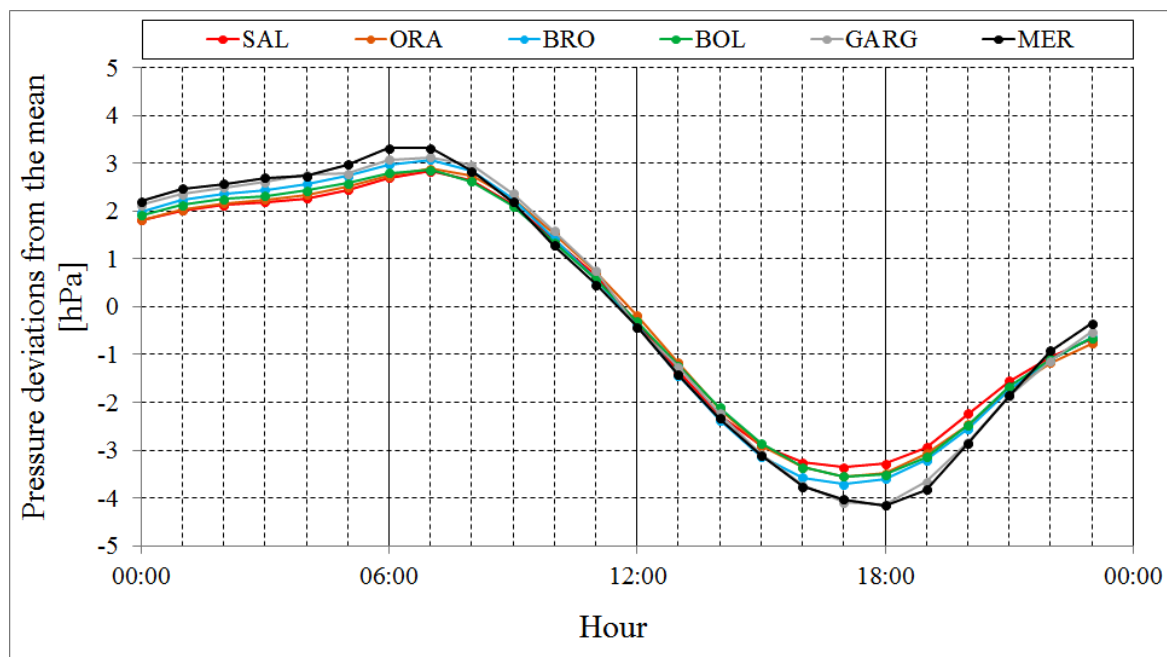
Figure 5.24: As in Fig. 5.23, but in the Province of Bolzano.

along-valley wind and the development of a down-valley wind at night and an up-valley wind during the day.

The only exception is Molino Vittoria, where the daily pressure range is lower than at Trento Sud, located some kilometers south. The lower values measured during the night at Molino Vittoria with respect to Trento Sud may be caused by an urban effect: as seen in Chapter 3 a quite strong UHI develops in the city of Trento at night in clear sky situations (and valley wind days are characterized by clear skies). Therefore the higher temperatures in the urban area may lead to lower pressure values. The higher pressure during daytime may be caused by the fact that in many days Molino Vittoria is influenced, as partly shown from the wind hodograph (Fig. 5.8) and as it will be more deeply investigated in Section 5.6, by the Ora del Garda, which is slightly cooler than the up-valley wind blowing in the Adige Valley and for this reason mitigates the pressure drop in the afternoon. This hypothesis seems confirmed observing that the pressure fluctuations at Trento Sud and S. Michele all'Adige are very similar in the afternoon, even though these two weather stations are 19 km far away. Therefore it can be supposed that the up-valley wind at the latter weather station is caused not only by the pressure differences with the southern sections of the valley, but also by the propagation towards north of the Ora del Garda. It can be observed that the cycles of the pressure fluctuations in the plain and in the valley are not in phase. In particular the minimum and maximum values in the plain are reached some hours later than in the valley, probably due to the different heating and cooling mechanisms. The reversal of the pressure gradient occurs around 1100 LST in the morning and around 2300 LST in the evening, fairly in agreement with the average along-valley wind cycles in Fig. 5.17.

Also the pressure daily cycles for the weather stations in the Province of Bolzano (Fig. 5.24) show higher ranges going toward the inner parts of the valley, with the exception of the weather station of Bolzano, which displays lower values at night and higher values during daytime with respect to Bronzolo, located south of Bolzano. The behavior of Bolzano is similar to what found for Molino Vittoria weather station, located in the city of Trento. Therefore during the night it is likely that the presence of the urban area of Bolzano plays a role in determining the lower pressure values with respect to Bronzolo. The lower daily pressure range may be also caused, as highlighted above, by the fact that Bolzano is placed in a relatively large basin, and as a consequence the heating and cooling rates of the air in the basin may be lower than in the valley.

Figures 5.25 and 5.26 show the average pressure gradients in the along-valley direction at different hours of the day and allow a clearer visualization of the pressure gradients leading to the development of down- and up-valley winds. Also in this case data from the weather stations in the Province of Trento and Bolzano have been separated. Focusing on the Province of Trento and the plain, at 0000 LST the pressure tends to slightly increase going from the plain (Cason) to the inner parts of the Adige Valley. The pressure gradients become then stronger in the
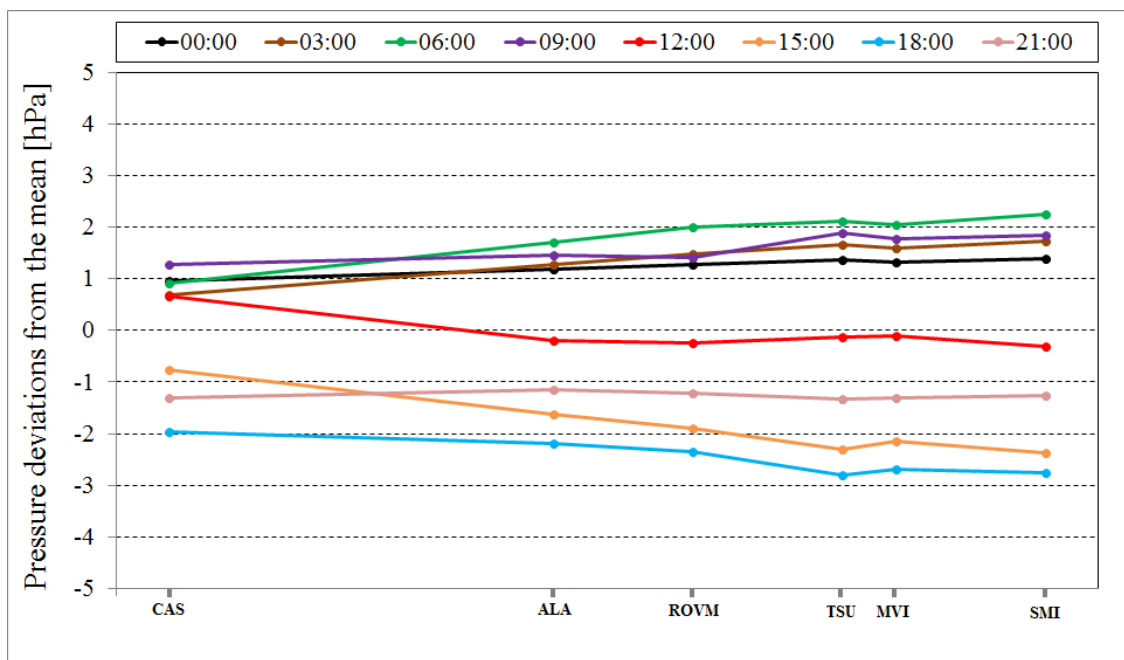
Figure 5.25: Average pressure gradients in the Adige Valley in the Province of Trento (plus Cason in the Po Plain) at different hours of the day. The proportions of the distances between the weather stations are respected in the x axis.
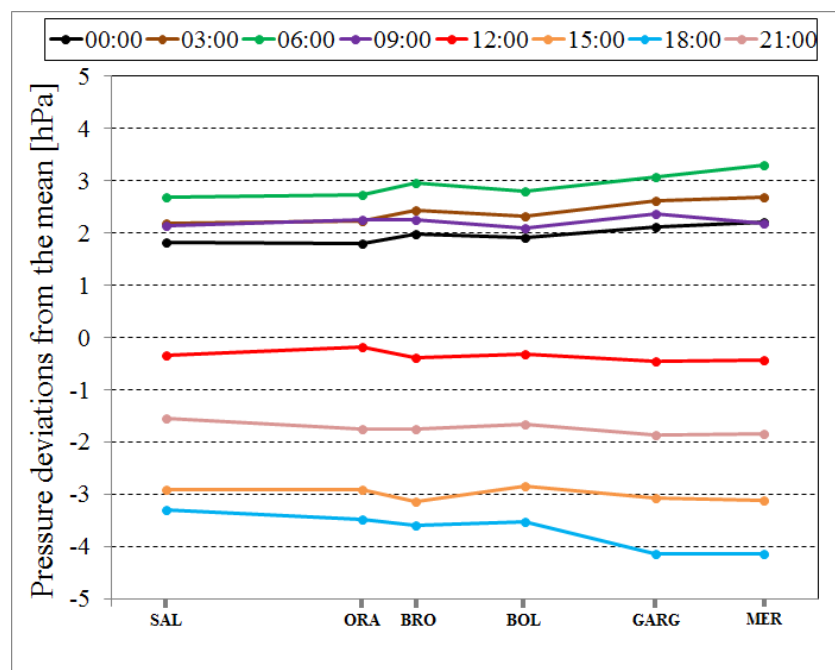
Figure 5.26: As in Fig. 5.25, but in the Province of Bolzano.

following hours of the night. As seen before, the "normal" pressure gradient is reversed from Trento Sud to Molino Vittoria. This behavior suggests that an "urban breeze", blowing from south to north, may occur between Trento Sud and Molino Vittoria, but observations does not support this hypothesis. However the weak down-valley wind present at night at Trento Sud (Fig. 5.17) may be a consequence of this particular effect. At 0900 LST pressure gradients weaken in the southern part of the valley, while become stronger between Rovereto and Trento Sud; accordingly in most days the down-valley wind at Trento Sud and Rovereto (and also at Molino Vittoria) reaches the highest intensity at this time of the day. At 1200 LST the pressure gradient is very weak between Ala and S. Michele all'Adige, while the pressure decreases from the plain (Cason) to the southernmost valley station (Ala). Therefore the pressure gradient reversal occurs earlier between the plain and the southernmost sections of the valley than between the inner sections of the valley. This behavior seems in agreement with the earlier onset of the up-valley wind at Ala. At 1500 LST the pressure decreases roughly linearly from Cason to Trento Sud, in accord with a well-developed up-valley wind. Going north, as said before, pressure increases from Trento Sud to Molino Vittoria, probably due to the influence of the Ora del Garda. The situation remains similar at 1800 LST, with a decrease of the pressure differences between the plain and the southernmost part of the valley. At 2100 LST pressure gradients are weak everywhere, with only a slight pressure increase between Cason and Ala, suggesting that the down-valley wind starts to blow earlier in the southernmost part of the valley.

In the Province of Bolzano (Fig. 5.26), at night the pressure gradient between Salorno and Ora is very weak, while stronger differences are observed between Ora and Bronzolo. As seen from the daily cycles in Fig. 5.24, at night the pressure decreases from Bronzolo to Bolzano, probably due to the combination of the urban and the basin effects. This pressure distribution is in agreement with the light up-valley wind blowing also at night at Bronzolo. North of Bolzano pressure increases again, suggesting that a down-valley wind is present in this part of the valley. However Fig. 5.18 showed that at Gargazzone the down-valley wind is very weak at night. On the other hand a significant down-valley wind is present at Merano. At 0900 LST the pressure gradient is weak between Salorno and Bronzolo, while the pressure still slightly decreases from Bronzolo to Bolzano and increases from Bolzano to Gargazzone. The pressure decrease between Gargazzone and Merano may explain the earlier onset of the up-valley wind at the latter weather station (Fig. 5.18). At 1200 LST gradients are weak everywhere, with the only exception of the pressure decrease between Ora and Bronzolo, which may be the cause of the onset of a stronger up-valley wind at Bronzolo at this hour. In the afternoon the "basin effect" causes a convex pressure distribution at Bolzano: this particular behavior probably determines the significant differences between the up-valley wind south of the basin and north of it. At 1800 LST the pressure increase from Bronzolo to Bolzano becomes less strong; in fact maximum wind velocities at Bolzano are registered around this hour. Finally at 2100 LST pressure gradients

become weak everywhere.

5.5 Analysis of local circulations in the Sarca and Lakes valleys

5.5.1 Wind odographs

Like in the Adige Valley, the wind hodographs of the weather stations in the Sarca and Lakes valleys are mainly oriented along the valley axis, following the cycle of down- and up-valley winds. Only at Terlago the wind hodograph is oriented in the west-east direction, probably due to local effects: in fact the highest part of the Lakes Valley presents a very complex morphology, with hills that divide the main valley in several minor gullies. The intensity of the down-valley wind is of order 1-2 m s^{-1}, with higher values only at Sarche, due to katabatic winds flowing down a gully joining the Lakes Valley nearby. The up-valley wind, the Ora del Garda, reaches intensities of 7-8 m s^{-1}, with the highest values at Riva del Garda, on Lake Garda shores.

Figure 5.31 shows, also in this case, the summary of all the wind odographs in the Sarca and Lakes valleys, along with the position of the weather stations to which they refer.

5.5.2 Along-valley wind daily cycles

In the Sarca and Lakes valleys only Arco weather station has a dataset of wind velocity and direction covering the whole time period 2004-2011. Data from Riva del Garda weather station cover the time period 2004-2010, data from Sarche weather station the time period 2010-2011, while data from Terlago starts from 2011. For this reason it was not possible to calculate the average along-valley wind daily cycles at these four weather stations using data from the same days. Thus it has been decided to use for each weather station all the data available, even though the comparisons between the daily cycles using this methodology may be not completely truthful. However an analysis of the single daily cycles has highlighted that, as in the case of the Adige Valley, the day-to-day variability is not very marked and therefore the calculation of the average cycles is not significantly affected by the use of different datasets.

The average daily cycles of the along-valley wind during "valley wind days" in the four weather stations in the Sarca and Lakes valleys are shown in Fig. 5.32. The onset of the up-valley wind occurs earlier at Riva del Garda (around 1000 LST) and then at the other weather stations. Indeed it looks like the Ora del Garda propagates from Riva del Garda north to Terlago, even though this analysis is somehow hindered by the scarce resolution of the data. At Sarche the wind intensity in the afternoon is considerably lower than at the other weather stations, while, as seen from the wind hodograph in Fig. 5.29, the down-valley wind at night is quite strong, especially in the first hours of the morning, and starts earlier than at the other weather stations (around 1900 LST). On the other hand at Terlago the down-valley wind is completely absent, probably due to the location of this weather station at the bottom of a small
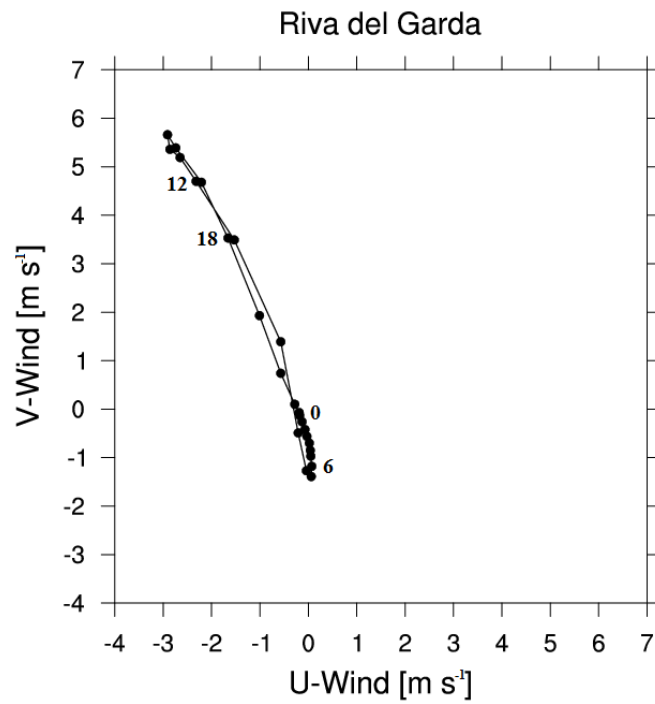
Figure 5.27: Wind hodograph at Riva del Garda weather station.
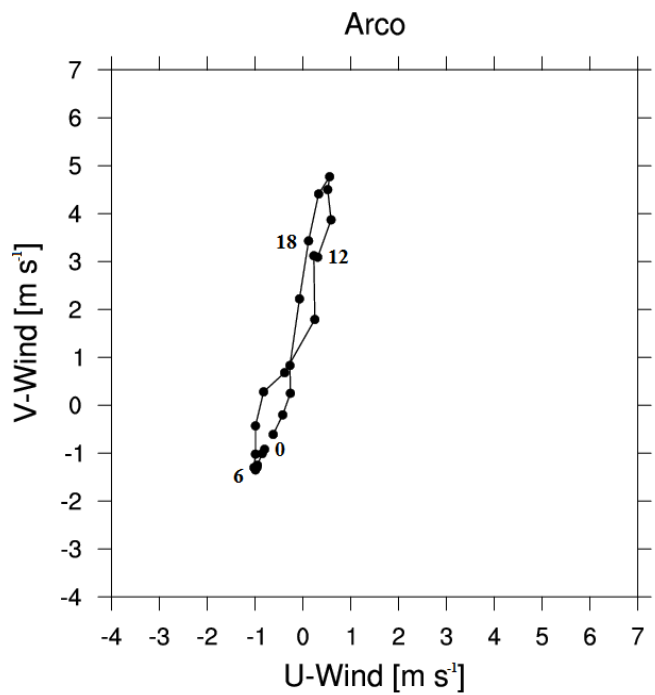
Figure 5.28: As in Fig. 5.27, but at Arco weather station.
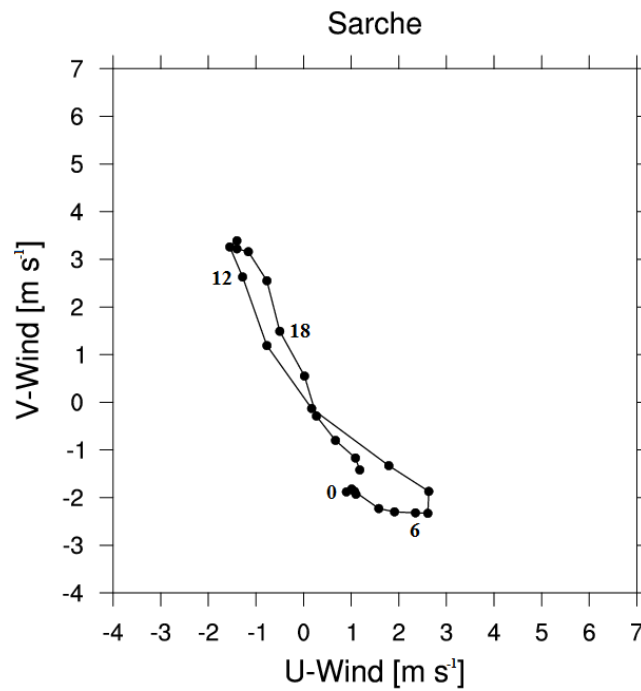
Figure 5.29: As in Fig. 5.27, but at Sarche weather station.
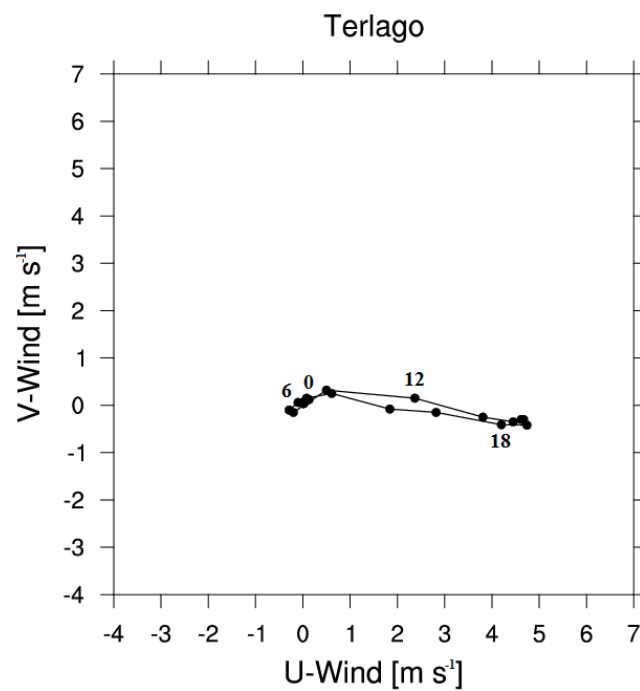
Figure 5.30: As in Fig. 5.27, but at Terlago weather station.
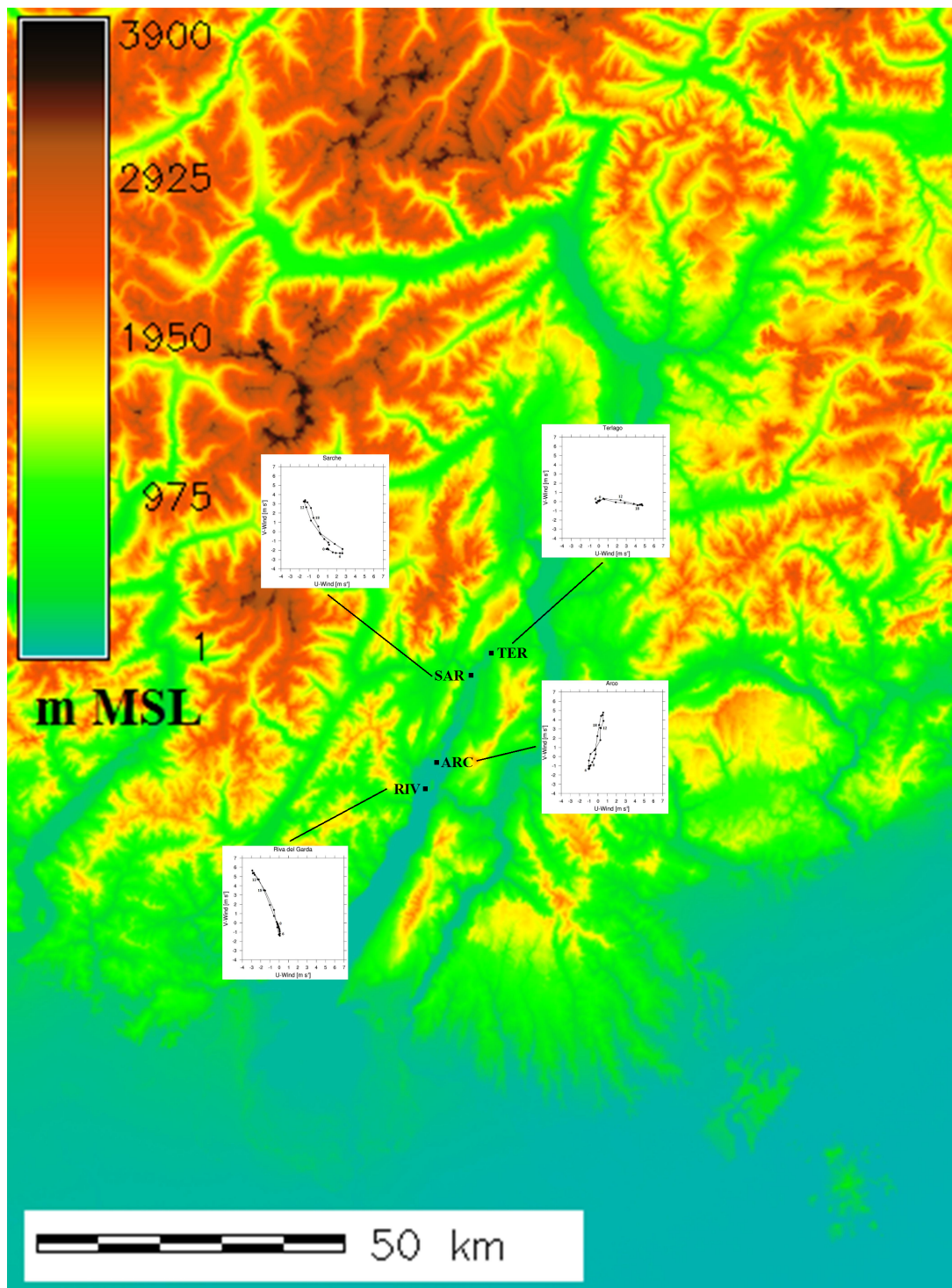
Figure 5.31: Summary of the wind odographs in the Sarca and Lakes valleys, along with the position of the weather stations to which they refer.

basin.
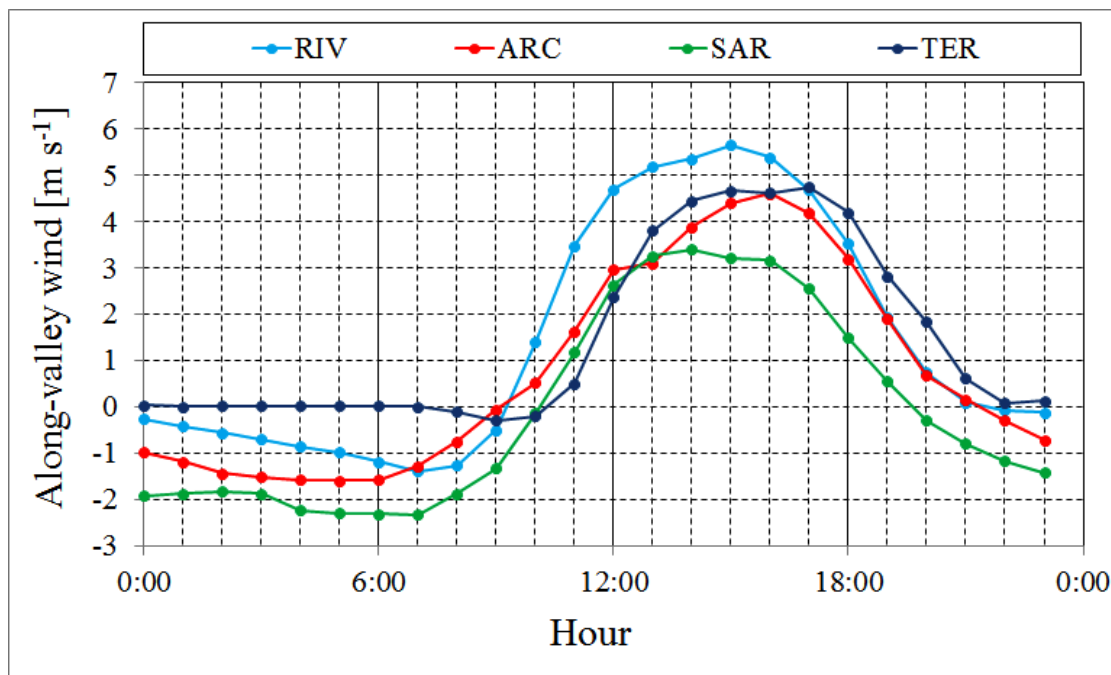
Figure 5.32: Average daily cycles of the along-valley wind during "valley wind days" for the weather stations in the Sarca and Lakes valleys.

In order to confirm the results found with the average cycles and to obtain more information about the propagation of the lake breeze, also in this case the single daily cycles have been analyzed. This analysis confirms that the onset of the up-valley wind at Arco weather station occurs in almost all the days an hour later than at Riva del Garda (not shown). On the other hand the situation becomes less clear when leaving the basin of Arco-Riva and going up in the Sarca and Lakes valleys. In most days the onset of the up-valley wind at Sarche and Terlago weather stations is at the same time, and an hour later with respect to Arco (Fig. 5.33). It can be supposed that the scarce temporal resolution of the data does not allow to see the propagation of the lake breeze from Sarche to Terlago, which are about 10 km far away. In some days the onset of the up-valley wind occurs at the same time at Arco, Sarche and Terlago (Fig. 5.34). In these situations it seems that a light up-valley wind starts to blow before the arrival of the lake breeze. This wind is probably a typical valley wind, caused by the different heating of the different sections of the valley. It is in fact likely that a typical valley circulation would blow in the Sarca and Lakes valleys if Lake Garda were not present. Results from investigations of this particular aspect by means of idealized numerical simulations are shown in Chapter 6.

The propagation of the lake breeze can be studied also analyzing the daily cycles of temperature at the same weather stations. In fact the arrival of the cooler air blowing from the lake
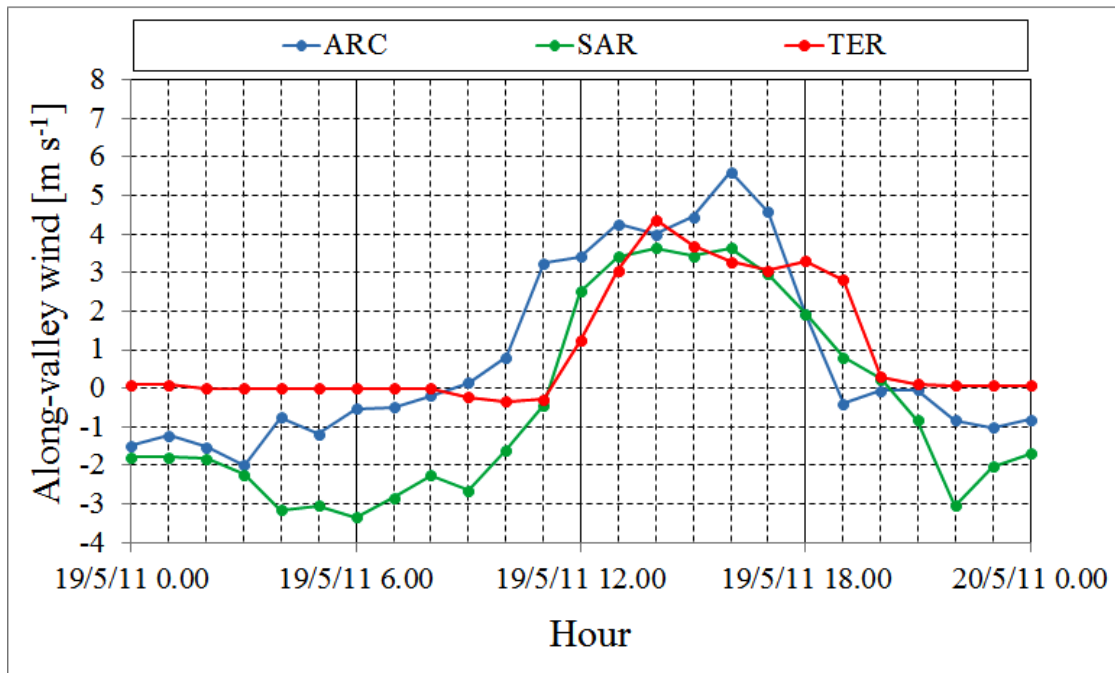
Figure 5.33: Daily cycles of the along-valley wind during 19 May 2011 for Arco, Sarche and Terlago weather stations.
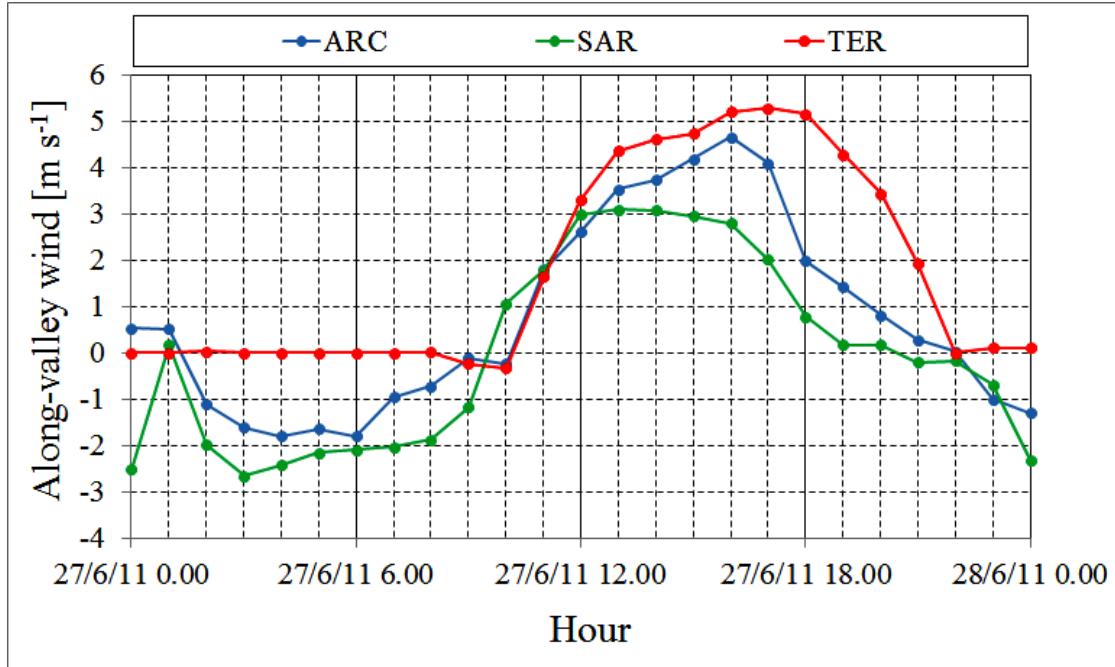
Figure 5.34: As in Fig. 5.33, but during 27 June 2011.

is marked in most days by a temperature drop, first at Riva del Garda and then at the other weather stations, as in the example shown in Fig. 5.35. Figure 5.35 shows also the daily cycle of temperature at Gardolo, located in the Adige Valley north of Trento, so as to highlight that the outbreak of the Ora del Garda mitigates the temperature in the afternoon also in this part of the Adige Valley. Furthermore it can be seen that at night the temperature at Terlago is considerably lower than at the other weather stations: also in this case this particular behavior is caused by the location of the weather station at the bottom of a small basin, where at night strong thermal inversions build up, leading to the development of a "cold pool".
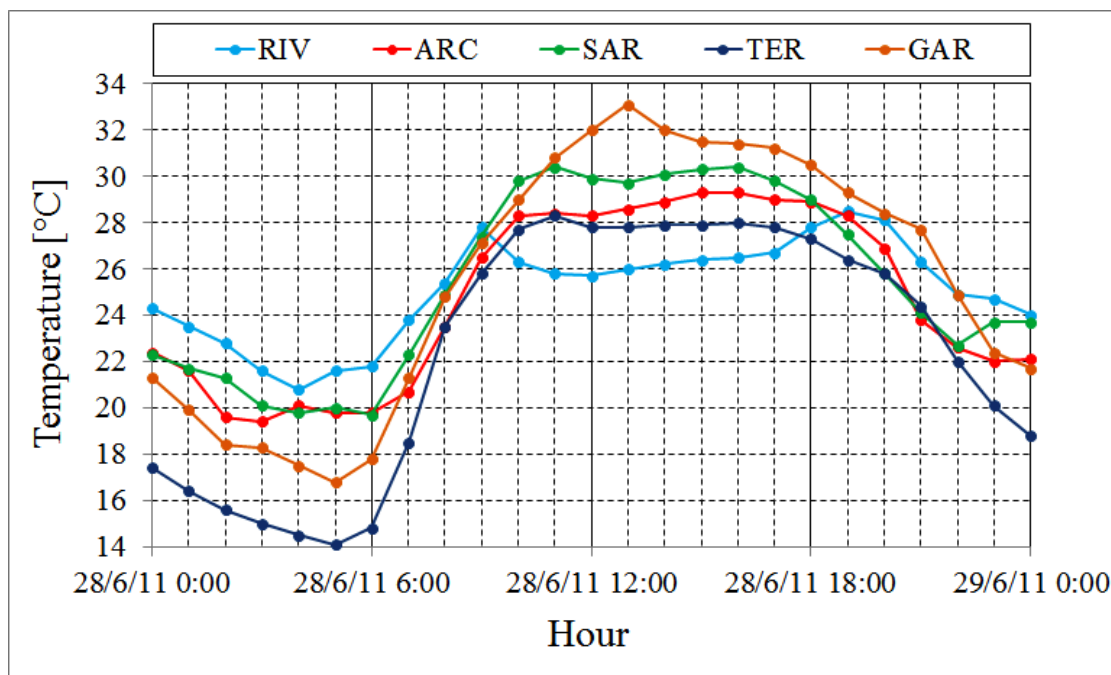
Figure 5.35: Daily temperature cycles during 28 June 2011 for Riva, Arco, Sarche, Terlago and Gardolo weather stations.

5.5.3   Monthly variations in the onset of the Ora del Garda

The histograms in Figs. 5.36 and 5.37 show the frequency distribution of the onset hour of the Ora del Garda at Riva del Garda and Arco weather stations respectively. It can be seen that in both stations there is a progressive delay going from May to August in the onset of the lake breeze. In fact at Riva del Garda the highest frequencies are at 0900 and 1000 LST in May, while at 1100 LST in August. This delay is probably due to the progressive heating of the lake water during the warm season: as a consequence the temperature contrasts which lead to the development of the lake breeze start later in the second part of the summer, when the lake water is warmer. Furthermore these histograms confirm that the onset of the Ora del Garda at
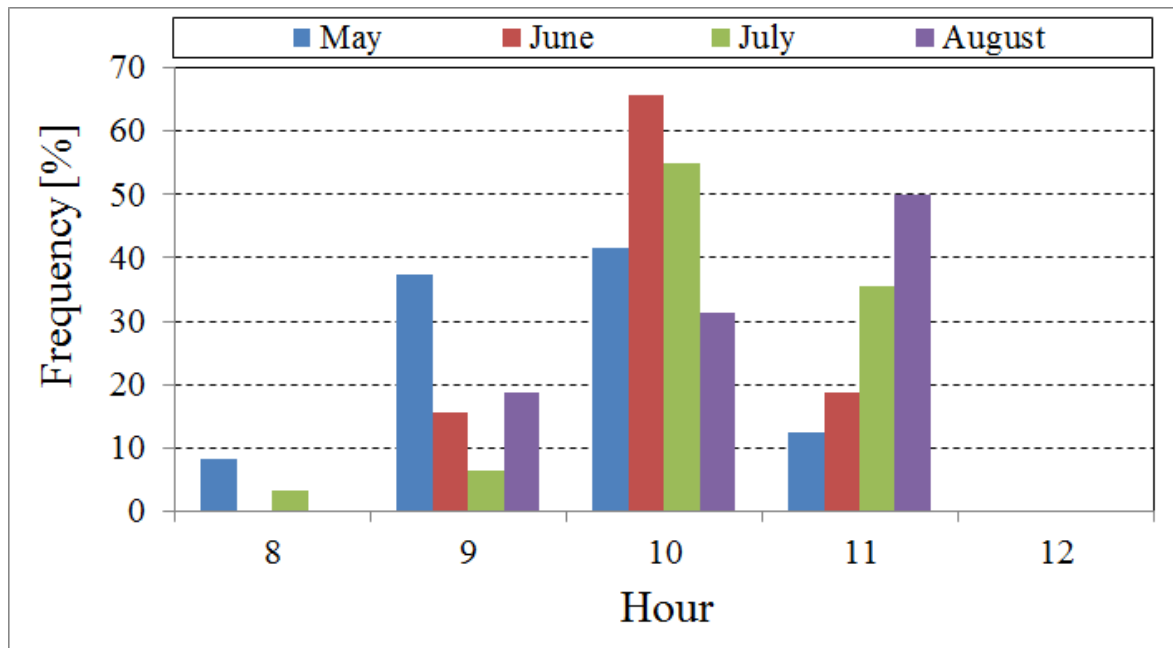
Figure 5.36: Frequency distribution of the onset hour of the Ora del Garda at Riva del Garda weather station.
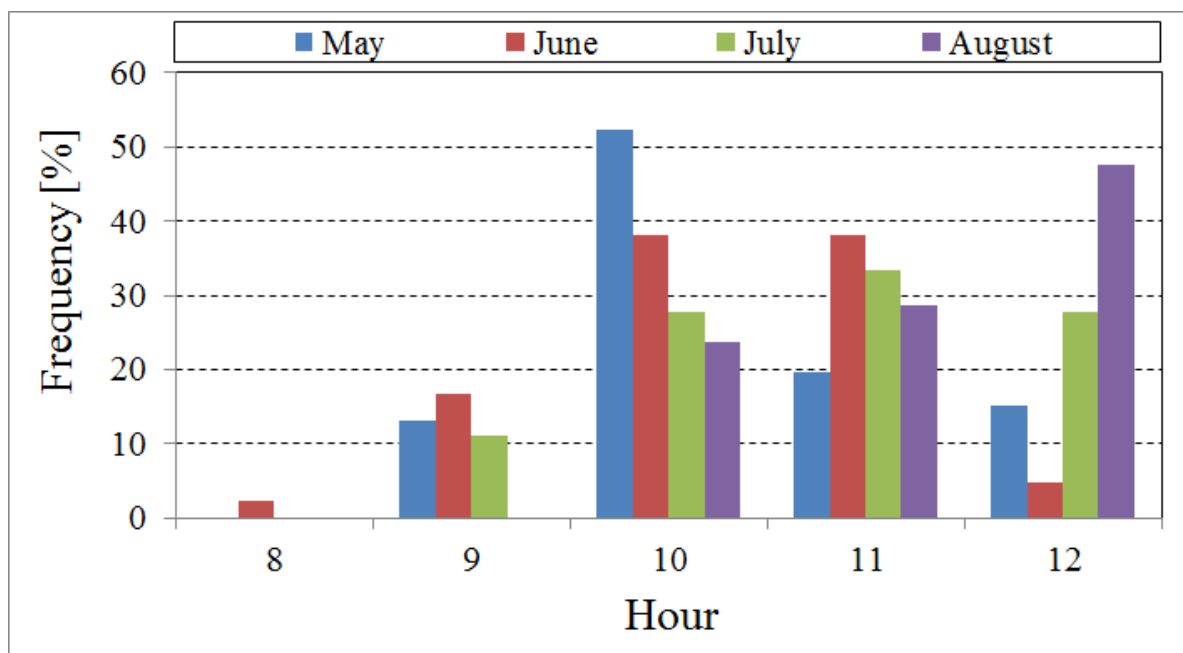
Figure 5.37: As in Fig. 5.36, but at Arco weather station.

Arco is about an hour later than at Riva del Garda.

5.6   Ora del Garda - Adige Valley up-valley wind interaction

In this Section the interaction between the Ora del Garda and the up-valley wind in the Adige Valley is investigated analyzing wind velocity and direction measurements at Trento Sud, Molino Vittoria and Gardolo weather stations, located south of Trento, in the city center and north of the city respectively. Data from Trento Sud and Gardolo are hourly averages, while data from Molino Vittoria are 10-min averages, so as it is possible to appreciate wind velocity and direction fluctuations. This analysis highlights that during the afternoon wind velocity and direction at Molino Vittoria exhibit a high day-to-day variability, in contrast with the other weather stations, where recurrent features are found during "valley wind days". Four different cases have been individuated and presented here.

In some days, as in the example in Fig. 5.38, in the late morning the up-valley wind starts to blow at Molino Vittoria, but it is soon replaced by a wind blowing from north, the branch of the Ora del Garda that flows from north to south, as shown in Fig. 5.2. In fact at Gardolo, north of Trento, the Ora del Garda is quite strong and starts to blow at the same time as the northerly wind replaces the up-valley wind at Molino Vittoria. On the other hand south of the city the up-valley wind continues to blow for all the afternoon, not affected by the Ora del Garda.

In other days the Ora del Garda is able to reach Molino Vittoria only in the second part of the afternoon for few hours, as shown in Fig. 5.39. It is interesting to notice that the Ora del Garda arrives at Molino Vittoria when the up-valley wind at Trento Sud weakens. In fact the point of interaction between the two opposing circulations is determined by their relative strength.

In some cases (Fig. 5.40), when the Ora del Garda is weaker, a typical valley wind daily cycle is present also at Molino Vittoria, with the alternation of down-valley and up-valley winds. In this case it seems that the Ora del Garda is not able to reach the city center and it can be supposed that the interaction with the up-valley wind of the Adige Valley is located far north, between Gardolo and Molino Vittoria weather stations.

Finally it has been found that in some days (Fig. 5.41) during the afternoon the wind direction continues to change at Molino Vittoria, probably because the interaction between the two opposing circulations occurs in the area of Molino Vittoria, and the point of interaction slightly oscillates in the along-valley direction. In these situations wind velocity at Molino Vittoria is quite weak. At Trento Sud the wind cycle shows a typical alternation between down- and up-valley wind also in this case, while at Gardolo the Ora del Garda replaces the up-valley wind in the early afternoon.

Similarly to what found in Fig. 5.35, the arrival of the Ora del Garda at Molino Vittoria

is marked by a temperature drop (not shown). As a consequence, when the Ora del Garda is strong enough, it is able to mitigate the afternoon temperature also in the urban area.

5.7 Conclusions

In this Chapter the main characteristics of local circulation systems, and in particular along-valley winds, in the valleys around the city of Trento have been investigated by means of the analysis of a dataset from surface weather stations. Suitable "valley wind days" have been chosen from the days in the months of May, June, July and August with cloud cover ≤ 2 oktas and well-developed valley wind daily cycles.

Local circulation systems in the Adige Valley generally follow the classical Defant's (1949) scheme, with a twice-a-day reversal of valley and slope winds. However the geometrical inhomogeneities of the valley may cause significant local alterations from the "normal" situation. As to along-valley winds, in the Province of Trento, where the valley has a quite regular geometry, the daily cycles present similar features at all the weather stations analyzed. During the night the down-valley wind is generally quite weak, with maximum intensities of order 1-2 m s^{-1}, while the up-valley wind is considerably stronger, reaching frequently intensities of 6-8 m s^{-1} in the afternoon. Local changes in the valley orientation can modify the along-valley wind daily cycle, due to the different penetration of solar radiation inside the valley and as a consequence the different heating of the valley atmosphere. This is the case of Roveré della Luna and Salorno weather stations, located in a west-east oriented part of the valley, where in many days the up-valley wind starts to blow earlier than at the weather stations located south of them. Moreover a strong down-valley wind in the first hours of the morning is often observed at Salorno. The geometry of the Adige Valley in the Province of Bolzano becomes more irregular. In particular south of the city of Bolzano a secondary valley develops parallel to Adige Valley, from which it is separated only by a low hill. Moreover the valley becomes larger going towards north, reaching the maximum width in the basin of Bolzano. As a consequence of these geometrical differences, the along-valley wind daily cycles change substantially, especially north of the basin of Bolzano, where the up-valley wind becomes very weak.

Characteristics of along-valley winds in the Adige Valley have been further investigated analyzing the pressure gradients in the along-valley direction. The daily pressure range generally becomes larger going from the plain to the inner parts of the Adige Valley, in agreement with the twice-a-day reversal of the along-valley wind and the development of the down-valley wind at night and the up-valley wind from midday to the evening. However the "normal" pressure distribution is reversed in the sections of the valley near the cities of Trento and Bolzano. In both cases it may be speculated that the presence of the urban area with a consequent UHI during the night determines lower pressures in comparison with the surrounding rural areas on the valley floor. However an "urban" breeze is not observed south of Trento, although the

down-valley wind at Trento Sud weather station, some kilometers south of the urban area, is very weak at night, maybe weakened by this effect. On the other hand south of Bolzano a weak up-valley wind is present also at night, but in this case it is probable that the particular geometry of the valley, which widens in the basin of Bolzano, is a concurrent cause of this behavior. It is supposed that the basin behaves as a "small plain", with lower heating and cooling rates, and as a consequence a lower pressure daily range. In fact it is found that during daytime the pressure at Bolzano is higher than in the surrounding sections of the valley both in the north and south directions. This higher pressure during daytime is probably the cause of the weak up-valley wind north of Bolzano.

The outbreak inside the Adige Valley in the area north of Trento of the Ora del Garda, the lake breeze flowing from Lake Garda, determines another alteration in the "normal" pressure distribution. In fact the cooler air associated with the lake breeze mitigates the pressure drop during the afternoon in the sections of the valley reached by this circulation. For this reason the pressure increases going north from Trento Sud, not reached by the Ora del Garda, to Molino Vittoria, where the lake breeze arrives in most days.

Focusing on the onset of the up-valley wind in the Province of Trento, where the valley is more regular, it has been found that the pressure contrasts develop earlier between the plain and the southernmost sections of the valley and then between the inner sections of the valley. Accordingly the up-valley wind tends to develop earlier at Ala, the southernmost weather station. On the other hand in the inner sections of the valley the onset of the up-valley wind seems dependent on local factors, as the geometry of the valley or the presence of solar radiation, and a breeze front developing from south to north is not present.

The analysis of the along valley wind daily cycles in the Sarca and Lakes valleys has highlighted the substantial differences with the local circulation in the Adige Valley. A typical lake breeze (Ora del Garda) develops in the morning from Lake Garda and goes up in the Sarca and Lakes Valley, outbreaking into the Adige Valley north of Trento in the first part of the afternoon. The arrival of the lake breeze front is clearly marked by a sudden increase of the wind from south in the basin of Arco-Riva, immediately north of the lake, while the propagation of the front in the Sarca and Lakes valleys can not always be clearly detected, being the arrival of the lake breeze masked by the presence of a valley wind in some days. However the passage of the lake breeze is evidenced by a characteristic temperature drop, which can be detected also in the Adige Valley in the areas north of Trento reached by the Ora del Garda.
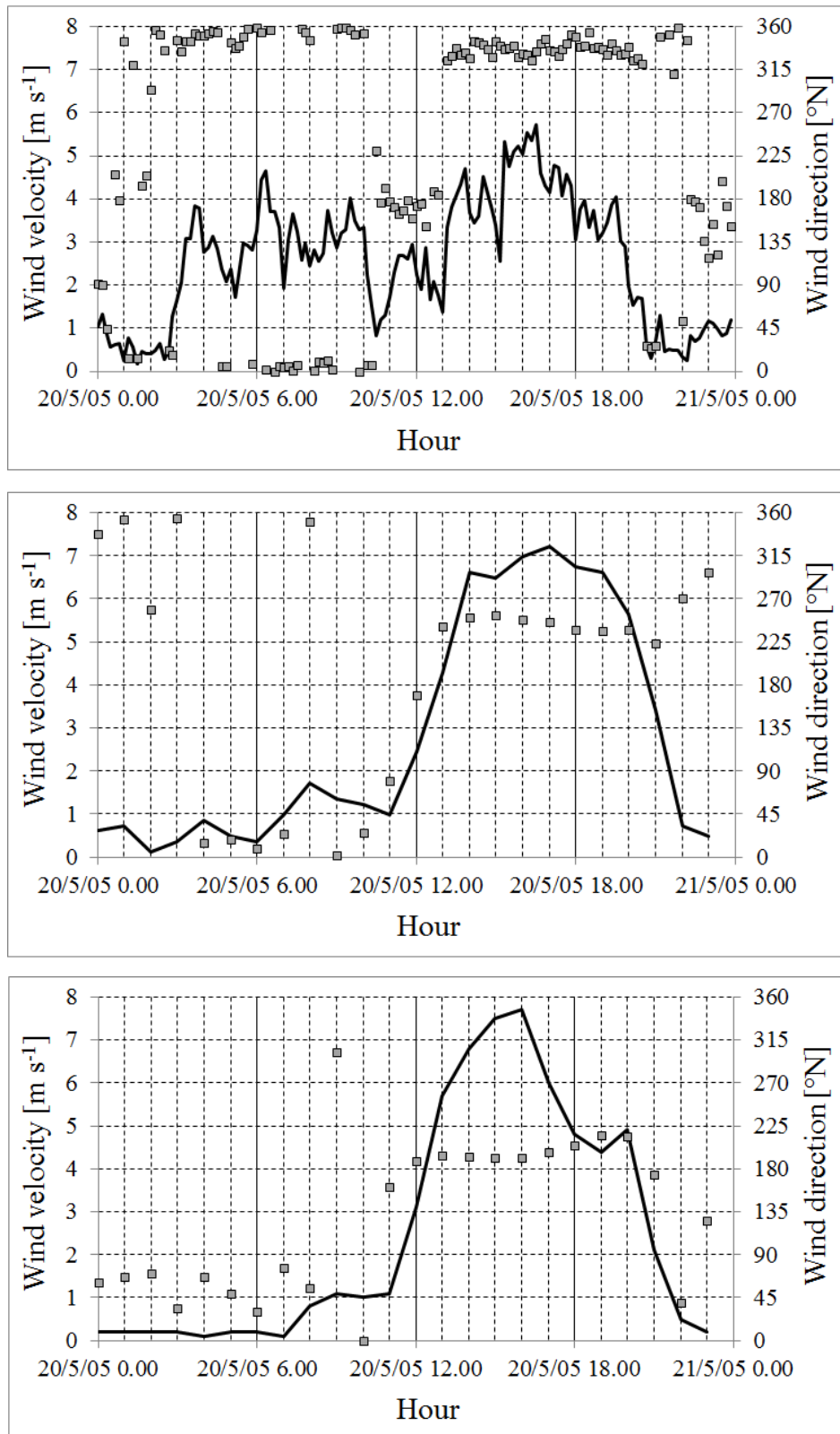
Figure 5.38: Wind velocity and direction at Molino Vittoria, Gardolo and Trento Sud weather stations on 20 May 2005.
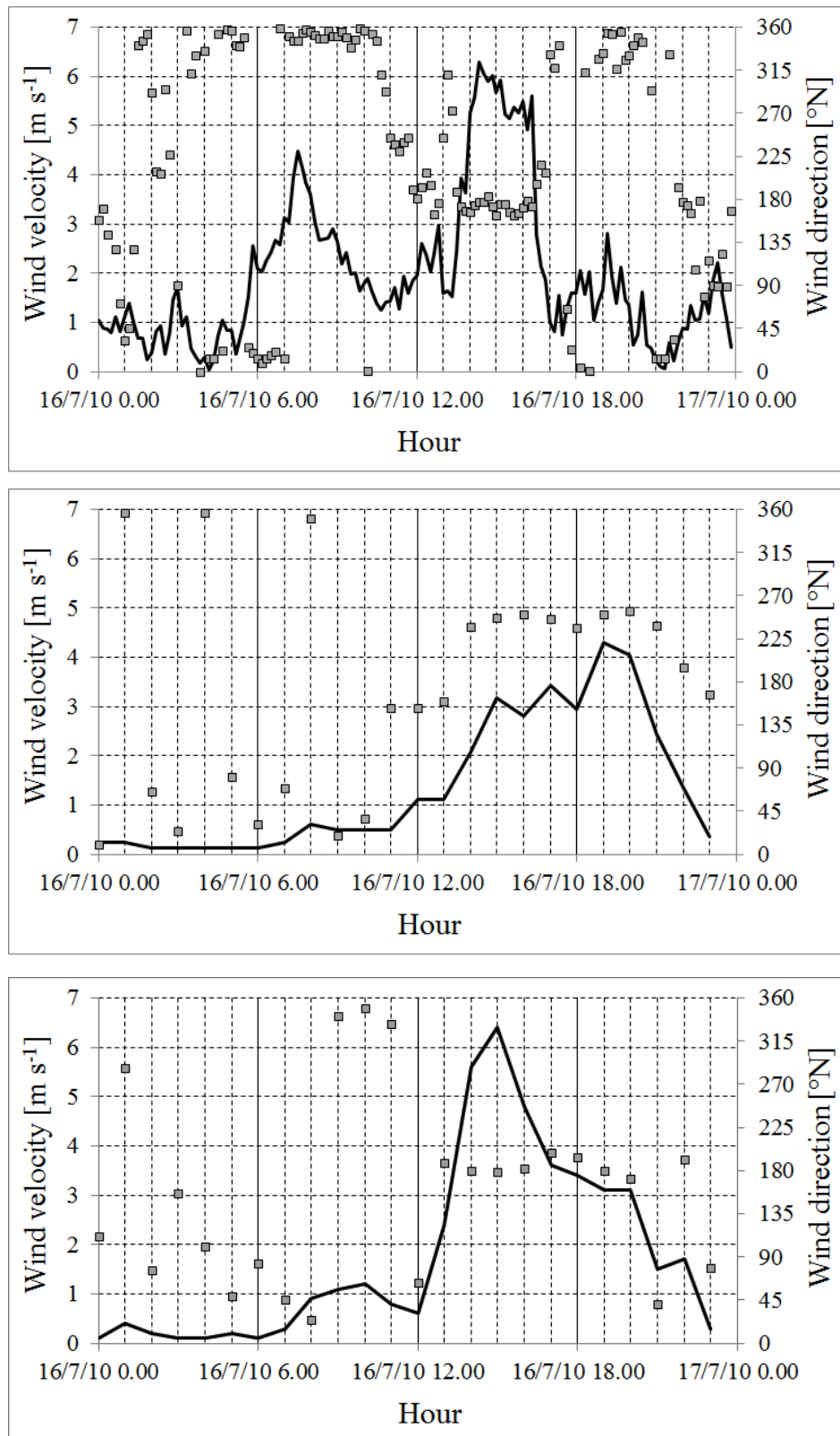
Figure 5.39: As in Fig. 5.38, but on 16 July 2010.
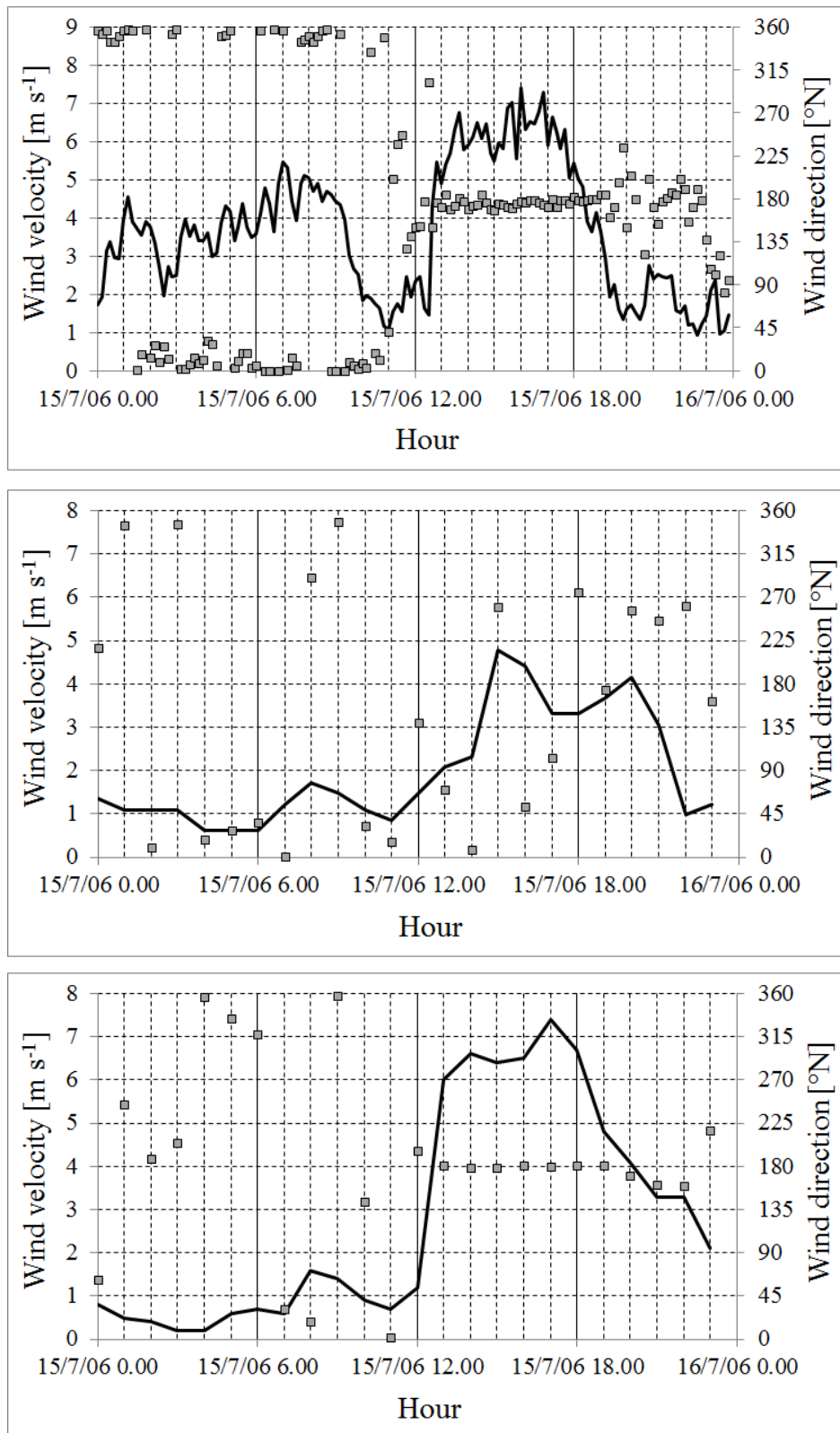
Figure 5.40: As in Fig. 5.38, but on 15 July 2006.
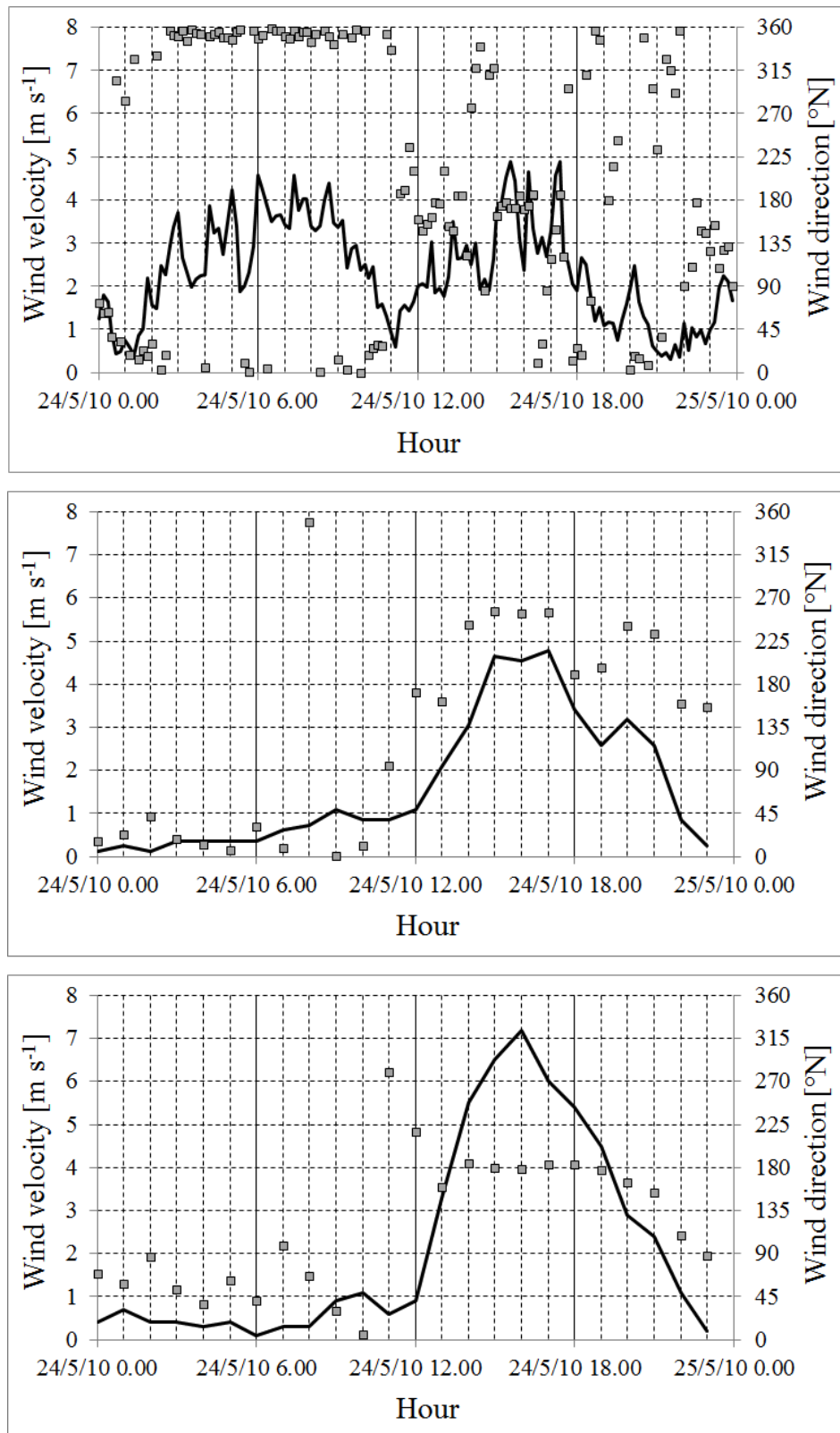
Figure 5.41: As in Fig. 5.38, but on 24 May 2010.

Chapter 6

High-resolution numerical simulations of valley boundary layer processes including urban areas

In the last few years, thanks to the progressive increase in available computational power, the horizontal resolution of simulations with mesoscale meteorological models has progressed to finer grid spacings, allowing the investigation of local-scale atmospheric processes, as local circulation systems and urban phenomena. In this Chapter simulations with the mesoscale meteorological model WRF (Skamarock et al. 2008), coupled with the BEP urban parameterization scheme (Martilli et al. 2002), are performed with a twofold aim: investigating the urban climate of Trento and the development of thermally driven local circulations in the valleys around the city.

As to local circulation systems, different studies have highlighted the ability of mesoscale models to capture the main features of boundary layer processes in mountain valleys. Zängl (2004) performed idealized numerical simulations with the mesoscale model MM5, with a horizontal resolution of 800 m in the inner domain, to study the development of valley winds in the Alpine Inn Valley. In these simulations he used a realistic topography, but idealized large-scale conditions, without synoptic forcing. The author compared some of the results of these simulations with measurements taken during an intensive field campaign, when valley winds were well-developed. This comparison indicated that the model was able to reproduce the main features of valley winds, even though no extensive comparisons were performed. Direct comparisons between numerical simulations with the RAMS mesoscale model and observations in the Alpine Riviera Valley were performed by de Wekker et al. (2005), referring to a clear sky day with light synoptic wind of the MAP-Riviera field study (Rotach et al. 2004). They found that numerical results reproduced with a reasonable accuracy the observations, even though some discrepancies were found. For example the model was not able to capture the ground-based

thermal inversion and postponed the timing of the transition between down-valley and up-valley winds for two hours. Recently Schmidli et al. (2011) performed an intercomparison of different mesoscale models to test their ability to simulate daytime valley wind systems in an idealized case. The results highlighted that there is a general agreement between the different models, but some discrepancies, especially in the timing of the starting of the up-valley wind, in the vertical structure of the boundary layer and in the vertical profile of the along-valley wind, were found.

As shown in Section 2.5, in the last few years several studies have utilized mesoscale meteorological models coupled with urban parameterization schemes to simulate the effects of urban areas on local climatic conditions and in particular on thermal and wind fields. These studies generally focused on big cities, especially in flat areas, where climatic conditions are mainly determined by synoptic forcings and urban effects can be easily detected. Moving to cities located in inhomogeneous terrain, where daily-periodic circulation systems may develop and deeply influence the local climate, only few works are present in the literature. As instance Thompson et al. (2007) and Dandou et al. (2009) analyzed climatic conditions of cities in coastal regions, where the development of the sea breeze may interact with the urban area, while Salamanca et al. (2011a) utilized the WRF model to evaluate the UHI of Madrid, located in moderately complex terrain. However, to the author's knowledge, the analysis presented in this Chapter represents the first attempt to model the urban climate of a city in a valley and the interactions between an urban area and valley winds. These objectives are particularly challenging due to the highly complex terrain surrounding the urban area of Trento, which is relatively small and located in a narrow valley.

Recent investigations of urban climatic conditions with mesoscale models coupled with urban parameterization schemes highlighted the importance of using high-resolution input datasets of urban morphology and anthropogenic heat flux to improve the accuracy of the results (cf. Salamanca et al. 2011b). Therefore for the analysis presented here, as it will be shown in the next Sections, particular attention has been devoted to obtain the relevant datasets for the city of Trento, from which maps of urban morphology and anthropogenic heat flux releases have been built.

6.1 The WRF model

The WRF model (Skamarock et al. 2008) is a state-of-the-art numerical weather prediction system for both operational and research activities developed at the National Center for Atmospheric Research (NCAR) in Boulder, Colorado. The equations integrated by the model are the compressible, non-hydrostatic Euler equations, formulated using a terrain-following mass vertical coordinate η:

$$\eta = \frac{p_{dh} - p_{dht}}{\mu_d} \tag{6.1}$$

where $\mu_d = p_{dhs} - p_{dht}$, p_{dh} is the hydrostatic component of pressure of the dry atmosphere and p_{dhs} and p_{dht} are the values at the surface and at the top boundary respectively. The moist Euler equations are:

$$\frac{\partial U}{\partial t} + \nabla \cdot \mathbf{V}u + \mu_d \alpha \frac{\partial p}{\partial x} + \left(\frac{\alpha}{\alpha_d}\right)\frac{\partial p}{\partial \eta}\frac{\partial \phi}{\partial x} = F_U \tag{6.2}$$

$$\frac{\partial V}{\partial t} + \nabla \cdot \mathbf{V}v + \mu_d \alpha \frac{\partial p}{\partial y} + \left(\frac{\alpha}{\alpha_d}\right)\frac{\partial p}{\partial \eta}\frac{\partial \phi}{\partial y} = F_V \tag{6.3}$$

$$\frac{\partial W}{\partial t} + \nabla \cdot \mathbf{V}w - g\left[\left(\frac{\alpha}{\alpha_d}\right)\frac{\partial p}{\partial \eta} - \mu_d\right] = F_W \tag{6.4}$$

$$\frac{\partial \Theta}{\partial t} + \nabla \cdot \mathbf{V}\Theta = F_\Theta \tag{6.5}$$

$$\frac{\partial \mu_d}{\partial t} + \nabla \cdot \mathbf{V} = 0 \tag{6.6}$$

$$\frac{\partial \phi}{\partial t} + \mu_d^{-1}\left[(\mathbf{V} \cdot \nabla \phi) - gW\right] = 0 \tag{6.7}$$

$$\frac{\partial Q_m}{\partial t} + \nabla \cdot \mathbf{V}q_m = F_{Q_m} \tag{6.8}$$

$$\frac{\partial \phi}{\partial \eta} = -\alpha_d \mu_d \tag{6.9}$$

$$p = p_0 \left(\frac{R_d \theta_m}{p_0 \alpha_d}\right)^\gamma \tag{6.10}$$

where $\mathbf{V} = \mu_d \mathbf{v}$, $\Theta = \mu_d \theta$, $\phi = gz$, α_d is the inverse density of dry air $1/\rho_d$, α is the inverse density taking into account the full parcel density, $\theta_m = \theta(1 + (R_v/R_d)q_v)$, $Q_m = \mu_d q_m$, q_m is the water mixing ratio and $\gamma = c_p/c_v$. The terms on the right-hand sides F_i represent the forcing terms.

Model variables are staggered in space on a C grid, with scalars defined at the center of grid boxes and normal velocity components on the corresponding box faces. As to the discretization in time, WRF uses a time-split integration scheme. Slow or low-frequency modes are integrated using a third-order Runge-Kutta time integration scheme, while the high-frequency acoustic modes are integrated over smaller time steps to prevent numerical instability.

6.1.1 Urban parameterization schemes

The WRF model can be coupled to a series of urban parameterization schemes with different degrees of complexity, in order to take into account the effects of urban areas on local climatic

conditions (Chen et al. 2011). The simplest approach is the "Bulk urban parameterization", where the effects of urban areas are simply parameterized changing the values of the roughness length, of the green vegetation fraction and of the properties of the surface materials. The second urban parameterization scheme that can be used in WRF is the single-layer model developed by Kusaka et al. (2001), which is very similar to the model presented in Chapter 4. The next urban scheme is the the multi-layer Building Environment Parameterization (BEP) model developed by Martilli et al. (2002), which represents the most sophisticated urban modeling in WRF. BEP takes into account the three-dimensional structure of urban areas and calculates the effects of horizontal and vertical surfaces on momentum, temperature and turbulent kinetic energy (TKE). Similarly to the single-layer model, also in BEP the urban area is represented by a series of urban street canyons, but with buildings of different heights. Also BEP takes into account the shadowing inside the street and the multiple reflections of long-wave and short-wave radiations. BEP can also be coupled to a Building Energy Model (BEM, Salamanca et al. 2010), to improve the estimate of the heat exchanged between the buildings and the atmosphere. BEM takes into account the diffusion of heat through the surfaces, the radiation exchanged through windows and between indoor surfaces, natural ventilation, the generation of heat due to occupants and equipments, air conditioning and heating. Moreover BEM can simulate the temperature evolution for different floors in the same building.

6.2   Set-up of the simulations
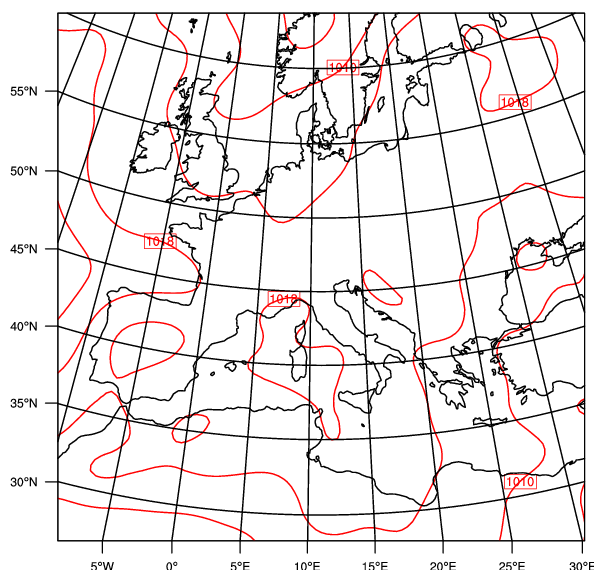
Figure 6.1: Sea-level pressure at 1200 UTC 1 August 2010.

Simulations focus on a completely sunny summer day, 1 August 2010, when daily-periodic local circulation systems were well developed. Figure 6.1 shows that North Italy was influenced by a relative high pressure with weak gradients. The 30-h simulations begin at 1800 UTC 31 July 2010 and finish at 0000 UTC 2 August 2010; the first 6 h are not considered for the analysis of the results. The horizontal domain used for the simulations (Fig. 6.2) is composed of five two-way nested domains with 100x100, 91x91, 91x100, 121x151, 193x241 cells, and grid spacings of 40.5, 13.5, 4.5, 1.5, 0.5 km, respectively, to cover all scales, from synoptic to local scales. 40 vertical levels, with higher resolutions near the ground, have been used. Finer vertical resolutions have been prevented by numerical stability problems, which rise in simulations in complex terrain. The initial and boundary conditions are supplied by the National Center for Environmental Prediction (NCEP) Operational Global Analysis data on 1.0x1.0 degree grids and with a temporal resolution of 6 h. The model output is written every 15 min.

The present simulations are run using the BEP model as urban parameterization scheme, coupled with the NOAH land surface model (Chen and Dudhia 2001), and the one-and-a-half-order closure Bougeault and Lacarrére (1989) turbulent scheme. As to the physical properties of the urban materials, it has been decided to use the default values contained in the URB-PARM.TBL file.
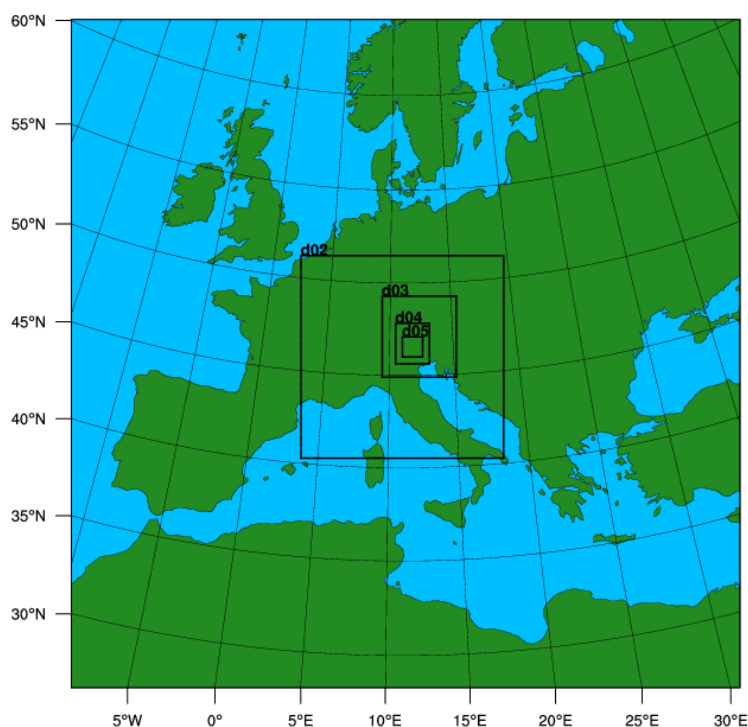
Figure 6.2: Five nested domains utilized for the simulations.

6.2.1 Topography

In order to perform realistic high-resolution simulations in complex terrain, it is important to use
a high-resolution topography dataset. The default topography dataset included in WRF has a
spatial resolution of 30" ($\sim$ 1 km), which is too coarse for the purpose of the simulations. For this
reason the topography data obtained from the website http://www.viewfinderpanoramas.org/
with a spatial resolution of 1" ($\sim$ 30 m) have been used, slightly smoothed (one smooth pass
with the 1-2-1 smooth filter) to prevent numerical instability. The topography of the inner
domain is shown in Fig. 6.3.
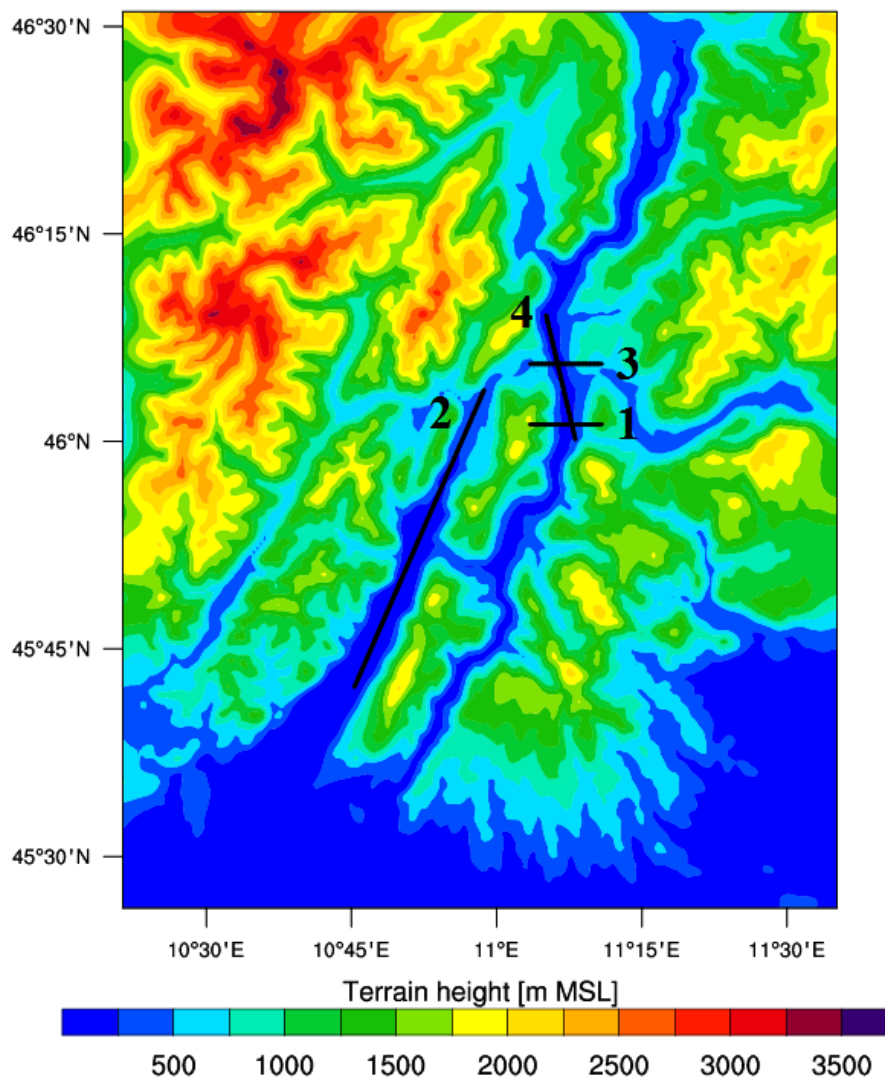
Figure 6.3: Topography in the inner domain, along with the cross sections that will be analyzed in this
Chapter.

6.2.2   Land use

Similarly to the topography, also the default land use in WRF has a spatial resolution of 30" (Modis), too coarse for the scopes of the simulations. In this case it has been decided to use Corine Land Cover (CLC) dataset (2006) from the European Environment Agency (http://www.eea.europa.eu), which has a spatial resolution of 100 m and 44 classes. Since most land use classes in CLC dataset do not match the 20 classes (+3 special classes for urban land use) in the Modis dataset, the CLC dataset has been cross-referenced in order to use the WRF look-up tables for the Modis dataset (see Tab. 6.1). Figure 6.4 shows the land use categories in the inner domain.
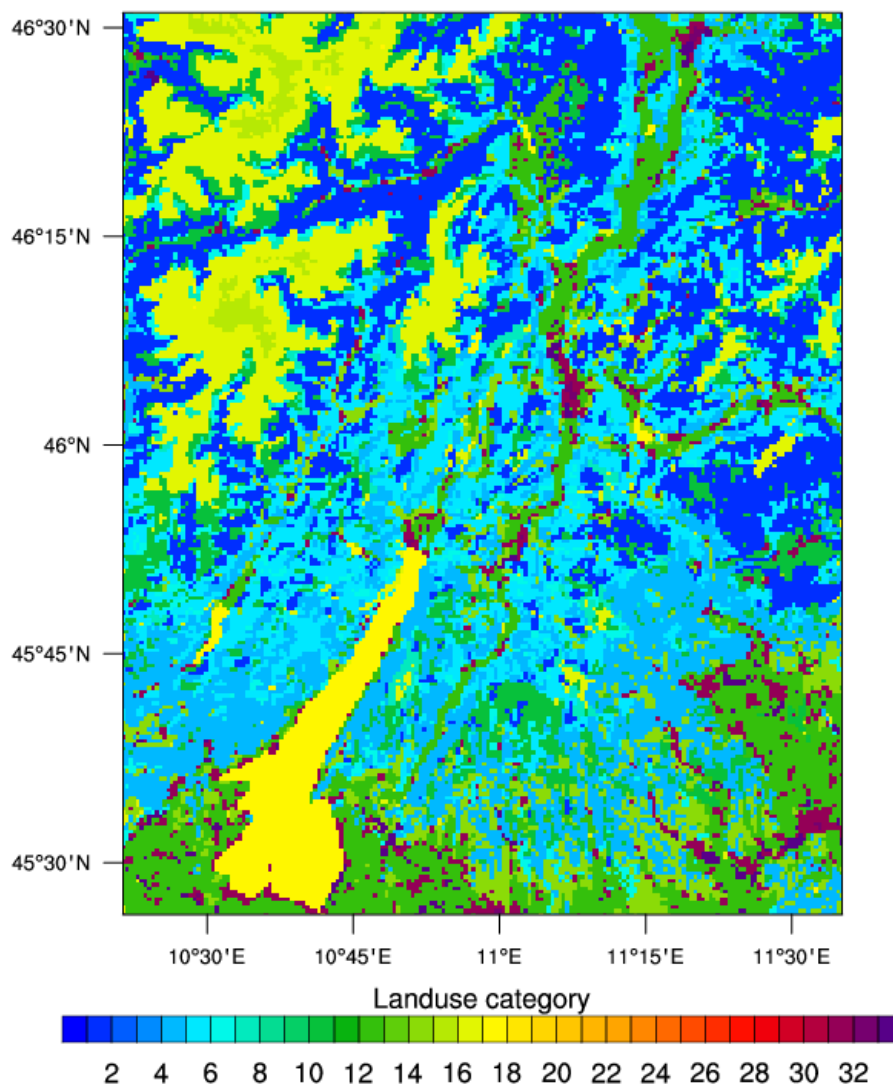
Figure 6.4: Land use categories in the inner domain.

6. High-resolution numerical simulations of valley boundary layer processes including urban areas

Table 6.1: Remapping of the 44 CLC dataset categories into the 20+3 Modis categories

CORINE	MODIS
1 Continuous urban fabric	32 High intensity residential
2 Discontinuous urban fabric	31 Low intensity residential
3 Industrial or commercial units	33 Industrial or commercial
4 Road and rail networks and associated land	33 Industrial or commercial
5 Port areas	33 Industrial or commercial
6 Airports	33 Industrial or commercial
7 Mineral extraction sites	16 Barren or sparsely vegetated
8 Dump sites	33 Industrial or commercial
9 Construction sites	33 Industrial or commercial
10 Green urban areas	10 Grasslands
11 Sport and leisure facilities	33 Industrial or commercial
12 Non-irrigated arable land	12 Croplands
13 Permanently irrigated land	12 Croplands
14 Rice fields	11 Permanent wetlands
15 Vineyards	12 Croplands
16 Fruit trees and berry plantations	12 Croplands
17 Olive groves	12 Croplands
18 Pastures	12 Grasslands
19 Annual crops associated with permanent crops	12 Croplands
20 Complex cultivation patterns	12 Croplands
21 Land principally occupied by agriculture, with significant areas of natural vegetation	14 Cropland/Natural vegetation mosaic
22 Agro-forestry areas	14 Cropland/Natural vegetation mosaic
23 Broad-leaved forest	4 Deciduous broadleaf forest
24 Coniferous forest	1 Evergreen needleleaf forest
25 Mixed forest	5 Mixed forest
26 Natural grasslands	10 Grasslands
27 Moors and heathland	7 Open shrublands
28 Sclerophyllous vegetation	2 Evergreen broadleaf forest
29 Transitional woodland-shrub	6 Closed shrublands
30 Beaches, dunes, sand	16 Barren or sparsely vegetated
31 Bare rocks	16 Barren or sparsely vegetated
32 Sparsely vegetated areas	16 Barren or sparsely vegetated
33 Burnt areas	16 Barren or sparsely vegetated
34 Glaciers and perpetual snow	15 Snow and ice
35 Inland marshes	11 Permanent wetlands
36 Peat bogs	11 Permanent wetlands
37 Salt marshes	11 Permanent wetlands

continued from previous page

CORINE	MODIS
38 Salines	11 Permanent wetlands
39 Intertidal flats	11 Permanent wetlands
40 Water courses	17 Water
41 Water bodies	17 Water
42 Coastal lagoons	17 Water
43 Estuaries	17 Water
44 Sea and ocean	17 Water

6.2.3 Urban morphology

As said in the first part of this Chapter, one of the crucial aspects when using an urban parameterization scheme coupled to a mesoscale model is the specification of the large number of urban morphology parameters needed to characterize in an adequate way the spatial characteristics of the urban area. The version of the WRF model used here was modified by dr. Alberto Martilli and dr. Francisco Salamanca to directly ingest the following gridded urban parameters as input for the BEP scheme:

- Building planar area fraction $\lambda_p = A_p/A_t$, where A_p is the plan area of buildings, A_t is the total area;

- Building surface area to plan area ratio $\lambda_b = (A_p + A_w)/A_t$, where A_w is the wall surface area;

- Average building height h_m;

- Distribution of building heights (every 5 m);

- Urban fraction.

In the present case urban morphology parameters have been obtained with GIS techniques from the high-resolution (horizontal accuracy of 1 m and vertical accuracy of 0.15 m) lidar data of the Autonomous Province of Trento (Fig. 6.5) and the land use map of the Municipality of Trento. Figures 6.6 - 6.9 show the maps obtained and used as input for the BEP scheme, on a grid of 500 m. It can be seen that the highest values of λ_p, λ_b and h_m are present in the central part of the city, indicating a more compact urban morphology with higher buildings.
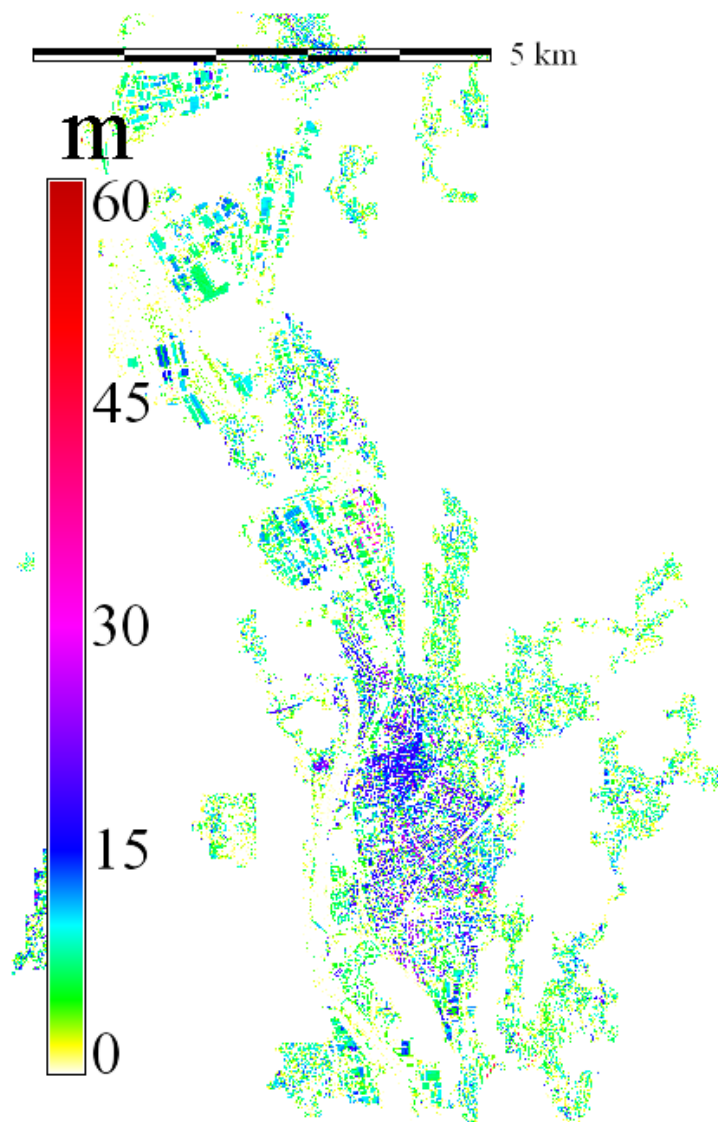
Figure 6.5: Map of the height of the buildings in the city of Trento, extracted from the high-resolution lidar data of the Autonomous Province of Trento.

6.2.4   Anthropogenic heat flux

As said in the Introduction, the anthropogenic heat flux may be an important additional heat source in urban areas, with considerable effects on the urban climate. Spatially and temporally detailed anthropogenic heat gridded fields are required to take into account these possible effects in mesoscale meteorological models. The determination of these gridded fields, referring to the anthropogenic heat flux released by the different sectors (buildings, industry, vehicular traffic), is often a difficult task, due to the lack of availability of the relevant data. For this reason in many studies, when data are not available, simplifications in the temporal and spatial variations
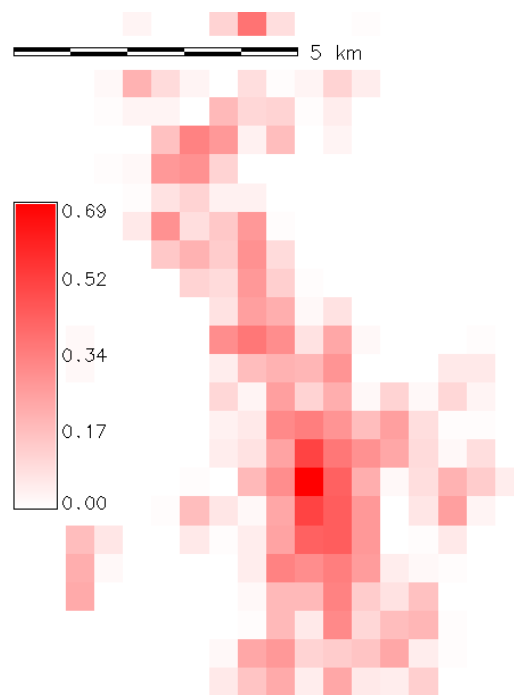
Figure 6.6: Map of the building planar area fraction λ_p in the city of Trento on a grid of 500 m extracted from the high-resolution lidar data of the Autonomous Province of Trento.
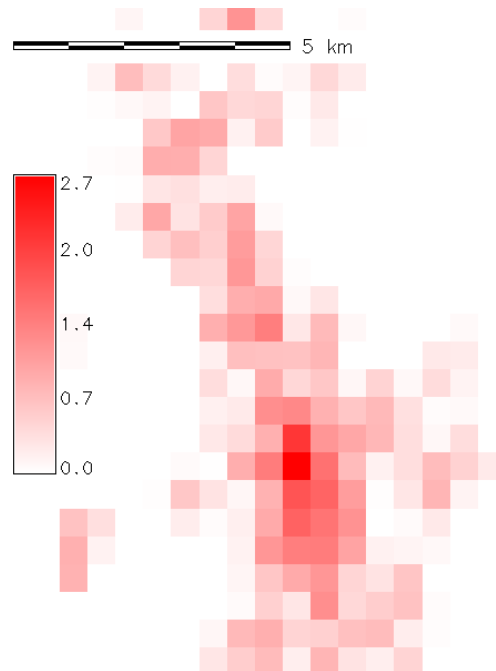
Figure 6.7: As in Fig. 6.6, but for building surface area to plan area ratio λ_b.
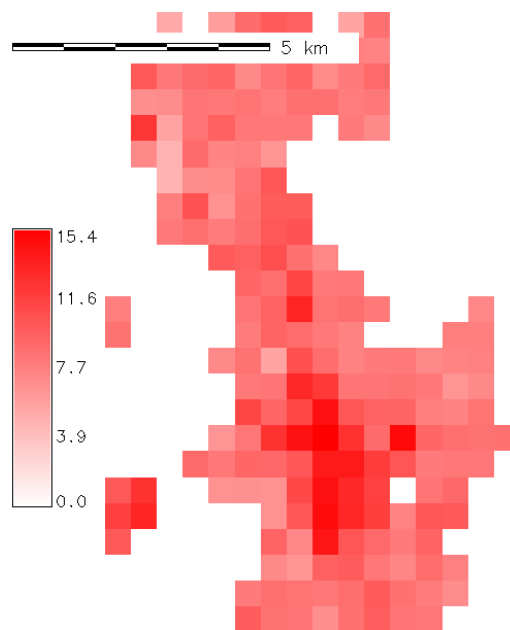
Figure 6.8: As in Fig. 6.6, but for the height of the buildings h_m (m).
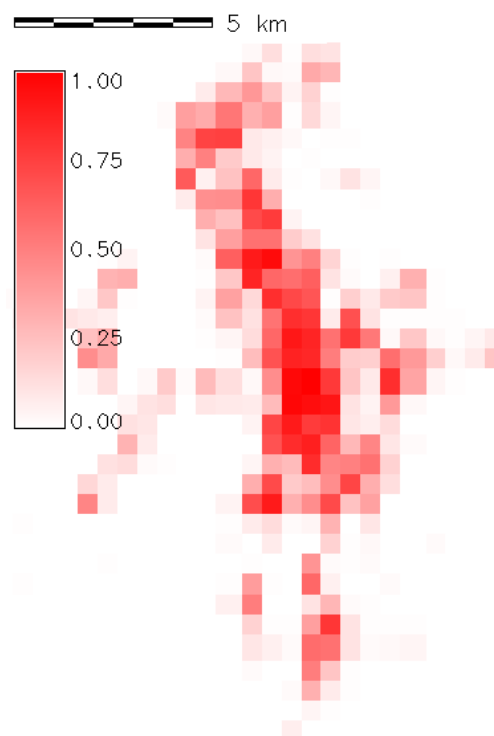
Figure 6.9: Map of the urban fraction in the city of Trento on a grid of 500 m obtained from a high-resolution land use map of the Municipality of Trento.
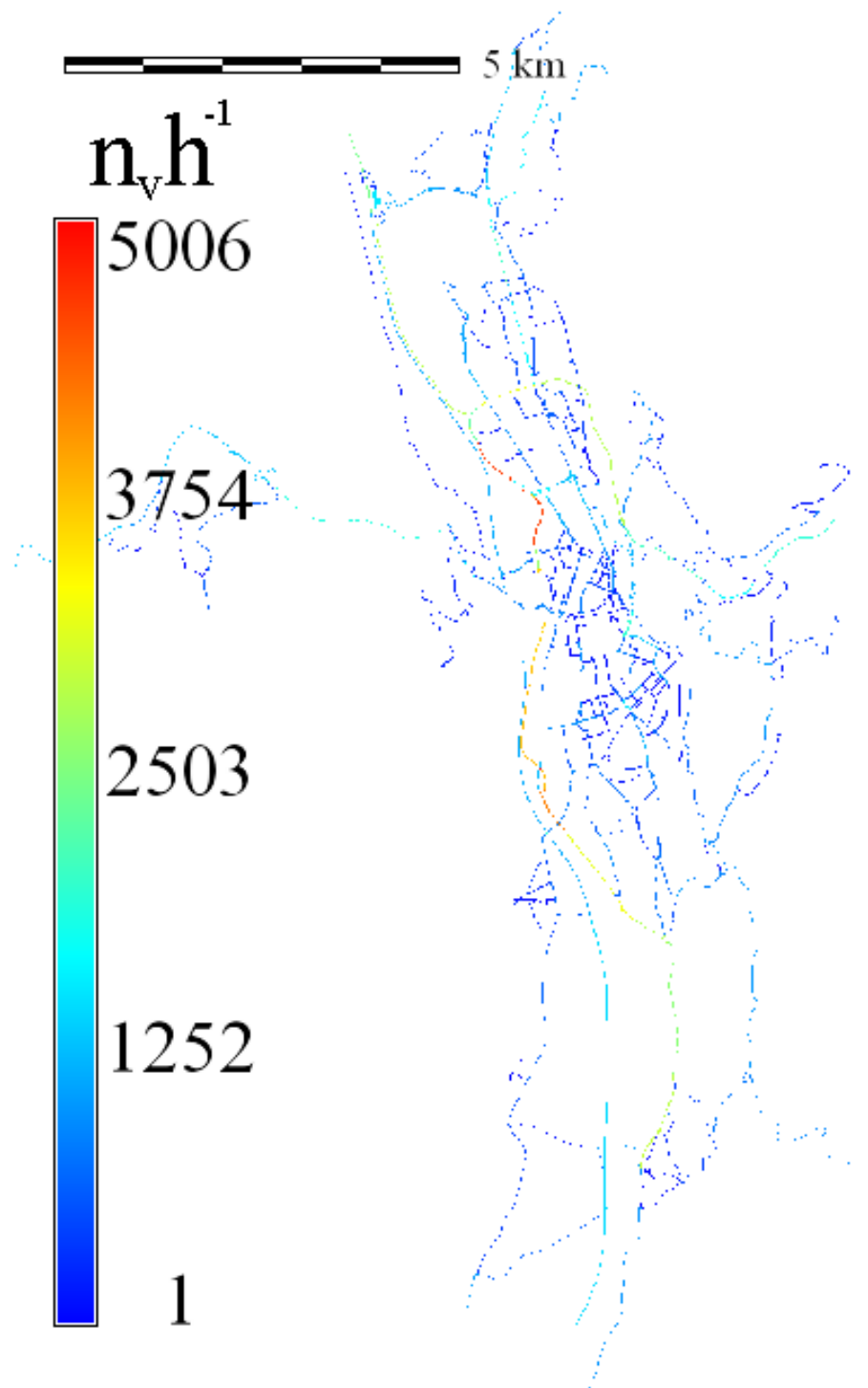
Figure 6.10: Average hourly vehicular fluxes along the roads in the Municipality of Trento (number of vehicles per hour), obtained from the Urban Mobility Plan of Trento.

of the anthropogenic heat flux are assumed (Sailor and Lu 2004). In the present case detailed data regarding vehicular traffic and energy consumption were present and for this reason it was possible to calculate hourly gridded fields of anthropogenic heat flux to use as input data for the BEP scheme.

The anthropogenic heat flux from vehicular traffic was estimated from the vehicular fluxes data contained in the Urban Mobility Plan of Trento and from the hourly vehicular fluxes profiles measured in different streets of the city of Trento. The Urban Mobility Plan of Trento supplies an estimate of the average vehicular fluxes along the roads in the Municipality of Trento, obtained from simulations with the software "Cube" and validated with measurements performed in different streets of the urban area. GIS techniques have been utilized to obtain the relevant maps: Fig. 6.10 shows, as an example, the average hourly fluxes along the roads in the Municipality of Trento. It can be seen that the highest vehicular traffic is present along the highway in the western part of the valley.
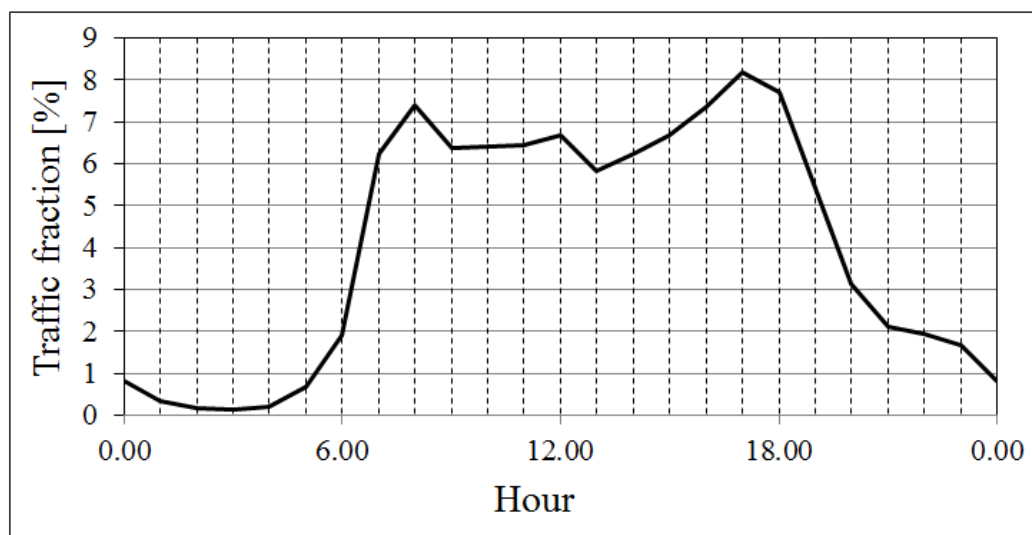
Figure 6.11: Hourly fractional traffic profile for the city of Trento obtained from measurements performed by the Municipality of Trento in different roads of the urban area.

Starting from the average hourly data contained in the Urban Mobility Plan, the actual hourly vehicular fluxes were calculated utilizing the real traffic measurements performed by the Municipality of Trento along different roads of the urban area, converted to fractions of daily traffic occurring within each hour (Fig. 6.11). The shape of the curve obtained from the traffic measurements is similar to those observed in other cities (cf. Grimmond 1992; Sailor and Lu 2004), with two peaks corresponding to the rush hours in the morning and in the evening. Finally the anthropogenic heat flux from vehicular traffic Q_v for each grid cell in the model was
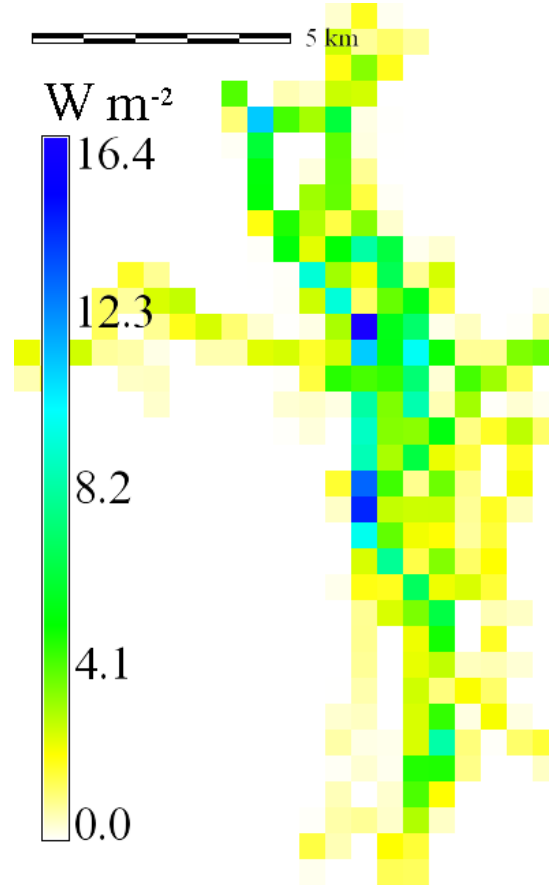
Figure 6.12: Average anthropogenic heat flux from vehicular traffic in the city of Trento on 500 m grid cells.

estimated using the expression proposed by Grimmond (1992):

$$\begin{cases} Q_v = \frac{n_v D_v EV}{A \cdot 3600} & [\text{W m}^{-2}] \\ EV = \frac{NHC\rho_f}{FE} & [\text{J m}^{-1}] \end{cases} \tag{6.11}$$

where n_v is the hourly vehicular flux, D_v [m] the length of the road, A [m^2] the area of the grid cell, NHC [J kg^{-1}] the net heat of combustion, ρ_f [kg l^{-1}] the density of fuel, and FE [m l^{-1}] the mean fuel economy. The values of NHC, ρ_f and FE have been chosen from typical values present in the literature ($NHC = 45 \cdot 10^6$ J kg^{-1}, $\rho_f = 0.75$ kg l^{-1}, $FE = 8500$ m l^{-1}, Sailor and Lu 2004). Figure 6.12 shows, as an example, the average anthropogenic heat flux from vehicular traffic calculated on 500 m grid cells.

Gridded fields of anthropogenic heat flux from buildings and industries were estimated, similarly to what suggested by Sailor and Lu (2004), through an inventory approach. The data available for these analyses, obtained also in this case from the Municipality of Trento, were the
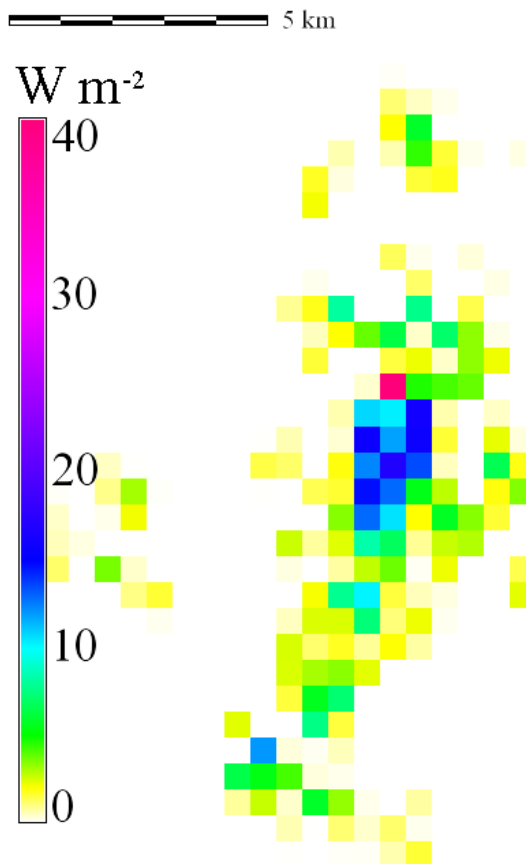
Figure 6.13: Average anthropogenic heat flux from buildings and industries in the city of Trento on 500 m grid cells.

yearly natural gas consumption for each user in the Municipality of Trento (more than 50 000 data) and the total yearly energy consumption for the different energy vectors (solid fuels, LPG, fuel oil, natural gas, electric energy). Since information about the spatial distribution of energy consumptions but the natural gas was not present, it was assumed that this spatial distribution can be extended also to the other energy vectors. This simplification may lead to some errors, especially because the fraction of energy vectors used by the building and industry sectors is different: the building sector utilizes, especially in the winter period, a higher fraction of natural gas, while the industry sector a higher fraction of electric energy. Also the daily and monthly cycles of energy consumption in the city of Trento were not available and for this reason the temporal behavior was estimated from typical cycles for the north-east part of Italy. Starting from these energy consumption data, the corresponding anthropogenic heat flux releases were calculated assuming a nominal heating value for the natural gas of $43 \cdot 10^6$ J m^{-3} and a thermal combustion efficiency of 80% (Sailor and Lu 2004). Figure 6.13 shows, as an example, the average anthropogenic heat flux releases from buildings and industries in the urban area of

Trento. The highest values occur in the city center and in the northern part of the urban area, where there are some shopping centers. It can be supposed that the releases are underestimated in the area north of the shopping centers, where there is the industrial area of Trento, due to the lack of data about the spatial distribution of the electric energy consumptions.
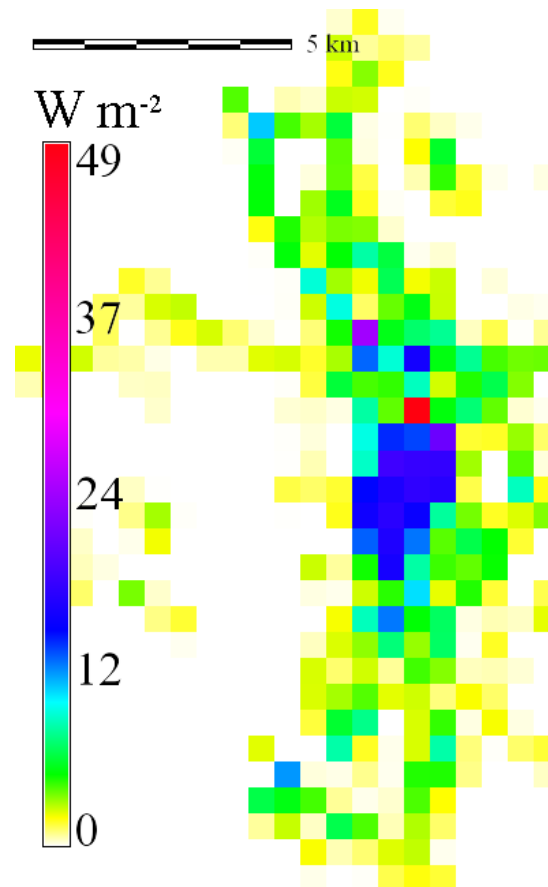
Figure 6.14: Total average anthropogenic heat flux in the urban area of Trento.

Finally the releases from the different sources were summed; Fig. 6.14 shows the total average anthropogenic heat flux in the urban area of Trento. The values found are quite low if compared with big cities (e.g. Miao et al. 2009), but not so different from what found in Salt Lake City (Sailor and Lu 2004), slightly bigger than Trento, but with a similar climate.

In the present analysis the water vapor releases from human activities have been neglected. Moreover, using the inventory approach for estimating the anthropogenic heat flux from building and industry sectors, it has been assumed that there is no time lag between consumptions and emissions (Sailor 2011).

6.3   Analysis of the results

6.3.1   Synoptic situation
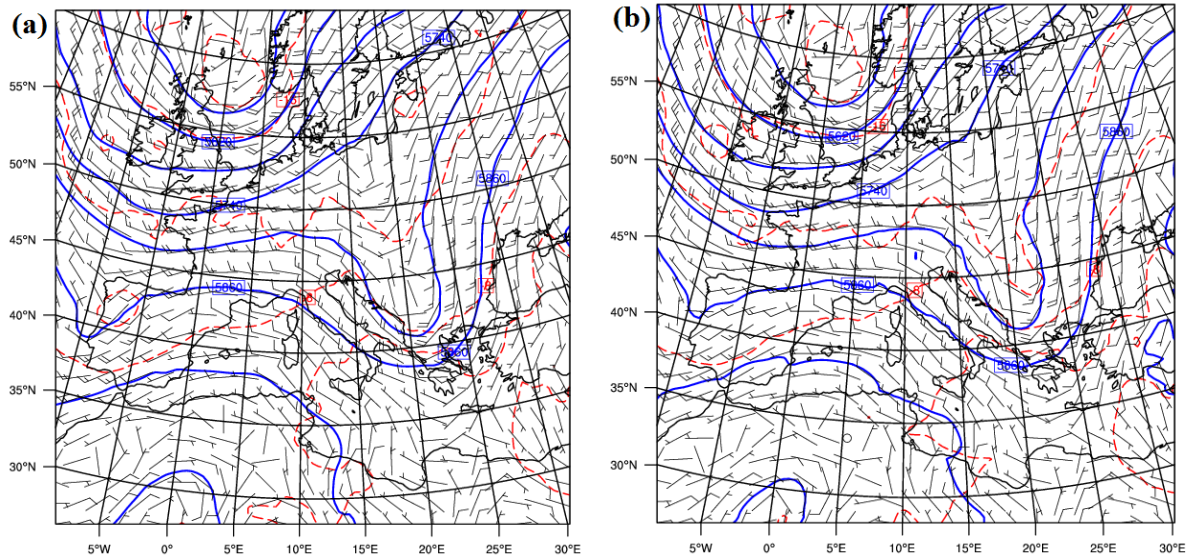
Figure 6.15: Synoptic weather conditions from (a) reanalysis and (b) simulation in the first domain at 500 hPa at 0000 UTC 1 August 2010, showing geopotential height (m, blue lines), temperature (°C, red dashed lines) and wind vectors.
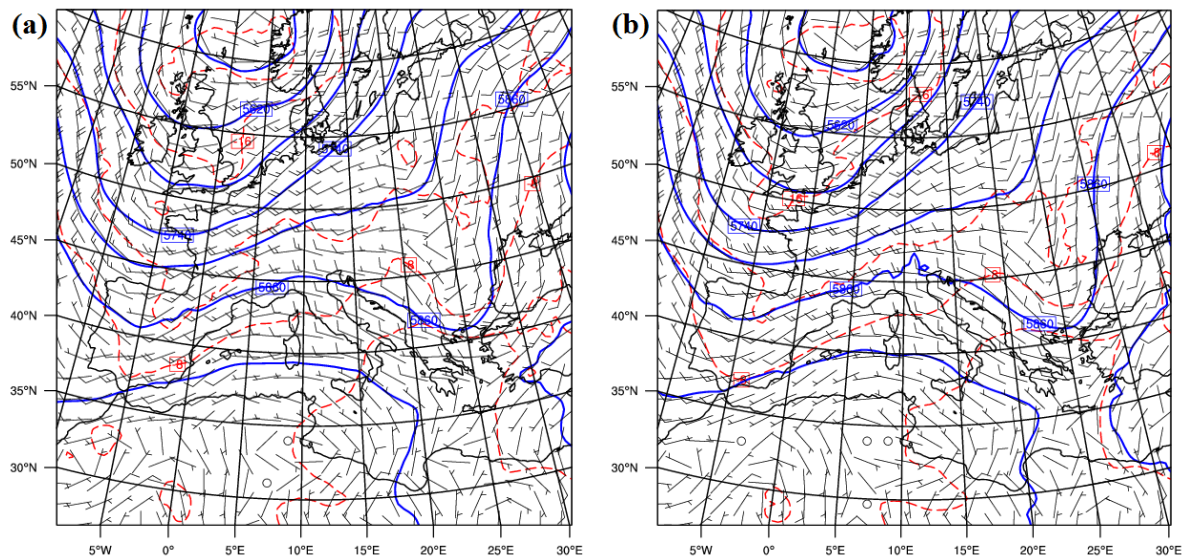
Figure 6.16: As in Fig. 6.15, but at 1200 UTC 1 August 2010.
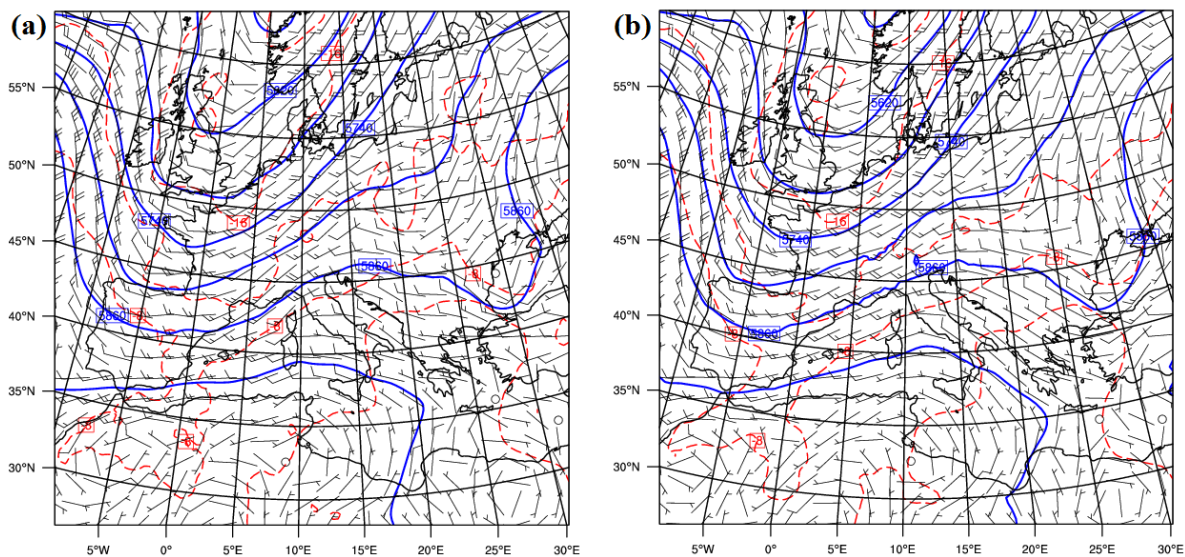
Figure 6.17: As in Fig. 6.15, but at 0000 UTC 2 August 2010.

Figures 6.15 - 6.17 show that the model well simulates the synoptic situation in the first domain, characterized by the presence of a trough north of Great Britain, moving towards south-east. In particular in both the reanalysis and the simulation wind at 500 hPa over North Italy is from north-west at 0000 UTC 1 August 2010, and then turns from south-west at 0000 UTC 2 August 2010.

6.3.2 Along-valley wind daily cycles

The along-valley wind simulated by the model at 10 m AGL in the Adige, Sarca and Lakes valleys has been tested against measurements from surface weather stations. All data reported are hourly averages. In the Adige Valley (Figs. 6.18 - 6.22) the main features of the daily cycle are well captured, with a light down-valley wind at night and the onset of a stronger up-valley wind in the late morning until evening. However some minor errors are present. The onset of the up-valley wind in the simulation is about an hour earlier than in the observations, while its intensity is slightly underestimated at Ala and Trento Sud. On the other hand the up-valley wind is overestimated at Bolzano.

Figure 6.21 shows the along-valley wind daily cycle simulated at Roveré della Luna; unfortunately data from this weather station were not available for this day. However it is noticeable that the model sees an up-valley wind lasting until 0200 UTC, as in the average along-valley wind daily cycle shown in Fig. 5.17 and in the daily cycle in Fig. 5.19. Therefore the model is able to capture also the local modifications in the along-valley wind daily cycles, induced by changes in the geometry of the valley. On the other hand the strength of the up-valley wind is probably overestimated in the evening.

Ala
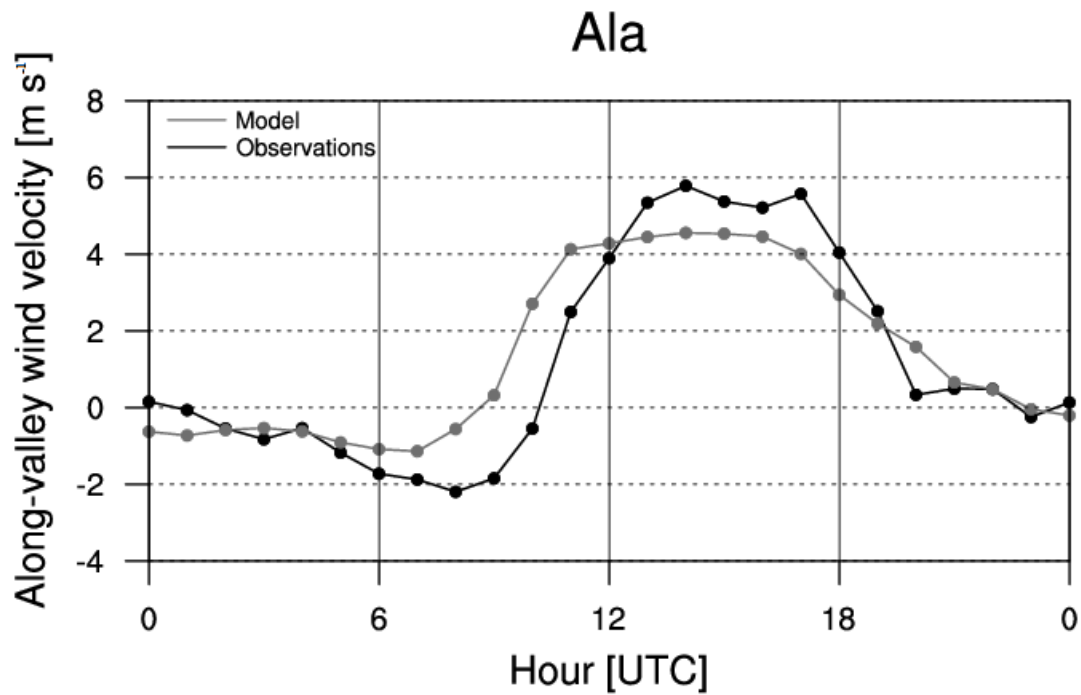
Figure 6.18: Along-valley wind daily cycle at 10 m AGL at Ala weather station on 1 August 2010 obtained from model results (gray line) and observations (black line).
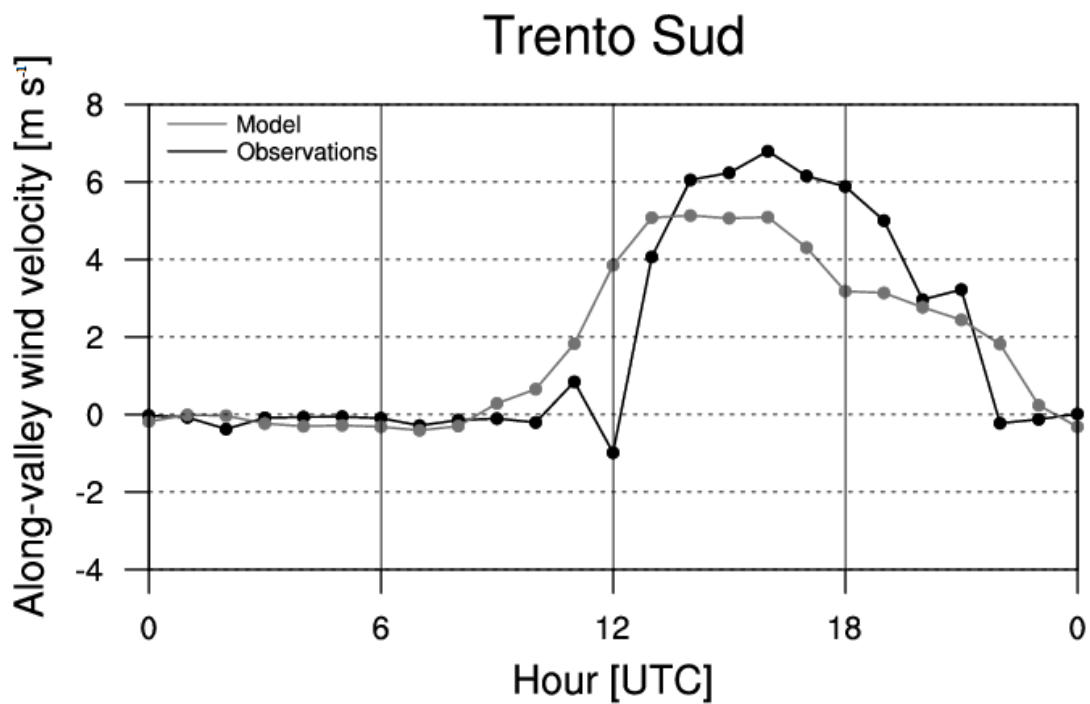
Trento Sud

Figure 6.19: As in Fig. 6.18 but at Trento Sud weather station.
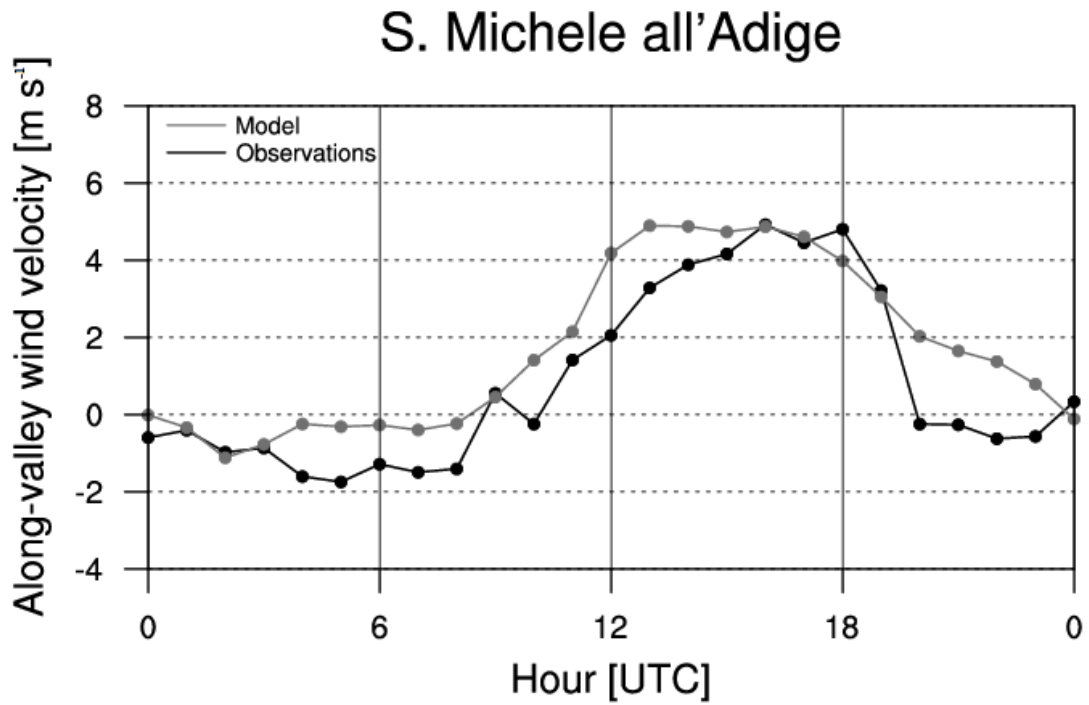
S. Michele all'Adige

Figure 6.20: As in Fig. 6.18 but at S. Michele all'Adige weather station.
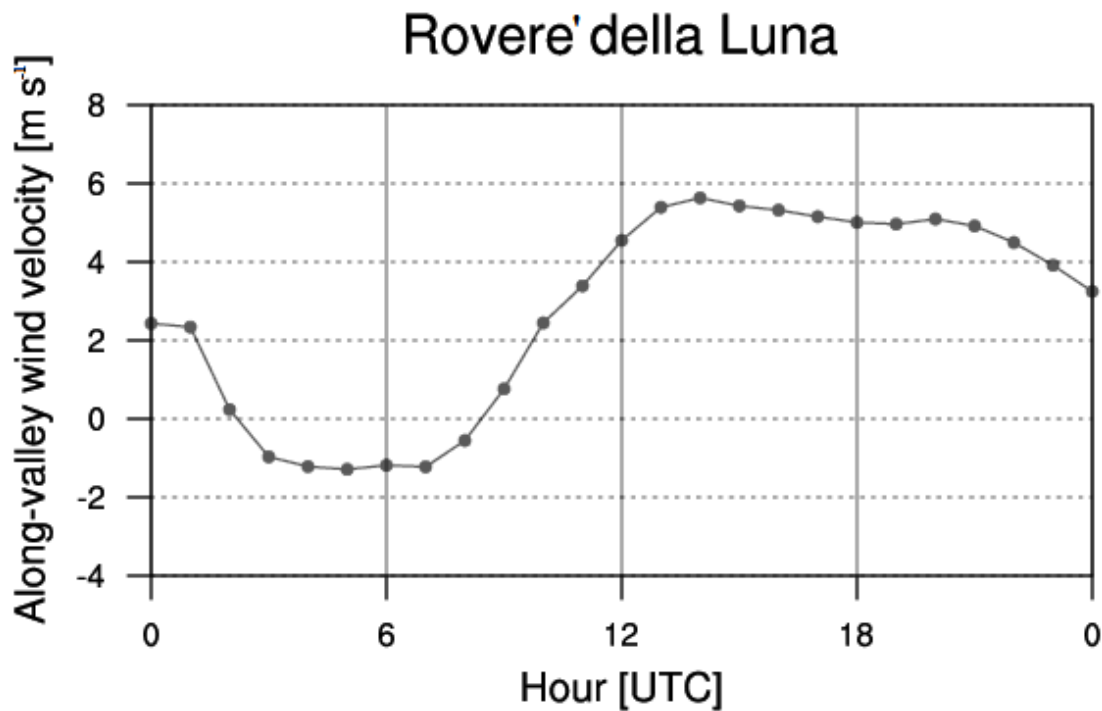
Rovere' della Luna

Figure 6.21: Along-valley wind daily cycle at Roveré della Luna weather station on 1 August 2010 from model results.
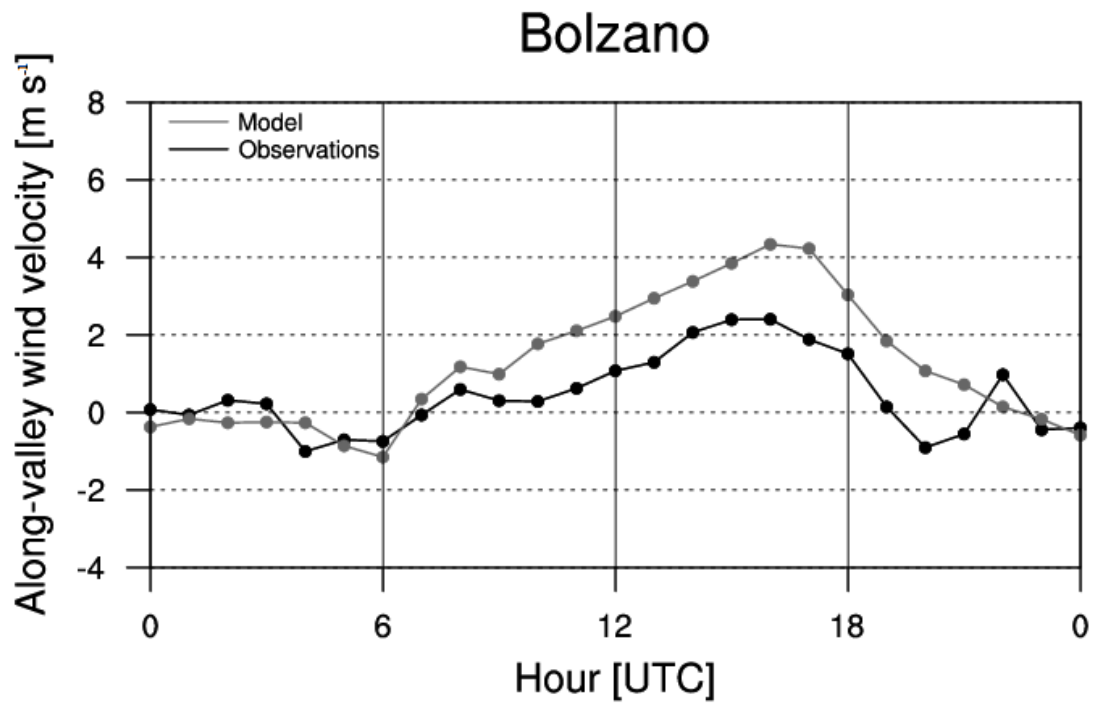
Bolzano

Figure 6.22: As in Fig. 6.18 but at Bolzano weather station.
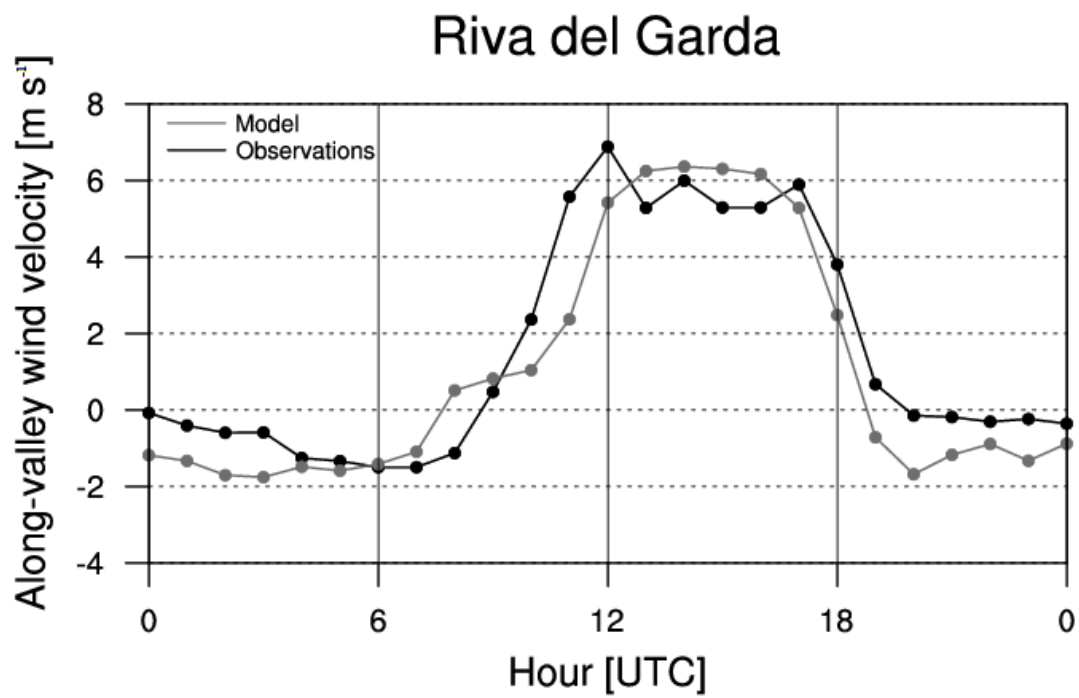
Riva del Garda

Figure 6.23: As in Fig. 6.18 but at Riva del Garda weather station.
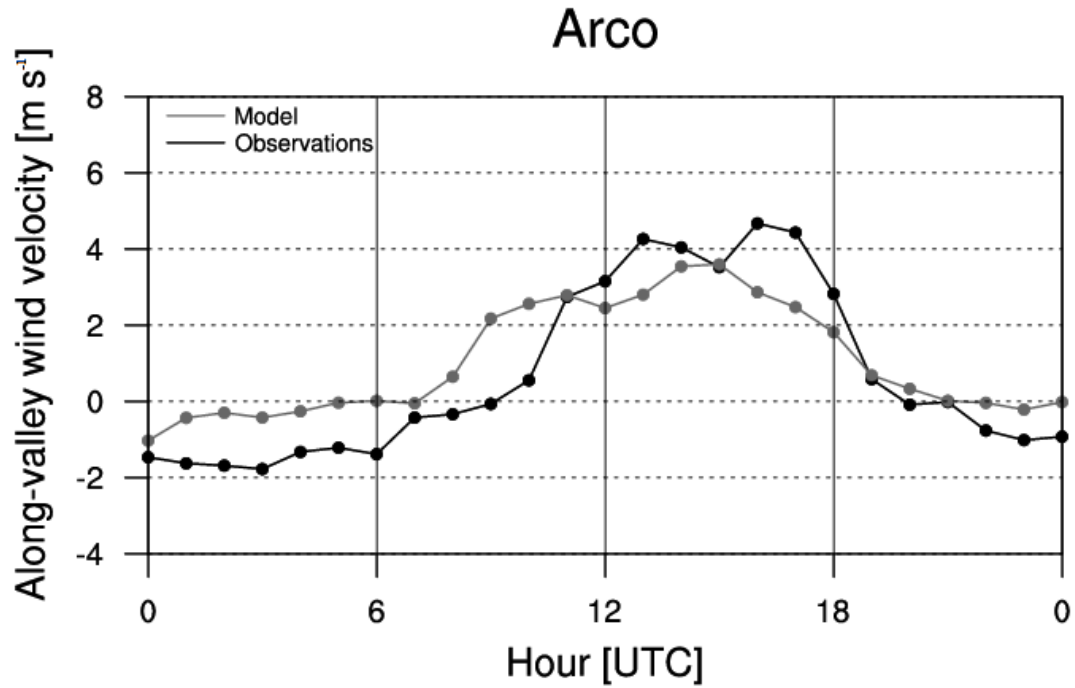
Figure 6.24: As in Fig. 6.18 but at Arco weather station.
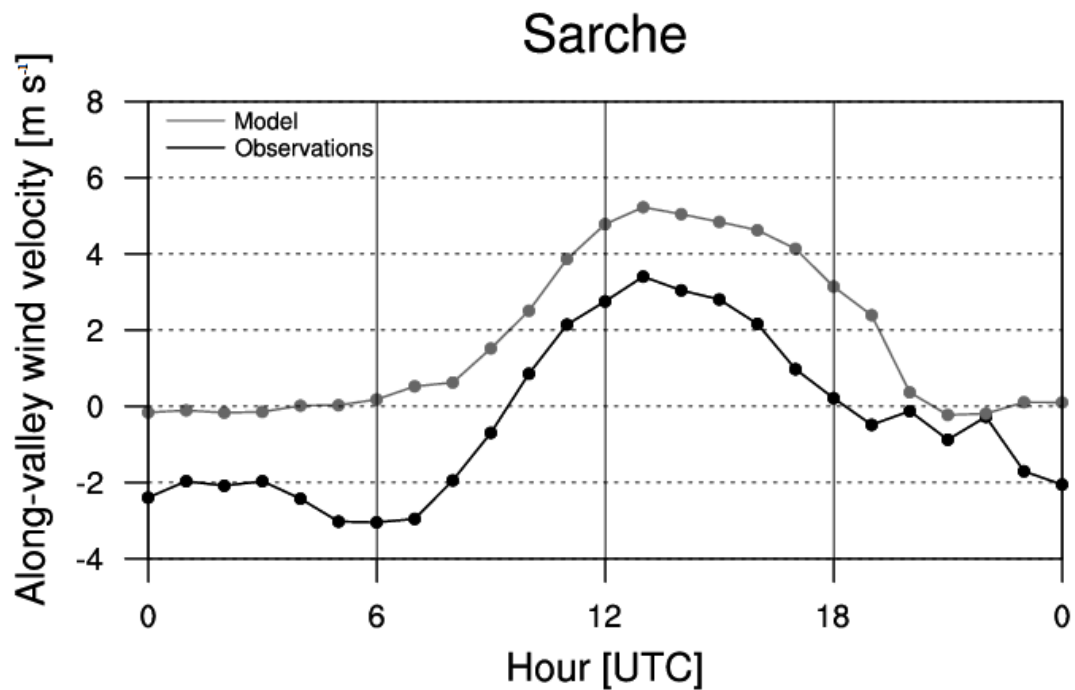
Figure 6.25: As in Fig. 6.18 but at Sarche weather station.

Moving to Sarca and Lakes valleys, Fig. 6.23 shows that there is a good agreement between model results and observations at Riva del Garda. In particular the onset of the Ora del Garda in the morning and its intensity in the afternoon are well captured by the model. A good agreement is present also at Arco, even though the down-valley wind is underestimated and the wind reversal in the morning is anticipated by two hours. It seems that in the simulation an up-valley wind starts to blow at Arco before the arrival of the lake breeze front. Thus, as in the Adige Valley, the model anticipates the onset of the up-valley wind in the morning. At Sarche the model results are not satisfactory: the model underestimates the down-valley wind at night, while it overestimates the up-valley wind during daytime.

6.3.3 Cross-valley circulations

Figures 6.26 - 6.33 show the evolution of the flow and of the potential temperature in a cross section of the Adige Valley located where the city of Trento lies (cross-section 1 in Fig. 6.3), so as to evaluate the vertical profile of the along-valley wind and the development of cross-valley circulations. It has to be noticed that the vertical resolution close to the ground utilized in this work is not sufficiently fine to give a complete representation of cross-valley winds, which typically present shallow vertical extensions (see Section 5.1), and are generally investigated by means of numerical simulations in idealized valleys with simple and regular geometries (cf. Serafin and Zardi 2010a,b).

At 0300 UTC light and very shallow down-slope winds are present on both sidewalls. The down-valley wind layer has a depth of about 700-800 m, while above this height a light up-valley wind is present. At 0600 UTC on the east-facing slope, which starts to be heated by solar radiation, there is the development of light up-slope winds, whereas on the west-facing sidewall down-slope winds continue. The down-valley wind is stronger, reaching a maximum velocity of 2.5 m s^{-1} in the center of the valley, 300 m above the valley floor. An up-valley wind is still present at higher heights, with maximum velocities 1000-1500 m above the valley floor.

Later in the morning, as the sun begins to heat also the west-facing slope, light up-slope winds begin to develop also on this sidewall, while the along-valley wind, which reverses from down- to up-valley, is very weak in the low layers (Fig. 6.28). The potential temperature distribution shows the heating of both slopes and the presence of potentially cooler air in the center of the valley. At 1200 UTC a quite strong up-valley wind develops in the low levels in the center of the valley, where potentially cooler air is still present. The up-slope wind on the eastern slope is quite strong and probably overestimated by the model. A well-mixed layer then develops during the day, as shown in Fig. 6.30, referring to 1500 UTC. In these hours the up-valley wind is well developed, with maximum velocities of about 7-8 m s^{-1}, especially in the center of the valley and near the ground. The up-valley wind layer reaches a depth of
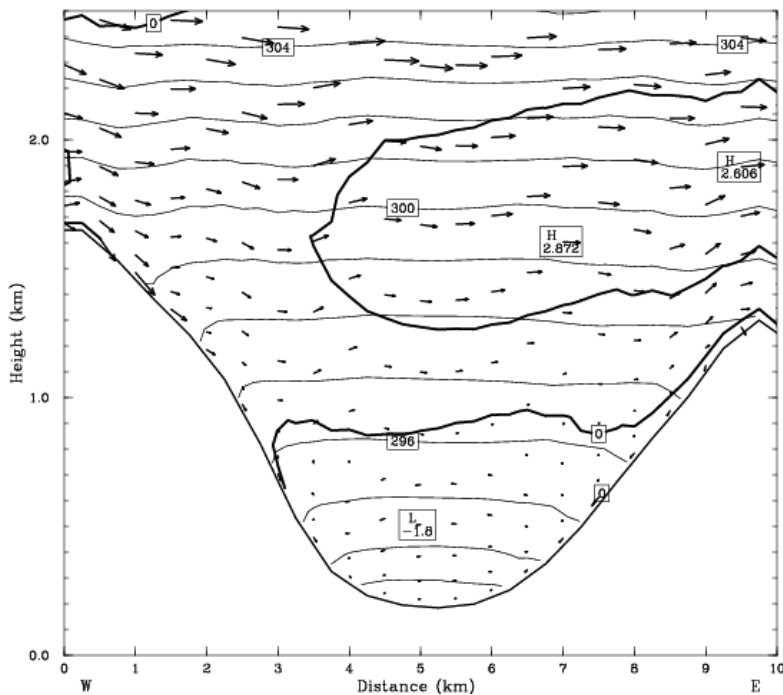
Figure 6.26: Cross valley section at 0300 UTC 1 August 2010 (cross section 1 in Fig. 6.3) showing cross-valley wind vectors, along-valley wind velocity (bold contours: contour interval = 2 m s^{-1}), and potential temperature (thin contours: contour interval = 1 K).
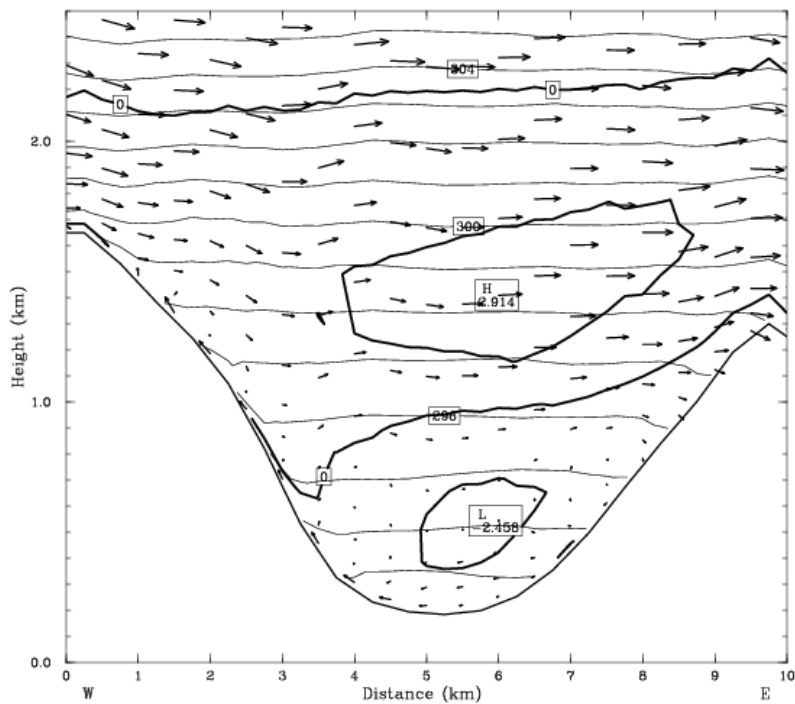
Figure 6.27: As in Fig. 6.26 but at 0600 UTC 1 August 2010.
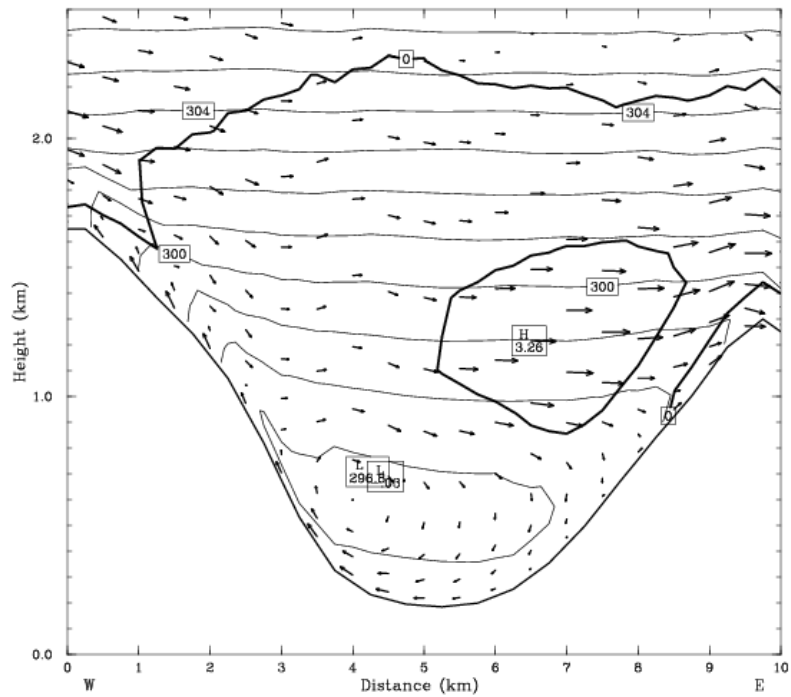
Figure 6.28: As in Fig. 6.26 but at 0900 UTC 1 August 2010.
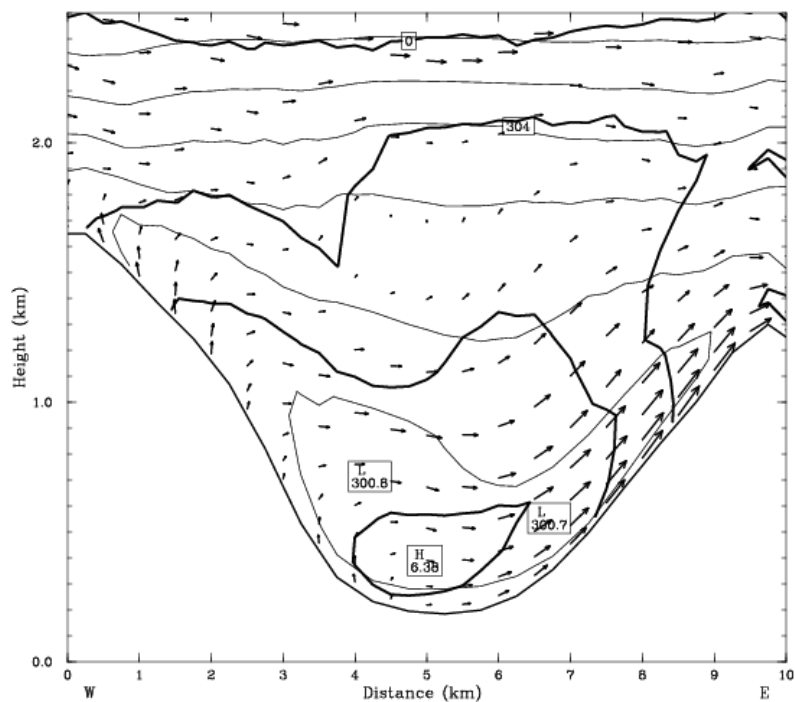
Figure 6.29: As in Fig. 6.26 but at 1200 UTC 1 August 2010.
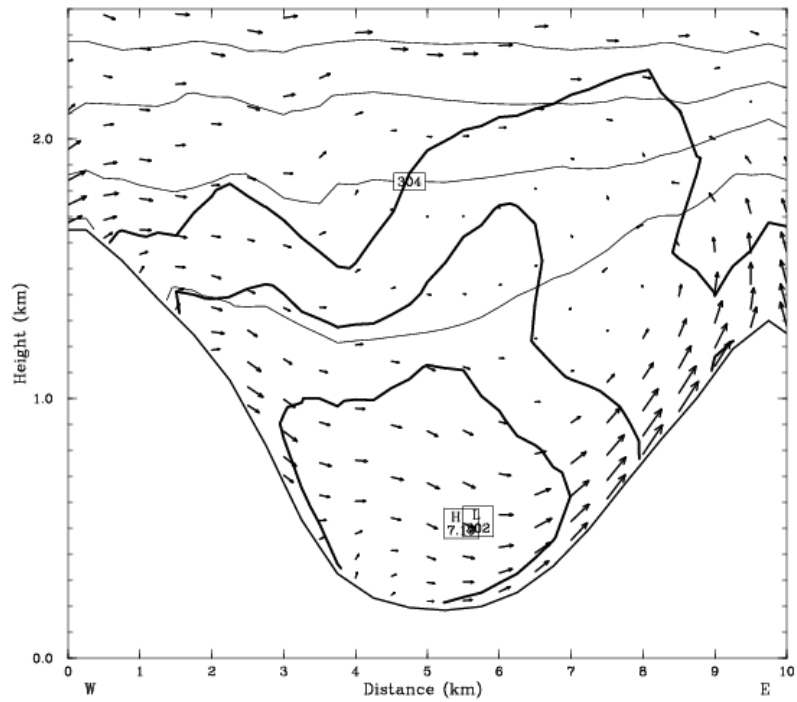
Figure 6.30: As in Fig. 6.26 but at 1500 UTC 1 August 2010.
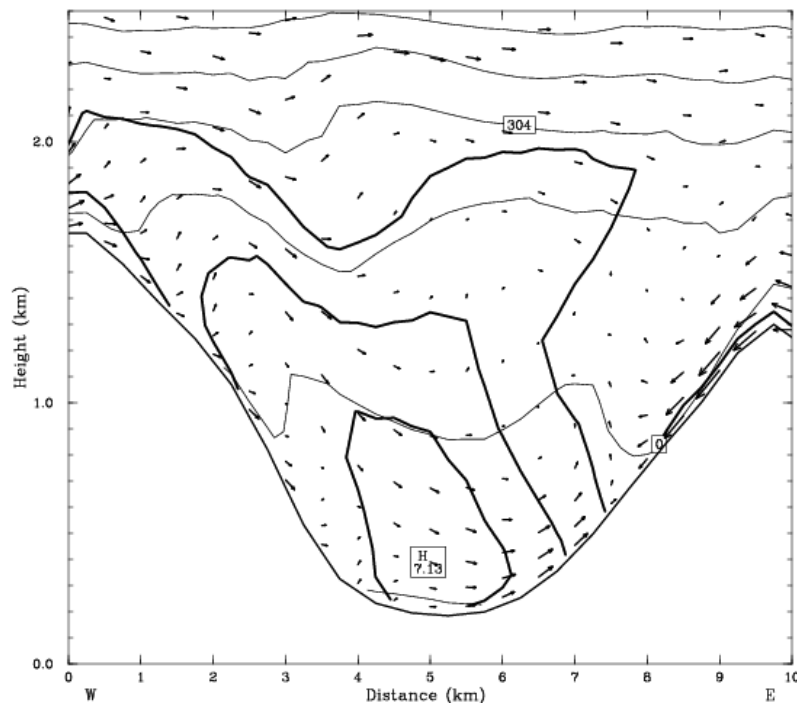
Figure 6.31: As in Fig. 6.26 but at 1800 UTC 1 August 2010.
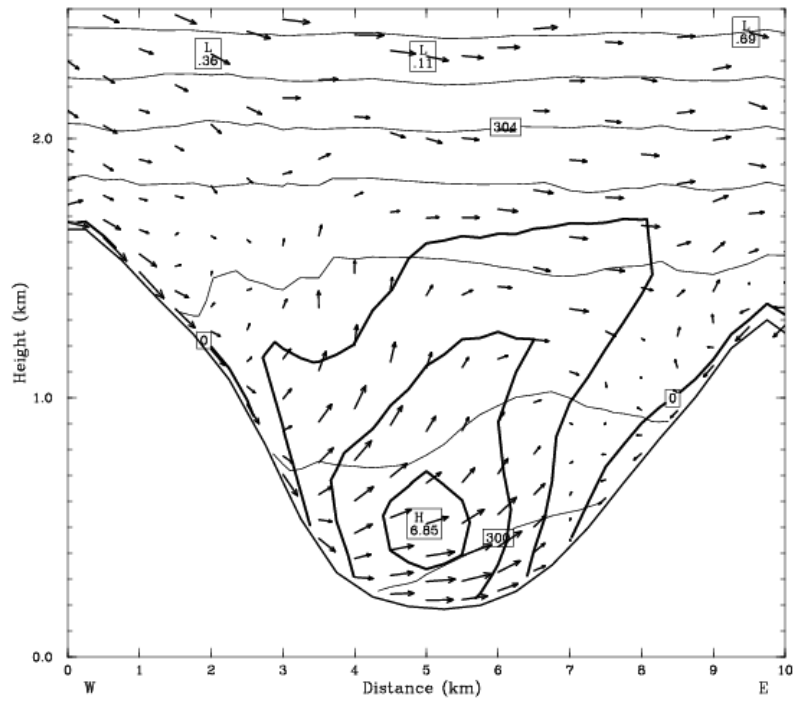
Figure 6.32: As in Fig. 6.26 but at 2100 UTC 1 August 2010.
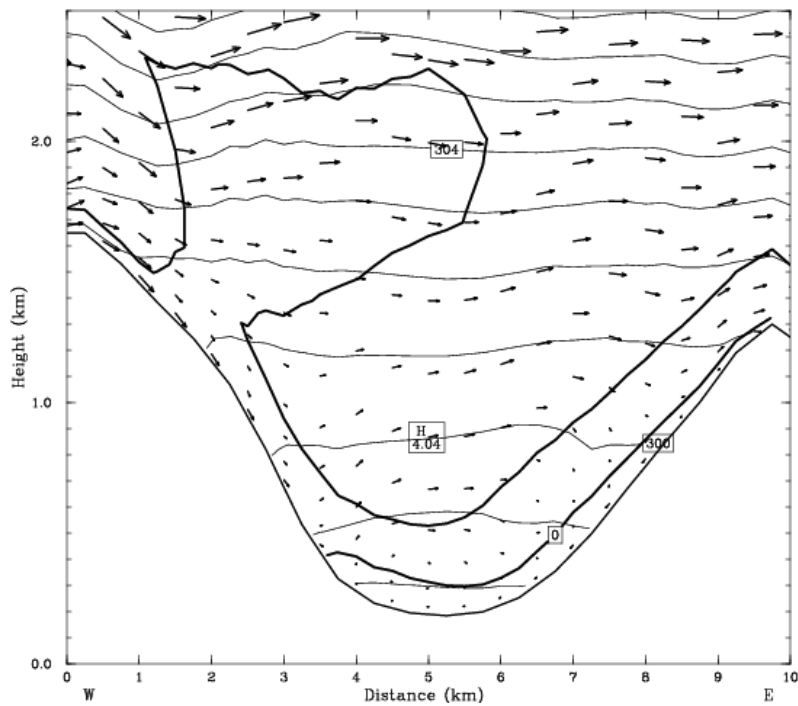
Figure 6.33: As in Fig. 6.26 but at 0000 UTC 2 August 2010.

about 2000 m. Up-slope winds are still present on the eastern slope, while they cease and begin to reverse on the western sidewall. At 1800 UTC the up-valley wind continues with similar intensities, while down-slope winds start to blow also at the top of the the eastern slope. The potential temperature distribution shows that the slopes and the valley floor begin to cool. Three hours later down-slope winds are present on both sidewalls, while the up-valley wind is still quite strong in the center of the valley, extending to a height of about 1500 m. Finally at 0000 UTC a shallow down-valley wind begins to develop near the ground, while 300 m above the valley floor a quite strong up-valley wind is still present.

6.3.4   Temperature daily cycles

Similarly to the analysis performed for the along-valley wind, near-surface temperature daily cycles simulated by the model have been validated against measurements from surface weather stations. Also in this case results presented refer to hourly averages. At Ala and Trento Sud (Figs. 6.34 - 6.35) the agreement is very satisfactory, with only minor differences between numerical results and observations. In particular in both stations there is an earlier heating in the morning and a too quick cooling in the evening. It can be supposed that the earlier heating in the morning may play a role in the earlier onset of the up-valley wind in the simulations, as seen in Section 6.3.2. At S. Michele all'Adige the timing of the morning heating is correct, but the daily temperature range is too small, with an overestimation of the nighttime temperatures and an underestimation during daytime.

Analyzing Figs. 6.37 and 6.38, which show the comparison between model results and measurements in the Sarca and Lakes valleys at Arco and Sarche (data from Riva del Garda were not available for 1 August 2010), it can be seen that the model overestimates and anticipates the cooling due to the arrival of the Ora del Garda. Moreover also in these weather stations the model simulates an earlier heating in the morning.

6.3.5   Pressure daily cycles in the Adige Valley

Figure 6.39 shows the hourly-averaged along-valley pressure gradients in the Adige Valley simulated by the model at different hours of the day. In this graphic hours refer to LST, so as to directly compare the results with the average cycles obtained from measurements in Figs. 5.25 and 5.26. The weather stations of Gargazzone and Merano are not present in this analysis, because these locations are outside the inner domain. Moreover it is worth remembering that observations refer to average values over several days, while the numerical results to a single day; as a consequence comparisons may be influenced by this mismatch. However numerical results and observations are fairly in agreement, thus confirming the ability of the model to simulate the mechanisms leading to the development of valley winds. At 0000 LST the pressure increases from Cason to Trento Sud, while it is roughly constant from Trento Sud to Molino

Ala
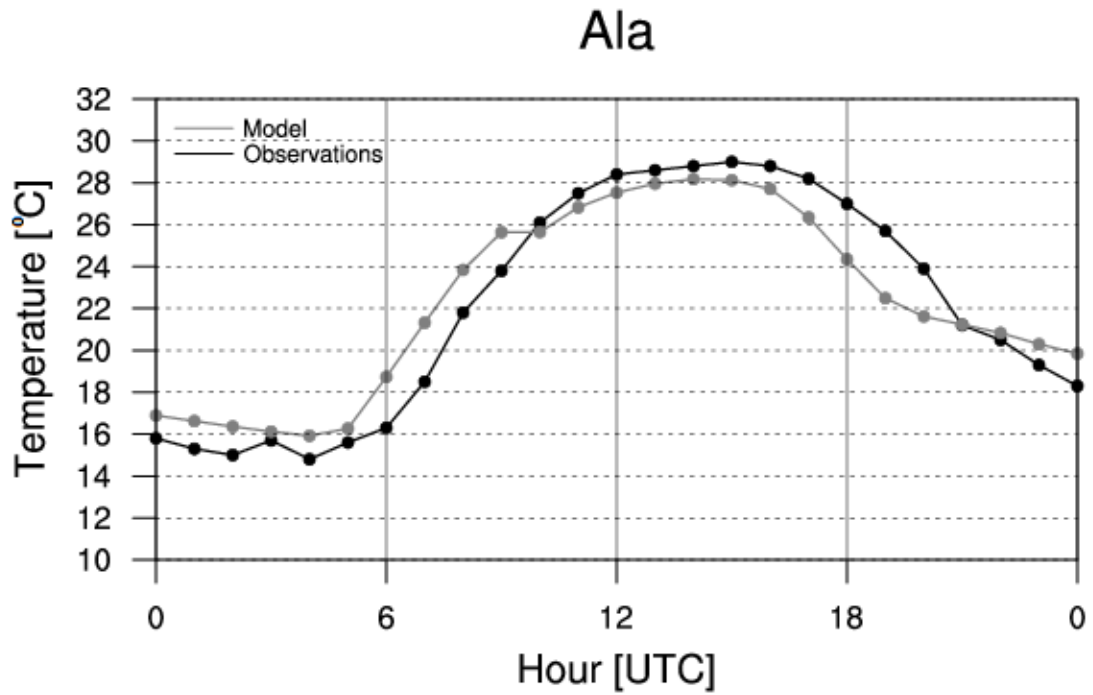
Figure 6.34: Temperature daily cycle at Ala weather station at 2 m AGL for 1 August 2010 obtained from model results (gray line) and observations (black line).
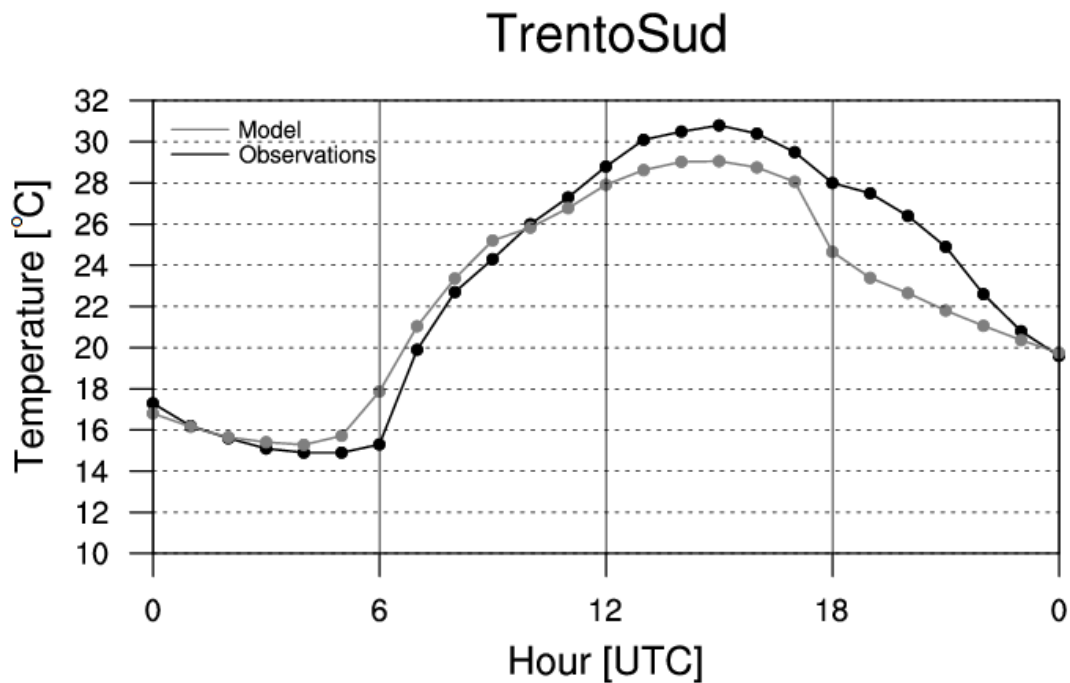
TrentoSud

Figure 6.35: As in Fig. 6.34, but at Trento Sud weather station.
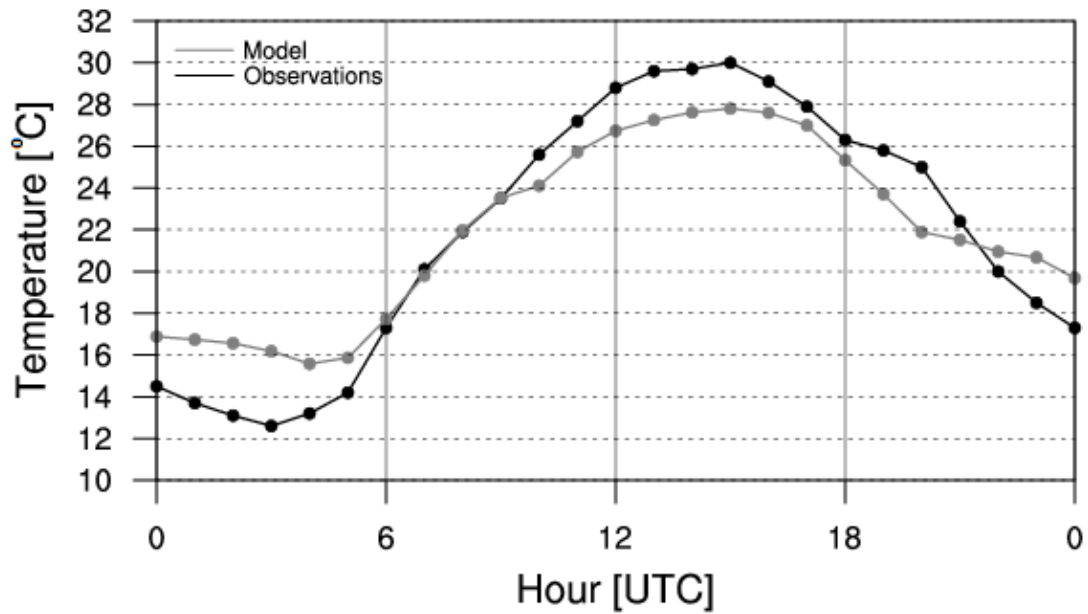
Figure 6.36: As in Fig. 6.34, but at S. Michele all'Adige weather station.
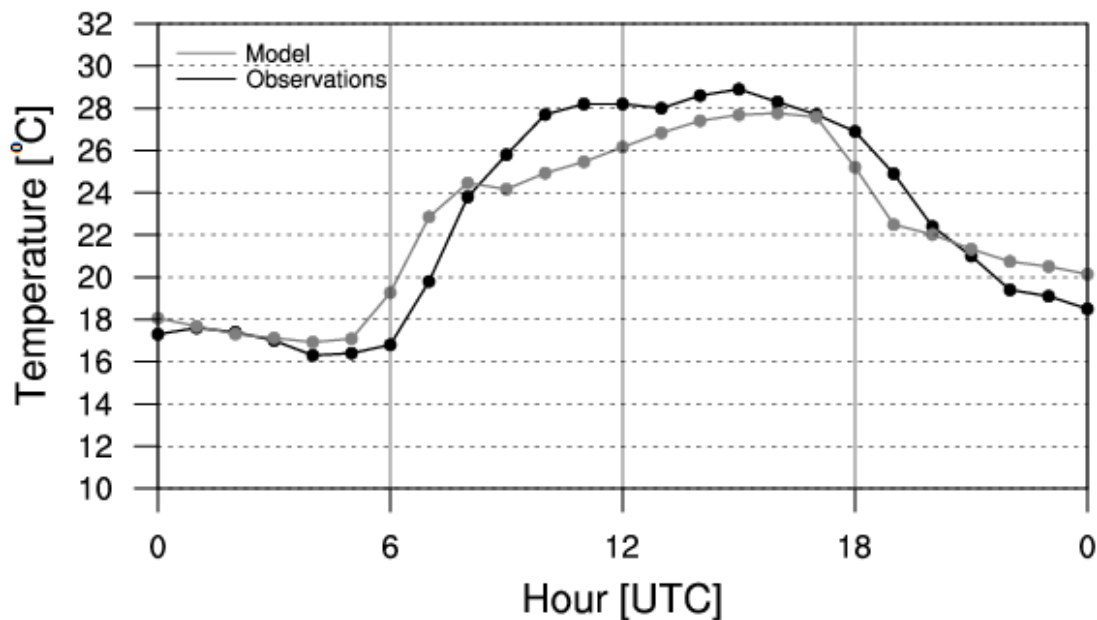
Figure 6.37: As in Fig. 6.34, but at Arco weather station.
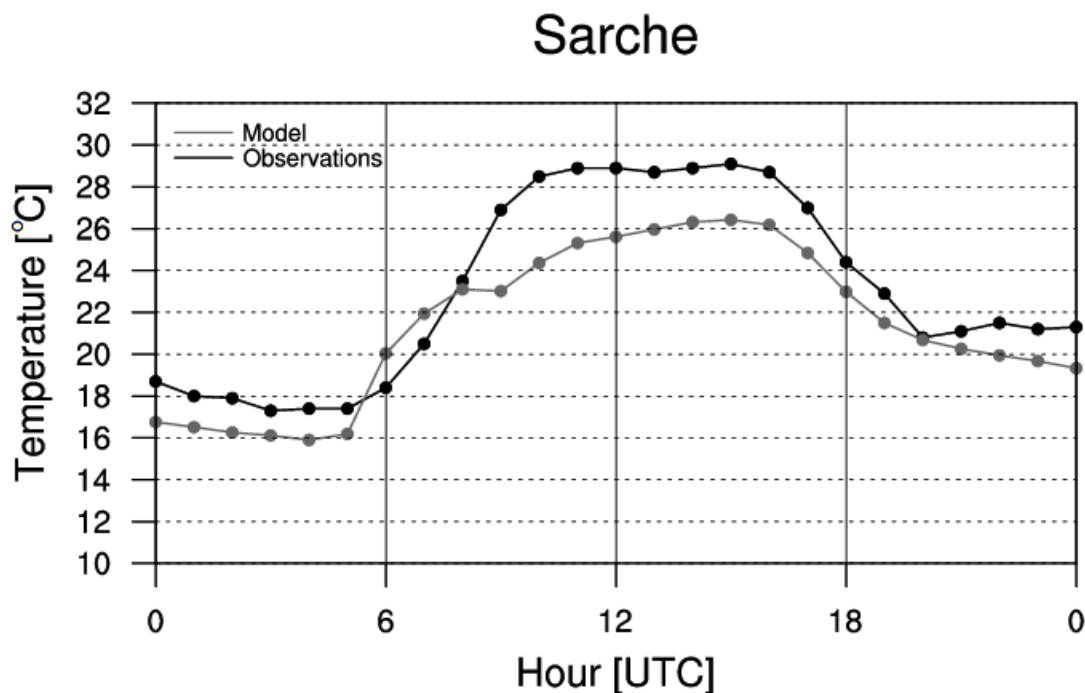
Figure 6.38: As in Fig. 6.34, but at Sarche weather station.

Vittoria. Observing that later in the night the pressure slightly decreases from Trento Sud to Molino Vittoria, it might be supposed that the model results confirm the influence of the urban area on the pressure distribution at night, as hypothesized in Section 5.4.3. However an identical pressure distribution has been found also in an idealized simulation without the urban area (see Section 6.3.7 for more details); this hypothesis is therefore not supported. North of Molino Vittoria the pressure increases towards S. Michele all'Adige, while there is a decrease between this latter weather station and Salorno. This decrease may be the cause of the persistence of the up-valley wind until 0200-0300 LST at Roveré della Luna, located between S. Michele all'Adige and Salorno. Going north, the pressure increases from Salorno to Bronzolo, while, as in the measurements, it decreases going towards the basin of Bolzano. The situation remains similar during the night and in the first part of the morning. At 1200 LST the pressure strongly decreases from the plain to the southernmost part of the valley, confirming, as found from observations, the earlier onset of the up-valley wind in the southernmost part of the valley, as a consequence of the plain-valley pressure contrasts. On the other hand the model sees that pressure gradients are already developed, though less strong, also between Ala and S. Michele all'Adige, while Fig. 5.25 showed weak pressure differences in this part of the valley. This pressure distribution is coherent with the earlier onset of the up-valley wind in the model with respect to observations. At 1500 LST pressure gradients become stronger from Ala to
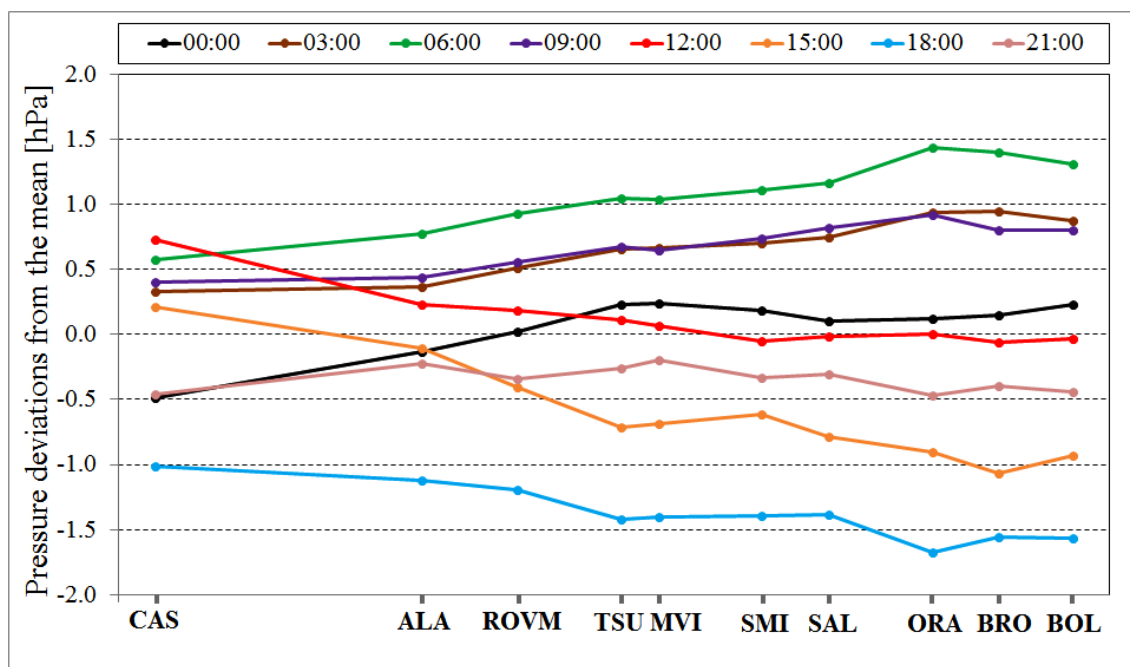
Figure 6.39: Along-valley pressure gradients as simulated by the model at different hours [LST] of the day.

Trento Sud, while the pressure increases from Trento Sud to S. Michele all'Adige, probably due to the presence of the cooler Ora del Garda. Going further north the pressure decreases from S. Michele all'Adige to Bronzolo, while in the observations pressure gradients were weak. On the other hand, as in the observations, the pressure increases from Bronzolo to Bolzano, thus confirming that the basin of Bolzano behaves as a "small plain". At 1800 LST the situation remains similar, but with weaker pressure gradients, while at 2100 LST, as in the observations, gradients are weak everywhere, with only a pressure increase from Trento Sud to Molino Vittoria, behavior difficult to explain. Moreover the pressure slightly increases from Cason to Ala, confirming the earlier onset of the down-valley wind in the southernmost part of the valley.

6.3.6 Ora del Garda

As seen in Section 5.5, the Ora del Garda starts to blow in the morning on Lake Garda shores and then flows towards north in the Sarca and Lakes valleys, outbreaking into the Adige Valley in the first part of the afternoon. In this Section the characteristics of the lake breeze and its propagation are investigated analyzing the model results. Figure 6.40 shows the lake breeze front moving in the morning from Lake Garda towards north (cross section 2 in Fig. 6.3). The lake breeze is associated with potentially cooler air which reaches a depth of about 600-700 m. Moreover it can be seen that a southerly wind (an up-valley wind) is present also ahead of the lake breeze front.
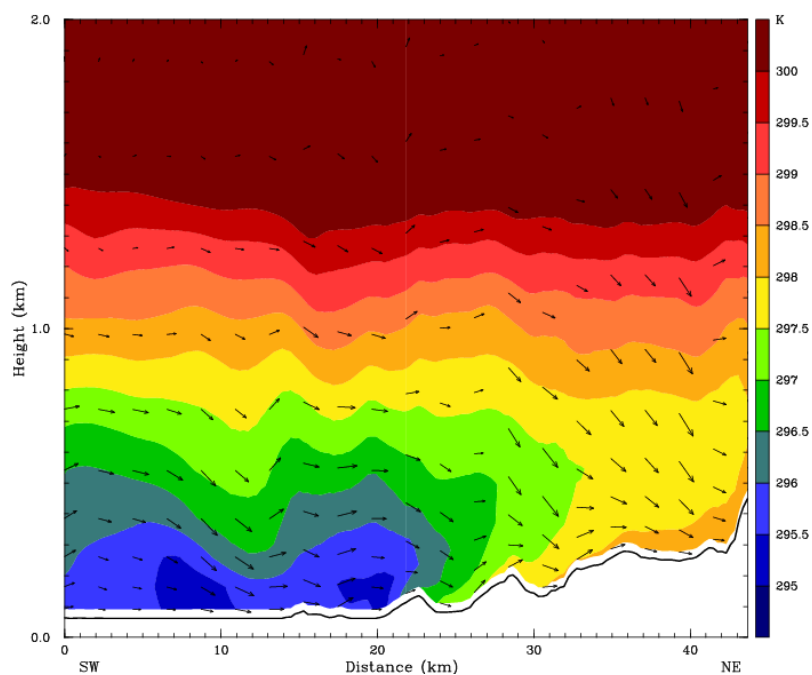
Figure 6.40: Along-valley section of the Sarca and Lakes valleys (cross section 2 in Fig. 6.3) at 1000 UTC 1 August 2010, showing along-valley wind vectors, and potential temperature (contour interval = 0.5 K).

Figure 6.41, showing the near-surface temperature and wind vectors at 1500 UTC in the central part of the inner domain, highlights that north of Trento, in agreement with the wind odograph in Fig. 5.9, wind direction is from west-southwest, due to the outbreak of the Ora del Garda into the Adige Valley. Moreover it can be seen that the interaction with the up-valley wind of the Adige Valley occurs over the urban area. The cross sections in Figs. 6.42 and 6.43 (cross section 3 in Fig. 6.3) show that the Ora del Garda, marked by the presence of potentially cooler air, reaches the Adige Valley floor flowing close to the western slope of the valley (Terlago saddle), where the highest wind velocities are reached. The arrival of the lake breeze induces an inhomogeneity in the cross-valley potential temperature field. Moreover it seems that a vortex develops inside the valley, with a quite strong up-slope flow on the eastern slope and a light return flow aloft, about 1300-1500 m above the valley floor. The along-valley wind component is almost negligible close to the valley floor, whereas an up-valley wind is present at higher levels.

The along-valley section in Fig. 6.44 (cross section 4 in Fig. 6.3), referring to 1500 UTC, shows that, as supposed by Schaller (1936), the up-valley wind flows over the potentially cooler air coming from the Lakes Valley. The interaction between the two circulations is highlighted by a zone where the along-valley wind component is weak, whereas the outbreak of the Ora del Garda is marked by a strong cross-valley wind, reaching a height of about 600-700 m above the valley floor. The highest cross-valley wind intensities are reached near the ground.

The effects of the Ora del Garda on climatic conditions in the Sarca, Lakes and Adige
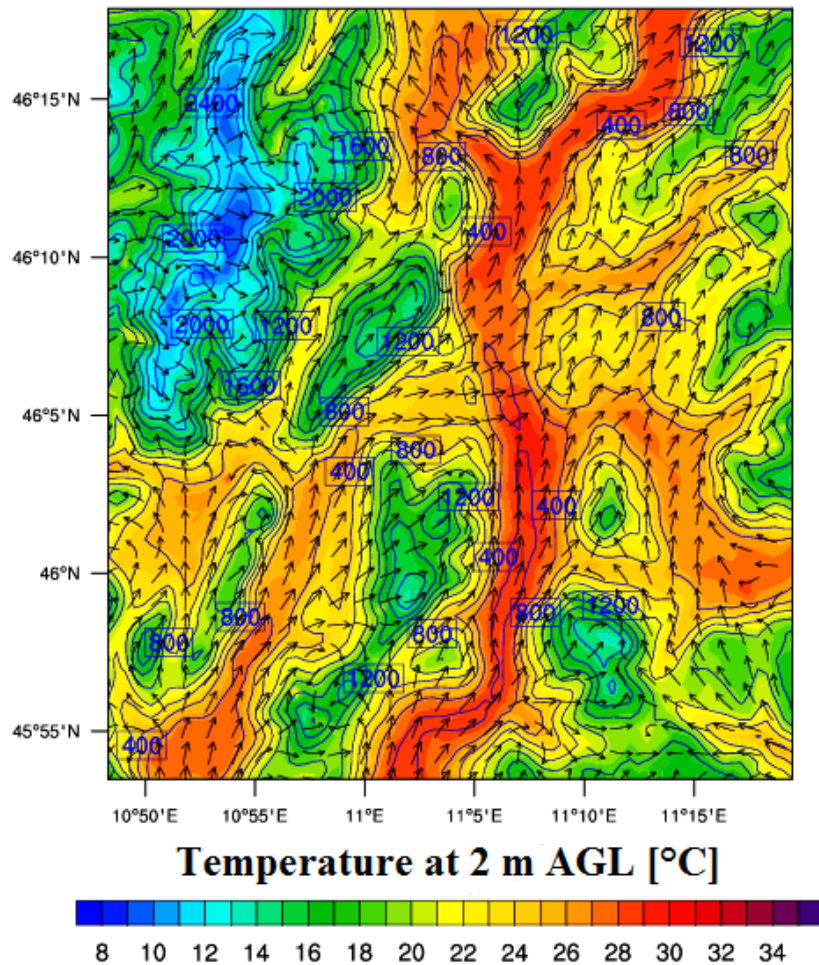
Figure 6.41: Temperature at 2 m AGL (°C) and horizontal wind vectors at 10 m AGL in the central part of the inner domain at 1500 UTC 1 August 2010.

valleys have been analyzed performing also an idealized simulation, in which all lake land use grid points in the inner domain have been replaced by cropland. Figures 6.45-6.51 show the temperature differences at 2 m AGL between the reference run and the idealized simulation without lakes at different hours of the day. During the night the presence of Lake Garda causes higher temperatures in the basin of Arco-Riva, as can be seen in Fig. 6.45, referring to 0500 UTC. On the other hand starting from 0800 UTC the propagation from Lake Garda towards north of the lake breeze front lowers temperatures first in the basin of Arco-Riva, then in the Sarca and Lakes valleys, and at 1300 UTC also in the Adige Valley north of Trento (Figs. 6.46 - 6.51). In the basin of Arco-Riva temperatures at 2 m AGL are about 3°C lower in the reference run than in the simulation without lakes. Differences are lower in the Sarca and Lakes valleys (~ 2°C), and in the Adige Valley in the area north of Trento (~ 1°C). It can be supposed that these differences may be slightly overestimated, as the comparisons presented in Section 6.3.4
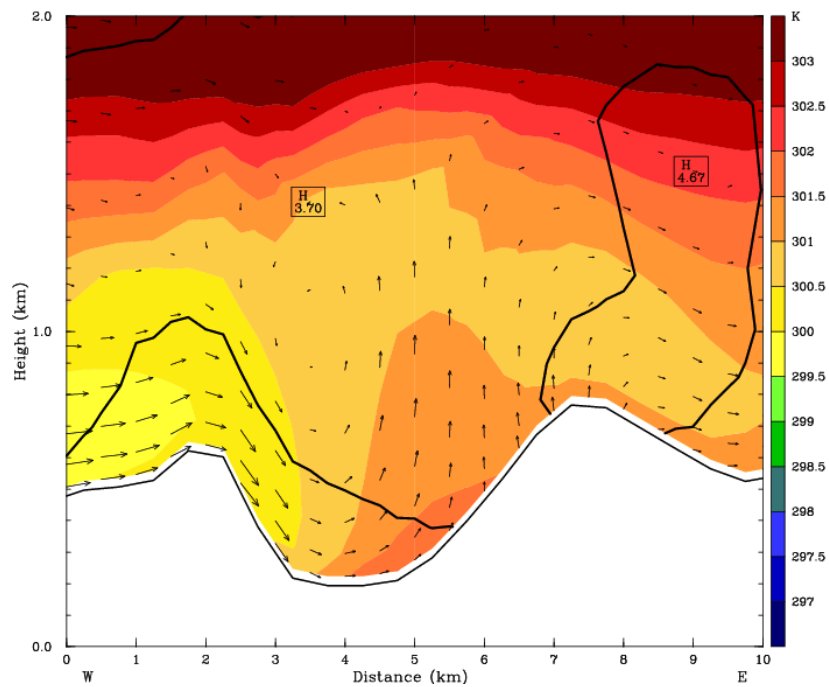
Figure 6.42: Cross section of the Adige Valley north of Trento (cross section 3 in Fig. 6.3) at 1200 UTC 1 August 2010, showing cross-valley wind vectors, along-valley wind velocity (bold contours: contour interval = 2 m s^{-1}), and potential temperature (contour interval = 0.5 K).
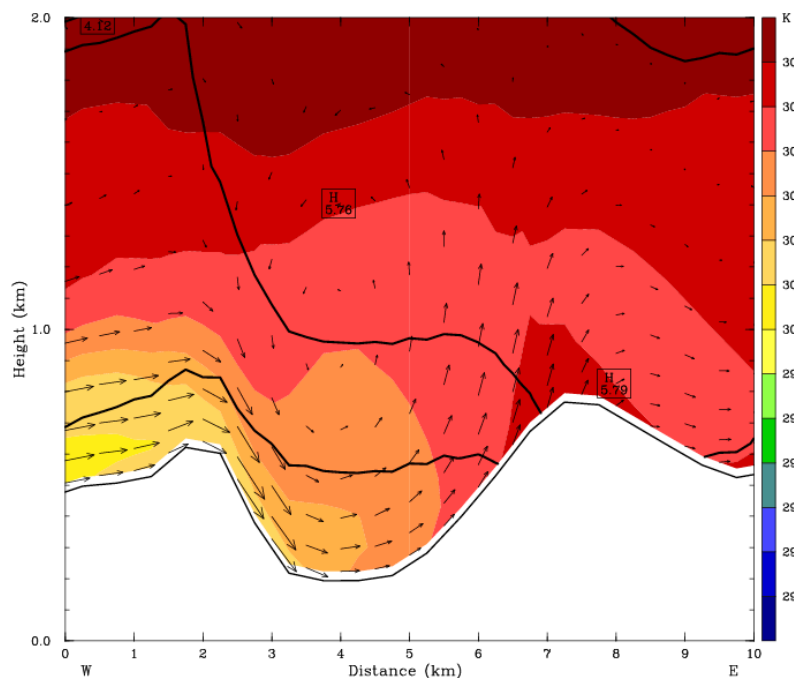
Figure 6.43: As in Fig. 6.42, but at 1600 UTC 1 August 2010.
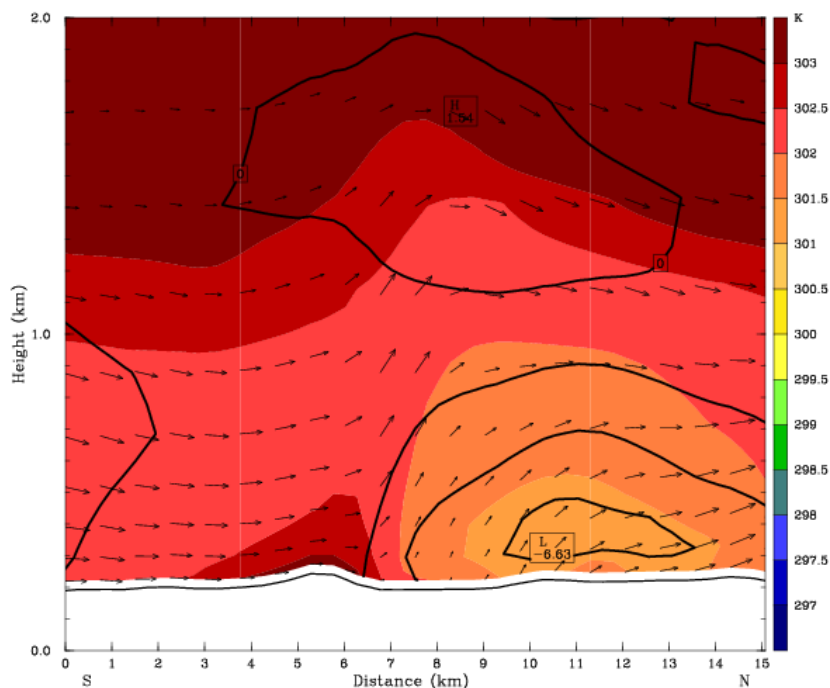
Figure 6.44: Along-valley section of the Adige Valley in the area of Trento (cross section 4 in Fig. 6.3) at 1500 UTC 1 August 2010, showing along-valley wind vectors, cross-valley wind velocity (bold contours: contour interval = 2 m s^{-1}), and potential temperature (contour interval = 0.5 K).

have shown that the model overestimates the temperature drop at the arrival of the lake breeze front.

The influence of the lake breeze on the vertical profile of temperature can be estimated analyzing the comparisons shown in Figs. 6.52 - 6.54. At Riva del Garda, on the shores of the lake, at 0500 UTC the presence of the lake inhibits the development of a ground-based thermal inversion and the higher temperatures in the reference run extend to about 500 m AGL. On the other hand at 1300 UTC the lake breeze lowers the temperature up to about 700 m AGL. Temperature differences are maximum near the ground and progressively decrease with height. A similar behavior is found also in the Adige Valley north of Trento (Gardolo, Fig. 6.54), where the temperature differences between the two simulations are lower, but still significant.

Results of the idealized simulation without lakes have been analyzed to evaluate also the effects of Lake Garda on the near-surface wind field. In the early morning higher wind velocities are present in the reference run in the basin of Arco-Riva, due to the onset of the lake breeze (Fig. 6.55). Later in the morning the lake breeze moves towards north, but wind intensities in the reference run are only slightly higher than in the simulation without lakes in the Sarca and Lakes valleys, because a quite strong up-valley wind is present also in the latter simulation (not shown). The comparison at 1300 UTC (Fig. 6.56) shows great differences above Lake Garda, where, as expected, wind intensity is stronger in the reference run. On the other hand
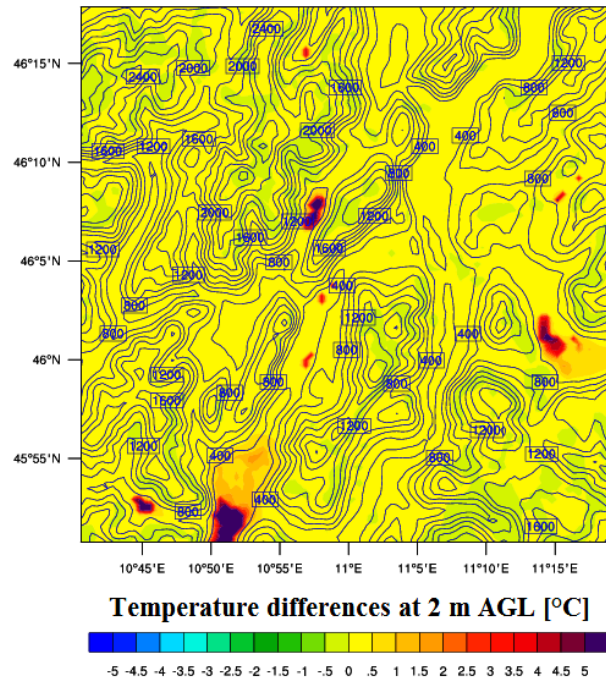
Figure 6.45: Temperature differences at 2 m AGL (°C) in the central part of the inner domain at 0500 UTC 1 August 2010 between the reference run and the run where the lake land use grid points are replaced with cropland.
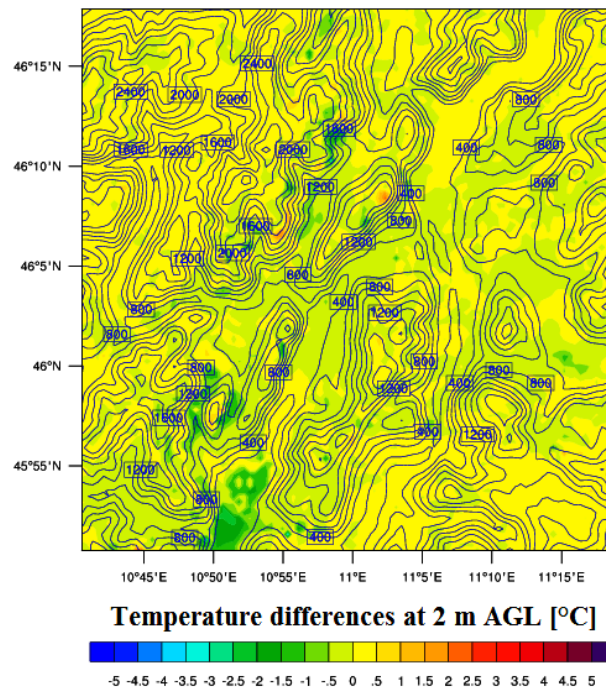
Figure 6.46: As in Fig. 6.45, but at 0800 UTC 1 August 2010.
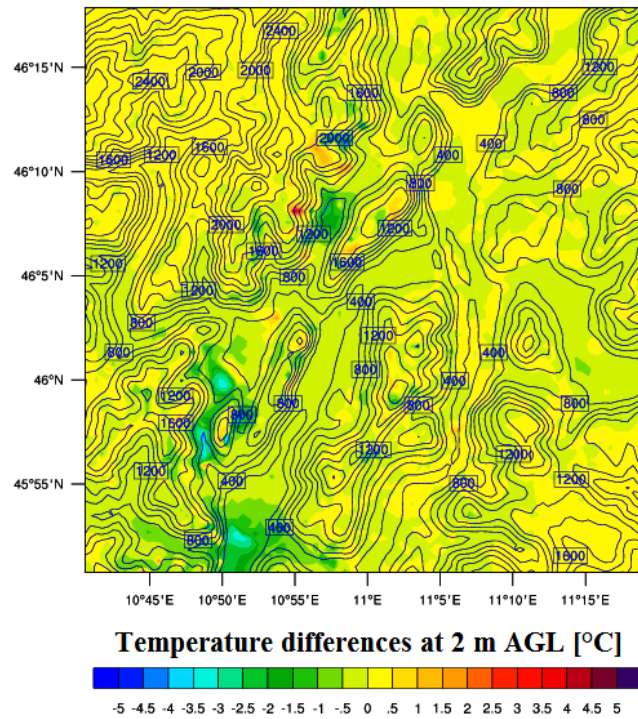
Figure 6.47: As in Fig. 6.45, but at 0900 UTC 1 August 2010.
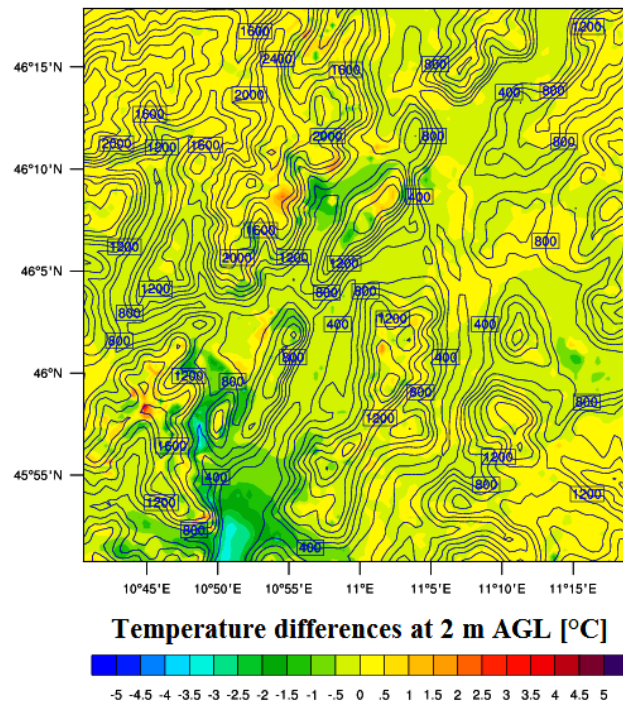
Figure 6.48: As in Fig. 6.45, but at 1000 UTC 1 August 2010.
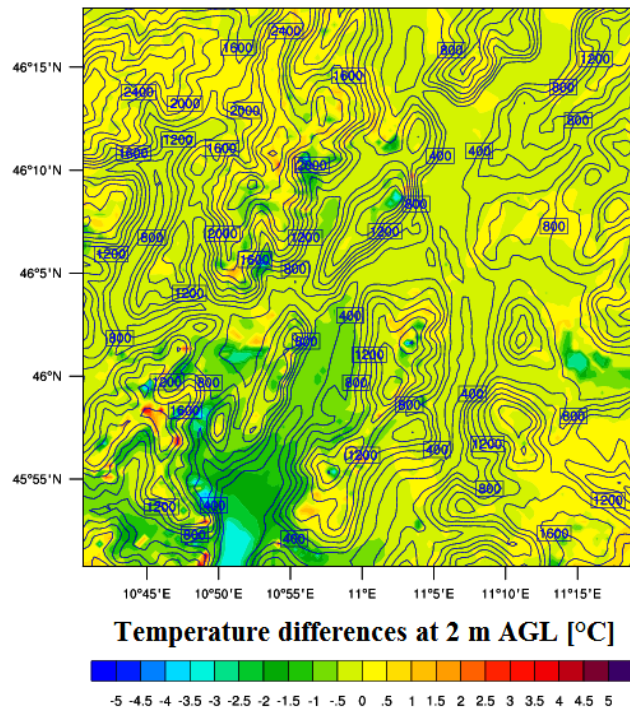
Figure 6.49: As in Fig. 6.45, but at 1100 UTC 1 August 2010.
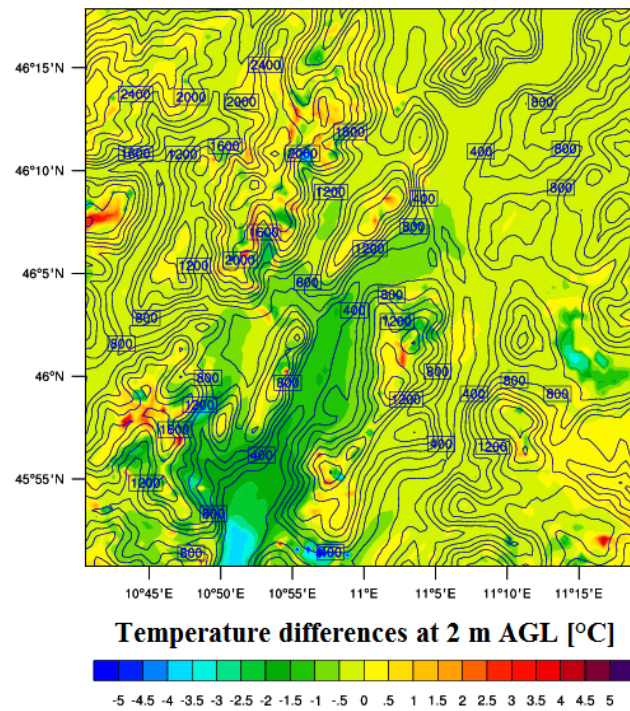
Figure 6.50: As in Fig. 6.45, but at 1200 UTC 1 August 2010.
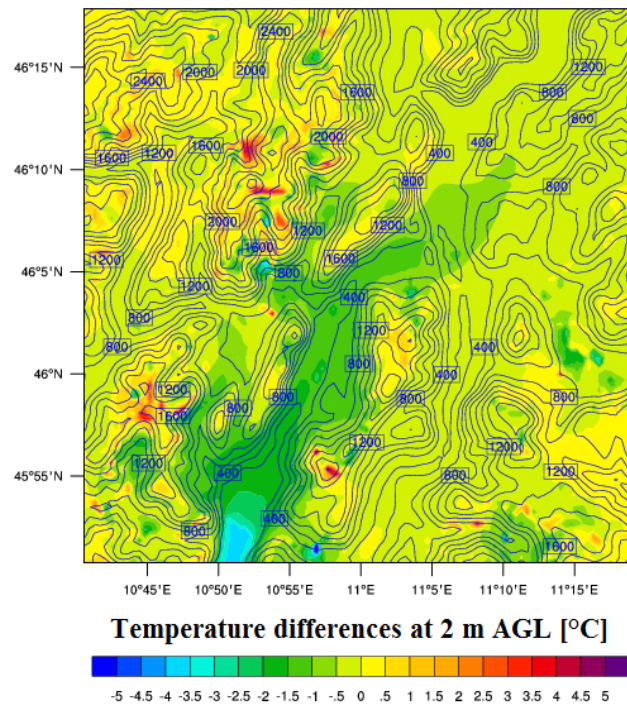
Figure 6.51: As in Fig. 6.45, but at 1300 UTC 1 August 2010.

the presence of the lake lowers the wind intensity in the basin of Arco-Riva, a behavior difficult to explain. Similarly to what found in the morning, slightly higher wind velocities occur in the Sarca and Lakes valleys in the reference run, while stronger differences are found in the area north of Trento, due to the outbreak of the Ora del Garda into the Adige Valley.

6.3.7   Urban effects

In this Section the urban effects captured by the WRF model coupled with the BEP urban scheme are analyzed and commented. Figure 6.57, showing near surface temperature and wind at 0000 UTC 2 August 2010, highlights that a strong UHI develops at night in the city of Trento, in the central part of the map. The temperature is quite homogeneous inside the city and the UHI boundaries follow the extension of the urban land use. Furthermore also the other smaller urban areas on the valley floor are marked by the presence of higher temperatures. On the other hand in the morning (Fig. 6.58 refers to 0900 UTC 1 August 2010) the temperature field on the valley floor is more homogeneous and urban effects are not present. These findings are confirmed by the daily cycle of the UHI simulated by the model, calculated as the temperature differences at 2 m AGL between the urban station of Molino Vittoria and the rural station of Aldeno, located on the valley floor 6 km south of the city, chosen because certainly not affected by urban effects (Fig. 6.59). Similarly to what found in Chapter 3, where the UHI of the city of Trento was investigated in detail, the model simulates a strong UHI during the night and at
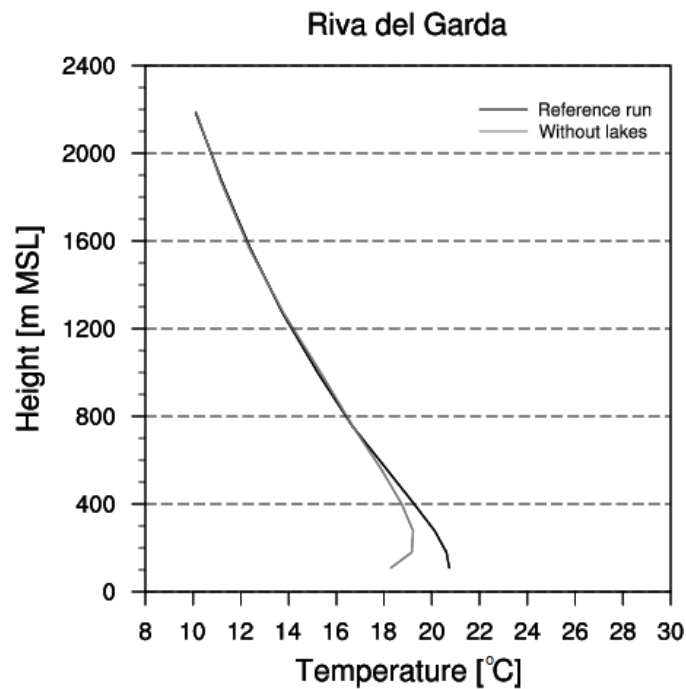
Figure 6.52: Vertical temperature profiles (°C) at Riva del Garda at 0500 UTC 1 August 2010 for the reference run (black line) and the run where the lake land use grid points are replaced by cropland (gray line).
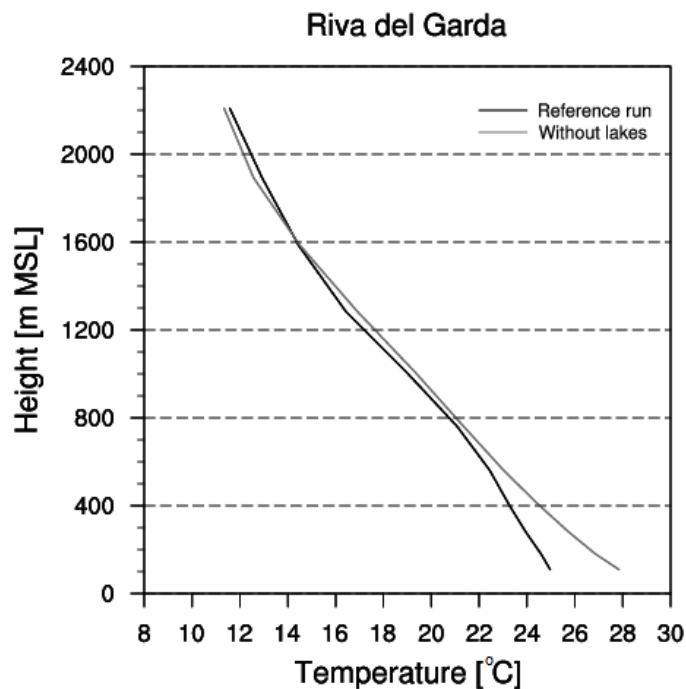
Figure 6.53: As in Fig. 6.52, but at 1300 UTC 1 August 2010.
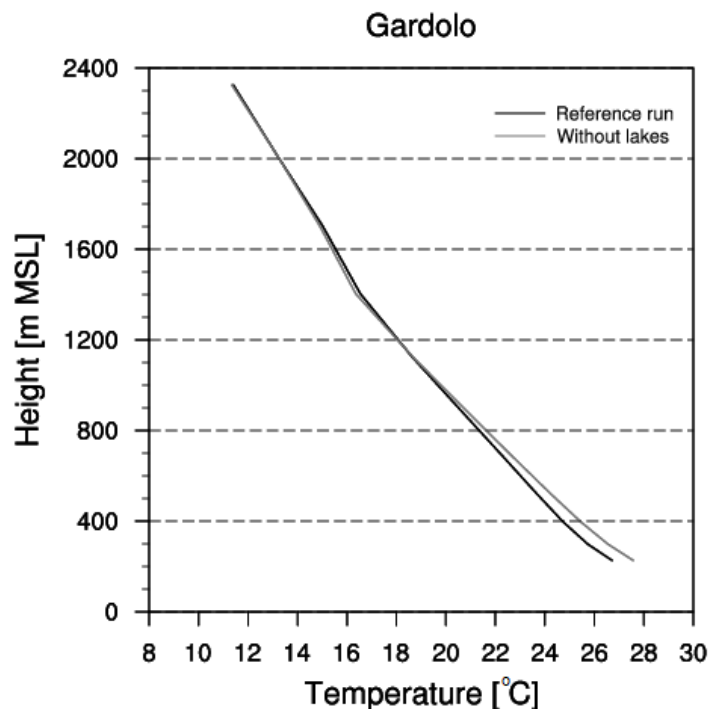
Figure 6.54: As in Fig. 6.52, but at Gardolo and at 1300 UTC 1 August 2010.

evening and low or negligible intensities in the morning and in the central hours of the day. The comparison with the observed values highlights that the model simulates very well the strong UHI intensity at night, but the urban cool island in the morning is underestimated. Moreover in the evening the model sees a strong UHI starting from 1800 UTC, while observations show high intensities only from 2300 UTC. It is worth remembering that Molino Vittoria weather station is located well above rooftop level, while model results refer to values at 2 m AGL. Following the results of the field campaign carried out in an urban canyon of Trento in summertime (Chapter 4), it can be supposed that UHI intensity would be roughly 1°C higher at street level with respect to the observed values in Fig. 6.59. Therefore it is likely that the model slightly underestimates the UHI intensity at night, while the underestimation of the urban cool island in the morning is probably less important.

Similarly to what done when analyzing the Ora del Garda in Section 6.3.6, urban effects simulated by the model have been evaluated performing an idealized run, in which all urban land use grid points in the inner domain have been replaced by cropland. Figures 6.60 - 6.64 show the near-surface temperature differences between the two simulations at different hours of the day. At 0000 UTC (Fig. 6.60) temperature differences, i.e. the urban effects, are strong at Trento, with slightly higher values in the central and south parts of the city, where the urban area is more compact and there are higher buildings. Furthermore it can be seen that inside the city small areas with considerably lower temperatures are present, probably due to lower urban
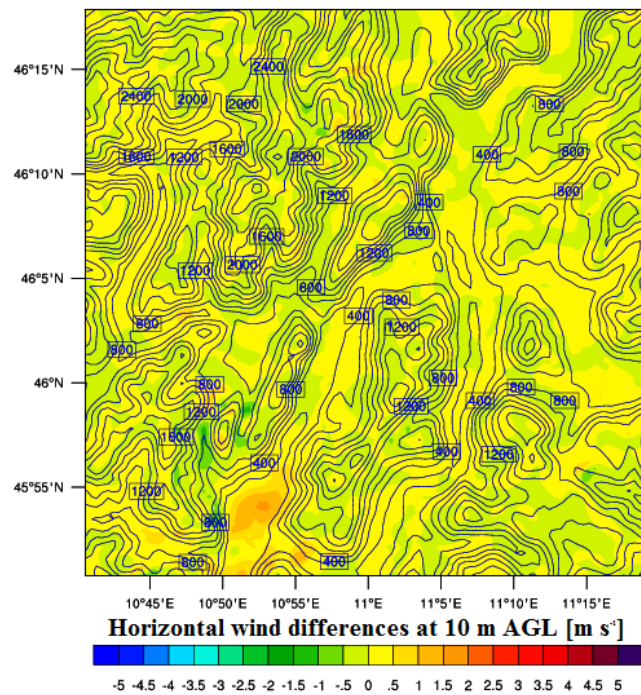
Figure 6.55: Horizontal wind velocity differences at 10 m AGL (m s^{-1}) in the central part of the inner domain at 0800 UTC 1 August 2010 between the reference run and the run where the lake land use grid points are replaced by cropland.
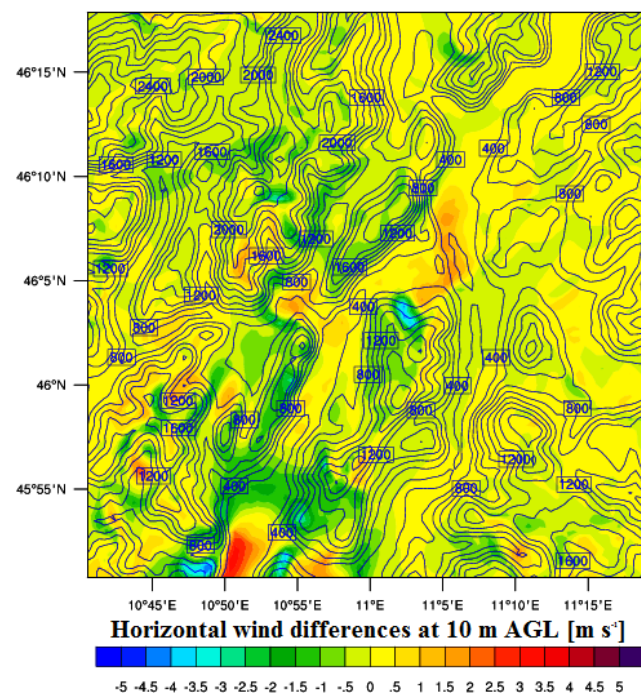

Figure 6.56: As in Fig. 6.55, but at 1300 UTC 1 August 2010.
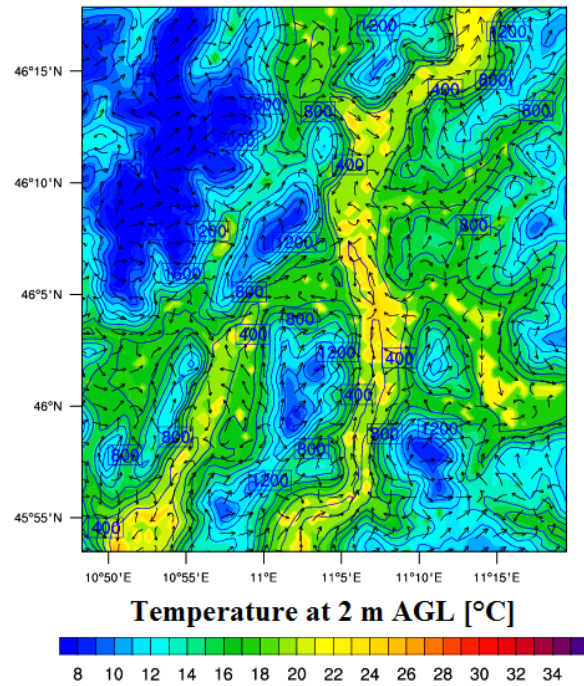
Figure 6.57: Temperature at 2 m AGL (°C) and horizontal wind vectors at 10 m AGL in the central part of the inner domain at 0000 UTC 2 August 2010.
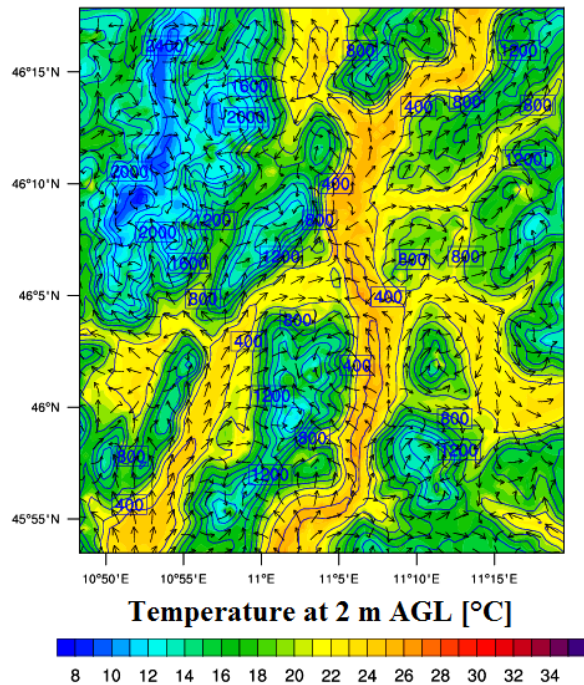
Figure 6.58: As in Fig. 6.57, but at 0900 UTC 1 August 2010.
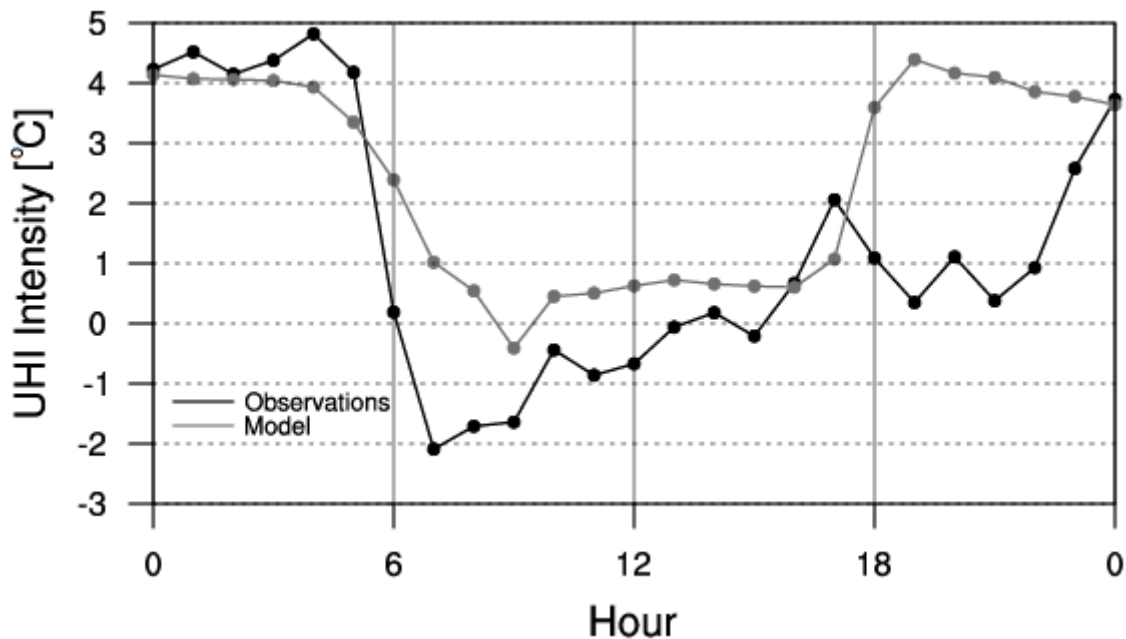
Figure 6.59: Comparison between UHI daily cycles (calculated as the temperature difference between Molino Vittoria and Aldeno weather stations, °C) on 1 August 2010 obtained from model results (gray line) and observation (black line).

fractions (see Fig. 6.9). The situation remains similar until 0400 UTC, when temperature differences begin to weaken. At 0600 UTC (Fig. 6.61) urban effects are negligible, while in the following hours the presence of the urban area causes lower temperatures in Trento, with maximum differences between the two simulations at 0800 UTC (Fig. 6.62). These differences are slightly stronger in the northern part of the city, with respect to the more compact central part of the urban area. In the central hours of the day urban effects become weak again, with only slightly higher temperatures in the reference run in the central part of the city and lower values at the northern and southern boundaries of the urban area (Fig. 6.63). After 1700 UTC, the temperature differences between the two simulations begin to become stronger, starting from the city center (Fig. 6.64), and in the evening the situation is again similar to 0000 UTC, with strong urban effects, indicating the presence of a strong UHI (not shown).

The idealized simulation without cities allows to evaluate also the effects of the urban area of Trento on the wind field. At night, when the down-valley wind is weak, no appreciable differences are present (not shown), while in the early morning wind velocities over the city are slightly higher in the reference run (Fig. 6.65). At 1000 UTC (Fig. 6.66) wind velocity is still slightly higher in the south part of the city in the reference run, whereas in the northern part wind intensities are considerably lower. Further analyses have highlighted that these lower wind intensities permit an earlier outbreak of the Ora del Garda into the Adige Valley. In fact at 1100 UTC (Fig. 6.67) north of the city wind velocity is considerably higher in the reference
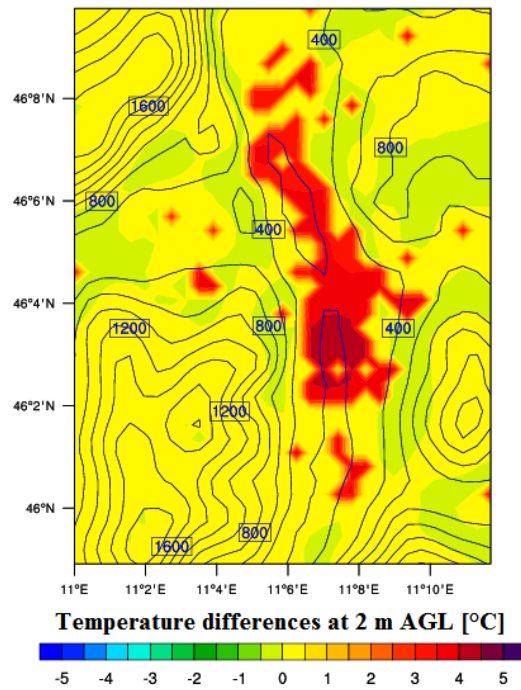
Figure 6.60: Temperature differences at 2 m AGL (°C) in the city of Trento and surroundings at 0000 UTC 1 August 2010 between the reference run and the run where the urban land use grid points are replaced by cropland.
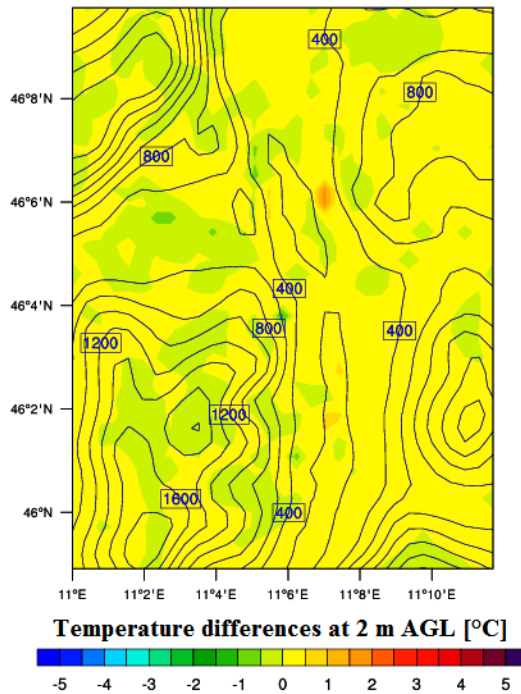
Figure 6.61: As in Fig. 6.60, but at 0600 UTC 1 August 2010.
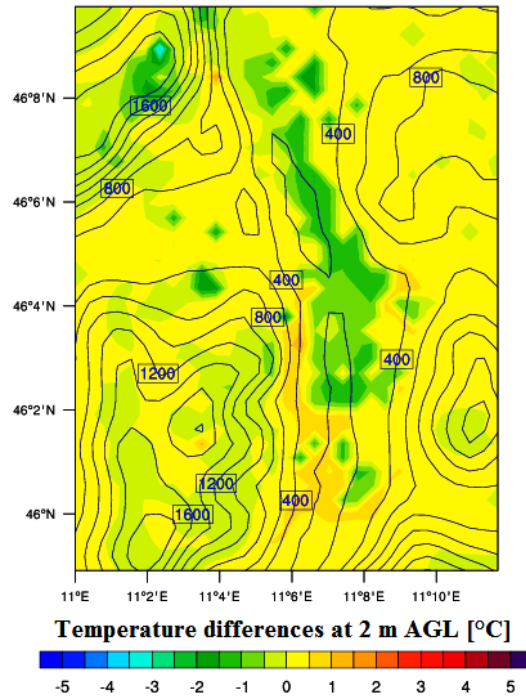
Figure 6.62: As in Fig. 6.60, but at 0800 UTC 1 August 2010.
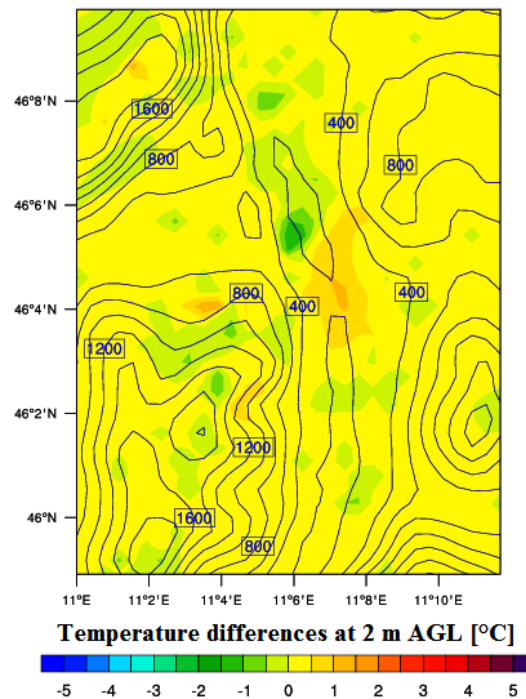
Figure 6.63: As in Fig. 6.60, but at 1200 UTC 1 August 2010.
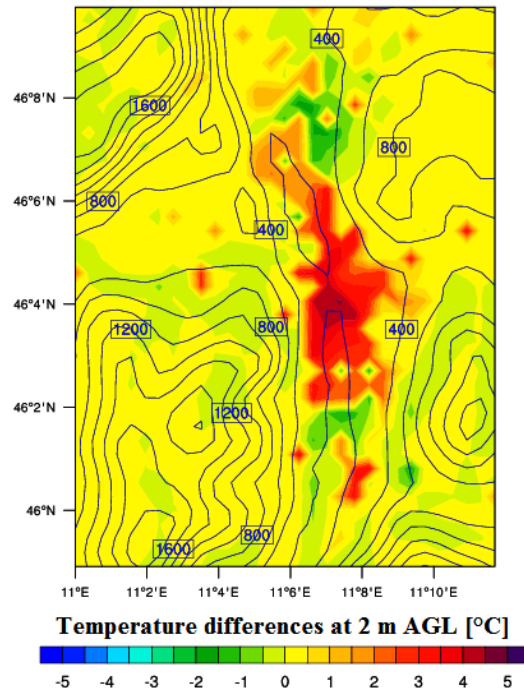
Figure 6.64: As in Fig. 6.60, but at 1800 UTC 1 August 2010.
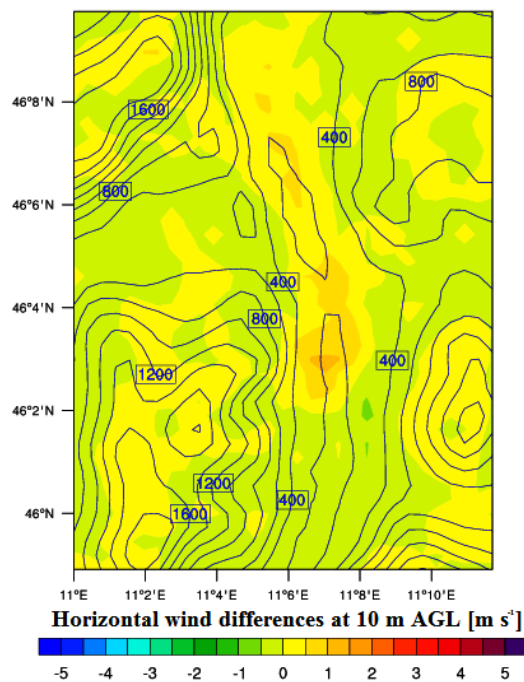
Figure 6.65: Horizontal wind velocity differences at 10 m AGL (m s^{-1}) in the city of Trento and surroundings at 0800 UTC 1 August 2010 between the reference run and the run where the urban land use grid points are replaced by cropland.
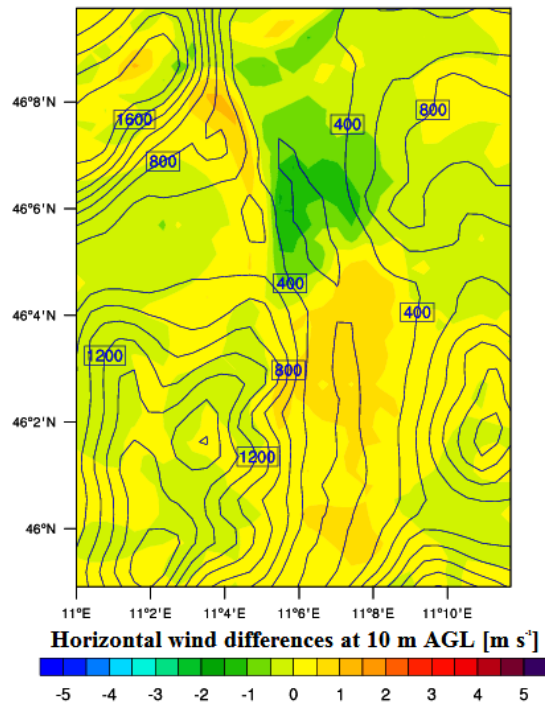
Figure 6.66: As in Fig. 6.65, but at 1000 UTC 1 August 2010.
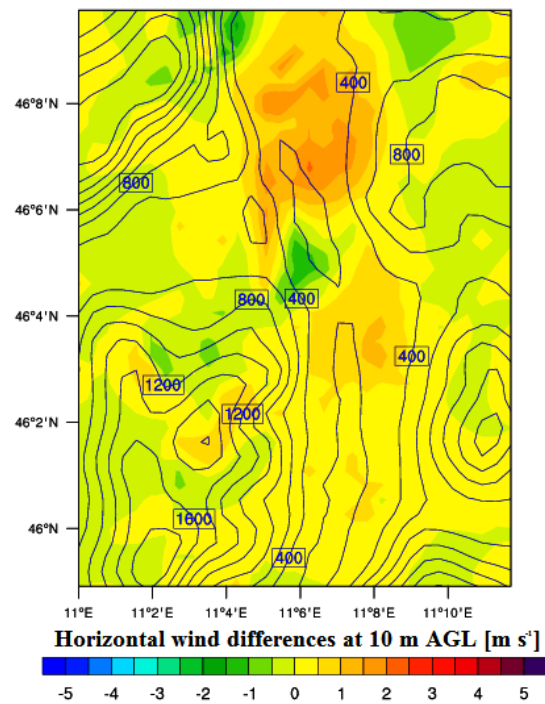
Figure 6.67: As in Fig. 6.65, but at 1100 UTC 1 August 2010.
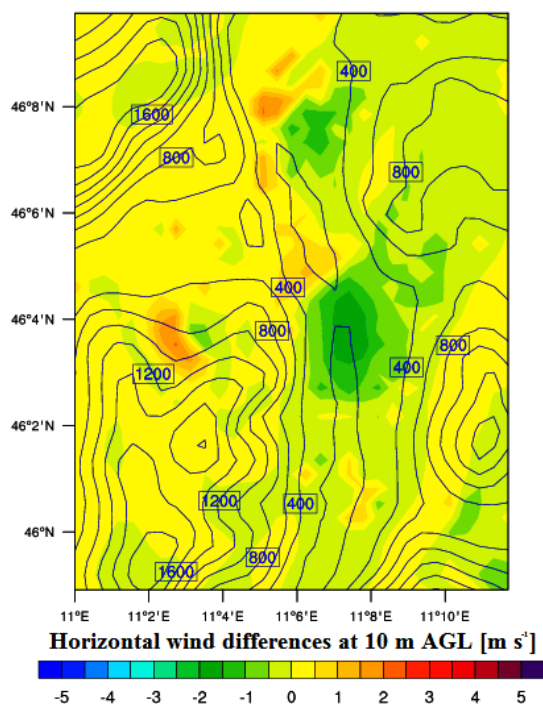
Figure 6.68: As in Fig. 6.65, but at 1500 UTC 1 August 2010.

run with respect to the simulation without cities. In the afternoon the presence of the city weakens the up-valley wind (Fig. 6.68), probably due to the high roughness of the urban area. As a consequence the interaction between the Ora del Garda and the up-valley wind of the Adige Valley is slightly moved towards north in the simulation without cities, especially in the first part of the afternoon. Finally in the evening wind intensity differences between the two simulations are negligible again (not shown).

6.3.8 Sensitivity to urban parameters

In order to assess how the anthropogenic heat flux, the albedo of the buildings and the morphology of the city affect the urban climate, idealized simulations artificially changing these parameters have been performed.

The results of a simulation without anthropogenic heat releases have highlighted that this variable does not considerably affect climatic conditions in Trento: only small temperature differences with the reference run have been found at any time of the day (not shown). This result is reasonable, because anthropogenic heat releases are much lower than the solar energy input in the summer period. The same comparison has been performed also for a cold sunny winter day, 3 January 2009, highlighting that in wintertime the anthropogenic heat flux has a slightly stronger influence on the temperature field, especially in the evening, even though the differences between the two simulations are still low, of order 0.3-0.4°C. Figure 6.69, showing

6. High-resolution numerical simulations of valley boundary layer processes including urban areas
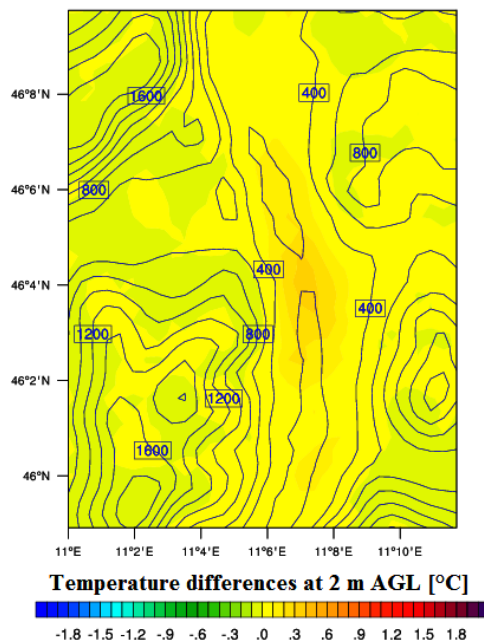
Figure 6.69: Temperature differences at 2 m AGL (°C) in the city of Trento and surroundings at 1900 UTC 3 January 2009 between the reference run and the simulation without anthropogenic heat flux releases.

the temperature differences in the city of Trento and surroundings between the two wintertime simulations at 1900 UTC 3 January 2009, highlights that the effects of the anthropogenic heat flux are low, with slightly higher values in the city center, where there are stronger anthropogenic releases.

As to the albedo of the buildings, a simulation has been performed changing the value for walls and roofs from 0.2 to 0.4. The increase of the albedo causes, as expected, a slight decrease of the temperature, of order 0.5°C, especially in the central part of the city and in the morning (Fig. 6.70). In the afternoon temperature differences between the two simulations are weaker and appreciable only in the city center.

In another idealized simulation the values of the urban morphology parameters λ_p and λ_b, which represent the compactness of the city structure, have been halved over the whole urban area, to simulate a city with larger streets than Trento. The comparison with the reference run highlights that the compactness of the urban area does not affect appreciably the temperature field. In fact only small temperature differences have been found, with slightly lower temperatures in the central part of the city in the idealized simulation (not shown). On the other hand when halving also the urban fraction, thus simulating a city with greater green spaces, the temperature differences with the reference run become important. At night the temperature is only slightly higher in the reference run in the city center, but during the day the differences raise to 0.7-0.8 °C, especially in the city center, as shown in Fig. 6.71, referring to 1300 UTC. In
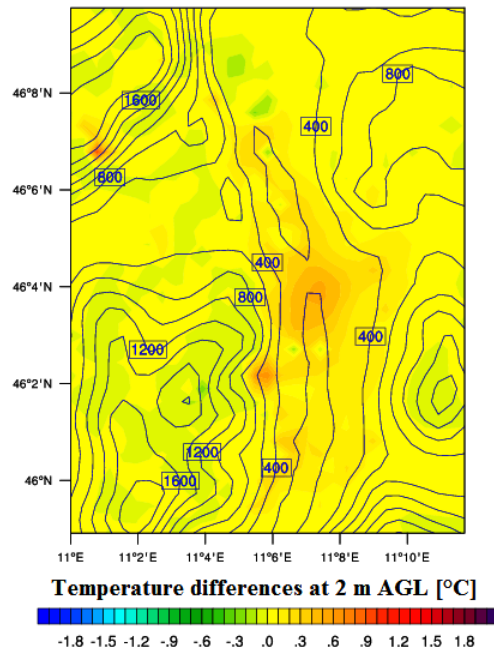
Figure 6.70: Temperature differences at 2 m AGL (°C) in the city of Trento and surroundings at 0800 UTC 1 August 2010 between the reference run and the simulation where the albedo of walls and roofs has been changed from 0.2 to 0.4.
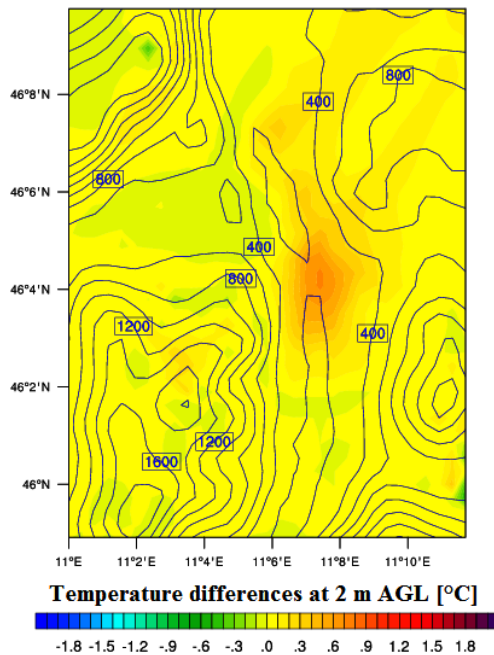

Figure 6.71: Temperature differences at 2 m AGL (°C) in the city of Trento and surroundings at 1300 UTC 1 August 2010 between the reference run and the simulation where λ_p, λ_b and the urban fraction have been halved.

the afternoon the temperature differences are slightly lower, but still significant, of order 0.5°C (not shown), while in the evening they become again very low.

6.4 Conclusions

High-resolution numerical simulations with the mesoscale WRF model, coupled with the BEP urban parameterization scheme, have been performed to investigate boundary layer processes, and in particular local circulation systems, in the valleys around the city of Trento, as well as the modifications induced by the urban area on local climatic conditions.

Particular attention has been devoted to the creation of high-resolution input datasets, especially for the urban parameterization scheme. Urban morphology parameters have been calculated with GIS techniques from high-resolution lidar data, while the anthropogenic heat flux from detailed information about vehicular traffic fluxes and energy consumption.

It has been found that the model well simulates the along-valley pressure gradients in the Adige Valley and, as a consequence, the development of valley winds. In fact comparisons with observations from surface weather stations have highlighted that the model captures the main characteristics of the along-valley wind daily cycles, with only minor errors in the timing of the onset of the up-valley wind in the late morning and in the determination of its maximum strength in the afternoon. The down-valley wind layer reaches a depth of about 700-800 m at night, with maximum intensities of 2.5 m s^{-1} in a cross section of the valley where the city of Trento lies. On the other hand during daytime the up-valley wind layer is considerably thicker, reaching a depth of about 2000 m in the afternoon. The analysis of the along-valley pressure gradients has confirmed many of the features observed in Chapter 5, where data from surface weather stations were analyzed. Simulations confirmed that in the morning pressure gradients develop earlier between the plain and the valley and then between the inner sections of the valley. Moreover also from model results it seems that the basin of Bolzano behaves as a "small plain", with a smaller pressure range than in the valley. On the other hand the influence of the city of Trento on pressure distribution at night is not seen by the model.

Model results have been used to investigate also the evolution of the Ora del Garda from the shores of Lake Garda to its outbreak inside the Adige Valley. In the morning the lake breeze, marked by a front with a thickness of about 700 m, develops on the shores of Lake Garda and then moves towards north in the Sarca and Lakes valleys. As to the outbreak into the Adige Valley, it has been found that, as proposed by Schaller (1936), the Ora del Garda flows under the local up-valley wind. Moreover it seems that the outbreak of the lake breeze causes the development of a vortex inside the valley. The temperature of the lake breeze is probably underestimated by the model; in fact comparisons of the numerical results with observations from surface weather stations have highlighted that the temperature drop at the arrival of the lake breeze front is overestimated. This error is probably to be attributed to an

incorrect initialization of the lake water temperature, but further tests are needed to prove this hypothesis.

As to urban effects, the model is able to simulate the daily cycle of the urban-rural temperature differences, with a strong UHI at night and low or negligible intensities in the central hours of the day, similarly to what found in Chapter 3. According to the model, at night the boundaries of the UHI follow the urban land use, with a sharp temperature increase at the city boundaries, similarly to the "cliff" proposed by Oke (1987) (Fig. 2.6). This behavior seems confirmed by the fact that the weather stations on the valley floor considered for the analysis of the UHI of Trento in Chapter 3 are placed close to the boundaries of the city, but seem not affected by urban effects. In particular Roncafort weather station is located only 200 m north of the city boundaries (Fig. 3.1), but it registers strong temperature differences with the urban site at night. On the other hand the temperature inside the city is roughly constant, similarly to the "plateau" in Fig. 2.6, with only slightly higher values in the central part of the urban area, which displays a more compact urban morphology. Furthermore in the evening the UHI begins to develop from the city center and then it spreads to the whole urban area. Idealized simulations in which all the urban grid cells have been replaced by cropland have highlighted that, as expected, the presence of the city lowers the up-valley wind in the afternoon, probably due to the high roughness of the urban area. In the morning the results found are more difficult to explain. In the early morning wind velocity is slightly stronger when the urban area is present. On the other hand the presence of the city leads to lower velocities in the northern part of the urban area at 1000 UTC, and, as a consequence, the Ora del Garda outbreaks an hour earlier into the Adige Valley.

Sensitivity tests have shown that anthropogenic heat flux releases in Trento do not affect considerably temperatures, even though it has been found that during wintertime, when solar radiation is weaker and natural gas consumptions are higher, these effects can be slightly stronger. As a further step, the use of the Building Energy Model (BEM), which is already available in WRF, will allow to directly take into account energy exchanges between buildings and the atmosphere, and thus might give further information about this aspect. As to the urban morphology parameters, it seems that the urban fraction is the variable which most influences the temperature field inside the urban area.

Chapter 7

Conclusions and future developments

The common thread of this work has been the investigation of the climate of the city of Trento, taken as a particular case study of urban boundary layer processes occurring in a midsized city located in a narrow mountain valley. Two typical urban meteorology themes, the evaluation of the UHI of the city and of the microclimatic conditions inside an urban canopy, have been tackled at first, whereas in the second part of this work the analysis has moved to a larger spatial scale, investigating more deeply the peculiarity of a city located in a narrow valley. Therefore local circulation systems, typically developing in mountain valleys, have been also investigated, to evaluate the possible mutual interactions with the urban area.

The first characterization of the urban climate of Trento by means of the analysis of data from surface weather stations has highlighted that the city, though quite small, develops a strong UHI at night in clear sky conditions with low winds. On the other hand in the morning the temperature raises more quickly in rural areas than in the city, with the development of an urban cool island in the central hours of the day. The weather station taken as a reference for the urban area in this analysis is located close to the city center, but above the mean rooftop level. In order to evaluate climatic conditions also at street level, two field measurements, one in the summertime and one in the wintertime, were carried out inside a north-south oriented urban canyon located in the city center. Results have shown that the temperature in the urban canopy is slightly higher than above roof level both in summer and in winter. The highest differences are observed in the summertime, probably due to the stronger solar radiation, which can penetrate for a longer time period inside the canyon, causing, as a consequence, a stronger overheating of the walls and of the road. For this reason the UHI intensity at street level is even higher with respect to the values found above roof level, while the urban cool island effect is less strong, especially in the summer period. However it is likely that during wintertime an urban cool island is present in the morning also inside the urban canopy, due

to overshadowing. The results of these field campaigns suggest that, as found in other cities, the microclimatic conditions inside the urban canopy are mainly controlled by the penetration of the solar radiation inside the street. As a consequence, results found are site-specific and thermal conditions may change in streets with different geometries. In order to overcome this limitation, the performances of a simple single-layer model, similar to the scheme proposed by Kusaka et al. (2001), which simulates climatic conditions in the urban canopy, have been tested against observations. Comparisons have demonstrated that this simple scheme is an useful tool to evaluate in an easy, but reliable way, surface and air temperatures inside the urban canopy. In particular wall surface measurements collected in a physical model and independently from this work (Idczak et al. 2007) have been very well reproduced, simulating correctly both the heating due to direct solar radiation and that induced by the multiple reflections occurring inside urban canyons.

The main features of local atmospheric processes developing in the valleys around Trento, with a particular attention to along-valley winds, have been investigated both analyzing data from surface weather stations and performing high-resolution simulations with the mesoscale WRF model. Both methods have highlighted the substantial differences occurring between the local circulation system developing in the Adige Valley, and that blowing in the Sarca and Lakes valleys. The former is a typical valley wind, while the latter is a combination of a lake breeze and a valley wind. The lake breeze, the so called Ora del Garda, starts to blow from the shores of Lake Garda in the morning and then propagates with its cooler air in the Sarca and Lakes valleys, outbreaking into the Adige Valley north of Trento in the first part of the afternoon. In some days the lake breeze is even able to reach the central part of the urban area of Trento, thus lowering the temperature in the city in hot summer afternoons. As to the Adige Valley, it has been found that the features of local circulation systems are mainly determined by the local geometry of the valley, which controls the penetration of solar radiation and the heating of the valley slopes. For this reason the onset of the up-valley wind is generally not associated with the propagation of a front, as in the case of the lake breeze, but caused by the local pressure gradients developing irregularly along the valley. Only in the southernmost part of the valley, close to its end in the Po Plain, it is likely that an up-valley wind front propagating north is present, as the pressure contrasts which cause the onset of the valley wind develop earlier between the plain and the southernmost part of the valley, and then between the inner sections of the valley. These results, though found in a particular context, are likely to be extended also to other valleys with geometric characteristics and solar forcing similar to the Adige Valley.

The WRF model, coupled with the BEP urban parameterization scheme, has been used also to obtain more information about the urban climate of Trento. The model is able to simulate with a good accuracy the daily cycle of the UHI, confirming that the city of Trento alters considerably the near surface temperature field on the valley floor. Moreover results suggest that the UHI follows the boundaries of the city, with slightly higher intensities in the areas

where the urban morphology is more compact. The analysis of the impact of the city on the wind field has highlighted, as expected, that the high roughness of the urban area lowers the intensity of the up-valley wind in the afternoon. On the other hand the presence of the city seems to have an impact also on the timing of the outbreak of the Ora del Garda into the Adige Valley, which is anticipated by an hour.

In the present thesis, besides characterizing exhaustively the urban climate processes in the city of Trento, a series of methods, which can be easily exported to other contexts, have been implemented and tested. Furthermore these methods, along with the results obtained, could be useful in view of possible future applications in several different fields. For example the simple numerical scheme positively validated against observations in urban canyons might be an useful tool not only to simulate climatic conditions in the canopy layer, but also in building energetics, as it could provide the atmospheric boundary conditions to a building energy model. Moving to a larger spatial scale and considering the entire urban area, the methodology followed for the modeling study with the WRF model, with the creation of high-resolution input gridded fields of urban morphology and anthropogenic heat flux, allows to study the influence of these factors on urban climatic conditions, thus obtaining important information on the possible strategies for the mitigation of the UHI. Moreover, as a further step, the use of the Building Energy Model (BEM), already included in the WRF model, may allow to directly take into account the exchange of energy between the buildings and the outdoor atmosphere, thus evaluating the impact of the building characteristics on energy consumption. This strategy is alternative to the inventory approach followed in this work, and a comparison of the results obtained with the two different methods might be performed to validate the estimates of anthropogenic heat flux releases. The numerical simulations of valley boundary layer processes including urban areas performed in this work are also a fundamental instrument for the study of pollutants dispersion in complex terrain. The methodology developed in this thesis will be particularly useful in view of a project aiming at evaluating the transport and dispersion of air pollutants emitted by the vehicular traffic moving on the highway, which run on the valley floor of the Adige Valley.

Finally the complete analysis of the urban climate of Trento will prove useful also in view of the reconstruction and analysis of the long temperature time series (1816-2010) of the city (Rea et al. 2003), as it will provide criteria to discriminate between temperature variations due to climatic change and those caused by the growth of the city in the last two centuries (cf. Andrighetti et al. 2009). In fact since 1816 temperature measurements were performed in several observatories, placed in different part of the city, and some of these locations were later progressively incorporated in the urban area.

Bibliography

Andrighetti, M., D. Zardi, and M. de Franceschi, 2009: History and analysis of temperature series of Verona (1769-2006). *Meteor. Atmos. Phys.*, **103**, 267–277.

Baik, J.-J. and J.-J. Kim, 1999: A numerical study of flow and pollutant dispersion characteristics in urban street canyons. *J. Appl. Meteor.*, **38**, 1576–1589.

Bee, E., 2010: Analisi delle circolazioni a regime di brezza nella valle dell'Adige (Analysis of local circulation systems in the Adige Valley). 99 pp.

Bougeault, P. and P. Lacarrére, 1989: Parameterization of orography-induced turbulence in a mesobeta-scale model. *Monthly Weather Review*, **117**, 1872–1890.

Bourbia, F. and H. B. Awbi, 2004: Building cluster and shading in urban canyon for hot dry climate. part i: Air and surface temperature measurements. *Renewable Energy*, **29**, 249–262.

Brutsaert, W., 1975: On a derivable formula for long-wave radiation from clear skies. *Water Resour. Res.*, **11**, 742–744.

Carroll, J. J., 1985: Global transmissivity and diffuse fraction of solar radiation for clear and cloudy skies as measured and as predicted by bulk transmissivity models. *Solar Energy*, **2**, 105–118.

Cenedese, A. and P. Monti, 2003: Interaction between an inland urban heat island and a sea-breeze flow: a laboratory study. *J. Appl. Meteor.*, **42**, 1569–1583.

Chen, F. and Coauthors, 2011: The integrated WRF/urban modelling system: development, evaluation, and applications to urban environmental problems. *Int. J. Climatol.*, **31**, 273–288.

Chen, F. and J. Dudhia, 2001: Coupling an advanced land-surface/hydrology model with the Penn State/NCAR MM5 modeling system. Part I: Model implementation and sensitivity. *Monsoon Weather Review*, **129**, 569–585.

Chen, T. C., S. Y. Wang, and M. C. Yen, 2007: Enhancement of afternoon thunderstorm activity by urbanization in a valley: Taipei. *J. Appl. Meteor. Climatol.*, **46**, 1324–1340.

Coceal, O., A. Dobre, and T. G. Thomas, 2007: Unsteady dynamics and organized structures from dns over an idealized building canopy. *Int. J. Climatol.*, **27**, 1943–1953.

Coutts, A. M., J. Beringer, and N. J. Tapper, 2007: Impact of increasing urban density on local climate: spatial and temporal variations in the surface energy balance in Melbourne, Australia. *J. Appl. Meteor. Climatol.*, **46**, 477–492.

Dandou, A., M. Tombrou, and N. Soulakellis, 2009: The influence of the city of Athens on the evolution of the sea-breeze front. *Bound.-Layer Meteor.*, **131**, 35–51.

de Franceschi, M., G. Rampanelli, and D. Zardi, 2002: Further investigations of the ora del garda valley wind. *Proc. 10th Conference on Mountain Meteorology and Mesoscale Alpine Program MAP-Meeting 2002*, Yokohama, Japan, International Association for Urban Climate.

de Franceschi, M. and D. Zardi, 2007: *LOsservatorio meteorologico dellUniversit degli Studi di Trento al Molino Vittoria (The Meteorological Observatory of the University of Trento at the Molino Vittoria)*. Universit degli Studi di Trento Dipartimento di Ingegneria Civile e Ambientale, 36 pp.

de Franceschi, M., D. Zardi, M. Tagliazucca, and F. Tampieri, 2009: Analysis of second order moments in the surface layer turbulence in an alpine valley. *Quart. J. Roy. Meteor. Soc.*, **135**, 1750–1765.

de Wekker, S. F. J., D. G. Stein, J. D. Fast, M. W. Rotach, and S. Zhong, 2005: The performance of RAMS in representing the convective boundary layer structure in a very steep valley. *Envrionmental Fluid Mechanics*, **5**, 35–62.

de Wekker, S. F. J. and C. D. Whiteman, 2006: On the time scale of nocturnal boundary layer cooling in valleys and basins and over plains. *J. Appl. Meteor. Climatol.*, **45**, 813–820.

de'Donato, F. K. and Coauthors, 2008: Airport and city-centre temperatures in the evaluation of the association between heat and mortality. *Int. J. Biometeorol.*, **52**, 301–310.

Defant, F., 1949: Zur Theorie der Hangwinde, nebst Bemerkungen zur Theorie der Berg- und Talwinde. [A theory of slope winds, along with remarks on the theory of mountain winds and valley winds]. *Arch. Meteor. Geophys. Bioclimatol., Ser. A*, **1**, 421–450.

Doran, J. C., C. M. Berkowitz, R. L. Coulter, W. J. Shaw, and C. W. Spicer, 2003: The 2001 Phoenix Sunrise experiment: vertical mixing and chemistry during the morning transition in Phoenix. *Atmos. Environ.*, **37**, 2365–2377.

Erell, E. and T. Williamson, 2007: Intra-urban differences in canopy layer air temperature at a mid-latitude city. *Int. J. Climatol.*, **27**, 1243–1255.

Fast, J. D., J. C. Torcolini, and D. Redman, 2005: Pseudovertical temperature profiles and the urban heat island measured by a temperature datalogger network in Phoenix. *J. Appl. Meteorol.*, **44**, 2–13.

Gedzelman, S. D., S. Austin, R. Cermak, N. Stefano, S. Partridge, S. Quesenberry, and D. A. Robinson, 2003: Mesoscale aspects of the urban heat island around new york city. *Theor. Appl. Climatol.*, **75**, 29–42.

Georgakis, C. and M. Santamouris, 2006: Experimental investigation of air flow and temperature distribution in deep urban canyons for natural ventilation purposes. *Energy and Buildings*, **38**, 367–376.

Giovannini, L., D. Zardi, and M. de Franceschi, 2011: Analysis of the urban thermal fingerprint of the city of Trento in the Alps. *J. Appl. Meteor. Climatol.*, **50**, 1145–1162.

Giovannini, L., D. Zardi, and M. de Franceschi, 2012: Characterization of the thermal structure inside an urban canyon: field measurements and validation of a simple model. *submitted to the J. Appl. Meteor. Climatol.*

Goldreich, Y., 1984: Urban topoclimatology. *Prog. Phys. Geogr.*, **8**, 336–364.

Goldreich, Y., 2009: Updating the urban topoclimatology a review. *Extended Abstracts, The seventh International Conference on Urban Climate*, Park City, UT, Amer. Meteor. Soc.

Grigiante, M., F. Mottes, D. Zardi, and M. de Franceschi, 2011: Experimental solar radiation measurements and their effectiveness in setting up a real sky irradiance model. *Renewable Energy*, **36**, 1–8.

Grimmond, C. S. B., 1992: The suburban energy balance: methodological considerations and results for a mid-latitude west coast city under winter and spring conditions. *Int. J. Climatol.*, **12**, 481–497.

Grimmond, C. S. B., 2006: Progress in measuring and observing the urban atmosphere. *Theor. Appl. Climatol.*, **84**, 3–22.

Grimmond, C. S. B. and Coauthors, 2011: Initial results from phase 2 of the international urban energy balance model comparison. *Int. J. Climatol.*, **31**, 244–272.

Grimmond, C. S. B. and T. R. Oke, 1999: Heat storage in urban areas: local-scale observations and evaluation of a simple model. *J. Appl. Meteor.*, **38**, 922–941.

Howard, L., 1833: *Climate of London deduced from meteorological observations*, Vol. 1. Harvey and Darton, 348 pp.

Idczak, M., D. Groleau, P. Mestayer, J.-M. Rosant, and J.-F. Sini, 2010: An application of the thermo-radiative model SOLENE for the evaluation of street canyon energy balance. *Building and Environment*, **45**, 1262–1275.

Idczak, M., P. Mestayer, J.-M. Rosant, J.-F. Sini, and M. Violleau, 2007: Micrometeorological measurements in a street canyon during the joint ATREUS-PICADA experiment. *Bound.-Layer Meteor.*, **124**, 25–41.

Jauregui, E. J., 1987: Urban heat island development in medium and large urban areas in Mexico. *Erdkunde*, **41**, 48–51.

Johansson, E., 2006: Influence of urban geometry on outdoor thermal comfort in a hot dry climate: a study in Fez, Morocco. *Building and Environment*, **41**, 1326–1338.

Junk, J., A. Helbig, and J. Luers, 2003: Urban climate and air quality in Trier Germany. *Int. J. Biometeorol.*, **47**, 230–238.

Kanda, M., R. Moriwaki, and Y. Kimoto, 2005: Temperature profiles within and above an urban canopy. *Bound.-Layer Meteor.*, **115**, 499–506.

Kassomenos, P. A. and B. D. Katsoulis, 2006: Mesoscale and macroscale aspects of the morning urban heat island around athens, greece. *Meteor. Atmos. Phys.*, **94**, 209–218.

Kim, Y.-H. and J.-J. Baik, 2002: Maximum urban heat island intensity in Seoul. *J. Appl. Meteor.*, **41**, 651–659.

Kljun, N., P. Calanca, M. W. Rotach, and H. P. Schmid, 2004: A simple parameterisation for flux footprint predictions. *Bound.-Layer Meteor.*, **112**, 503–523.

Kusaka, H., H. Kondo, Y. Kinegawa, and F. Kimura, 2001: A simple single-layer urban canopy model for atmospheric models: comparison with multi-layer and slab models. *Bound.-Layer Meteor.*, **101**, 329–358.

Kuttler, W., A.-B. Barlag, and F. Rossmann, 1998: Influence of regional and local winds on urban ventilation in Cologne, Germany. *Atmos. Environ.*, **30**, 365–378.

Kuttler, W., D. Dutemeyer, and A.-B. Barlag, 1996: Study of the thermal structure of a town in a narrow valley. *Meteor. Z.*, **7**, 77–87.

Landsberg, H. E., 1981: *The urban climate.* Academic Press, 275 pp.

Lazar, R. and A. Podesser, 1999: An urban climate analysis of Graz and its significance for urban planning in the tributary valleys east of Graz (Austria). *Atmos. Environ.*, **33**, 4195–4209.

Lee, S.-H. and J.-J. Baik, 2010: Statistical and dynamical characteristics of the urban heat island intensity in Seoul. *Theor. Appl. Climatol.*, **100**, 227–237.

Lin, C.-Y., F. Chen, J. C. Huang, W.-C. Chen, Y.-A. Liou, W.-N. Chen, and S.-C. Liu, 2008: Urban heat island effect and its impact on boundary layer development and land-sea circulation over northern Taiwan. *Atmos. Environ.*, **42**, 5635–5649.

Lora, C., M. de Franceschi, M. Sitta, and D. Zardi, 2006: Determinazione delleffetto isola di calore urbana in una citt alpina mediante utilizzo di reti di sensori a basso costo (determination of the urban heat island effect in an alpine city with a network of low cost sensors). *XXX Convegno di Idraulica e Costruzioni Idrauliche IDRA 2006*, Rome, Italy.

Lowry, W. P., 1977: Empirical estimation of urban effects on climate: a problem analysis. *J. Appl. Meteor.*, **16**, 129–135.

Martilli, A., A. Clappier, and M. W. Rotach, 2002: An urban surface exchange parameterization for mesoscale models. *Bound.-Layer Meteor.*, **104**, 261–304.

Masson, V., 2000: A physically-based scheme for the urban energy budget in atmospheric models. *Bound.-Layer Meteor.*, **94**, 357–397.

Masson, V., 2006: Urban surface modeling and the meso-scale impact of cities. *Theor. Appl. Climatol.*, **84**, 35–45.

Miao, S., F. Chen, M. A. LeMone, M. Tewari, Q. Li, and Y. Wang, 2009: An observational and modeling study of characteristics of urban heat island and boundary layer structures in Beijing. *J. Appl. Meteor. Climatol.*, **48**, 484–501.

Miao, S., F. Chen, Q. Li, and S. Fan, 2011: Impacts of urban processes and urbanization on summer precipitation: a case study of heavy rainfall in Beijing on 1 August 2006. *J. Appl. Meteor. Climatol.*, **50**, 806–825.

Mills, G., 2004: The urban canopy layer heat island. *www.urban-climate.org*.

Mochida, A. and I. Y. F. Luna, 2008: Prediction of wind environment and thermal comfort at pedestrian level in urban area. *Journal of Wind Engineering and Industrial Aerodynamics*, **96**, 1498–1527.

Morris, C. J. G. and I. Simmonds, 2000: Associations between varying magnitudes of the urban heat island and the synoptic climatology in Melbourne, Australia. *Int. J. Climatol.*, **20**, 1931–1954.

Morris, C. J. G., I. Simmonds, and N. Plummer, 2001: Quantification of the influences of wind and cloud on the nocturnal urban heat island of a large city. *J. Appl. Meteor.*, **40**, 169–182.

Nkemdirim, L. C., 1980: Cold air drainage and temperature fields in an urban environment: a case study of topographical influence on climate. *Atmos. Environ.*, **14**, 375–381.

Noilhan, J., 1981: A model for the net total radiation flux at the surfaces of a building. *Building Environment*, **16**, 259–266.

Nunez, M. and T. R. Oke, 1977: The energy balance of an urban canyon. *J. Appl. Meteor.*, **16**, 11–19.

Offerle, B., I. Eliasson, C. S. B. Grimmond, and B. Holmer, 2007: Surface heating in relation to air temperature, wind and turbulence in an urban street canyon. *Bound.-Layer Meteor.*, **122**, 273–292.

Ohashi, Y., Y. Genchi, H. Kondo, Y. Kikegawa, H. Yoshikado, and Y. Hirano, 2007: Influence of air-conditioning waste heat on air temperature in Tokyo during summer: numerical experiments using an urban canopy model coupled with a building energy model. *J. Appl. Meteorol. Clim.*, **46**, 66–81.

Oke, T. R., 1973: City size and the urban heat island. *Atmos. Environ.*, **7**, 769–779.

Oke, T. R., 1976: The distinction between canopy and boundary layer urban heat islands. *Atmosphere*, **14**, 268–277.

Oke, T. R., 1981: Canyon geometry and the nocturnal heat island. comparison of scale model and field observations. *Journal of Climatology*, **1**, 237–254.

Oke, T. R., 1982: The energetic basis of the urban heat island. *Quart. J. Roy. Meteor. Soc.*, **108**, 1–24.

Oke, T. R., 1987: *Boundary Layer Climates.* 2d ed., Routledge, 435 pp.

Oke, T. R., 1988: The urban energy balance. *Prog. Phys. Geogr.*, **12**, 471–508.

Oke, T. R., 2006: Initial guidance to obtain representative meteorological observations at urban sites. Wmo instruments and observing methods, report n. 81, 47 pp.

Oke, T. R. and C. East, 1971: The urban boundary layer in montreal. *Bound.-Layer Meteor.*, **1**, 411–437.

Oke, T. R., R. A. Spronken-Smith, E. Jauregui, and C. S. B. Grimmond, 1999: The energy balance of central mexico city during the dry season. *Atmos. Environ.*, **33**, 3919–3930.

Pearlmutter, D., A. Bitan, and P. Berliner, 1999a: Microclimatic analysis of "compact" urban canyons in an arid zone. *Atmos. Environ.*, **33**, 4143–4150.

Pearlmutter, D., A. Bitan, and P. Berliner, 1999b: Modifications of a valley wind system by an urban area experimental results. *Meteor. Atmos. Phys.*, **71**, 117–125.

Piringer, M., et al., 2005: The surface energy balance in urban areas. Final report cost action 715, 76 pp.

Rampanelli, G., D. Zardi, and R. Rotunno, 2004: Mechanisms of up-valley winds. *J. Atmos. Sci.*, **61**, 3097–3111.

Rea, R., G. Rampanelli, and D. Zardi, 2003: The temperature series of Trento: 1816-2002. *Proc. 27th International Conference on Alpine Meteorology and MAP-Meeting*, Brig, Switzerland, 483.

Rotach, M. W., 1993a: Turbulence close to a rough urban surface part I: Reynolds stress. *Bound.-Layer Meteor.*, **65**, 1–28.

Rotach, M. W., 1993b: Turbulence close to a rough urban surface part II: variances and gradients. *Bound.-Layer Meteor.*, **66**, 75–92.

Rotach, M. W. and Coauthors, 2005: BUBBLE: an urban boundary layer meteorology project. *Theor. Appl. Climatol.*, **81**, 231–261.

Rotach, M. W. and M. Coauthors, 2004: Turbulence structure and exchange processes in an Alpine valley:the Riviera project. *Bull. Amer. Meteorol. Soc.*, **85**, 1367–1385.

Rotach, M. W. and D. Zardi, 2007: On the boundary layer structure over highly complex terrain: key findings from map. *Quart. J. Roy. Meteor. Soc.*, **133**, 937–948.

Runnals, K. E. and T. R. Oke, 2000: Dynamics and controls of the near-surface heat island of vancouver, british columbia. *Physical Geography*, **21**, 283–304.

Sadler, F. and A. Bellin, 2004: Analisi di serie storiche di precipitazione (analysis of historical precipitation time series). *Analisi climatologica delle serie storiche delle precipitazioni e temperature in Trentino (Climatologic analysis of historical precipitation and temperature time series in Trentino)*, A. Bellin and D. Zardi, Eds., Editoriale Bios.

Sailor, D. J., 2011: A review of methods for estimating anthropogenic heat and moisture emissions in the urban environment. *Int. J. Climatol.*, **31**, 189–199.

Sailor, D. J. and L. Lu, 2004: A top-down methodology for developing diurnal and seasonal anthropogenic heating profiles for urban areas. *Atmos. Environ.*, **38**, 2737–2748.

Sakakibara, Y., 1996: A numerical study on the effect of urban geometry upon the surface energy budget. *Atmos. Environ.*, **30**, 487–496.

BIBLIOGRAPHY

Salamanca, F., A. Krpo, A. Martilli, and A. Clappier, 2010: A new building energy model coupled with an urban canopy parameterization for urban climate simulations-part i. formulation, verification and sensitivity analysis of the model. *Theor. Appl. Climatol.*, **99**, 331–344.

Salamanca, F., A. Martilli, M. Tewari, and F. Chen, 2011a: A study of urban boundary layer using different urban parameterizations and high-resolution urban canopy parameters in wrf. *J. Appl. Meteor. Clim.*, **50**, 1107–1128.

Salamanca, F., A. Martilli, and C. Yague, 2011b: A numerical study of the urban heat island over Madrid during the DESIREX (2008) campaign with WRF and an evaluation of simple mitigation strategies. *Int. J. Climatol.*

Santamouris, M., N. Papanikolaou, I. Koronakis, I. Livada, and D. Asimakopoulos, 1999: Thermal and air flow characteristics in a deep pedestrian canyon under hot weather conditions. *Atmos. Environ.*, **33**, 4503–4521.

Santin, M., 2007: Analisi del ciclo diurno delle variabili meteorologiche connesse allo sviluppo di circolazioni locali nella val d'Adige (Analysis of the daily cycle of meteorological variables that causes the development of local circulations in the Adige Valley. 196 pp.

Schaller, E., 1936: Aerologische untersuchung des periodischen talwindsystems von Trient (Aerologic investigation of the periodic valley-wind system of Trento). 62 pp.

Schmidli, J. and Coauthors, 2011: Intercomparison of mesoscale model simulations of the daytime valley wind system. *Monthly Weather Review*, **67**, 3033–3047.

Schmidli, J. and R. Rotunno, 2010: Mechanism of along valley winds and heat exchange over mountainous terrain. *J. Atmos. Sci.*, **67**, 3033–3047.

Serafin, S. and D. Zardi, 2010a: Daytime heat transfer processes related to slope flows and turbulent convection in an idealized mountain valley. *J. Atmos. Sci.*, **67**, 3739–3756.

Serafin, S. and D. Zardi, 2010b: Structure of the atmospheric boundary layer in the vicinity of a developing upslope flow system: a numerical model study. *J. Atmos. Sci.*, **67**, 1171–1185.

Skamarock, W. C., J. B. Klemp, J. Dudhia, D. O. G. abd D. M. Barker, M. Duda, X.-Y. Huang, W. Wang, and J. G. Powers, 2008: A description of the advanced research wrf version 3. NCAR Technical Note TN-475+STR, 125 pp. [Available from NCAR, P.O Box 3000, Boulder, CO 80307].

Sofer, M. and O. Potchter, 2006: The urban heat island of a city in an arid zone: the case of Eilat, Israel. *Theor. Appl. Climatol.*, **139**, 1389–1409.

Steinecke, K., 1999: Urban climatological studies in the Reykjavk subarctic environment, Iceland. *Atmos. Environ.*, **33**, 4157–4162.

Stewart, I. D., 2010: A systematic review and scientific critique of methodology in modern urban heat island literature. *Int. J. Climatol.*, **31**, 200–217.

Stull, R. B., 1988: *An introduction to boundary layer meteorology.* Kluwer Academic Publisher, 435 pp.

Svensson, M. K., 2004: Sky view factor analysis implications for urban air temperature differences. *Meteorol. Appl.*, **11**, 201–211.

Tan, J. and Coauthors, 2010: The urban heat island and its impact on heat waves and human health in Shanghai. *Int. J. Biometeorol.*, **54**, 75–84.

Thompson, W. T., T. Holt, and J. Pullen, 2007: Investigation of a sea breeze front in an urban environment. *Quart. J. Roy. Meteor. Soc.*, **133**, 579–594.

UNFPA, cited 2007: State of world population 2007. Unleashing the potential of urban growth.

Unger, J., Z. Sumeghy, and J. Zoboki, 2001: Temperature cross-section features in an urban area. *Atmospheric Research*, **58**, 117–127.

Unsworth, M. H. and J. L. Monteith, 1975: Long-wave radiation at the ground. *Quart. J. Roy. Meteor. Soc.*, **101**, 13–24.

Unwin, D. J., 1980: The synoptic climatology of Birminghams heat island. *Weather*, **35**, 43–50.

Vergeiner, I. and E. Dreiseitl, 1987: Valley winds and slope winds - observations and elementary thoughts. *Meteor. Atmos. Phys.*, **36**, 264–286.

Wagner, A., 1932: Neue Theorie der Berg- und Talwinde [New theory of mountain and valley winds]. *Meteor. Z.*, **49**, 329–341.

Wagner, A., 1938: Theorie und beobachtung der periodischen gebirgswinde (theory and observation of periodic mountain winds). *Gerlands Beitr. Geophys.*, **52**, 408–449.

Wanner, H. and J. A. Hertig, 1984: Studies of urban climates and air pollution in switzerland. *J. Climate Appl. Meteor.*, **23**, 1614–1625.

Weigel, A. P., F. K. Chow, M. W. Rotach, R. L. Street, and M. Xue, 2006: High-resolution large-eddy simulations of flow in a steep Alpine valley. Part II: Flow structure and heat budgets. *J. Appl. Meteor. Climatol.*, **45**, 87–107.

Whiteman, C. D., 1990: Observation of thermally developed wind systems in mountainous terrain. atmospheric processes over complex terrain. Amer. Meteor. Soc., No. 45 in Meteor. Monogr., 5–42.

Whiteman, C. D., J. M. Hubbe, and W. J. Shaw, 2000: Evaluation of an inexpensive temperature datalogger for meteorological applications. *J. Atmos. Ocean. Tech.*, **17**, 76–81.

Xiaomin, S., H. Zhen, and W. Jiasong, 2006: The impact of urban street layout on local atmospheric environment. *Building and Environment*, **41**, 1352–1363.

Yoshikado, H., 1992: Numerical study of the daytime urban effect and its interaction with the sea breeze. *J. Appl. Meteor.*, **31**, 1146–1164.

Zajic, D., H. J. S. Fernando, R. Calhoun, M. Princevac, M. J. Brown, and E. R. Pardyjak, 2011: Flow and turbulence in an urban canyon. *J. Appl. Meteor. Climatol.*, **50**, 203–223.

Zängl, G., 2004: A reexamination of the valley wind system in the Alpine Inn Valley with numerical simulations. *Meteor. Atmos. Phys.*, **87**, 241–256.

Zardi, D. and C. D. Whiteman, 2011: Diurnal mountain wind systems. *Mountain Weather Research and Forecasting*, Amer. Meteor. Soc., AMS Meteorological Monographs, chap. 2, (submitted).